

DA126217

RADC-TR-82-328

Final Technical Report

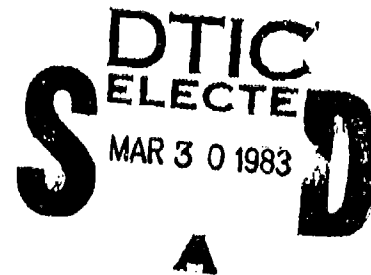
December 1982



JAM RESISTANT COMMUNICATIONS SYSTEMS TECHNIQUES

The Ohio State University

A. A. Ksienski



APPROVED FOR PUBLIC RELEASE; DISTRIBUTION UNLIMITED

DTIC FILE COPY

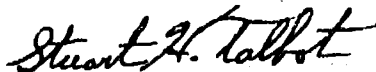
**ROME AIR DEVELOPMENT CENTER
Air Force Systems Command
Griffiss Air Force Base, NY 13441**

88 03 30 052

This report has been reviewed by the RADC Public Affairs Office (PA) and is releasable to the National Technical Information Service (NTIS). At NTIS it will be releasable to the general public, including foreign nations.


RADC-TR-82-328 has been reviewed and is approved for publication.

APPROVED:



STUART H. TALBOT
Project Engineer

APPROVED:



BRUNO BEEK
Technical Director
Communications Division

FOR THE COMMANDER:



JOHN P. HUSS
Acting Chief, Plans Office

If your address has changed or if you wish to be removed from the RADC mailing list, or if the addressee is no longer employed by your organization, please notify RADC (DCCR) Griffiss AFB NY 13441. This will assist us in maintaining a current mailing list.

Do not return copies of this report unless contractual obligations or notices on a specific document requires that it be returned.

UNCLASSIFIED

SECURITY CLASSIFICATION OF THIS PAGE (When Data Entered)

REPORT DOCUMENTATION PAGE		READ INSTRUCTIONS BEFORE COMPLETING FORM
1. REPORT NUMBER RADC-TR-82-328	2. GOVT ACCESSION NO. AD A126217	3. RECIPIENT'S CATALOG NUMBER
4. TITLE (and Subtitle) JAM RESISTANT COMMUNICATIONS SYSTEMS TECHNIQUES		5. TYPE OF REPORT & PERIOD COVERED Final Technical Report Feb 79 - May 82
		6. PERFORMING ORG. REPORT NUMBER ESL-711679-11 ✓
7. AUTHOR(s) A. A. Ksienski	8. CONTRACT OR GRANT NUMBER(s) F30602-79-C-0068	
9. PERFORMING ORGANIZATION NAME AND ADDRESS The Ohio State University/Electroscience Lab Dept of Electrical Engineering Columbus OH 43212		10. PROGRAM ELEMENT, PROJECT, TASK AREA & WORK UNIT NUMBERS 62702F 45196308
11. CONTROLLING OFFICE NAME AND ADDRESS Rome Air Development Center (DCCR) Griffiss AFB NY 13441		12. REPORT DATE December 1982
		13. NUMBER OF PAGES 302
14. MONITORING AGENCY NAME & ADDRESS (if different from Controlling Office) Same		15. SECURITY CLASS. (of this report) UNCLASSIFIED
		15a. DECLASSIFICATION/DOWNGRADING SCHEDULE N/A
16. DISTRIBUTION STATEMENT (of this Report) Approved for public release; distribution unlimited.		
17. DISTRIBUTION STATEMENT (of the abstract entered in Block 20, if different from Report) Same		
18. SUPPLEMENTARY NOTES RADC Project Engineer: Stuart H. Talbot (DCCR)		
19. KEY WORDS (Continue on reverse side if necessary and identify by block number) Cascaded Processors Degrees of Freedom (See reverse) LMS Processor Element Placement Power Inversion Processor Array Pattern Computation Adaptive Array Geometric Theory of Diffraction (GTD) Modeling Thinned Array Aircraft Mounted Antenna Pattern Simulation		
20. ABSTRACT (Continue on reverse side if necessary and identify by block number) The objective of this effort was to develop techniques to increase the jam resistant capability of communication systems. The effort involved the assessment of the limitations, both theoretical and practical, that restrict the effectiveness of adaptive arrays operating in various environments, and wherever possible to overcome these limitations by appropriate design changes. A technique was developed to predict adaptive array performance and		

DD FORM 1 JAN 73 1473

EDITION OF 1 NOV 65 IS OBSOLETE

UNCLASSIFIED

SECURITY CLASSIFICATION OF THIS PAGE (When Data Entered)

UNCLASSIFIED

SECURITY CLASSIFICATION OF THIS PAGE(When Data Entered)

provide guidelines for the design of adaptive arrays on complex structures to produce specified performance levels. A cascaded adaptive array consisting of a power inversion stage followed by an LMS stage has been designed, built and tested showing improved dynamic range performance. An angle of arrival estimation system capable of providing accurate angle estimates in the presence of multiple high powered jammers has been developed.

The angle of arrival estimate could be utilized to provide pointing information in a demand assignment TDMA SATCOM system employing high gain switchable downlink beams.

A four phase modulation system for communication systems utilizing adaptive arrays has been developed, built and tested with experimental results in close agreement with the theoretical analysis. Computational codes have been developed that provide very accurate antenna patterns for antennas located on aircraft structures. A conformal array study was carried out to replace reflector type antennas on C-135 aircraft for satellite communication. A delay lock loop incorporating a Kalman filter was designed to provide low error rates for a TDMA system operating at very high data rates.

Block 19 (cont'd)

Microcircuit Multiplier

Kalman Predictor Sampled Delay Lock Loop

UNCLASSIFIED

SECURITY CLASSIFICATION OF THIS PAGE(When Data Entered)

ACKNOWLEDGEMENT

The research reported in this final report on Contract #F30602-79-C-0068 represents the effort of several researchers. The names of those whose contributions were published in separate reports appear with the titles of the summaries in Section III. Major contributors to the research effort not previously reported are Dr. W.G. Swarner (Sections III and IV), Dr. H.D. Brown (Section IV), Mr. H.S. Eilts (Sections V and VI), Mr. E. Yu (Section VI), Dr. E.K. Walton (Section VIII), and Dr. I.J. Gupta (Sections IX and X). Mr. R.C. Taylor and R.W. Evans made significant contributions to all experimental work performed under this contract.

Mr. Stuart Talbot was the RADC Program Monitor for this research.



Accession For	
NTIS GRA&I	<input checked="checked" type="checkbox"/>
DTIC TAB	<input type="checkbox"/>
Unannounced	<input type="checkbox"/>
Justification	
By	
Distribution/	
Availability Codes	
Dist	Avail and/or Special
A	

TABLE OF CONTENTS

	Page
LIST OF TABLES	viii
LIST OF FIGURES	ix
SECTION I	
INTRODUCTION	1
SECTION II	
DOCUMENTED RESEARCH PERFORMED UNDER THE PRESENT CONTRACT	5
A. THE PERFORMANCE OF A SAMPLED DATA DELAY LOCK LOOP	5
B. AIRBORNE ANTENNA PATTERN CODE USER'S MANUAL	6
C. A WEIGHT STORAGE AND RECALL SYSTEM FOR USE IN AN EXPERIMENTAL ADAPTIVE ARRAY	8
D. ANGLE OF ARRIVAL ESTIMATION USING AN ADAPTIVE ARRAY	9
E. A FOUR-PHASE MODULATION SYSTEM FOR USE WITH AN ADAPTIVE ARRAY	11
F. DEPENDENCE OF ADAPTIVE ARRAY PERFORMANCE ON CONVENTIONAL ARRAY DESIGN	14
G. AN ALGORITHM TO SELECT ELEMENT LOCATIONS OF AN ADAPTIVE ARRAY	16
H. PREDICTION OF ADAPTIVE ARRAY PERFORMANCE IN A MULTIPLE JAMMER ENVIRONMENT	17

	Page
I. THE SINR PERFORMANCE OF CASCADED ADAPTIVE ARRAYS	19
J. GENERAL 3-D AIRBORNE ANTENNA RADIATION PATTERN CODE- USER'S MANUAL	20
K. REFERENCES	21
 SECTION III	
EXPERIMENTAL CASCADED ADAPTIVE ARRAY	24
A. BACKGROUND	24
B. CONCEPT OF THE CASCADED ADAPTIVE ARRAY	27
C. EXPERIMENTAL CASCADED ARRAY	32
1. Configuration	32
2. Implementation	35
3. Multipliers	43
4. Circuit Description and Diagrams	48
D. ARRAY PERFORMANCE AND RESULTS	58
1. Tests Using CW Signals	58
2. Tests with PN Coded Signals	63
3. Tests with Spectrum Matched Jamming Signals	72
E. SUMMARY AND CONCLUSIONS	75
F. REFERENCES	79
 SECTION IV	
MICROCIRCUIT MULTIPLIER DEVELOPMENT	82
 SECTION V	
A KALMAN PREDICTOR SAMPLED DATA DELAY LOCK LOOP EXPERIMENT	87

	Page
A. EXPERIMENTAL HARDWARE	88
B. RESULTS	91
C. CONCLUSIONS AND RECOMMENDATIONS	93
D. REFERENCES	94
SECTION VI	
THE MODIFIED-LMS FEEDBACK LOOP	97
A. INTRODUCTION	97
B. MODIFIED-LMS FEEDBACK LOOP	99
C. IMPLEMENTATION AND PERFORMANCE	108
D. MULTIPLIER FEEDTHROUGH	117
E. CONCLUSION	121
F. REFERENCES	122
SECTION VII	
COMMUNICATION SYSTEM APPLICATIONS STUDY	124
A. REFERENCES	129
SECTION VIII	
CONFORMAL ARRAYS ON C-135 AIRCRAFT FOR SATELLITE COMMUNICATION	130
A. INTRODUCTION	130
B. BLOCKAGE EFFECTS	132
1. The Aircraft Model	132
2. Example Far Field Plot	135
C. SINGLE ELEMENT PATTERNS	137
1. Mapping Procedure	140

	Page
2. Computer Program Description	142
3. Single Element Mappings	145
a. Antenna Element On Fuselage (25 deg. Roll 12.525 Inches Tailward Of Reference Point)	145
b. Antenna Element on Fuselage (65 deg. Roll 12.525 Inch Tailward of Reference Point) -RHP-	149
c. Antenna Element on Fuselage (65 deg. Roll 12.525 Inch Tailward of Reference Point) -LHP-	150
D. ARRAY PATTERN	150
1. Array Pattern Computation	150
2. Mapping Of Array Gain Coverage	155
3. Directional Gain vs. Satellite Direction	157
E. CONCLUSIONS	157
F. REFERENCES	160
SECTION IX	
DEGREES OF FREEDOM OF AN ADAPTIVE ARRAY	161
A. DEGREES OF FREEDOM OF AN ADAPTIVE ARRAY	161
B. DEGREES OF FREEDOM OF AN ADAPTIVE ARRAY IN A CONICAL CUT	163
C. EFFECT OF THE DISTRIBUTION OF PROJECTED ELEMENTS IN A CUT ON THE NUMBER OF DEGREES OF FREEDOM OF AN ADAPTIVE ARRAY	183

	Page
D. ADAPTIVE ARRAY PERFORMANCE WHEN ALL JAMMERS ARE NOT IN THE SAME CUT	190
E. CONCLUSIONS	200
F. REFERENCES	200
 SECTION X	
ELEMENT PLACEMENT FOR ADAPTIVE ANTENNA ARRAYS	201
A. INTRODUCTION	201
B. THE ELEMENT PLACEMENT ALGORITHM	202
C. ELEMENT LOCATIONS OF A LINEAR ARRAY IN THE PRESENCE OF ONE JAMMER	208
D. ELEMENT PLACEMENT OF A LINEAR ARRAY IN THE PRESENCE OF MULTIPLE JAMMERS	219
E. PLANAR ARRAY TO PROVIDE COVERAGE IN A THREE DIMENSIONAL SPACE	232
F. SUMMARY	258
G. REFERENCES	259
 SECTION XI	
CONCLUSIONS AND RECOMMENDATIONS	260
 APPENDIXES	
A. CASCADED ARRAY DIAGRAMS	265
B. HYBRID ELECTRONICS PROJECT	281
C. APPROPRIATE RELATIONSHIPS FOR THE KALMAN TRACKING LOOP EXPERIMENT	299

LIST OF TABLES

TABLE	Page
VIII-1. PARAMETERS OF MODEL OF THE KC135 AIRCRAFT	133
X-1. VARIOUS SYMBOLS AND CORRESPONDING LEVELS	238
A1. CASCADED ADAPTIVE ARRAY AMPLIFIER SPECIFICATIONS	280

LIST OF FIGURES

FIGURE	Page
III-1. Cascaded adaptive array configuration (3x3 fully implemented array).	28
III-2. Dynamic range of cascaded array (steady state solution).	31
III-3. Experimental 4x4 cascaded array configuration (partial implementation).	34
III-4. Self-excited I-F adaptive array feedback controller.	37
III-5. I-F weighted adaptive array controller with baseband integrators.	42
III-6. Passive mixer multiplier characteristics.	45
III-7. Pumped mixer multiplier characteristics.	46
III-8. Configuration for cw testing of the cascaded adaptive array.	59
III-9. Cascaded array performance with cw signals.	61
III-10. Cascaded array test configuration for bit error rate testing with TDMA modems.	64
III-11. Cascaded array performance in a pn-coded TDMA link with cw jammer (downlink S/N = 12 dB in 10 KHz BW).	66
III-12. Cascaded array performance in a pn-coded TDMA link with cw jammer (downlink S/N = 34 dB in 10 KHz BW).	67
III-13. Cascaded array performance in a pn-coded TDMA link with cw jammer (downlink S/N = 15 dB in 10 KHz BW).	68
III-14. Cascaded array performance with spectrum matched jammer, multiplier pump oscillators off.	73
III-15. Cascaded array performance with spectrum matched jammer, multiplier pump oscillators on.	74
IV-1. Microcircuit multiplier measured characteristics.	84
IV-2. Developmental microcircuit active multiplier.	85

FIGURE		Page
V-1.	Block diagram of the sampled-dealy lock loop (SDDL).	88
V-2.	Experimental hardware.	90
V-3.	Experimental and theoretical performance of the Kalman SDDL.	91
VI-1.	The LMS feedback loop.	100
VI-2.	The modified feedback loop.	102
VI-3.	The normalized time constants for the modified-LMS loop.	105
VI-4.	The time constant spread of the modified-LMS loop for several values of c' .	106
VI-5.	A block diagram of the modified-LMS loop implementation.	109
VI-6.	Waveforms of weights (lower trace) and their derivatives (upper trace). Horizontal: 50 μ sec/div. (a) LMS array (b) Modified-LMS array.	111
VI-7.	Spectrum of the array output. Horizontal: 100 KHz/div. Vertical: 10 dB/div. (a) LMS array (b) Modified-LMS array.	113
VI-8.	Bit error rate vs jammer to signal ratio for four different adaptive array configurations with pulse desired signal.	115
VI-9.	Bit error rate vs jammer to signal ratio for four different adaptive array configurations with continuous desired signal.	116
VI-10.	Weight multiplier characteristics.	118
VI-11.	The modified-LMS feedback loop with multiplier feedthrough.	119
VIII-1.	Prolate spheroid model of KC135 with attached plates.	134
VIII-2.	Field plot for single antenna element. Scan angle is 38° off fuselage axis.	136
VIII-3.	Elevation angle to geostationary satellite located at 135° west longitude as a function of geographic location.	138

FIGURE		Page
VIII-4.	Operational performance envelope of array based on Figure VIII-3.	139
VIII-5.	Observation point mapping scheme.	141
VIII-6.	Flowchart of computer program linkages.	143
VIII-7.	Signal strength map due to single antenna element.	146
VIII-8.	Signal strength map (RHP) due to single antenna element.	147
VIII-9.	Signal strength map (LHP) due to single antenna element.	148
VIII-10.	Initial distribution of array elements.	154
VIII-11.	Signal strength map due to sum of the signal amplitude of each of the 20 elements.	156
VIII-12.	Plot of array gain and operational performance map for conformal array.	158
IX-1.	A linear array in a 3-dimensional space.	164
IX-2.	An arbitrary conical cut in a 3-dimensional space.	167
IX-3.	A five element array in a 3-dimensional space.	170
IX-4.	A linear array of five isotropic elements.	175
IX-5.	Output SINR of the linear array of five isotropic elements in the xy plane.	176
IX-6.	Output SINR of the linear array of five isotropic elements in the yz plane in the presence of four (—) and five (----) jammers.	177
IX-7.	a) Crossed array of five isotropic elements, b) Projection of array in the xy plane.	179
IX-8.	Output SINR of the crossed array in the xy plane in the presence of two (—) and three (----) jammers.	180
IX-9.	a) θ_r cut in the coordinate system, b) Projection of the array elements in the θ_r cut.	181

FIGURE	Page
IX-10. Output SINR of the crossed array in $\theta_r = 60^\circ$ cut in the presence of (—) three jammers, (----) four jammers.	182
IX-11. Output SINR of a linear array of four isotropic elements in the presence of three jammers.	184
IX-12. Output SINR of a linear array of four isotropic elements in the presence of three jammers.	185
IX-13. Output SINR of a linear array of four isotropic elements in the presence of four jammers.	188
IX-14. Output SINR of a linear array of four isotropic elements in the presence of four jammers for different θ_{14} .	189
IX-15. Output SINR of the crossed array in the presence of (—) four jammers, (----) five jammers vs desired signal in the xy plane.	194
IX-16. Output SINR of the crossed array of five elements in the xy plane in the presence of one jammer in the yz plane.	195
IX-17. Output SINR of the crossed array of seven elements in the xy plane in the presence of one jammer in the yz plane.	197
IX-18. Output SINR of the crossed array of five elements in the xy plane in the presence of one jammer in $\theta_r = 60^\circ$ cut.	198
IX-19. Output SINR of the crossed array of seven elements in the xy plane in the presence of one jammer in $\theta_r = 60^\circ$ cut.	199
X-1. A linear of N isotropic elements with one incident jammer and a desired signal.	207
X-2. Unperturbed pattern (F) of a linear array of two elements (constraint elements).	209
X-3. Output SINR of a two element (constraint elements) array in the presence of one jammer vs. the jammer direction.	210
X-4. Unperturbed pattern (F) of a three element array (constraint elements plus one resolution element).	214
X-5. Output SINR of a three element array (constraint elements plus one resolution element) in the presence of one jammer vs. the jammer direction.	215

FIGURE	Page
X-6. Unperturbed pattern (F) of a four element array (constraint elements plus two resolution elements).	216
X-7. Output SINR of a four element array (constraint elements plus two resolution elements) in the presence of one jammer vs. the jammer direction.	218
X-8. Unperturbed pattern (F) of a linear array of four elements (constraint elements).	221
X-9. Unperturbed pattern (F) of a linear array of five elements (constraint elements plus one resolution element).	222
X-10. Unperturbed pattern (F) of a linear array of six elements (constraint elements plus two resolution elements).	223
X-11. Unperturbed pattern (F) of a linear array of seven elements (constraint elements plus three resolution elements).	224
X-12. Unperturbed pattern (F) of a completely filled linear array of fourteen elements.	226
X-13. Unperturbed pattern (F) of a linear array of six elements (constraint elements).	227
X-14. Unperturbed pattern (F) of a linear array of seven elements (constraint elements plus one resolution element).	229
X-15. Unperturbed pattern (F) of a linear array of eight elements (constraint elements plus two resolution elements).	230
X-16. Unperturbed pattern (F) of a linear array of nine elements (constraint elements plus three resolution elements).	231
X-17. Coordinate system for a three dimensional space.	233
X-18. A linear array for three incident jammers.	235
X-19. Unperturbed pattern of the linear array.	236
X-20. Output SINR of the linear array in the presence of three jammers vs. the third jammer direction.	237
X-21. A thinned rectangular array.	241
X-22. Unperturbed pattern of the rectangular array.	242

FIGURE	Page
X-23. Output SINR of the rectangular array in the presence of three jammers vs. the third jammer direction.	243
X-24. The crossed array.	245
X-25. Unperturbed pattern of the crossed array.	246
X-26. Output SINR in the presence of one jammer vs. the jammer direction.	249
X-27. Output SINR of the crossed array in the presence of three jammers vs. the third jammer direction.	250
X-28. Unperturbed pattern of a uniform circular array of fourteen elements.	252
X-29. Output SINR of a uniform circular array of fourteen elements in the presence of three jammers vs. the third jammer direction.	254
X-30. Unperturbed pattern of a tapered circular array of fourteen elements.	256
X-31. Output SINR of a tapered circular array of fourteen elements in the presence of three jammers vs. the third jammer direction.	257
A1. Cascaded adaptive array - converters and I-F amplifiers.	266
A2. Cascaded adaptive array - power inversion controllers, 4 x (2,3,3,2) configuration.	267
A3. Cascaded adaptive array - power inversion feedback loops, 4 x (2,3,3,2) configuration.	268
A4. Cascaded adaptive array - LMS controllers.	269
A5. Cascaded adaptive array - LMS feedback loop and output/reference converters.	270
A6. Cascaded adaptive array - pump oscillators and amplifiers.	271
A7. Cascaded adaptive array feedback controllers (PI and LMS).	272
A8. Cascaded adaptive array baseband integrators.	273
A9. Cascaded adaptive array weight control and mode switching.	274

FIGURE	Page
A10. Cascaded adaptive array I-F amplifier gain control and power wiring.	275
A11. Cascaded adaptive array power distribution.	276
A12. Cascaded array power supply APS-2.	277
A13. Cascaded array power supply regulator circuit board.	278
A14. Adaptive array element signal simulator (70 MHz).	279
B1. CA 3049L Data Sheet.	283
B2. a) Illustrated in the background is a ceramic board with 20 circuit patterns. b) Illustrated in the middle right is the device substrate. c) Illustrated in the upper portion is the complete device before capping.	284
B3. Conductor pattern and pin-out configuration of the hybrid circuit.	285
B4. Mechanical drawing of metalized ceramic device substrate.	287
B5. Twenty device substrates after sawing is complete.	289
B6. Complete device before capping.	290
B7. Test circuit.	291
C1. The noise performance of the Kalman predictors as a function of model parameters.	304

SECTION I

INTRODUCTION

The objective of this effort was to develop techniques to increase the jam resistant capability of communication systems. The effort involved the assessment of the limitations, both theoretical and practical, that restrict the effectiveness of adaptive arrays operating in various environments, and wherever possible to overcome these limitations by appropriate design changes. The concern regarding the limitations of adaptive arrays grew as the attempts to implement them ran into unexpected difficulties and indicated that the very impressive (A/J) protection predicted from theoretical considerations and idealized models were not achievable in practice. A major source of degradation appeared to be related to the electromagnetic properties of the array and its environment. For example, an array of widely spaced elements that would produce grating lobes in its conventional mode of operations would be subject to "grating nulls" in its adaptive mode. In general, the adaptive array performance appeared to be strongly affected by the antenna element types, their distribution and their particular locations on the airframe (for aircraft antennas) and the airframe itself. Moreover, the performance was also found to vary significantly with signal and jammer scenarios. This apparent unpredictability of the adaptive array performance required exhaustive tests to determine the

performance and yet no assurance could be given that a particular scenario would not cause excessive performance degradation. As a result of the present research effort, the relationship between the adaptive array performance and the electromagnetic properties of the array has been established leading not only to the predictability of performance for arbitrary scenarios but also to design guidelines that would assure adequate performance under the worst scenarios. Concepts such as the number of degrees of freedom simply linked to the number of nulls of an array have been shown to be inadequate and were appropriately modified to assure reliable communication in jamming environments.

Another area of considerable concern was that of the dynamic range of adaptive arrays which was found to be disappointingly small. The difficulty appeared to be related to the fact that in the presence of strong jammers the LMS array would fail due to the excessive speed of adaptive loops which would either demodulate the desired signal or modulate the interference to appear like the reference signal, thus permitting the entry of the jammer signal into the communication link. In an attempt to overcome this problem, two approaches were proposed; 1) to utilize a cascade of two adaptive arrays consisting of a power inversion array followed by an LMS array. This combination, it was hoped, would reduce significantly the input power levels to the LMS array preventing the excessive response speed of its loops. And 2), to implement the Compton modified LMS array which essentially equalizes the response time of the loops and reduces them to a prespecified rate of response. Both approaches were implemented with initial indications

that a significant increase in dynamic range is attainable; the details are discussed in the body of the report.

Another aspect of adaptive array performance which evoked concern, related to its ability to respond to a desired signal within a reasonably short time and yet not accept a deceptive jamming signal. In other words, rapid acquisition of desired signal and resistance to smart jammers. The first requirement leads to short codes; the second to very long ones. To accommodate these mutually contradictory requirements, a four-phase modulation system was developed that satisfies both rapid acquisition and good protection against both smart as well as brute force jammers. The system involving the adaptive array was designed, built and tested, with the results confirming the theoretical prediction.

One area of concern arose in connection with the introduction of adaptive arrays into a beam switching TDMA system, namely, the adaptive array may not be able to direct a beam (adapt) to the terminal within a fraction of a slot unless the weights were at least approximately preset. To provide that capability, a weight storage and recall system was designed and analyzed in sufficient detail to permit ready implementation.

Other studies involved the more general problem of satellite communication in a TDMA context. In particular, to allow higher data rates without incurring higher bit error rates due to timing inaccuracies, it was proposed to introduce more sophisticated processing into the delay lock loops of the timing correction circuitry. The performance of a sampled data delay lock loop with a Kalman loop filter

which was designed for this purpose was analyzed and computer simulated. The results confirmed significant performance improvements over the presently used sample averaging circuit. Another study dealt with angle of arrival estimation which is of particular importance for a TDMA beam hopping SATCOM system communicating with mobile terminals in the close vicinity of powerful jammers. The study resulted in a proposed approach which can estimate the angle of arrival of a desired signal to within a fraction of a beamwidth and can do that even in the presence of main beam jammers.

A study was carried out dealing with the possibility of utilizing conformal arrays on C-135 aircraft for satellite communications. The results indicate that this can be accomplished by a single contiguous array properly located on the fuselage of the airplane. Additional topics investigated are summarized below.

In Section II, summaries are provided of major research items which were documented separately by means of technical reports. Sections III to X include results of research work not covered in previous reports. Section XI presents our conclusions and recommendations for future work.

SECTION II

DOCUMENTED RESEARCH PERFORMED UNDER THE PRESENT CONTRACT

A. THE PERFORMANCE OF A SAMPLED DATA DELAY LOCK LOOP IMPLEMENTED WITH A KALMAN LOOP FILTER (ESL Report 711679-1 ; Henry S. Eilts)

In the OSU/RADC signalling scheme, pseudo-noise (PN) coding is used to provide some degree of interference and multipath immunity. Tracking loops are provided at the receiver to generate a local PN code synchronized with the received code. In the present modems, Sampled Data Delay Lock Loops (SDDLL) are used to track the received code. These provide very good code tracking with low PN code rates and stationary terminals. The desire to increase the PN code rates and utilize maneuvering terminals (e.g., terminals on aircraft) motivated a study into the integration of Kalman estimation techniques with the SDDLL.

The above report documents the performance of a SDDLL implemented with the Kalman prediction algorithm. It is divided into three sections:

1. Noise (jitter) performance.
2. Maneuver performance.
3. Transient or lock-up performance.

The jitter performance of the Kalman SDDLL was evaluated by using both analytical and Monte Carlo techniques. The maneuver performance was

evaluated by simulating two typical aircraft maneuvers and using the simulated propagation delays as inputs to the Kalman algorithm. It was found that the tracking jitter could be reduced to arbitrarily small values by reducing the bandwidth of the Kalman estimator. This degraded the maneuver tracking accuracy, however. Conversely, the tracking errors for the maneuvers could be reduced by increasing the estimator bandwidth. This raises the jitter due to noise. It was shown that it is possible, however, to adjust the bandwidth so that both the jitter performance and the maneuver tracking performance are simultaneously adequate.

Acquisition or lock-up performance was also evaluated by means of computer simulation. A comparison of the Kalman algorithm using time variable gains with the same algorithm using fixed (steady-state) gains was made. The fixed gain algorithm is much simpler computationally. It was shown that acquisition performance with fixed gains is generally poor. With time variable gains, the acquisition performance is good, and lock-up performance should not be a significant concern.

The data presented in this report were also presented in a Master's Thesis [1] and in a journal publication [2].

B. AIRBORNE ANTENNA PATTERN CODE USER'S MANUAL

(ESL Report 711679-2 by W.D. Burnside and T. Chu)

In order to investigate the radiation patterns of antennas in a complex environment such as on an aircraft, a Fortran IV computer code has been developed. The computer code is used to compute the near zone radiated fields for antennas mounted on an elliptic cylinder and in the

presence of a set of finite flat plates. The analysis applied in the development of the code is based on the geometrical theory of diffraction (GTD) [3,4]. The code allows the user to simulate a wide variety of complex electromagnetic radiation problems using the cylinder/plates model. For example, the elliptic cylinder can be used to simulate the fuselage or jet intake of an aircraft; whereas, the plates are used to represent the wings, stabilizers, stores, etc. Note that the plates can be attached to the cylinder and/or to other plates. In fact, the plates can be connected together to form a box. In terms of special sections in the input data set, antennas mounted on missile configurations are discussed. The T-tail effect and mutual coupling effect of antenna arrays mounted on a nearly flat fuselage are also illustrated by examples. The code has the flexibility to handle arbitrary pattern cuts. In addition, an arbitrary antenna type can be analyzed provided the current distribution across the aperture is known. The code can, also, treat a monopole or monopole arrays; however, the length of each element cannot exceed a quarter wavelength.

The mutual coupling effect for monopole arrays mounted on a fuselage is handled by thin-wire theory [5], if the region near the array is nearly flat. For engineering purposes, image theory can be applied to calculate the relative current distributions as equivalent dipole arrays. The relative current value on each dipole is then taken to be part of the input data for each monopole source specification. The final pattern is the superposition of the contributions from each individual monopole.

The present form of the computer code is not large in terms of computer storage and executes a pattern for a single antenna element very efficiently. The present code requires approximately 200 K bytes of storage. It will run a pattern cut of 360 points for a simple aircraft model with one antenna element in approximately 30 seconds on a CDC-6600 computer.

This user's manual is designed to give an overall view of the operation of the computer code, to instruct a user in how to use it to model structures, and to show the validity of the code by comparing various computed results against measured data whenever available.

C. A WEIGHT STORAGE AND RECALL SYSTEM FOR USE IN AN
EXPERIMENTAL ADAPTIVE ARRAY

(ESL Report 711679-3 by H.S. Eilts and W.G. Swarner)

A weight storage recall system (WSR) was proposed for an adaptive array used for uplink protection in a Time Division Multiple Access (TDMA) satellite communications system [6]. In this system, the various users are assigned sequential time slots in which to communicate. This poses some problems for the adaptive array. When a time slot occurs, the adaptive array must direct its beam (i.e., adapt) to the desired transmitter before communication can occur. This requires that an adaption preamble precede the data on each transmission. Without a WSR system, the array must adapt each time the user's time slot occurs. With a WSR system, the adaptive weights are sampled and stored at the end of a user's time slot. Then, when the time slot reoccurs, the stored weights are recalled. During the time slot, adaption proceeds from

weights which are already very near their final adapted values. Thus, the adaption preamble can be eliminated from all user transmissions subsequent to the first one. This will significantly increase the signalling efficiency of the system.

In TDMA systems, transmissions must be retrodirected from the satellite back toward the user. This requires that the satellite have a knowledge of the position of the receiver. This knowledge can be gained from the uplink weights. Estimation schemes are currently under study for this purpose [7]. These methods use computer processing of the weights to gain position information. The storage portion of a WSR system facilitates this processing by providing weights in digital format.

The above report describes the design of a WSR system for use on an experimental adaptive array [8]. Analysis is provided which indicates that a 12 bit system offers a good compromise between cost and performance. Sample, hold, and conversion hardware is described. This description includes schematic diagrams and part lists. For the actual weight storage, a Hewlett Packard 2116 computer is used. Computer programs were written for the computer operation and are presented along with flow charts and explanation.

D. ANGLE OF ARRIVAL ESTIMATION USING AN ADAPTIVE ARRAY

(ESL Report 711679-4 by Bengt V. Andersson)

The objective of this study was to develop an angle of arrival estimation technique that could perform reliably in the presence of high powered jammers stronger, by up to several orders of magnitude, than the desired signal whose angle is to be estimated. The angle estimate is

aimed at a demand assignment TDMA SATCOM system employing high gain switchable down link beams. A high accuracy estimate would provide a reliable communication link where quality would greatly exceed that of a system employing an earth coverage beam.

Various approaches have been previously used to accomplish angle of arrival (AoA) estimation. The best known is the monopulse system. This system provides a good AoA estimate as long as the noise present is receiver noise or uniformly distributed background noise. The presence of strong directional interfering signals (jammers) would drastically degrade the estimation, however, and the monopulse system would no longer be useful.

Adaptive arrays are ideally suited for the suppression of jammers and the maximization of signal to interference plus noise ratios. It would then appear to be very advantageous if an angle of arrival estimation system would incorporate an adaptive array in its processor. Indeed, Davis, et al. [9], extended the theory of adaptive arrays to the angle estimation problem. Based on the maximum likelihood theory of angle estimation, they proposed an AoA estimator which can be readily implemented using adaptive arrays. The estimator requires the knowledge of the covariance matrix of the element signals in the absence of the desired signal. This requirement can be accommodated in a TDMA system, and consequently, the estimator was studied in this report under different jamming scenarios. The estimator involves sum and difference beams, which are analogous to those used in conventional monopulse systems. The estimator, therefore, was termed the monoestimator. It was shown that if one has some prior knowledge of the AoA of the desired

signal, the mon estimator provides an accurate estimate of the AoA (within a fraction of a beamwidth). If, however, the expected AoA is not within a half beamwidth of the actual AoA, the mon estimator generally breaks down. An alternative estimator was, therefore, proposed in this work. It also is based on the maximum likelihood theory of angle of arrival estimation and requires the knowledge of the covariance matrix. But no prior approximate knowledge of the AoA is needed. The new estimator called the "Q estimator" can also be implemented using adaptive arrays. It was shown that the Q estimator provides very accurate estimates of the AoA (within a tenth of a beamwidth) as long as the jammers are outside the main beam of the array. As the angular separation between the desired signal and the jammer decreases, the accuracy of the Q estimate degrades. However, the estimated AoA still remains within a quarter of a beamwidth of the true AoA and is, therefore, adequate for a switched down link beam of a TDMA system. Furthermore, the Q estimate can be used as an initial estimate for the mon estimator, further improving the final accuracy for close-in jammer scenarios. The overall system would provide angle estimates accurate to within a tenth of a beamwidth even with jammers located within the main beam of the array.

E. A FOUR-PHASE MODULATION SYSTEM FOR USE WITH AN ADAPTIVE ARRAY
(ESL Report 711679-5 by Jack Winters)

The purpose of this research was to develop a four-phase communication system for use with an adaptive array. This system was developed to improve upon a previously developed biphasic system [10].

The four-phase system was analyzed both theoretically and experimentally. The analytical and experimental results demonstrate the rapid acquisition and jammer protection of the four-phase system.

The four-phase system was developed by first examining the previous biphas system and then studying the four-phase modulation techniques which overcome the biphas system's shortcomings. The biphas system was shown to have two shortcomings: 1) short codes must be used for reasonable acquisition times, but short codes may not have adequate security for many applications, and 2) the biphas system is vulnerable to repeat jammers with biphas remodulation. To overcome the first shortcoming, a long and a short code were shown to be required on the signal. Several modulation techniques were given which combined the two codes. Because these signals were to be used with an adaptive array, reference signal generation techniques were developed. To overcome the second shortcoming, a data modulation method other than biphas was shown to be required. Several data modulation techniques were presented and reference signal generation methods for these techniques were discussed. A particular type of four-phase signal was shown to be able to overcome the biphas system shortcomings. A communication system was developed for this system. The four-phase signal consists of two orthogonal biphas signals. One signal contains a short code for rapid acquisition. The other contains a long code to be used for protection against smart jammers. The reference signal generation technique uses the same reference signal generation loop as in the biphas system, but a biphas reference signal partially correlated with the received signal is generated. The signal acquisition technique involves a multi-step

process. The short code timing is first acquired by a sliding correlation method. With the short code used in reference signal generation, the long code timing is rapidly acquired by the Rapid Acquisition by Sequential Estimation method [11]. The long code is then used in reference signal generation.

To assure rapid acquisition of the signal at the receiver, the acquisition procedure was analyzed in detail. The acquisition of the short code timing by the sliding correlation method was studied first. The acquisition trajectory of the delay lock loop was shown without noise present with the signal. Equations were derived that describe the acquisition process with noise in terms of the delay lock loop parameters. The tracking jitter of the delay lock loop was then analyzed. Equations were developed which determine the tracking jitter in terms of the delay lock loop parameters. Next, the long code acquisition process was analyzed. Differential detection of the four-phase signal in the acquisition process was studied in detail. An appropriate model for the acquisition process was analyzed. Computer simulation results for the actual process were carried out. It was shown that very long codes (those that repeat once a year or less often) can be acquired rapidly even with low received signal-to-noise ratios. To assure that the long code can provide security in the system, the long code structure was studied. Nonlinear codes were shown to be more secure than linear codes, but even linear codes were seen to provide reasonable security.

The effect was then studied of various jamming techniques on the acquisition procedure. It was shown that conventional jamming, repeat

jamming with remodulation, and biphase jamming with the short code could not jam the system.

An experimental four-phase system was implemented and experimental results analyzed. The system provided an example of how the analytical results of this study can be used to develop a system to meet specific requirements. Circuit schematics showed how the acquisition procedure can be implemented. Experimental results verified the analytical results. The experimental results also demonstrated the rapid acquisition and conventional jamming protection of the system. The conventional jamming protection was shown to be close to that of the biphase system and could be increased with code frequencies greater than the 175.2 kHz used. Finally, it was shown that although a smart jammer may slightly increase the acquisition time, it is no more effective in preventing acquisition than a cw jammer. Thus, the four-phase system is not vulnerable to the same type of jamming techniques as the biphase system.

F. DEPENDENCE OF ADAPTIVE ARRAY PERFORMANCE ON CONVENTIONAL ARRAY DESIGN

(ESL Report 711679-6 by I.J. Gupta and A.A. Ksienski)

The adaptive array provides significant advantages over the conventional array in both communication and radar systems. It is often, however, assumed that because of its flexibility in using the available array elements, the adaptive array can overcome most, if not all, of the deficiencies in the design of the basic or conventional array that is to be used in an adaptive mode. One can, it seemed,

ignore the conventional goals such as low sidelobes and narrow beamwidth in the array design. Recent work has been drawing attention to the fact that this is not so and that very serious problems, such as grating nulls, will arise with improper element distribution and patterns [12]. This work showed the dependence of the adaptive array performance on the soundness of the design of the basic, or conventional, array that is to be used in an adaptive mode. In particular, expressions were derived showing that the output signal-to-interference-plus-noise ratio (SINR) of an adaptive array is related to the conventional array characteristics as represented by the adaptive array pattern responding to a single desired signal in the absence of any interfering signals. This direct relationship permits one to evaluate the performance of an adaptive array without having to resort to exhaustive tests for a large variety of desired signal and jammer scenarios. Indeed, one can predict the signal and jammer locations for which the array will provide its best and worst performance by observing the unperturbed, namely the conventional, array pattern. One can then directly compute the SINR performance under these conditions. By using the expressions derived in the report, one can design the physical array including element location, radiation characteristics, number of elements, etc., to provide specified SINR performance levels without going through elaborate and expensive cut and try attempts which would at best only statistically predict the adaptive array performance.

G. AN ALGORITHM TO SELECT ELEMENT LOCATIONS OF AN ADAPTIVE ARRAY
(ESL Report 711679-7 by I.J. Gupta and W.D. Burnside)

It has been noticed that improper element patterns and/or placement can lead to serious degradation in the output signal-to-interference-plus noise ratio (SINR) of an adaptive array for certain angles of arrival. Ishide and Compton [12] characterized this problem in terms of a grating null phenomena and found that using elements with unequal (appropriate) radiation patterns the grating nulls can be avoided. In most applications, for example, airborne adaptive arrays, one does not have much control over the element patterns and thus the element placement becomes important. In this work an algorithm was derived which provides the appropriate element placement such that all the dips in the output SINR below a specified threshold can be avoided. The algorithm is based on dividing the total number of array elements into two parts:

a) The Constraint Elements: If there are m interference signals incident on the adaptive array, at least $m+1$ elements will be needed in this part of the array. These elements are closely spaced and are placed such as to ensure that there are no dips in the output SINR. These elements will be referred to as the constraint elements and provide the required degrees of freedom.

b) The Resolution Elements: Since the constraint elements are closely spaced, they may not provide the required resolution. As a result, some additional elements may be required to achieve the desired

resolution. These elements are placed at large distances and constitute the resolution part of the array. These elements will be called the resolution elements.

The constraint elements are specified first. Once the spacings of the constraint elements are decided, one adds resolution elements until the required resolution is achieved without introducing extra dips.

A single incident jammer is discussed in this report, but the method may be extended to multiple interference signals. The method is, first, applied to a linear array of isotropic elements and then it is extended to conformal arrays. It is shown that the method can be used for arrays mounted on conducting cylinders. The effect of scattered fields on the performance of an adaptive array mounted on complex structures such as an aircraft fuselage is addressed. It is shown that the scattered fields can cause extra dips in the output SINR. This specific problem is discussed in this report and is resolved by adding additional compensating elements.

H. PREDICTION OF ADAPTIVE ARRAY PERFORMANCE IN A MULTIPLE JAMMER ENVIRONMENT

(ESL 711679-8 by I.J. Gupta and A.A. Ksienski)

It is generally accepted that the performance of an adaptive array is affected by the interfering signals (jammers) scenario. Mesiwala and Widrow [13] found that the angular location of interfering signals affect the adaption time of an adaptive array, but it appears that to

date no quantitative estimates of the effect on the steady state performance of an adaptive array have been reported. Such an estimate is obtained in this work. It is shown that there exists a direct relation between the conventional array characteristics as represented by its radiation pattern and the adaptive array performance both in a single and multiple jammer environment. For a single incident jammer, the degradation in the array performance depends on the angular location of the jammer with respect to the desired signal and is determined by the sidelobe structure of the array. For a multiple jammer environment the location of jammers with respect to the desired signal as well as with respect to each other are important factors in determining the array performance. First, as one would expect, multiple jammers incident from the same direction can be treated as a single jammer. Jammers with small angular separations, however, can cause significant degradation in the performance of an adaptive array. For large angular separation between the jammers, the degradation of the adaptive array performance is the direct cumulative addition of the degradation due to each jammer separately.

The level of degradation of the adaptive array performance is illustrated by using linear arrays of several sizes. Various signal and jamming scenarios are used to show the effects of closely spaced and widely spaced jammers and it is shown that the margin of the number of degrees of freedom over the expected number of jammers is a critical parameter in avoiding drastic degradation in performance.

I. THE SINR PERFORMANCE OF CASCADED ADAPTIVE ARRAYS

(ESL Report 711679-9 by H.S. Eilts)

The least mean square (LMS) adaptive array is sometimes used in communication systems for interference and multipath suppression. The LMS algorithm has the characteristic that the speed of response of the weights is proportional to the input signal power [14]. This causes some problems. With very strong signals (such as jammers), the weights can respond too fast. This can cause signal distortion (modulation by the weights). It can also cause the interference to acquire the signal structure of the desired signal (again through weight modulation). If this occurs, the array no longer can differentiate between desired signals and interference, resulting in a failure to suppress the interference.

To overcome the speed of response problem, it has been proposed that each LMS input be preceded by a power inversion (PI) array. PI arrays have an input power threshold, above which all signals are suppressed. The idea behind this proposal is to use the PI arrays to suppress the strong signals which cause the problems in the LMS array. We call these systems cascaded arrays.

Now, the LMS array (by itself) is known to maximize the steady-state output signal to interference plus noise ratio (SINR) [15]. This report addresses the question of whether or not preceding each LMS input with a PI array destroys this property. That is, is the steady state output SINR of cascaded arrays maximized (optimized)?

This report shows that the steady-state output SINR of cascaded arrays is maximized whenever the LMS inputs are linearly independent.

For the "fully implemented" cascaded array¹, linearly independent LMS inputs are guaranteed by choosing the PI steering vectors to be linearly independent. The full configuration for N elements uses N^2+N weight control loops. Configurations which have fewer control loops were also examined. In general, as control loops are removed from the PI arrays, restrictions must be placed on the PI steering vectors to maintain linearly independent signals at the LMS inputs. Configurations which have fewer than N inputs to the LMS array are shown to be suboptimal.

Of course, other considerations (transient response, weight dynamic range, etc.) are also important in choosing a cascaded array configuration. These are the subject of current research. The value of this report is that it permits further research efforts to be directed toward optimal configurations.

J. GENERAL 3-D AIRBORNE ANTENNA RADIATION PATTERN CODE-USER'S MANUAL
(ESL Report 711679-10 by H.H. Chung)

This report presents the advanced version of report 711679-2 which provides a computational code for obtaining airborne antenna patterns. The major advance achieved in the present code is the introduction of a prolate spheroid to model the fuselage of an aircraft instead of the elliptic cylinder which was used in the previous version of the code. The prolate spheroid model permits the computation of radiation patterns in the nose and tail directions which was, of course, impossible with

¹A "fully implemented" cascaded array has N elements, N N-element PI arrays, and an N-input LMS array.

the elliptical cylinder representation, since it extends to infinity in those directions, i.e., it is not a finite body. The introduction of the prolate spheroid which is a doubly curved body, as compared to the singly curved cylinder, provides good polarization properties as compared with experimental data since it models much more accurately the fuselage of the airplane, particularly in the nose and tail regions where the double curvature of the fuselage becomes pronounced.

Another range of aspect angles where the prolate spheroid provides the essential model characteristics previously not available, is the shadow region where there is no direct illumination by the antenna and the energy travels following the geodesics of the body. The model geodesics must represent reasonably well those of the actual fuselage to provide agreement with experimental data.

K. REFERENCES

- [1] H.S. Eilts, "The Performance of a Sampled Data Delay Lock Loop Implemented with a Kalman Loop Filter", M.S. Thesis, The Ohio State University, March 1979.
- [2] H.S. Eilts, "A Sampled Data Delay Lock Loop Implemented as a Kalman Predictor", IEEE Trans AES, Vol AES-16, No. 6, Nov. 1980, pp. 800-810.
- [3] R.G. Kouyoumjian and P.H. Pathak, "A Uniform Geometrical Theory of Diffraction for an Edge in a Perfectly-Conducting Surface", Proc. IEEE, Vol. 62, November 1974, pp. 1448-1461.

- [4] R.G. Kouyoumjian, "The Geometrical Theory of Diffraction and Its Applications", Numerical and Asymptotic Techniques in Electromagnetics, edited by R. Mittra, Spring-Verlag, New York, 1975.
- [5] J.H. Richmond, "Radiation and Scattering by Thin-Wire Structures in the Complex Frequency Domain", Report 2902-10, July 1973, The Ohio State University ElectroScience Laboratory, Department of Electrical Engineering; prepared under Grant No. NGL 36-008-138 for National Aeronautics and Space Administration.
- [6] H.S. Eilts and W.G. Swarner, "A Weight Storage and Recall System for Use in an Experimental Adaptive Array", Technical Report 711679-3, The Ohio State University ElectroScience Laboratory, Department of Electrical Engineering; prepared under contract F30602-79-C-0068 for Rome Air Development Center.
- [7] B.V. Andersson, "Angle of Arrival (AoA) Estimation Using an Adaptive Array", Technical Report 711679-4, The Ohio State University ElectroScience Laboratory, Department of Electrical Engineering; prepared under contract F30602-79-C-0068 for Rome Air Development Center.
- [8] T.W. Miller, R. Caldecott, and R.J. Huff, "A Satellite Simulator with a TDMA-System Compatible Adaptive Array", Technical Report 3364-4, January 1976, The Ohio State University ElectroScience Laboratory, Department of Electrical Engineering; prepared under Grant No. NGR 36-008-177 for NASA/Langley Research Center.

- [9] R.C. Davis, L.E. Brennan and L.S. Reed, "Angle Estimation with Adaptive Arrays in External Noise Fields", IEEE Trans. on AES, Vol. AES-12, No. 2, March 1976, p. 179.
- [10] R.T. Compton, Jr., "An Adaptive Array in a Spread-Spectrum Communication System", Proc. IEEE, Vol. 66, March 1978, p. 289.
- [11] R.B. Ward, "Acquisition of Pseudonoise Signals by Sequential Estimation", IEEE Trans., COM-13, December 1965, p. 475.
- [12] A. Ishide and R.T. Compton, Jr., "On Grating Nulls in Adaptive Arrays", IEEE Trans. on Antennas and Propagation, Vol. AP-28, pp. 467-475, July 1980.
- [13] H. Mesiwala and B. Widrow, "Compression of Eigenvalue Range by Using a Surplus of Adaptive Antenna Elements", Electroprofessional Program, Sharaton, New York, April 25-26, 1979.
- [14] T.W. Miller, "The Transient Response of Adaptive Arrays in TDMA Systems", Technical Report 4116-1, June 1976, The Ohio State University ElectroScience Laboratory, Department of Electrical Engineering; prepared under Contract No. F30603-75-C-0061 for Rome Air Development Center.
- [15] C.A. Baird, Jr. and C.L. Zahm, "Performance Criteria for Narrowband Array Processing", 1971 IEEE Conf. on Decision and Control, Miami Beach, Florida, December 15-17.

SECTION III

EXPERIMENTAL CASCADED ADAPTIVE ARRAY

A. BACKGROUND

The use of adaptive arrays for uplink protection of a TDMA satellite communications system, as well as for other applications, has been extensively investigated both theoretically and experimentally under previous contracts by this laboratory [1-4], and by numerous others as well. Of the many algorithms which have been proposed for adaptive array applications, the LMS algorithm [5] and the power inversion algorithm [6-8] appear to be most useful when protection from potential jamming threats within the main beam of the receiving antenna is required for high data rate, high duty cycle, communications applications.

The LMS algorithm is superior, particularly when the angle of arrival of a desired signal is unknown a priori (as, for example, a TDMA system with moving terminals) since this algorithm causes the array to automatically beam up on desired signals in addition to suppressing interfering signals. This algorithm, however, requires a reference signal input (i.e., an approximate replica of the desired signal) which must be generated locally by some type of suitable bootstrap circuit. This may, or may not, be feasible depending upon particular system requirements.

The power inversion algorithm does not require a reference signal. This algorithm tends to null all signals, desired or undesired, which are above a given power threshold. It can be used to advantage when the desired signal is of low level and is relatively constant and known a priori at the receiving location, which is often the case for applications such as satellite system up-link protection. In addition, some form of steering vector input is required which tends to point a finite beam in a specific direction in the absence of received signals. Without the steering vector input, the array would simply shut down and receive nothing at all. For best performance, particularly in the absence of a jamming signal, the steering vector must point the quiescent beam in the direction from which the desired signal is expected. Since it is difficult to design a power inversion array which will yield an output SINR (signal to interference plus noise ratio) above 0 dB, some auxiliary form of processing gain (i.e., spectrum spreading via PN-code modulation, frequency hopping, or other means), is normally also required.

While both of these arrays have many potentially useful applications, they are limited in the dynamic range of input signals (i.e., the range of received signal power levels) for which they will function properly. The basic reason is that the time constants of the feedback loops for these algorithms are inversely proportional to the received signal power. In general, the array time constant must be short enough at low signal levels so that the array can respond to null a jamming signal (and/or beam up on a desired signal in the case of an LMS array) before intolerable data loss occurs; while for high signal

levels (notably, high jammer levels), the loop response time must not become so short that desired signal coherence is destroyed.

In particular, for an LMS array using a coded reference signal, at very high jammer levels, the array loop response may become fast enough so that the desired signal code modulation would be impressed upon a jamming signal. When this happens, the jammer is converted to a replica of the reference signal and is accepted by the array. This has been called the catastrophic failure mode and results in essentially complete obliteration of the desired signal information content. During cw testing of an LMS array, this condition can easily be mistaken for good array performance since the output spectrum under these conditions appears to have an excellent SINR. The data modulation, however, has been destroyed. The presence of an output spectrum generated by the array in this manner is readily verified by bit error rate testing using data-modulated signals (quantitative), or (qualitatively) by the simple expedient of temporarily removing the desired signal input and observing whether the (apparent) desired signal output spectrum still remains.

The power inversion array, having no reference signal, is not subject to the catastrophic failure mode, as such. It too, however, will ultimately destroy signal coherence due to weight jitter if the loop time constant becomes too short relative to the data or code chip rate. This has sometimes been described as resulting from partial coherence between the error signal (i.e., the array output signal) and the element input signal. It might also be thought of as due to incomplete filtering of array loop noise. This provides a signal in the feedback loop which produces cancellation of all signals within the loop

bandwidth. The manifestation of this effect at high input levels, and consequently high loop response rate, is a contribution to the weights which tends to "burn a hole" in the output spectrum proportional to the input power spectral density.

Whether or not an LMS array actually is performance limited by the catastrophic failure mode, or whether it too first fails due to the partial coherence effect is subject to some controversy. The fact that the catastrophic failure mode does indeed ultimately occur with increasing jammer input power is readily demonstrated experimentally. In any event, after optimizing an experimental adaptive array (LMS or power inversion) as well as possible for a specific application, the dynamic range of (jamming) signal levels over which it will provide adequate protection for data-modulated desired signals is typically found to be on the order of 20 to 30 dB. Achieving 50 to 60 dB protection using a single array of this type would appear to be highly unlikely in most cases, if not impossible.

B. CONCEPT OF THE CASCADED ADAPTIVE ARRAY

An adaptive array configuration which may be capable of achieving 50 to 60 dB, or more, of protection in a jamming environment was proposed by Huff [9]. A block diagram of this configuration, which has been designated the cascaded adaptive array, is given in Figure III-1. As shown in the figure (for a 3x3 fully implemented array), it consists basically of an M-element LMS array (with reference signal input $r(t)$) in which each element input is augmented by an N-element power inversion (PI) array. There are M actual antenna elements used, as for the

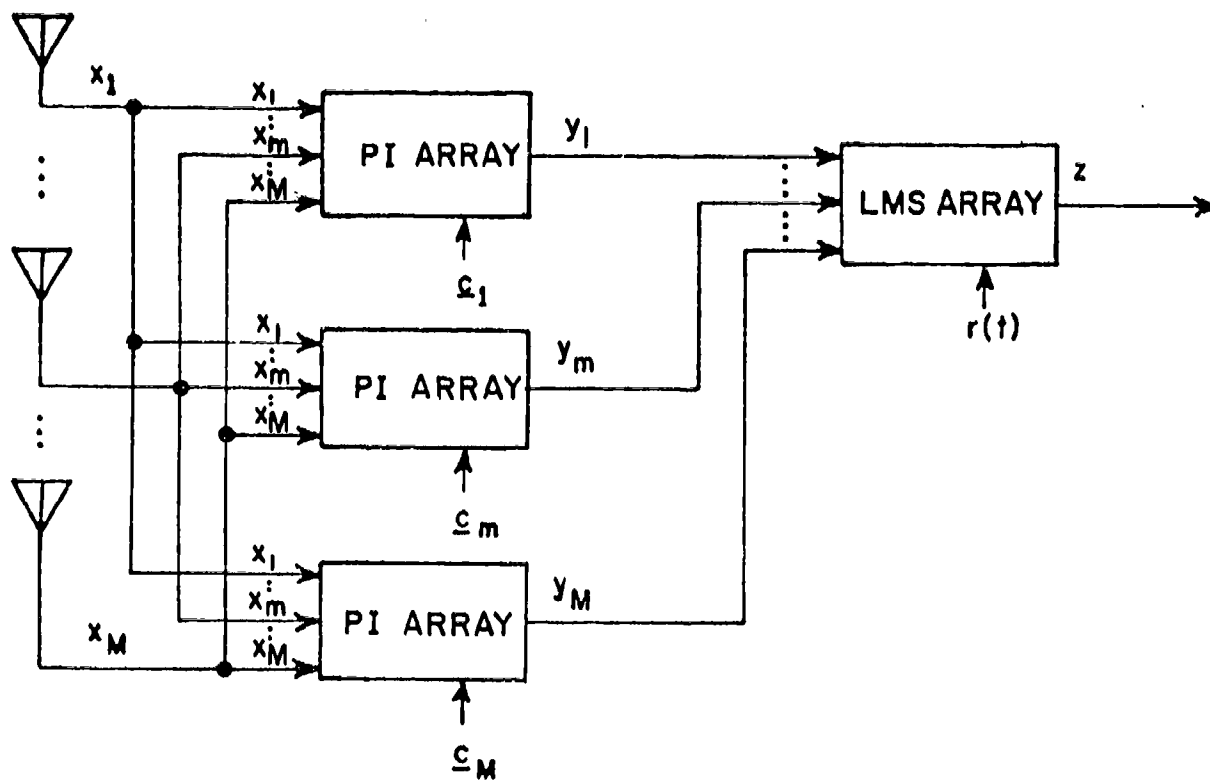


Figure III-1. Cascaded adaptive array configuration (3x3 fully implemented array).

conventional M-element LMS array. For the fully implemented array (i.e., $M=N$) each antenna element signal, x_m , is connected to each PI array, i.e., all of the PI arrays have identical inputs. The M PI array outputs, y_m , are then used as inputs for the LMS array, which weights and combines these signals to produce the array output, z .

In order for the LMS array to function properly, its inputs, y_m , must be linearly independent. For the fully implemented array (since all PI arrays are identical and have identical element signal inputs) this must be achieved by a suitable set of different steering vectors, c_m , which are applied to the PI arrays. In the case of a partially implemented cascaded array (i.e., $N < M$, as discussed more fully below) this independence may also be achieved, at least in part, by applying different combinations of element inputs to the various PI arrays.

The extended dynamic range capability of the cascaded array is achieved by choosing the threshold level for the PI arrays at the power level (normally jammer power level) above which the LMS array would fail. For power levels below this threshold, all signals are essentially ignored by the PI arrays and are handled by the LMS array in the conventional manner. If input power levels to the PI arrays exceed the threshold level, however, the PI arrays act to suppress the offending signal (or signals) below threshold (up to the suppression limit of the PI arrays, for sufficiently large inputs). Any significant residue is again suppressed by the LMS array.

It has been shown theoretically that, in steady state, the protection provided by the fully implemented cascaded array should be approximately double, in dB, that provided by the LMS array alone,

assuming that appropriate array parameters and steering vectors are chosen. In fact, the theoretical limit, R , as shown in Figure III-2, approaches the limit $2K+12$ dB for high performance arrays, where K is the dynamic range of the LMS array alone for a given application. In practice, somewhat less than this would be achievable due to circuit imperfections, some unavoidable overlap of the dynamic ranges of the LMS and PI arrays, and ultimately, difficulty in obtaining components of sufficient dynamic range with which to implement the loops. Protection on the order of 50 to 60 dB would appear to be realizable, however, using this approach.

Performance of the cascaded array configuration was studied by means of computer simulation to verify that steady state was indeed reached for typical array configurations and signal scenarios. No cases were found where problems with transient response were evident. For best performance, it appears that the transient response of the PI arrays should be made as rapid as possible, consistent with other requirements.

As is evident from the block diagram, Figure III-1, hardware requirements for fully implementing an M -element cascaded array could rapidly become prohibitive as M is increased. While a conventional M -element LMS array must contain a minimum of M vector control loops (often implemented as $2M$ scalar loops operating in phase quadrature, and with additional loops if tapped delay lines are used for broad-banding) the fully implemented cascaded array requires $M(M+1)$ vector control loops.

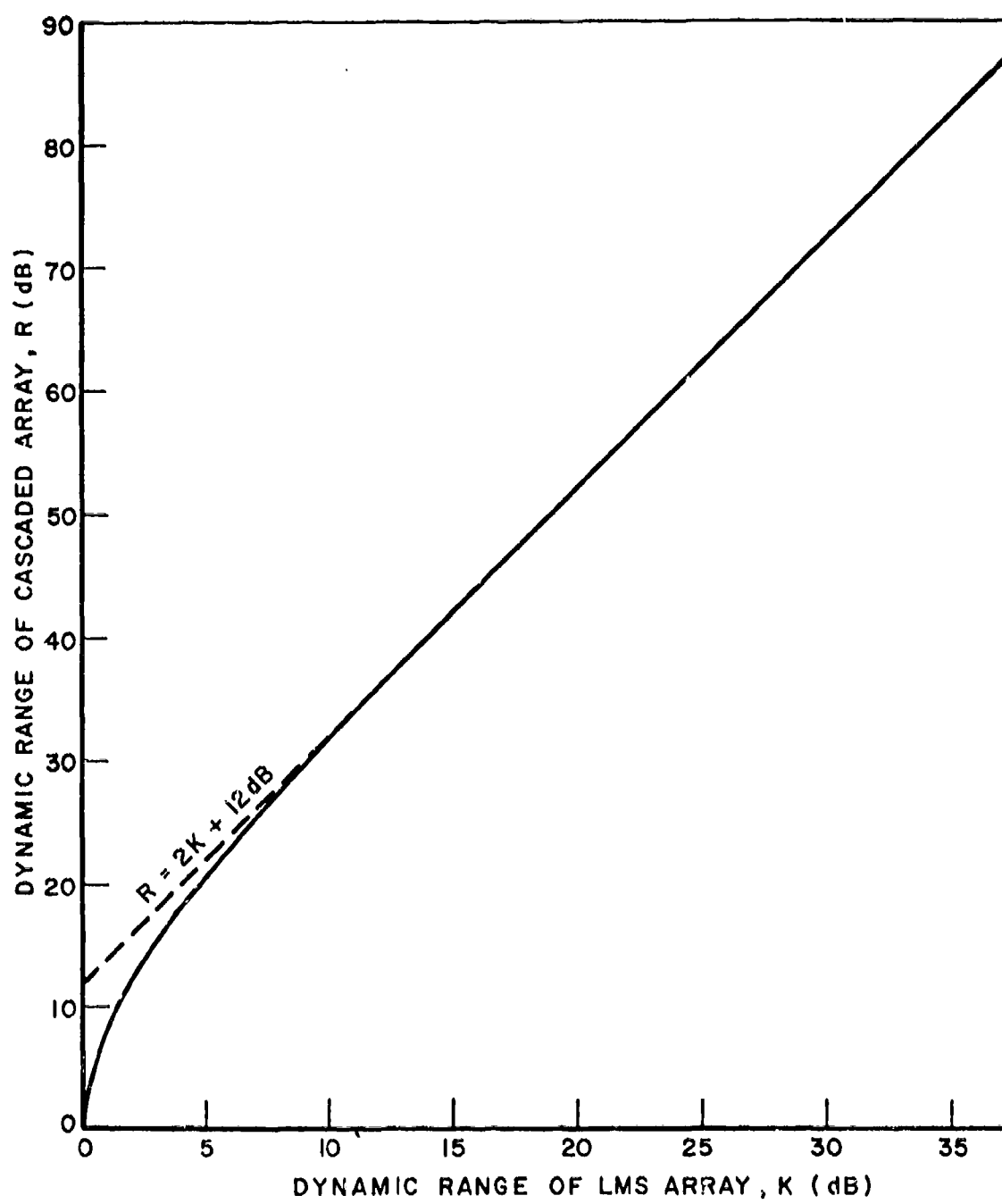


Figure III-2. Dynamic range of cascaded array (steady state solution).

Fortunately, it should seldom be necessary (or for that matter, even desirable) to fully implement an array in this manner. (The subject of partial implementation has been investigated separately [10] and is summarized in Section II of this report.) In general, it is only necessary to provide sufficient degrees of freedom in the PI arrays to handle the number of really big jamming signals expected; and considering the cost and difficulty of strategically locating and protecting such jammers, they would normally be expected to be rather few in number. In addition, such jammers may well be geographically localized with respect to a given operational scenario, and in this case further reductions in the number of PI control loops required might be realized by employing directional elements (or fixed sub-arrays) in the adaptive array configuration and supplying PI preprocessors only for those receiving signal power from the offending directions (i.e., a combination of the adaptive array and multiple beam array philosophies might be effective in certain scenarios).

Ultimately, a set of "control loop building blocks" might be considered which could be reconfigured as required, under processor control, to best meet a particular jamming threat using available resources.

C. EXPERIMENTAL CASCADED ARRAY

1. Configuration

The experimental cascaded array configuration, chosen to obtain the maximum useful information on cascaded array performance while minimizing hardware and construction costs, is given by the simplified

block diagram of Figure III-3. As shown in this figure, the cascaded array consists of a fully implemented 4-element LMS array augmented by 4 partially implemented 4-input PI arrays for which a total of 6 feedback controllers are currently available. These controllers may be used as desired to investigate various array configurations such as the 3x3 fully implemented array of Figure III-1, a 4x2 (MxN) symmetrical array, or the 4x(2,3,3,2) asymmetrical array of Figure III-3, provided that one direct "steering vector" input per array is used, as discussed below. Provisions for adding additional PI controllers at a later time, if desired, have also been included.

Theoretically, the basic cascaded array configuration of Figure III-3 is capable of simultaneously suppressing one large jamming signal and one or two medium jamming signals (two, if the residue of the large jammer remaining from the PI arrays is negligible) while placing a beam on the desired signal. Alternatively, if directional elements are used, the array could suppress two large jamming signals located in separate spatial directions while beaming on a desired signal of arbitrary location. How closely these theoretical limits can be approached in practice would depend on many things such as relative signal directions, element placement and desired signal and jammer bandwidths.

As indicated by the diagram, Figure III-3, one input to each PI array is hard-wired from an array element to the PI array summing junction and is not weighted by a feedback controller. The primary reason for this arrangement is the significant hardware savings thus achieved, with little loss in expected performance. These hard-wired inputs to the array perform the function of the steering vector applied

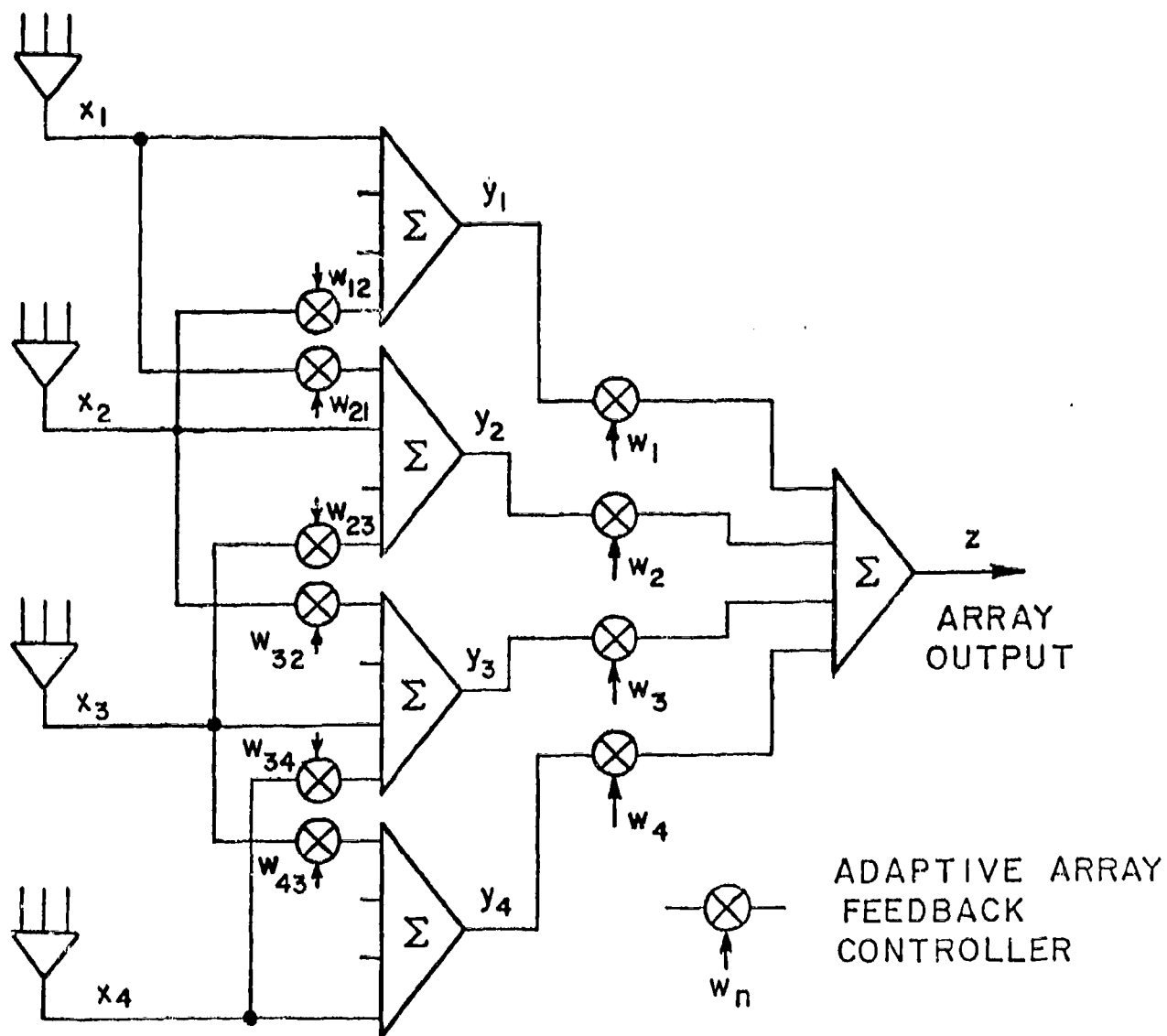


Figure III-3. Experimental 4x4 cascaded array configuration (partial implementation).

to a conventional PI array in that they prevent the array from shutting down in the absence of input signals (these inputs obviously cannot shut down --the controlled inputs do), and also provide a quiescent pattern which the array forms (in this case, an omni-directional pattern for each PI array) in the absence of input signals. Since a different element signal is hard-wired to each of the PI arrays, these "steering vector inputs" differ for each array so that the array outputs are linearly independent, and thus suitable as inputs for the LMS array.

Performance of a PI array configured in this manner is similar, although not identical, to a conventional adaptive array with a corresponding steering vector input. This array is somewhat more constrained in that it is not free to adjust overall signal level (relative to background noise, for example) but can only adjust the amplitudes and relative phases of coherent output signals by performing the vector addition of one or more controlled vector inputs with the fixed signal vector resulting from the hard-wired input.

2. Implementation

Several design goals were considered in the design of feedback controllers for implementing the cascaded array, particularly since a practical operational array may require a relatively large number of these controllers. These goals are: low cost, minimum complexity, reliability, component availability, performance, and standardization.

Most previous arrays have been constructed using some form of baseband (scalar) weighting applied to quadrature components of the input signal. Such an implementation has been found to work well when

carefully designed, constructed, and aligned; however, common shortcomings include dc offsets, signal leakage and feedthrough (at the multipliers, in particular) and alignment drift with temperature changes and component aging. Also, particularly significant for this application, $2N$ scalar loops are required to implement an N -loop array. In addition, suitable multipliers, for weighting and for correlation are in general difficult to construct and align, "temperamental", and expensive. Consequently, alternative approaches were considered.

In theory, an adaptive array feedback controller operating at a suitable I-F frequency can be implemented as shown in Figure III-4. Both correlator and weighting multiplier carry both phase and magnitude information so that only a single loop of this type is required to implement a vector controller, rather than two loops as required by a baseband system with quadrature signal processing. In addition, dc offset problems are completely eliminated since there are no dc or baseband signals anywhere in the loop, and leakage and feedthrough at the correlator and weighting multiplier are readily controlled via suitable filtering since a frequency translation occurs across these multipliers. Note that the loop configuration appears identical to a typical scalar baseband loop except that a bandpass filter replaces the integrator of the baseband loop. Consequently, hardware requirements for implementing an array using this technique would effectively be reduced by one half.

It can be shown theoretically that performance of this loop is identical with that of the two-loop scalar baseband processor provided that ideal components are assumed and that a single (proper) sideband

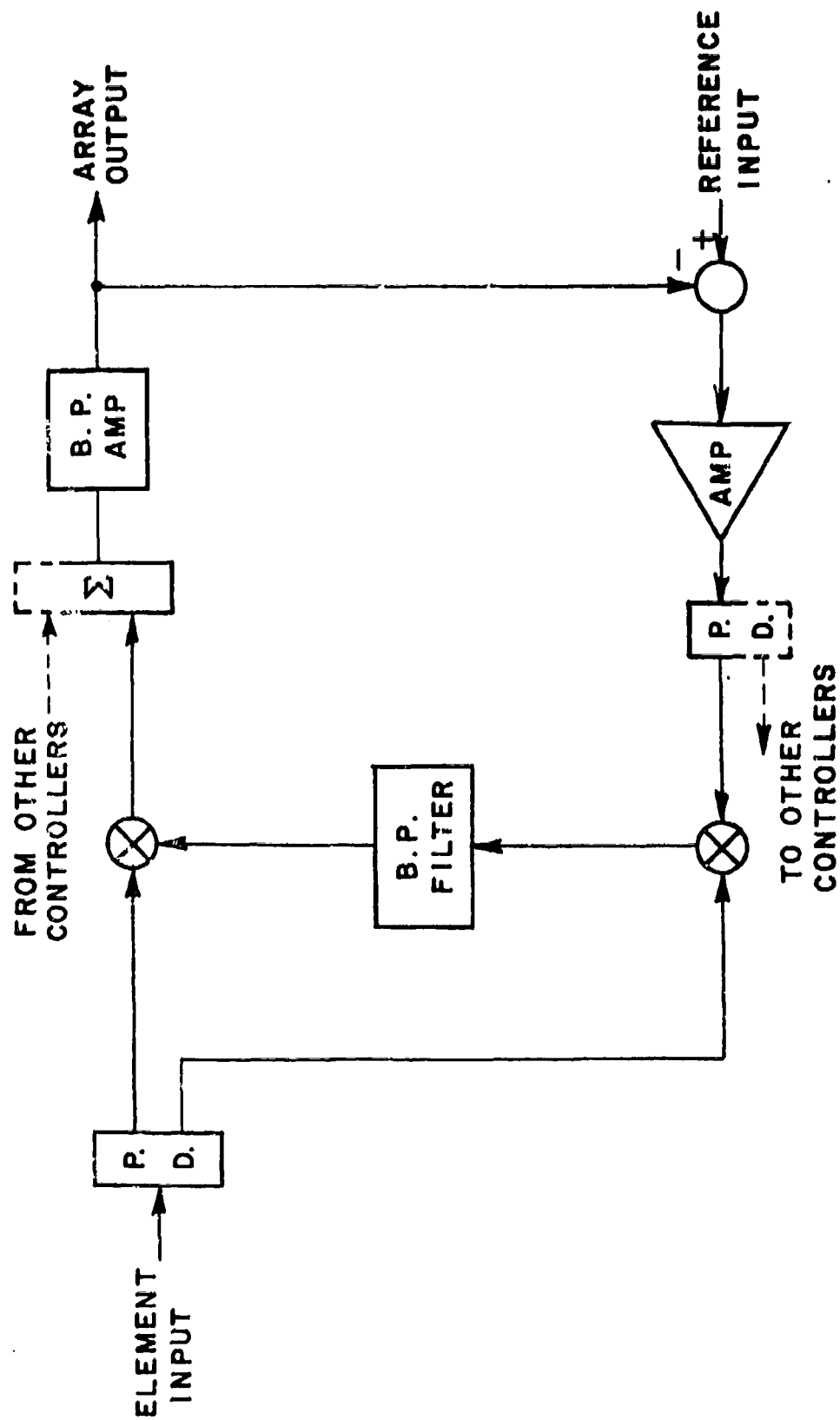


Figure III-4. Self-excited I-F adaptive array feedback controller.

is retained following each multiplier. In practice, however, two difficulties may arise. The first is that both sidebands are produced by the multipliers (plus, in general, other higher order cross products). At the correlation multiplier this is not a serious problem since the bandpass filter (counterpart of the baseband integrator) can effectively eliminate the unwanted sideband and cross-products. Following the weighting multiplier, however, both sidebands are present. In an ideal circuit having no group delay, both might be retained and utilized; but in a practical circuit it will not be possible to obtain the proper phase relationships around the loop for two widely differing frequencies over a finite bandwidth. Hence, one must be eliminated.

At least two potential methods exist for eliminating the unwanted sideband. First, a single-sideband mixer could be used to replace the conventional weighting multiplier. But this approach would reintroduce much of the circuit complexity we had hoped to eliminate. Also, performance specifications for currently available single-sideband mixers leave much to be desired. The second method is by means of a suitable bandpass filter. Extra poles in the loop transfer function introduced by this filter, and the resulting significant increase in group delay, can lead to instability problems, however. The I-F loop with this filter included (or with more than one pole-pair in the "integration" filter) is not unconditionally stable, as is the baseband loop. In practice, the potential stability problems introduced by this filter are manageable provided that the reference signal (if used) is suitably constrained (as, for example, through the use of a bootstrap

reference system) and that a filter having "compensating" poles is added to the element signal input branch to the correlator. This method is used successfully in the current experimental cascaded array.

The problem of imperfect components, in particular, lack of an adequate bandpass filter to replace the baseband integrator, is more difficult. Computer simulations have shown that for proper operation in an LMS array, a filter Q on the order of 10^6 would be required in a typical application. This is at least two orders of magnitude greater than could (hopefully) be obtained in any form of analog filter. Crystal filters perhaps come closest. Maximum Q for a practical crystal filter is on the order of 10^4 , but additional problems exist. The center frequency is generally limited to about 100 MHz or less (I-F frequency of the current array is 410 MHz); and for reasonable passband characteristics, considerably more than the desired one pole-pair (see above) is needed in constructing the filter. SAW filters have been constructed in the frequency range of interest which exhibit very high Q passband characteristics. These filters have extremely large group delay characteristics however, which, because of matching and stability problems, would appear to preclude their use in this application.

Two experimental I-F feedback loops were constructed using 2-section cavity filters ($Q=410$) to further investigate the behavior of these loops implemented with imperfect integration filters. As should be expected (particularly when aided by hindsight), it was discovered that: 1) a single loop, and also a 2-loop array, operate well relative to a single input signal, i.e., a jamming signal (no reference input) is suppressed; or a desired signal is made to track the reference signal

over a significant range of amplitude and phase variations, and

2) the loops will not operate independently, they always both produce essentially the same weighting vectors in a given signal environment. Consequently, it is not possible, for example, to simultaneously null a jamming signal while receiving a desired signal, even when a third (hard-wired) channel is added to the array to gain an extra degree of freedom.

A cursory analysis of the multiple-loop LMS array circuit reveals that the various loops can produce independent weighting vectors only by virtue of the storage capability of the integrator (i.e., charge storage in the case of the baseband integrator, and filter "ringing" in the case of the I-F counterpart). Hence, if this storage capability (filter Q) is too low, a multiple loop array will perform little better than a single loop array.

The fact that storage is the lacking component in this type of I-F feedback loop suggests that partial digitization of the loop, with digital storage supplied at this point, might be a very practical method of adapting this basic loop for practical applications. Because of time and funds limitations, this digital approach was not investigated further under the current contract, but is strongly recommended for future research. For a conventional PI array, a "leaky" integrator (i.e., a lowpass filter) is employed rather than a true integrator. Also, the steady state error signal is non-zero, and independence between steady state weights in the various loops is provided, at least in part, by a suitable steering vector. Consequently, the I-F loop in analog form may be more directly applicable to this type array. This possibility should also be further explored.

In order to construct an experimental array, within current contractual constraints, to verify the concept of the cascaded array while concurrently investigating some of the relative merits of the I-F feedback loop, the circuit shown in Figure III-5 was chosen for implementing the array controllers. This circuit is functionally identical to the basic I-F loop of Figure III-4 except that the integrating band pass filter is replaced by quadrature baseband integrators, with conversion from the I-F frequency to baseband prior to the integrators, and back again to I-F following the integrators. The single vector weighting multiplier and vector correlation multiplier of the basic I-F loops are retained, with frequency translation across the multipliers to alleviate feedthrough and leakage problems, and with bandpass filtering to remove the extra sideband. A compensating band pass filter (between the input power divider and correlator) has also been added for stability, as discussed above. Unfortunately, this conversion to baseband, and reversion to I-F, effectively eliminates the savings in hardware which could otherwise be realized, and also re-introduces the possibility of problems due to dc offsets. However, it does permit many aspects of the I-F control loop to be experimentally investigated, and provides the possibility for retro-fitting, following further development, to regain some of the advantages lost due to the current I-F to baseband conversion.

The configuration shown by the block diagram of Figure III-5 is used specifically for the LMS portion of the cascaded array. The PI array configuration is identical except that input and output frequencies (250 MHz and 160 MHz) are reversed, and no reference input

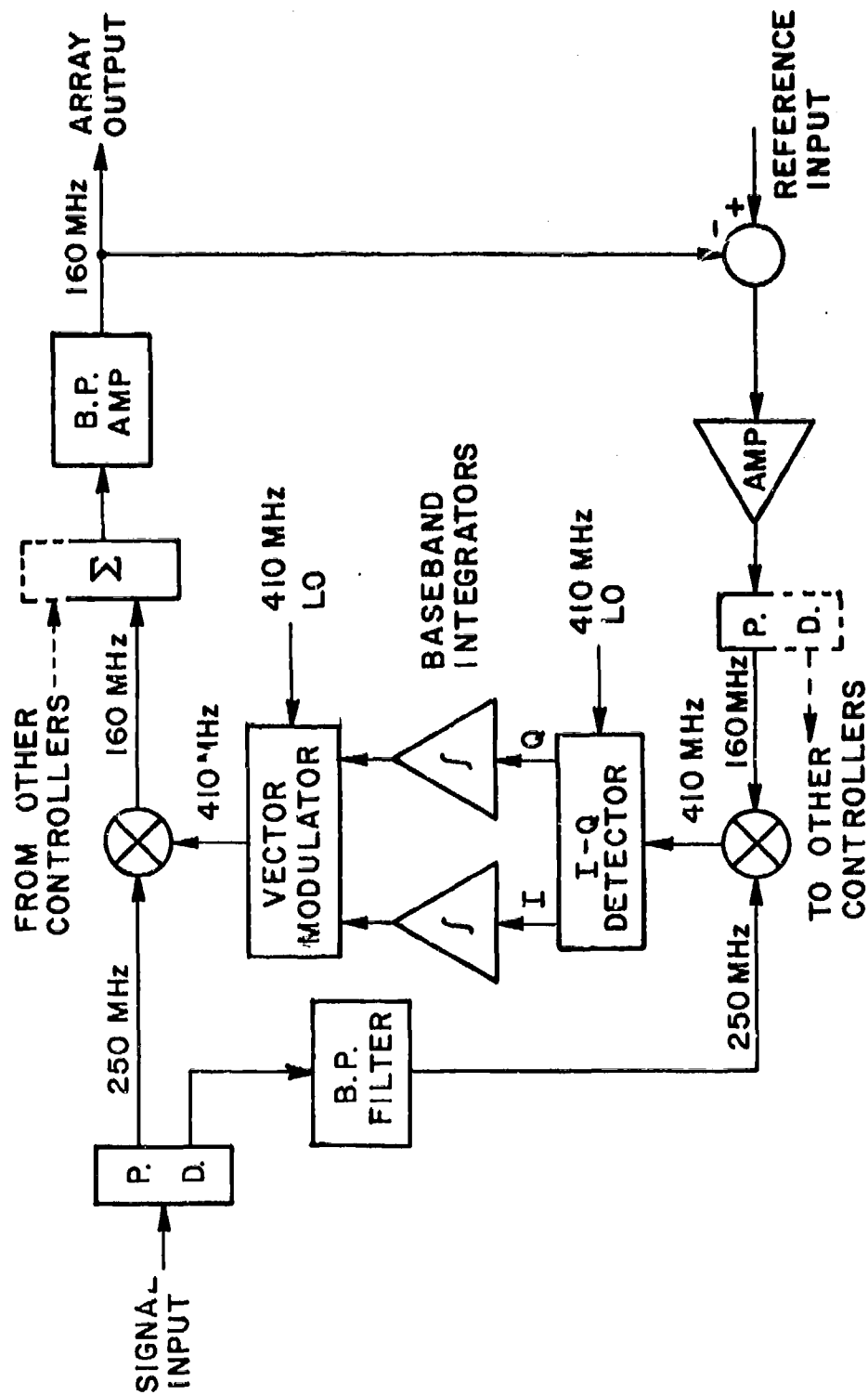


Figure III-5. I-F weighted adaptive array controller with baseband integrators.

is used. All array controllers, PI and LMS, are identical. Array circuitry external to the controllers differs primarily relative to the frequencies and bandwidths of the various filters used and in relative signal levels and loop gain.

3. Multipliers

As the frequencies and bandwidths for adaptive array applications are increased, and as more and more controllers are needed to fulfill operating requirements, the problem of availability, cost, and reliability of suitable multipliers for signal weighting and correlation becomes increasingly severe. Consequently, a certain amount of effort under the current contract has been devoted to investigating alternatives for the multipliers previously used. One such effort is the continuing development of microcircuit transconductance multipliers as discussed elsewhere in this report (see Section IV). Another, is an investigation of the use of passive double-balanced mixers which is discussed here.

The primary motivation for the use of passive double-balanced mixers as multiplying elements of an adaptive array is that they are inexpensive, reliable, stable, and readily available for nearly any frequency range (and bandwidth) of interest. And they are, after all, basically multiplying devices.

A primary limitation for use as a 4-quadrant multiplier is that, for proper signal multiplication to occur, at least one input signal must be relatively large and relatively constant. The local oscillator (LO) fulfills this requirement in normal mixer applications. This

requirement is very evident from the typical mixer characteristic curves of Figure III-6. From these curves, it is apparent that if one signal (in this case the 30 MHz signal) is held constant somewhere in the range of +5 to +15 dBm that the mixer output (at 70 MHz) remains essentially proportional to the lower level (100 MHz) signal input over at least a 70 dB dynamic range; i.e., the circuit operates properly as a multiplier under these conditions. If, however, the higher level signal (30 MHz) is varied while maintaining the lower level (100 MHz) signal constant, the output does not vary proportionally. In fact, if the largest input signal (30 MHz) is reduced much below about 5 dBm, the device completely fails to function as a multiplier.

Realizing that proper mixer performance is obtained by utilizing the larger input signal for reliable, symmetrical switching of the mixer diodes, the possibility of multiplying two lower level signals in the presence of a third, high-level "pump" signal introduced just for this purpose appears reasonable. In fact, it works; as shown by the pumped mixer multiplier characteristics of Figure III-7. To obtain these curves, a 250 MHz signal (applied to the mixer LO port) was multiplied by a 410 MHz signal (applied to the RF port) to produce an output product (IF) at 160 MHz. A 765 MHz pump signal at +7 dBm was used, added to the RF input via a matched summing junction. The output signal remained essentially proportional to the product of the two input signals over a dynamic range of at least 70 dB for one input signal (410 MHz) and 50 dB for the other (250 MHz).

There are, of course, other high level signals present in the output (essentially all combinations of the two signal inputs and the

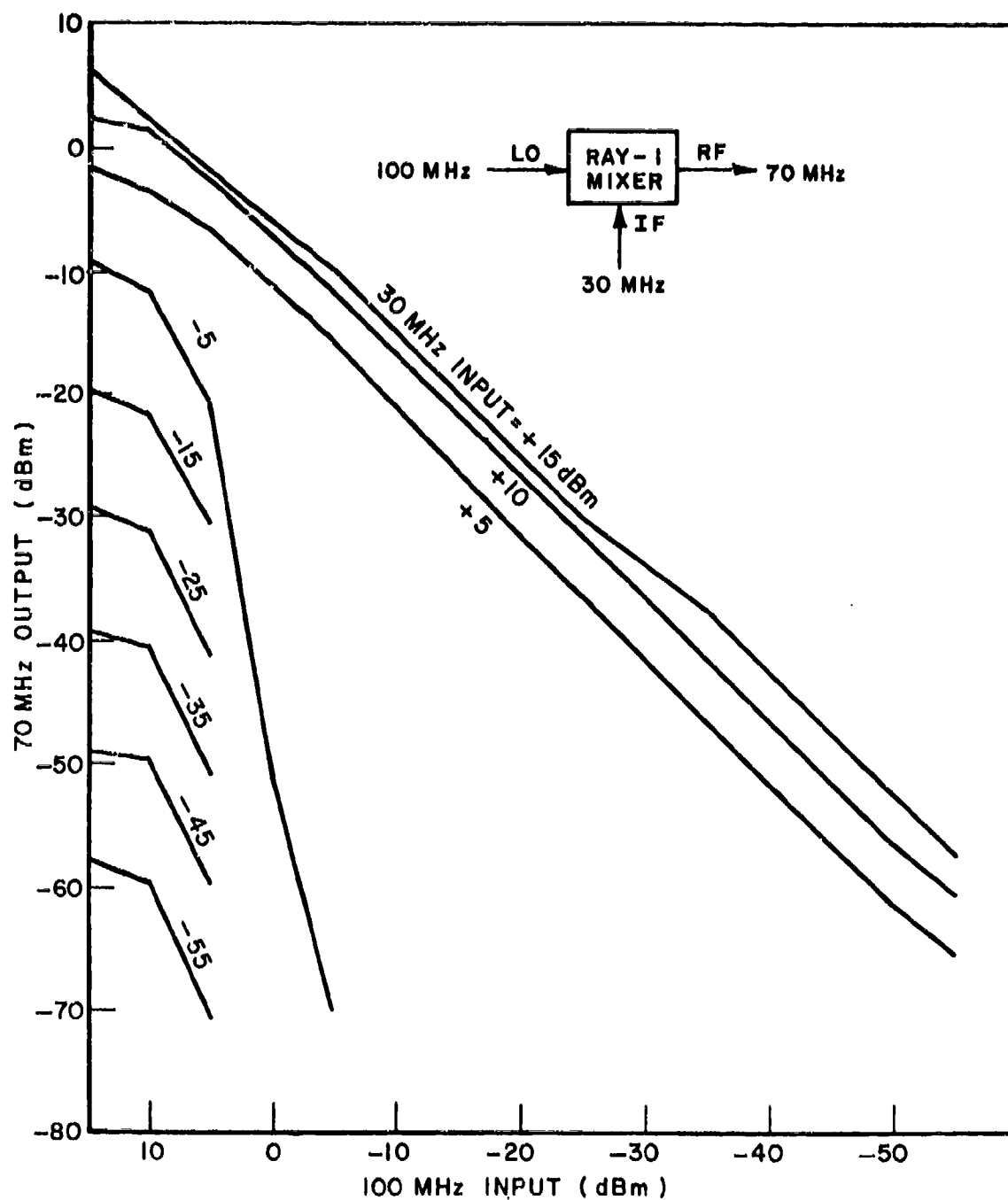


Figure III-6. Passive mixer multiplier characteristics.

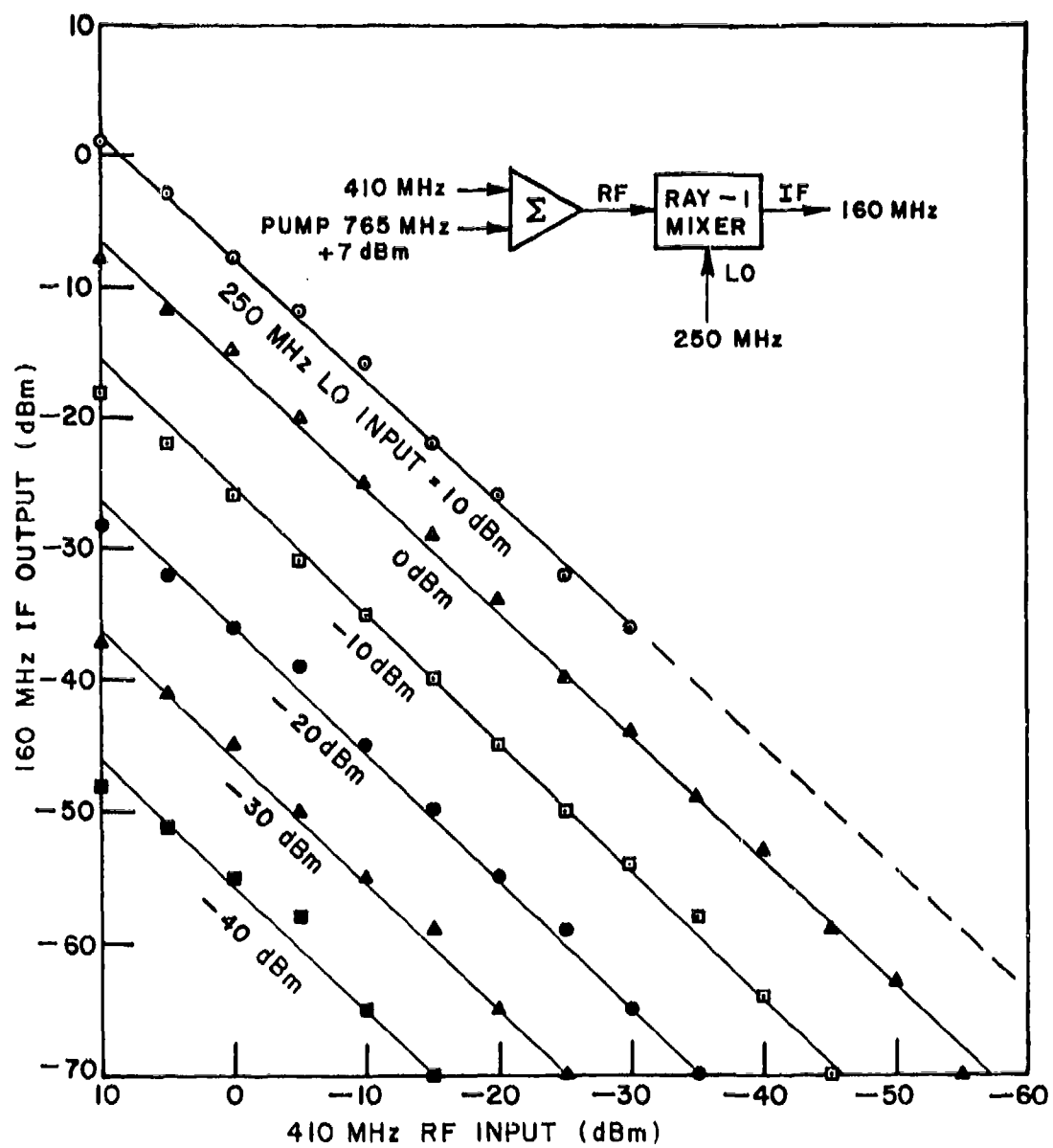


Figure III-7. Pumped mixer multiplier characteristics.

pump) in addition to the desired output product. These must be properly considered, and dealt with, in any potential application of the pumped multiplier circuit. Problems with extraneous signals can be minimized (as with any superhetrodyne circuit) by proper choice of the pump frequency so that spurious signals can be filtered out with minimum degradation of the desired circuit function. In general, the pump frequency should be significantly higher than the signal frequencies to be multiplied, but it must be low enough for proper operation with the mixer used, and the associated circuitry. Pump power level is also somewhat critical. It should be at least comparable to the highest input signal levels to be multiplied, but if too high, causes a degradation of performance; possibly due to saturation of mixer components (i.e., transformers). In practice, the optimum pump power level is typically less than the recommended LO input power level for the mixer used. For the example of Figure III-7, the recommended LO power level for the mixer used is +23 dBm while a pump level of +7 dBm was found to be nearly optimum.

Passive double-balanced mixer multipliers are used in the current experimental cascaded array as both weighting and correlation multipliers. They can be operated in either the pumped, or unpumped, mode as desired and/or as signal conditions require. If a high level input signal is present, as in the case of a large cw jamming signal, this signal alone is sufficient to obtain proper multiplying action from the mixer-multipliers and the pump signals can be turned off with little or no degradation of array performance. An AGC system is incorporated in the array which automatically adjusts the peak value of

such signals coincident with the upper limit of the array dynamic range, thus extending the usefulness of this operating mode over a considerable range of input signal levels. In the absence of a suitable input signal for switching the mixer diodes, as for example, when a broadband jamming signal is used, the pump signals must be used, otherwise severe degradation of array performance occurs.

4. Circuit Description and Diagrams

Circuit diagrams of the experimental cascaded array are presented, as a unit, in Appendix A for convenience and ready reference. Brief descriptions and explanations of circuit operation relative to these diagrams are given in this section. Figures A1 through A6 (see Appendix A) are detailed block diagrams of major sections of the array, each contained on a separate chassis. In general, the array is constructed of commercial components, as specified on the diagrams. For specialized components, further details are given by separate schematic diagrams (Figures A7-A14). Signal connections within each major array section are by semi-rigid coaxial cable (SMA interface), for excellent shielding and circuit stability; while interconnections between sections are by teflon-insulated double-shielded flexible coaxial cable.

Basically, the array operates at an I-F frequency of 160 MHz (input and output frequencies) with a signal bandwidth of 40 MHz. Internal to the array, the signal paths are converted to 250 MHz by the PI array weighting multipliers, and back again to 160 MHz by the LMS array weighting multipliers. Portions of the feedback control loops between the correlation multipliers and weighting multipliers operate at an I-F

frequency of 410 MHz, with integration performed at baseband. At the input and output of the array, conversion to/from 70 MHz has also been provided so that the array could be tested using the available OSU/RADC TDMA modems and the TDMA timing and bootstrap reference system of the satellite simulator adaptive spatial processor which operates at this frequency. When operated at 70 MHz in this manner, the maximum useful signal bandwidth of the array is reduced to approximately 15 MHz.

Figure A1 is a detailed block diagram of the converter and I-F amplifier section of the array. This section contains four identical parallel signal paths, one for each of the array element signal inputs. A mixer, LO input, and bandpass filter is first provided in each signal path for conversion from 70 MHz to the array input frequency of 160 MHz to permit testing with the TDMA modems, as mentioned above. If the array is to be used at 160 MHz, these converters should be disconnected and the element input signals should be applied directly to the IF amplifier inputs or to the bandpass filters if restriction of the input signal bandwidth is considered desirable (as, for example, to prevent overloading of the I-F amplifiers by out-of-band signals which may be present). Separate 160 MHz input ports (which could be provided via summing junctions) were not included in the array since this would increase the input noise figure.

The 4 I-F amplifiers (RHG ICEMT 160/40) are standard commercial units gain and phase matched to ± 1 dB and $\pm 5^\circ$ over a 50 dB gain control range. Maximum gain is 60 dB and maximum power output is +13 dBm. An AGC driver operating from the video output of the channel 1 amplifier sets the gain of all I-F amplifiers to achieve a given

maximum signal amplitude at the output, for pulsed, as well as for cw signals. Manual gain control is also provided and can be used instead of AGC, if desired. Each I-F amplifier is followed by a power amplifier and a 4-way power divider which provides signals for the 4 PI arrays which follow. Power level at each output of these power dividers is normally on the order of + 10 dBm. Connections to the PI array inputs are made via flexible double-shielded coaxial cables to facilitate connecting various array configurations, as desired.

The power inversion (PI) controller section of the array is shown by Figure A2. This section contains the input, converter, and feedback processor portions of the 4 PI arrays which make up the power inversion preprocessor section of the cascaded array. The configuration shown is for the basic $4 \times (2,3,3,2)$ configuration (see Section III-C-1, and Figure III-3). Hence, each of the 4 arrays contains either 2 or 3 signal paths.

One signal path for each array is hard-wired (i.e., does not include a feedback controller) to serve as a steering vector input as discussed previously. Since there is a frequency conversion (from 160 MHz to 250 MHz) performed by the weighting multipliers of the PI controllers, in order for these fixed signals to be summed at the array output, they too must be similarly converted. This is accomplished by means of a high-level mixer (with appropriate LO input) in each of these paths. A manually controlled attenuator (ARM-1) is also included in each path for optimizing the power level of each direct channel relative to the weighted outputs.

Each weighted signal channel contains a power divider (PDM 20-250) to provide signals for both the signal input branch and correlator input branch of the PI processor. The signal input is connected directly to the PI processor while the correlator input first passes through a bandpass filter and a delay line. This bandpass filter is the compensating filter discussed earlier in section (III-C-2). It, together with the delay line which is included to permit customized trimming to compensate for filter and/or circuit mismatch, is chosen to equalize the group delay in the element signal branch to the correlator relative to that in the error signal branch. This is necessary in order that the proper phase relationship (and hence loop stability) can be maintained at the correlator over a broad frequency band.

The PI processors (feedback controllers) which are shown by a separate diagram (Figure A7), also receive an error signal input from the corresponding PI feedback loop (see below) as well as pump and local oscillator inputs. Pump and local oscillator distribution circuits are also included in this section of the array as shown in Figure A2, as well as the 410 MHz crystal oscillator and associated amplifier which supplies the LO signal for converting the 410 MHz I-F signals to baseband, and back again to I-F (see Figure A7).

As for the input signals, the signal output and error input connections to the following section of the array are made via flexible coaxial cables, so that the array configuration can readily be changed, if desired.

The remaining circuits of the PI arrays are contained in the next major section of the array, the power inversion feedback loops, as shown

by Figure A3. This section contains 4 identical circuits, one for each of the PI arrays. Each circuit contains a 4-input summing junction, which performs vector addition of the signals from the corresponding array signal paths, followed by a bandpass filter to eliminate the unwanted sideband (and other spurious signals which may be present) created by the mixers and frequency-translating weighting multipliers. The desired sideband signal then passes through an adjustable attenuator (for loop gain control) and a high-gain amplifier. A power divider then provides signals for a front panel test jack, a PI array output signal to be used as input for the LMS section of the cascaded array, and an error signal for the feedback controllers. The error signal branch contains an adjustable phase shifter (PSM3-250) for setting error signal phase for proper negative feedback, an additional amplifier for increasing the error signal power to that required by the feedback controllers, and a 4-way power divider to distribute the error signal to the associated PI array controllers. In the present configuration only 1 or 2 of these outputs are used, however, up to 4 could be required for a fully implemented array.

The LMS controllers for the cascaded array are shown in Figure A4. This section of the array is similar to the power inversion controllers section described above (Figure A2) except that there is only one LMS array and this array is fully implemented, having 4 identical weighted signal channels, and no direct (hard-wired) inputs. Input signals for this array are the output signals from the four PI arrays, applied via flexible input cables. Configuration and operation of each signal channel is the same as that described earlier except that input and output frequencies are reversed; i.e., the input signals at 250 MHz,

are converted to 160 MHz by the frequency-translating weighting multipliers contained in the LMS processors. The LMS processors are physically identical to the PI processors and are shown in more detail in Figure A7. Since there is no reason to change the configuration of this array, the signal summing junction and error distribution power divider are also included in this section of the array and are connected to the LMS processors by semi-rigid cable.

The cascaded array LMS feedback loop and output/reference converters are shown in Figure A5. The single LMS feedback loop is similar to the PI feedback loops described earlier (Figure A3) except that an error junction (HJM-110) and associated reference signal input circuitry are provided. This reference junction performs the vector subtraction of the array output signal from the reference signal input, as required for the LMS algorithm. Test jacks for examining these signals for test and alignment purposes are also provided, and are phase matched relative to the error junction output so that a phase comparison of signals made at these ports will accurately represent signals at the error junction. An error test output jack is also provided for examining the resultant error signal (following amplification, since this signal, at the error junction, is normally a very low level signal).

A mixer, bandpass filter, and output power divider are provided to convert the 160 MHz array output to 70 MHz for array testing with the TDMA modems when desired, as mentioned previously. A similar mixer and bandpass filter permits conversion of a 70 MHz reference input (as obtained from the satellite simulator adaptive spatial processor

bootstrap reference system) to 160 MHz for use by the array. A separate reference input for use at 160 MHz is also provided. The 230 MHz crystal oscillator with associated LO distribution circuitry used for frequency conversion between 70 and 160 MHz is included in this section of the array, and is also connected to the input converter section (Figure A1) via a double-shielded flexible coaxial cable. A switch is provided for turning off this oscillator, when not needed, to eliminate the possibility of introducing spurious signals.

Figure A6 shows the pump oscillators and amplifiers used to pump the passive mixer multipliers used in the feedback controllers as discussed earlier (section III-C-3). Separate oscillator circuits are provided for use with the PI arrays and with the LMS array. Each circuit is tunable in frequency over a range of approximately 500 to 1000 MHz, so that an optimum pump frequency for each type of array can be selected. Pump amplitude can be varied, as required, by proper choice of the fixed attenuator pads used between the pump oscillators and amplifiers. A switch is also provided for turning off the pump oscillators, if desired, for testing, or for operation in the presence of a cw jamming signal for which use of the pumps is not needed (see section III-C-3).

A detailed block diagram of the cascaded array feedback controller, used in both the PI and LMS arrays, is given in Figure A7. This controller is basically the I-F vector implementation, discussed previously in section III-C-2, with integration performed at baseband. Except for the baseband integrators (shown separately by the schematic diagram, Figure A8) it is constructed of commercial components mounted

on microstrip. High-level passive double-balanced mixers (RAY-1) are used as multipliers with provisions for pumping so that proper operation can be obtained when only low level input signals are present. The upper (RAY-1) mixer in Figure A7 is the weighting multiplier while the lower one is the correlation multiplier. The internal I-F frequency, 410 MHz, generated by the correlation multiplier is converted to quadrature baseband signals for integration by the I-Q detector, with associated LO input. After integration the signals are reconverted to I-F by the vector modulator, amplified, and applied as an I-F weight input to the weighting multiplier.

A schematic diagram of the baseband integrators is given in Figure A8 and of the associated weight control and mode switching circuitry in Figure A9. There are two identical baseband integrators in each feedback controller, one for the in-phase (I) and the other for the quadrature (Q) signal component. During normal operation (ADAPT mode), each integrator (CA 3140) of Figure A8 receives an input signal (I or Q) from the I-Q detector. However, by means of the digitally controlled analog switches (DG 211) the integrator input can be connected to ground (ZERO mode), primarily for alignment purposes; or the output can be preset to an initial value applied via the initial weight input. This permits setting the weights to a desired, fixed value (RESET mode) for array testing, and could also be used for implementing weight storage and recall (applicable to TDMA systems) at a later time, if desired. If all switches are turned off (HOLD mode), the integrator holds the current value of output signal for periods up to several minutes or more.

Since the preset circuit is of low impedance (i.e., a short time constant) to permit rapid presetting of the weights (as required for implementing weight storage and recall), the differential driver (2N3904 and 2N3906) has been added to increase the available integrator output power. Although this driver employs no biasing circuitry, no "dead zone" results in the steady state output. When the output of the CA3140 becomes such that both transistors are cut off, the feedback circuit is effectively opened, the gain suddenly becomes extremely high, and the CA3140 output rapidly changes to the value required to cause one of the transistors to conduct, again closing the feedback circuit. Hence, at worst, there may be a small glitch (delay) in the transient response, but not in the steady state output.

The weight control and mode switching circuitry is shown in Figure A9. Two such circuits are used; one for the LMS array and the other for all PI array controllers, in parallel. The two circuits are identical except that for the LMS array only 4 pairs of initial weight potentiometers and 4 channels of the weight metering circuitry have been implemented since only 4 feedback controllers are used in this array. In addition to the ZERO, RESET, ADAPT, and HOLD modes discussed above, an additional AUTO mode is available via the mode selector switch. In this mode, external logic signals (TTL logic levels) can be applied for automatically selecting the adapt, reset, or hold modes, as desired. This may be used, for example, in TDMA applications where it is desired to preset the weights prior to a new data slot and/or hold the weights during a portion of each data bit to compensate for propagation delay through a bootstrap reference system.

Figures A10 and A11 show the cascaded adaptive array I-F amplifier gain control and power wiring, and the power distribution cables, respectively. These diagrams are essentially self-explanatory.

Diagrams of the cascaded array power supply and regulator circuit board (part of the power supply) are given in Figures A12 and A13. This power supply is constructed using 4 commercial modular power units furnishing regulated dc voltages of +28, +15, -15, and +5 volts. Additional outputs of +24, +12, and -12 volts are obtained from these by means of auxiliary regulator circuits mounted on the regulator circuit board. The power supply unit also contains fuses, indicators, voltage test points and adjustment controls, and circuits for the array cooling fans and for primary AC power control.

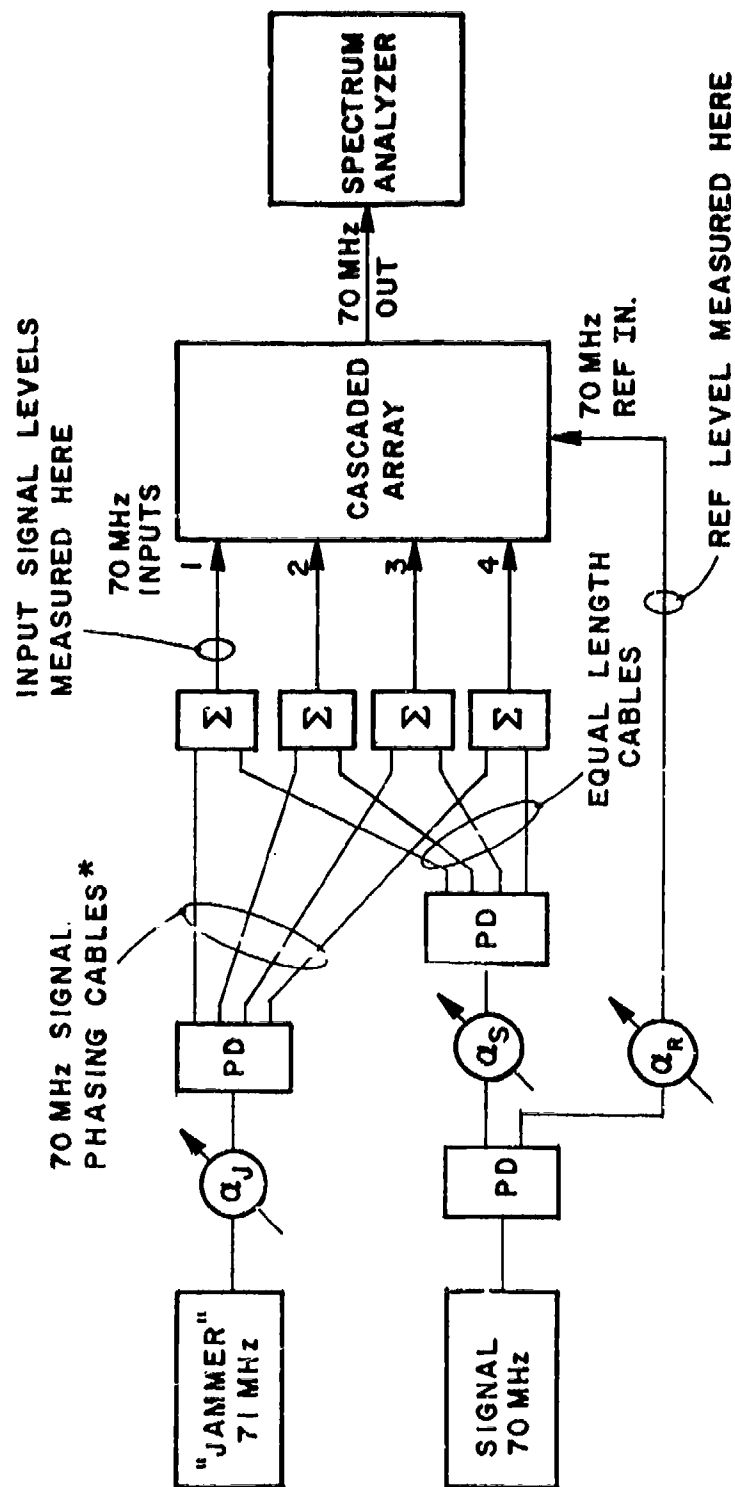
To facilitate cascaded array testing using the TDMA modems together with a suitable jamming signal the adaptive array element signal simulator of Figure A14 is used. The desired signal input is divided into 4 equal, in-phase components for application to the 4 array inputs, thus representing a signal incident broadside to a 4-element linear array. Uncorrelated noise may be added to these signal inputs to establish a given input signal to noise ratio, as desired. The jammer signal first passes through a pair of step attenuators which permit varying the jammer level in 1 dB steps over a 120 dB range. The signal is then divided into 4 paths, each path containing an adjustable phase shifter which may be set to simulate a desired angle of arrival of the jammer relative to the desired signal. These signals are then summed with the desired signals for application to the cascaded array element inputs.

A relatively large number of amplifiers having various specifications are required in the implementation of the cascaded array. To achieve a certain degree of standardization while at the same time providing the versatility needed for an experimental array, most of these were assembled from modular cascadable units utilizing standard circuit boards and cases. The components used for these amplifiers, together with the resultant amplifier specifications, are listed in Table A1 of Appendix A.

D. ARRAY PERFORMANCE AND RESULTS

1. Tests Using CW Signals

Initial tests of the cascaded array were performed using cw signals to represent both desired and jammer signal inputs. These tests were conducted using the equipment configuration shown in Figure III-8. A 70 MHz cw signal, representing a desired signal, was applied via an attenuator and power divider to the 4 array element inputs as shown. These signals are equal, and in-phase at the array inputs, representative of a signal arriving broadside to a linear array. A portion of this 70 MHz signal is also applied, via another attenuator, to the cascaded array (LMS section) reference signal input. A 71 MHz signal representing a jamming signal is similarly applied to the 4 array inputs, except that in this case, phasing cables which increase incrementally by approximately 58 electrical degrees each, from inputs 1 through 4, are used, so that this signal appears to arrive from a different spatial angle than the desired signal.



* PHASING CABLE LENGTHS INCREASE INCREMENTALLY BY APPROXIMATELY 58° AT 70 MHz, FROM #1 TO #4.

Figure III-8. Configuration for cw testing of the cascaded adaptive array.

Typical results obtained from these tests are given in Figure III-9. These curves show array output Signal to Jammer Ratio (S/J) as a function of Input (per element) Jammer to Signal Ratio for the cascaded array in several operating modes. The curve labelled "Cascaded Array" was obtained with the array fully operational. Those labelled "LMS Array" and "P.I. Array" were obtained with only the corresponding section of the cascade operational and the other part of the array reset. An additional curve, labelled "Arrays Reset", taken with all array control loops reset, is included in the figure as a basis for determining array performance. For this test series, in the reset mode, the control loops were set to a fixed value (approximating unity gain). Note that for an input J/S of 0 dB an output S/J of approximately 6 dB is obtained in the reset mode. This is due to arraying of the 4 elements. For later tests (see the following sections), an omni-directional pattern (single element on - others off) has been used for the reset mode; hence, if performance comparisons are made, this difference should be noted.

If an output S/J of 0 dB, or greater, is chosen as a performance criterion, then from the curves of Figure III-9 the cascaded array provides approximately 51 dB of Jammer protection relative to the fixed reset mode array pattern, while the LMS array alone provides approximately 32 dB protection. The PI arrays alone provide no significant protection for an output S/J threshold of 0 dB; however they do provide approximately 30 dB or more of protection if an output S/J of -14 dB or less can be used (as, for example if sufficient processing

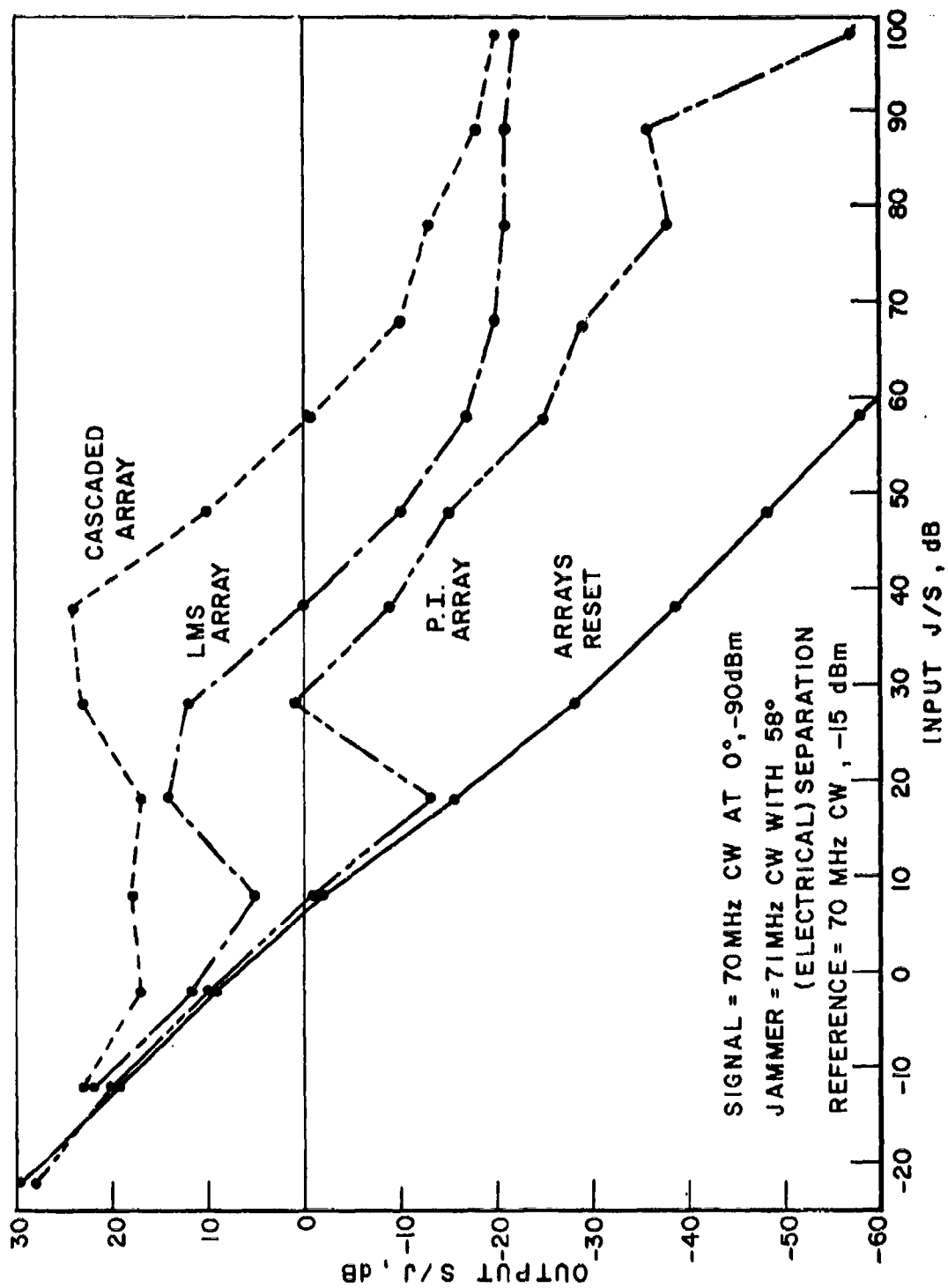


Figure III-9. Cascaded array performance with cw signals.

gain is available as a result of desired signal coding or spectrum spreading).

Testing of an adaptive array with cw signals can be deceptive unless care is used, particularly at high signal levels. For an LMS array in particular, at high signal levels, the time constants of the feedback loops (which are inversely proportional to input signal power) can become short enough that the weights may operate to transform a jamming signal to match the reference signal input (which indeed they will do under these conditions). When this occurs, the output S/J ratio, as determined via the output spectral density, approaches a constant value with increasing jammer input power. This effect is quite evident in the cascaded array and LMS array curves of Figure III-9 which are approaching a horizontal asymptote for high jammer levels. If this effect were not present, the curves of Figure III-9 should continue dropping with a slope of approximately minus one. Consequently, it would be grossly in error to conclude from these curves that jammer protection on the order of 80 dB could be achieved using this array if an S/J threshold of -20 dB is considered adequate. Values of jammer protection determined above for a 0 dB threshold should be representative of the performance achievable in a real signal environment, however, since the slopes of the curves at this value of S/J are still approximately correct. It can be seen also, from the PI array curve of Figure III-9 that the PI arrays, having no reference signal input, are not limited by this effect. Performance of these arrays too, however, eventually deteriorates at high jammer levels due to weight jitter and/or the partial coherence effects, as discussed earlier in section III-A.

2. Tests with PN Coded Signals

Bit error rate tests of cascaded array performance using pn coded bi-phase modulated TDMA signals were performed using the test configuration shown in Figure III-10. The OSU/RADC TDMA modems [11] were used for supplying the desired signal input to the array and for receiving and decoding the array output signal. These modems utilize a pulsed envelope signalling format for data, clock, and overhead signalling functions and employ spectrum spreading by a factor of 16, relative to the data rate, via a PN code of chip rate 175.2 Kbps. A bit error rate tester (BERT), synchronized with the TDMA modem clock supplied the data bit stream for transmission and, after synchronization of the received data stream with the transmitted data, detected and counted the bit errors which occurred.

The configuration used was chosen to simulate performance obtained over a typical TDMA satellite communications link, with the cascaded array employed for up-link protection. TDMA timing was performed over the link and the array reference signal was generated using a bootstrap reference system (borrowed from the OSU/RADC satellite simulator adaptive spatial processor [2]) as would be done in an actual satellite link. The four element inputs for the array, each containing a desired signal component (in-phase), an adjustable jamming signal component (skewed 60° from element to element), and uncorrelated noise (to establish a realistic up-link signal-to-noise ratio) were generated using the element signal simulator previously described (see section

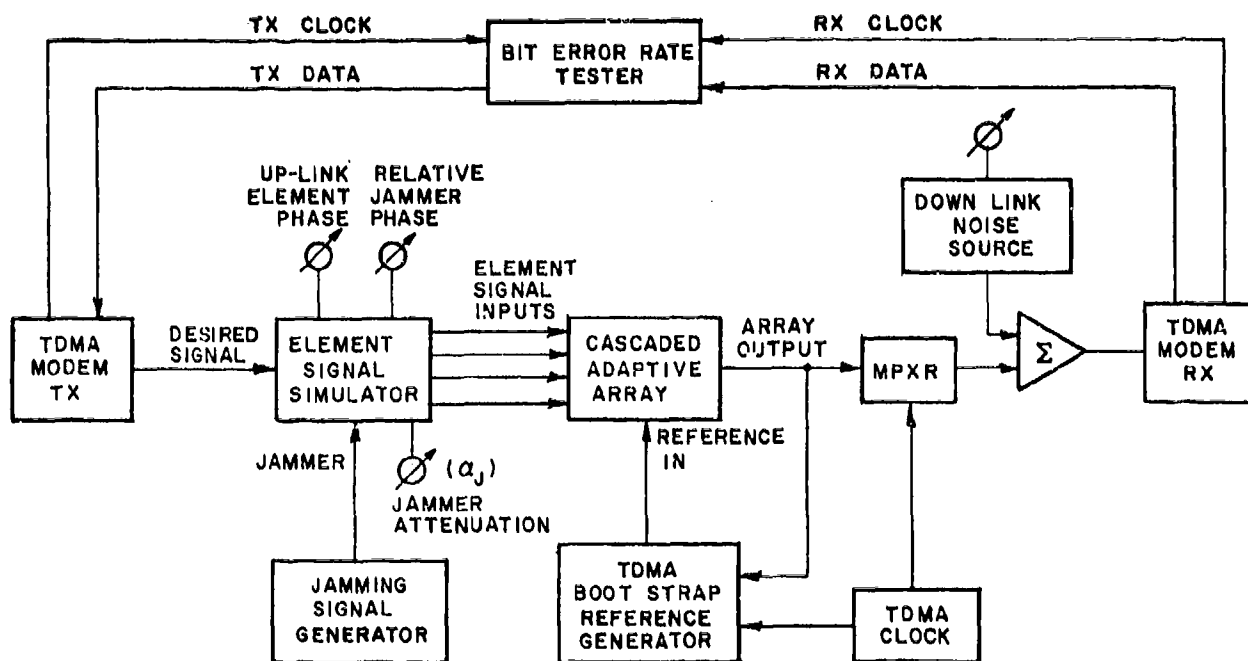


Figure III-10. Cascaded array test configuration for bit error rate testing with TDMA modems.

III-C-4 and Figure A14). The array output was multiplexed with the TDMA clock (also borrowed from the satellite simulator adaptive spatial processor) for TDMA modem timing purposes, mixed with uncorrelated down-link noise and then applied to the TDMA modem receiver.

An uplink signal-to-noise ratio of 0 dB was used, as measured in the 15 MHz array bandwidth established by the (70 MHz center frequency) array input filters. Downlink signal-to-noise ratio was chosen primarily to establish a reasonable bit error rate for obtaining statistically meaningful results in a reasonable time interval. In most cases, this signal-to-noise ratio is somewhat lower, and the bit error rate correspondingly higher than would be used in an actual communication link. Down-link signal-to-noise ratios were determined, and are given below, relative to a 10 KHz noise measurement bandwidth rather than the actual modem signal input bandwidth.

Typical results obtained from these measurements are given in Figures III-11 to III-13 which show curves of bit error rate as a function of jammer input power (i.e., decreasing jammer attenuation corresponds to increasing jammer input power) for the case of a cw jamming signal centered on the desired signal spectrum. This situation represents essentially worst case conditions for a continuous jammer of a given power level (assuming that the jammer cannot acquire the PN code, and code timing) since the power spectral density of the desired signal is highest at this point.

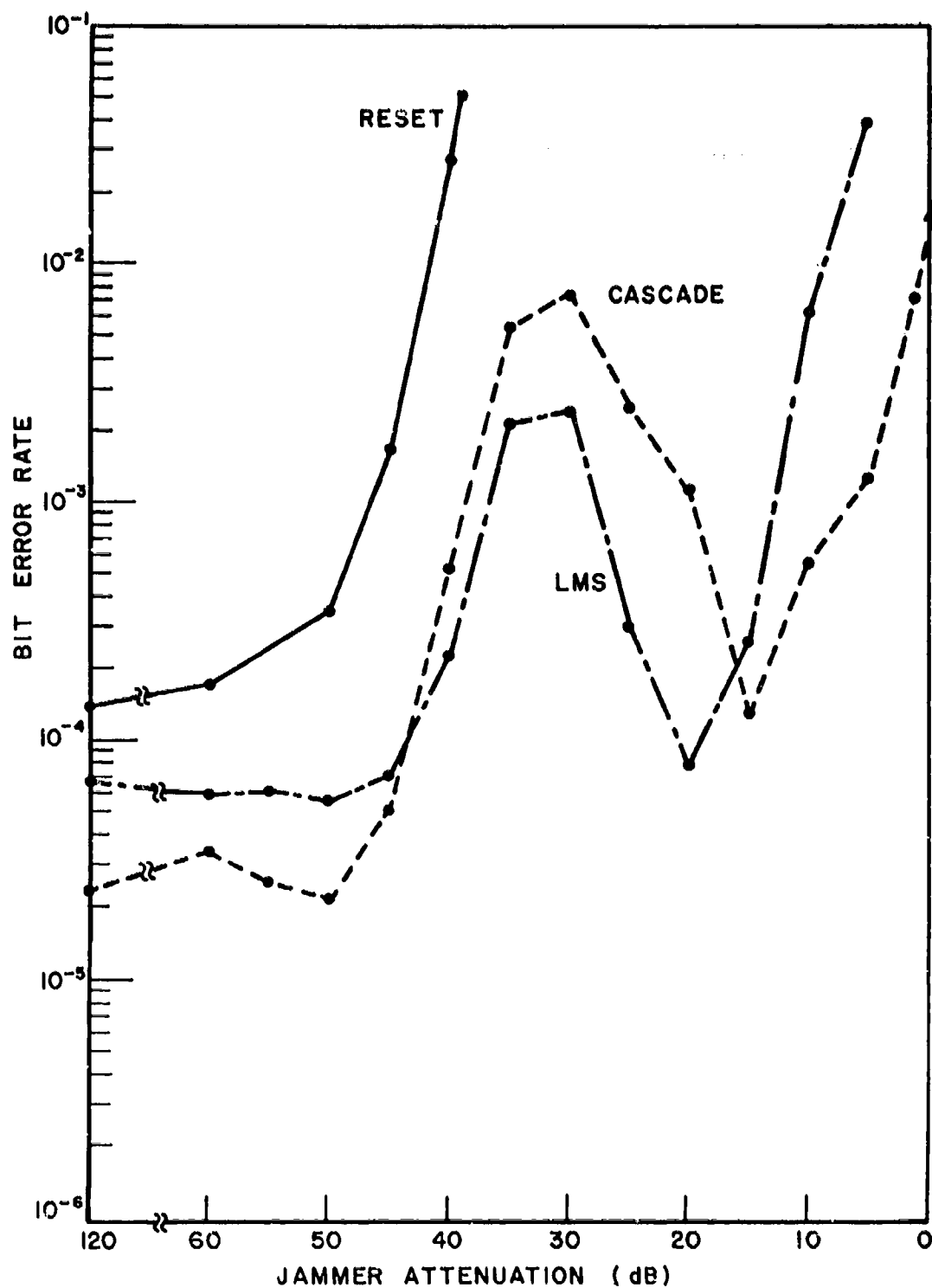


Figure III-11. Cascaded array performance in a pn-coded TDMA link with cw jammer (downlink S/N = 12 dB in 10 KHz BW).

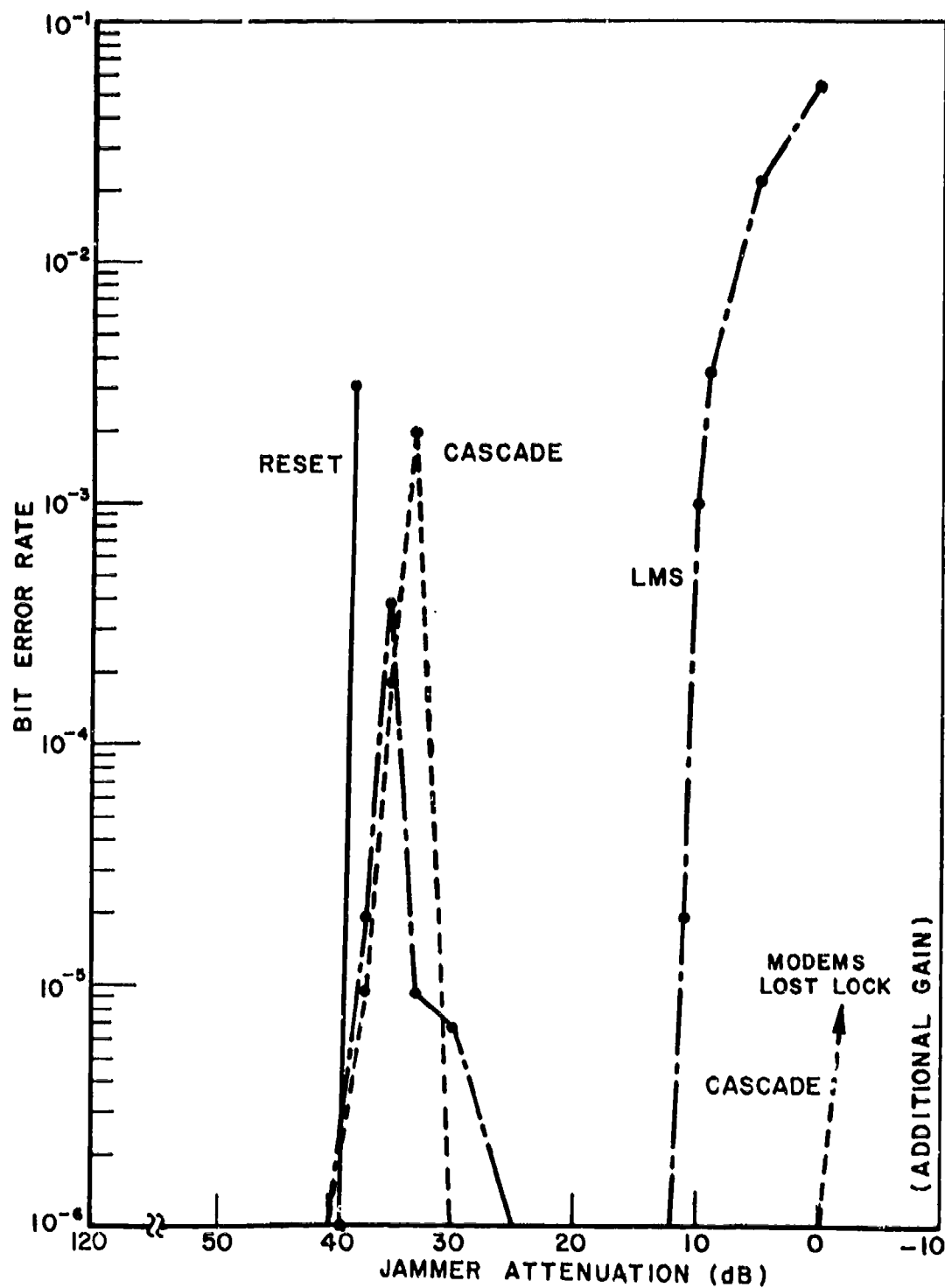


Figure III-12. Cascaded array performance in a pn-coded TDMA link with cw jammer (downlink S/N = 34 dB in 10 KHz BW).

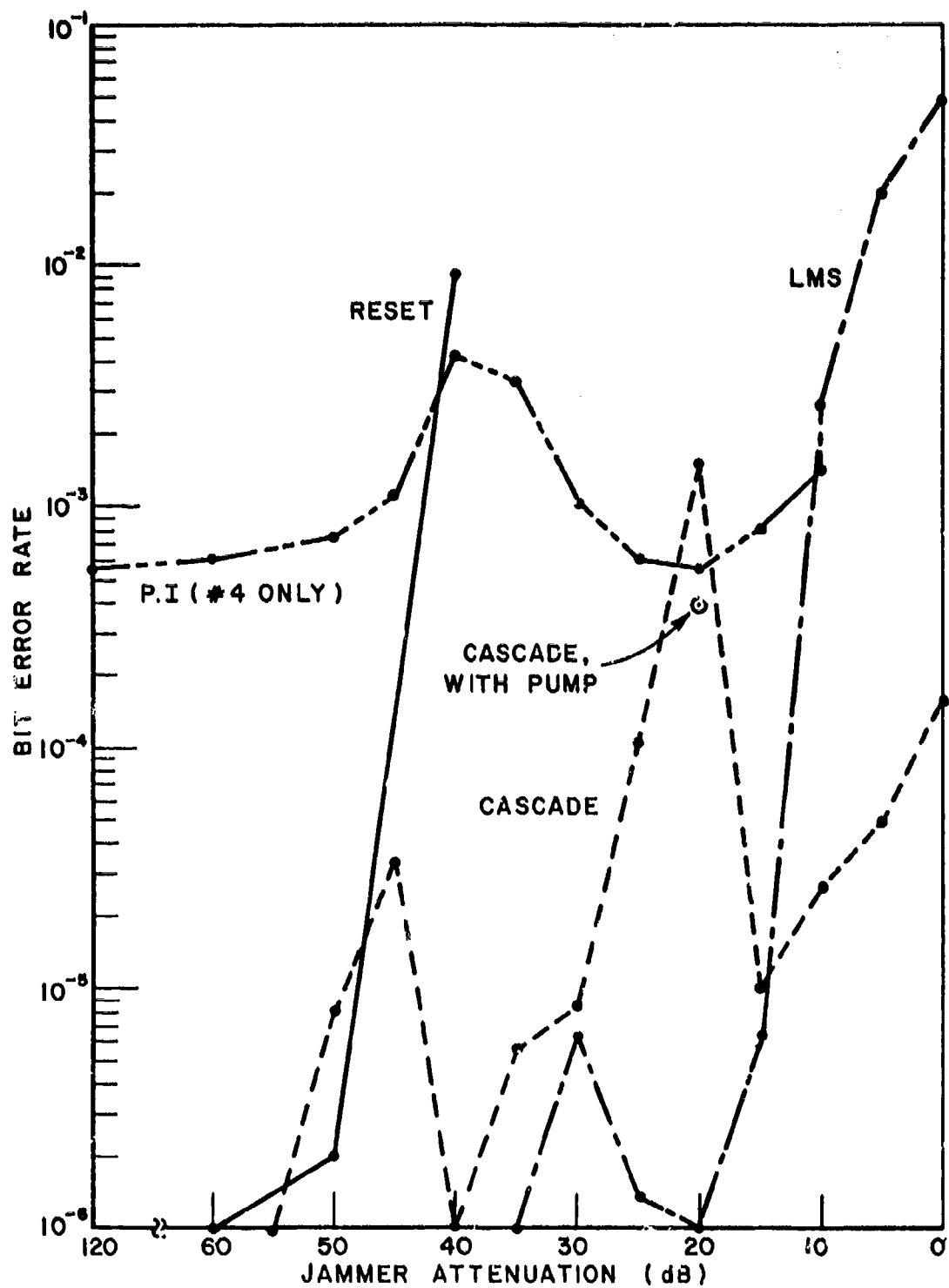


Figure III-13. Cascaded array performance in a pn-coded TDMA link with cw jammer (downlink S/N = 15 dB in 10 KHz BW).

The reset mode curves in these figures, relative to which array performance can be determined, were taken with all control weights set to zero except for the No. 4 LMS controller which had a finite, fixed weight (unity). Hence, the reset mode array patterns in these figures are omni-directional patterns. The PI array curve, also included in Figure III-12, represents the performance of PI array No. 4 only (rather than the combined performance of the 4 PI arrays as in the previous section) since contributions by the other three PI arrays are gated off by the (reset) LMS controllers.

The data of Figure III-11 were taken with a very low downlink S/N so that a relatively high (easily measurable) bit error rate occurs over a wide range of jammer input power levels in order to readily observe the general form of the resulting curves. At the left edge of these curves (essentially no jammer input) the "bit error rate floor", established in this case by the downlink S/N, is evident. The improvement due to the array factor (i.e., beaming up on the desired signal) for the "LMS" and "Cascade" curves is also evident. As jammer power is increased array performance essentially follows the reset curve (except for the array factor offset) until a threshold is exceeded, above which the array reacts to suppress the jammer thus reducing the bit error rate. Finally, when maximum jammer suppression (relative to the desired signal) has been reached, the error rate again increases along a curve essentially parallel to the reset curve. The horizontal distance (in dB) from the reset curve to the desired array mode curve gives the effective jammer suppression provided by the array. Maximum jammer suppression from these data (taken at a bit error rate of 10^{-2})

is approximately 32 dB for the LMS array alone (PI arrays reset - i.e., only the direct input signal branches of the PI arrays providing signals to the LMS array), and is approximately 41 dB for the cascade.

Figure III-12 shows similar curves obtained with no external noise added to the downlink ($S/N = 34$ dB in a 10 KHz BW). These curves are essentially similar to those of Figure III-11 except that the "bit error rate floor" previously established by downlink noise has been removed. In this case, the error rate for the cascaded array was only 10^{-6} for 0 dB jammer attenuation. An attempt was made to obtain measurements for higher jammer levels by adding an additional (10 dB) amplifier to the jammer signal input; however, the modems lost lock for higher jammer input levels, presumably due to timing jitter introduced by the array weights. (TDMA transmitter timing is established via ranging over the link containing the array.)

Figure III-13 shows array performance following a readjustment of various loop phase and gain adjustments in an attempt to 1) lower the threshold level at which array operation begins and 2) improve performance of the cascade for higher jammer levels. Downlink S/N for these curves is 15 dB in a 10 KHz bandwidth, 3 dB better than that used for the curves of Figure III-11. By comparing corresponding curves of Figure III-13 with those of Figures III-11 and III-12, it is evident that 1) the threshold level has been significantly reduced (i.e., the high error rate peaks at 30 to 40 dB jammer attenuation have been reduced by approximately 3 orders of magnitude), and 2) performance of the cascade for high jammer levels (below 15 dB attenuation) have been

improved to some degree. Performance of the cascade at a jammer attenuator setting of 20 dB has not improved however (it is approximately the same as in Figure III-11) and now appears excessively high relative to the remainder of the curve. In an attempt to discover the reason for this anomaly, a curve of PI array performance was also obtained (i.e., with the LMS array reset) and is included in Figure III-13. No abnormal behavior is apparent in this curve. However, due to the reset arrangement used, as discussed earlier, this curve represents the performance of only the No. 4 PI array so that abnormal behavior (as for example circuit instability or oscillation) of one of the other PI arrays is still a possibility.

The curves of Figures III-11 to III-13 were obtained with the pump oscillators (see Section III-C-3) turned off since, as previously discussed, they normally are not needed in the presence of a cw jamming signal. Since the point of highest bit error rate on the cascade curve of Figure III-13 is seen to coincide with the minimum of the PI curve, the possibility of insufficient residue signal (to properly "pump" the mixers of the LMS array) was suspected; hence, this point was remeasured with the pump oscillators turned on. Only a slight improvement in performance was obtained as shown by the point labelled "cascade, with pump", Figure III-13.

There are known to be rather serious hardware performance limitations in the quadrature detectors and vector modulators currently used in the cascaded array. This problem, which is discussed more fully in Section III-E below, may account at least in part, for the anomalous behavior noted above.

3. Tests with Spectrum Matched Jamming Signals

Additional measurements of array performance were made using the simulated satellite communications link of Figure III-10, but with the cw jamming signal replaced by a PN-coded bi-phase modulated jamming signal having a power spectral density envelope matched to that of the desired signal. The reset mode was also changed to that used in Section III-D-1 (all controllers set to unity gain) so that the combined performance of the 4 PI arrays could be determined. A downlink S/N of 15 dB (10 KHz bandwidth) was used. Other circuit parameters were the same as described above in Section III-D-2.

Results obtained from these tests are given in Figures III-14 and III-15. The curves of Figure III-14 were obtained with the multiplier pump oscillators turned off, as were all previous curves where cw jammers were used. Performance of the LMS array, in particular, and also of the cascade is seriously degraded, while the PI arrays provide approximately 27 dB of jammer protection for sufficiently high jammer levels.

The curves of Figure III-15 were obtained for conditions identical to those above except that the multiplier pump oscillators were turned on. Performance, in general, was greatly improved. For the cascade, jammer protection was increased from 17 dB to 42 dB, relative to the reset pattern, for a bit error rate of 10^{-4} . Or, relative to an omnidirectional pattern (obtained as for the reset curves of Figures III-11 to III-13) which is also included in Figure III-15 for comparison, 44 dB of jammer protection was obtained. Performance of the PI arrays

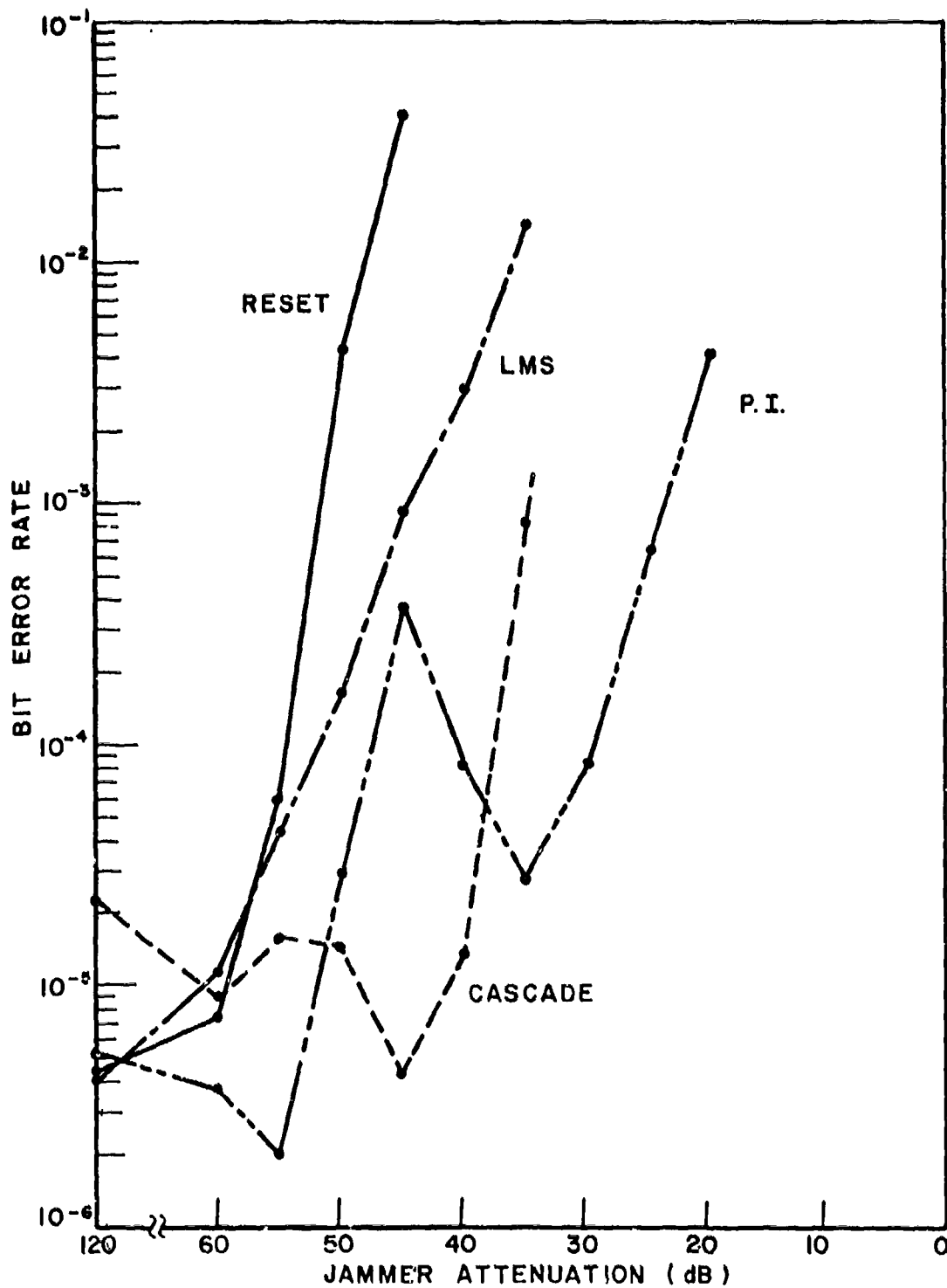


Figure III-14. Cascaded array performance with spectrum matched jammer, multiplier pump oscillators off.

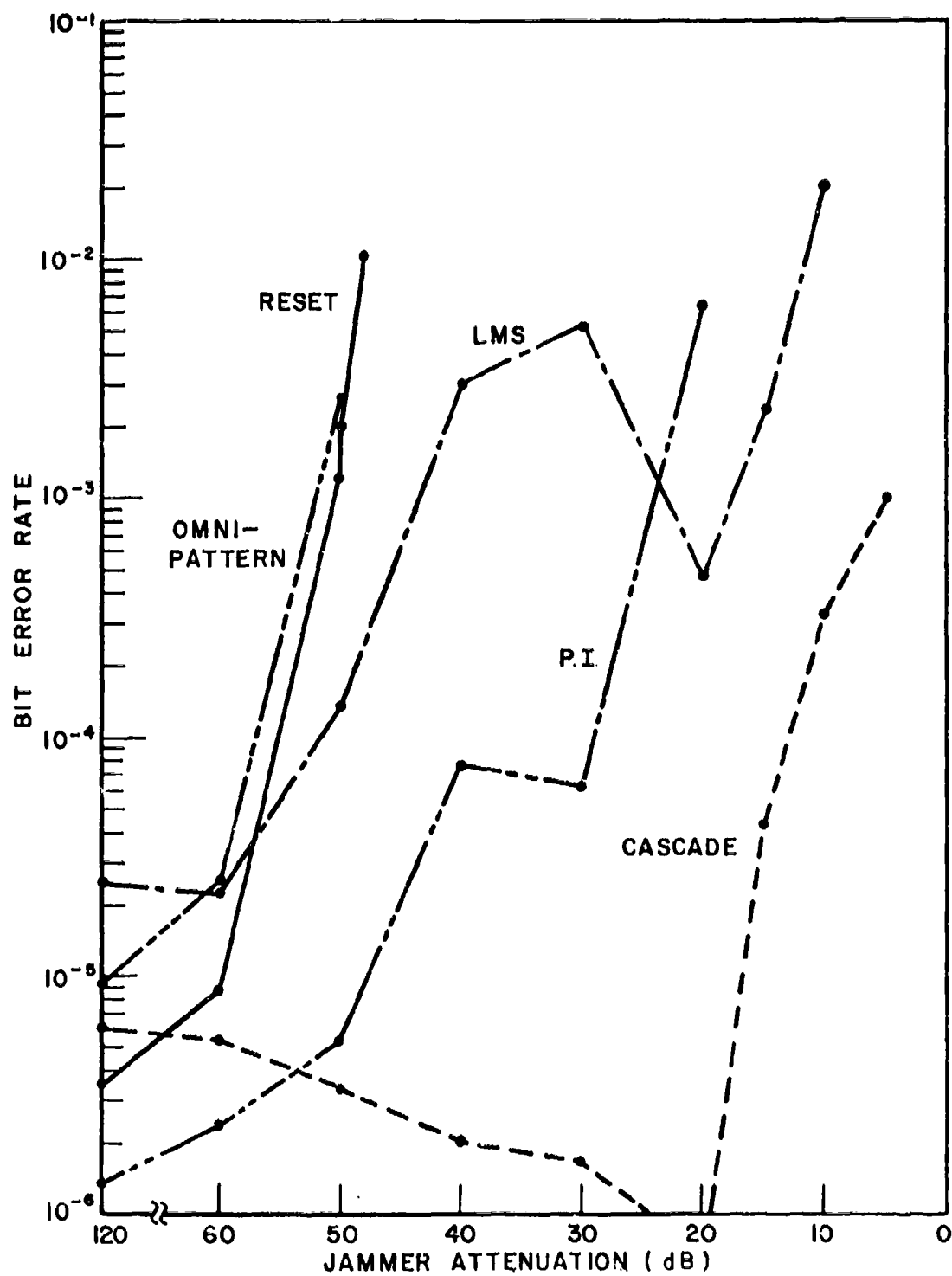


Figure III-15. Cascaded array performance with spectrum matched jammer, multiplier pump oscillators on.

at high jammer levels is approximately the same as before, but the threshold has been lowered (i.e., the peak in bit error rate occurring at 40 to 50 dB jammer attenuation, in Figure III-14, has been eliminated).

The LMS array curve also shows greatly improved performance at high jammer levels. However, this curve still exhibits a very high threshold level, similar to that of Figure III-11 which was obtained prior to loop phase adjustments. The LMS array obviously performs better than this curve would indicate when used in cascade with the PI arrays since the resulting good performance shown by the cascade curve at Figure III-15 could not otherwise be obtained. This is entirely reasonable, since the input signals applied to the LMS array would normally change significantly when the PI arrays are changed from the reset to the PI (operate) mode. Further implications of this behavior are discussed in the following section of this report.

E. SUMMARY AND CONCLUSIONS

A cascaded adaptive array configuration consisting of an LMS array with each element input augmented by a power inversion array for the purpose of greatly increasing the dynamic range of jamming signals which can be suppressed is presented and investigated experimentally. In addition, an I-F feedback loop configuration and pumped passive mixer multiplier circuits applicable to an array of this type are proposed, and are utilized in the experimental cascaded array. Test results obtained are presented. These include measured values of jammer suppression of cw jamming signals and of bit error rates obtained in a

simulated satellite TDMA communications link utilizing the cascaded array for uplink protection. Results obtained using the cascade configuration, and those obtained using only the LMS or PI portions of the array, are compared with those of a fixed array or omni-directional antenna.

Effective jammer suppression on the order of 50 dB relative to the desired signal was obtained during tests with cw signals. For the TDMA link tests which utilize a pulsed envelope spread spectrum pn coded bi-phase modulated signalling format, jammer protection of 41 dB was obtained relative to a cw jamming signal centered on the desired signal spectrum, and 44 dB relative to a spectrum-matched pn coded jamming signal.

The concept of the cascaded array in providing improved dynamic range capabilities relative to a conventional adaptive array in actual communications applications is amply demonstrated by this study. There are, however, some known deficiencies in the current implementation of the experimental array which, if corrected, should lead to improved performance. These are: 1) rather severe performance deficiencies in the quadrature detectors and vector multipliers used for conversion between the baseband integrators and the I-F feedback loop circuitry, 2) the possible effects of dc offsets and "dead zones" associated with the baseband integrators, and 3) somewhat less than ideal performance of the passive mixer multipliers for certain signal conditions. In addition, some further improvement in dynamic range of the current cascaded array might be achievable by adjusting relative signal levels in various parts of the feedback loops to more effectively utilize the available dynamic range of the individual loop components.

Several examples of anomolous array performance were observed relative to the data of the previous section; for example, the high array threshold levels observed in Figures III-11 and III-12, and again in Figure III-15. As noted previously, relative to the curves of Figure III-13, these can generally be reduced by appropriate phase and/or gain adjustments of the various feedback loops. However, it is generally found that an optimum adjustment for one input signal scenario is not necessarily optimum for another. In addition, the high bit error rate "spike" observed in Figure III-13 was not eliminated by this procedure. These performance limitations indicate that the current array, while basically capable of good performance in most cases, is excessively sensitive to specific input signal parameters.

The principle cause of this problem appears to be performance limitations of the quadrature detectors and vector multipliers, as mentioned above. These devices which are essentially "first of a kind" production units recently marketed by a well known manufacturer of signal processing components, consist of two mixers, a quadrature hybrid, and a power divider or summing junction. These components are all interconnected and prepackaged in a single small enclosure ideally suited for microstrip circuit applications. Unfortunately, performance of these units leaves much to be desired. Tests of these components revealed that large deficiencies exist in orthogonality between the (supposed) orthogonal components as well as gross mismatches in amplitude and phase of the transfer function from unit to unit, and also from one orthogonal component to the other. The reason for this may be stray coupling (inadequate shielding or isolation) between the various

components within the enclosure, since individually packaged components of the same type obtained from the same manufacturer have generally been found to be of excellent quality.

As a result of this deficiency, the array would experience difficulty in producing certain signal vectors, while others might readily be produced. Hence array performance would be somewhat erratic relative to a changing signal environment, which is the behavior observed with the current experimental array.

There are also "dead zones" (i.e., regions in which a changing input signal does not produce a corresponding change in output) associated with the vector modulators, and as in any baseband system, the possibility of dc offsets exists. These limitations affect primarily the array transient response (not considered particularly critical for the current conceptual demonstration array) and the array performance at low signal levels. If too severe, dc offsets can also lead to instability, but this has not been a problem with the current array. At the expense of increased circuit complexity, the dead zones could be compensated by suitable biasing of the driver circuitry, but this was not considered necessary for the current demonstration array.

The passive mixer multipliers used in the cascaded array generally performed well, at least within known performance limits. The linearity and dynamic range, however, are not as good as could be obtained using active multiplying circuits (see Section IV), particularly when use of the pump oscillators is necessary. The presence of the high level pump signals reduces, to some degree, the upper level of jammer and/or desired signal power which the circuits could otherwise accommodate.

Also, the additional spurious signals produced could cause difficulty, particularly relative to low level desired signals. These limitations should be carefully evaluated relative to their advantages (i.e., low cost, simplicity, availability, drift-free performance, and long-term reliability) when considering their possible use in future systems.

For further research and development of the cascaded array to obtain improved performance it is recommended that replacement of the baseband integrators and associated quadrature detectors and vector modulators, and possibly also the correlators, by digital processors should be considered. Development of active multiplier circuits having improved frequency, bandwidth, linearity, and dynamic range characteristics should be continued. Also, an investigation of the broadband nulling capabilities of the array should be made, with further development as necessary to achieve a desired nulling bandwidth. Although the current cascaded array has a nominal signal bandwidth of 40 MHz, and the feedback loops remain stable over this band, no detailed investigation of nulling bandwidth, per se, has been performed under the current contract.

F. REFERENCES

- [1] Swarner, William G., "Advanced TDMA Techniques and Bit Synchronous Design and Array Component Evaluation", Final Report 710300-5, April 1979, The Ohio State University ElectroScience Laboratory, Department of Electrical Engineering; prepared under Contract F30602-75-C-0061 for Rome Air Development Center.

- [2] T.W. Miller, R. Caldecott, and R.J. Huff, "A Satellite Simulator with a TDMA-System Compatible Adaptive Array", Report 3364-4, January 1976, The Ohio State University ElectroScience Laboratory, Department of Electrical Engineering; prepared under Contract F30602-72-C-0162 for Rome Air Development Center (RADC-TR-76-98) (AD/B011048L).
- [3] W.G. Swarner and A.J. Berni, "An Adaptive Antenna Array and Angle of Arrival Estimation System for Sensor Communications", Report 3435-2, April 1974, The Ohio State University ElectroScience Laboratory, Department of Electrical Engineering; prepared under Contract DAAG-72-C-0169 for Department of the Army, Harry Diamond Laboratories (AD780163).
- [4] T.W. Miller, "The Transient Response of Adaptive Arrays in TDMA Systems", Report 4116-1, June 1976, The Ohio State University ElectroScience Laboratory, Department of Electrical Engineering; prepared under Contract F30602-75-C-0061 for Rome Air Development Center (RADC-TR-76-390).
- [5] B. Widrow, P.E. Mantey, L.J. Griffiths and B.B. Goode, "Adaptive Antenna Systems, " Proc. IEEE, 55, December 1967, P. 2143.
- [6] R.T. Compton, Jr., "Adaptive Arrays: On Power Equalization with Proportional Control", Report 3234-1, December 1971, The Ohio State University ElectroScience Laboratory, Department of Electrical Engineering; prepared under Contract N00019-71-C-0219 for Naval Air Systems Command.

- [7] C.W. Schwegman and R.T. Compton, Jr., "Power Inversion in a Two-Element Adaptive Array", Report 3433-3, December 1972, The Ohio State University ElectroScience Laboratory, Department of Electrical Engineering; prepared under Contract N00019-72-C-0184 for Naval Air Systems Command (AD 758690).
- [8] C.L. Zahm, "Application of Adaptive Arrays to Suppress Strong Jammers in the Presence of Weak Signals", IEEE Trans., AES-9, March 1973, p. 260.
- [9] Ronald J. Huff, "On the Augmentation of a LMS Adaptive Array with Power Inversion Processors", unpublished technical memorandum, July 1977, The Ohio State University ElectroScience Laboratory, Department of Electrical Engineering; prepared under Contract F30602-75-C-0061 for Rome Air Development Center.
- [10] H.S. Eilts, "The SINR Performance of Cascaded Adaptive Arrays", Technical Report 711679-9, March 1982, The Ohio State University ElectroScience Laboratory, Department of Electrical Engineering; prepared under Contract F30602-79-C-0068 for Rome Air Development Center.
- [11] R.C. Taylor and R.J. Huff, "A Modem/Controller for TDMA Communications Systems", Report 3364-5, December 1976, The Ohio State University ElectroScience Laboratory, Department of Electrical Engineering; prepared under Contract F30602-72-C-0162 for Rome Air Development Center (RACS-TR-76-362).

SECTION IV

MICROCIRCUIT MULTIPLIER DEVELOPMENT

One of the most critical components required for practical implementation of an adaptive array, and on which good array performance ultimately depends, is the 4-quadrant multiplier needed for signal weighting and for correlation of the error signal with the corresponding element input signal for each feedback loop. In previous arrays, many types of devices have been used to perform these functions. These include passive mixers, active transconductive multipliers of various configurations, PIN diodes, programmable attenuators and/or phase shifters, and various types of FET multiplying circuits. All have various shortcomings which hopefully might be improved. Digital circuits are also becoming practical for correlation purposes, but are much too slow for application as a weighting multiplier in a typical communications link adaptive array.

Adaptive arrays constructed in recent years at this laboratory which operate at an I-F frequency of 70 MHz have successfully employed active transconductance multipliers (see references [2] and [3] of Section III) while the current cascaded array employs pumped passive mixers (see Section III-C-2). These transconductance multiplier circuits, which were constructed using discrete passive components together with a commercial dual differential amplifier (CA 3049), perform very well at the design frequency when properly aligned, but

performance is seriously degraded at much higher frequencies due to stray circuit capacitance and inductance, and the resultant signal leakage paths caused by the relatively large physical sizes of components and their arrangement required for implementation. The active device itself, which is rated to 500 MHz, does not, in general, limit multiplier performance. The pumped passive mixer multipliers employed in the current array (at I-F frequencies of 160, 250, and 410 MHz) also perform well, within known limitations; however, they are less linear, introduce additional spurious signal components, and have a somewhat smaller dynamic range than do the active transconductance multipliers.

Consequently, some effort has been devoted to the development of improved transconductance multiplier circuits for higher frequency operation in adaptive array applications. It is hoped that this work can be continued to upgrade existing capabilities in this area. As a first step, completed under the current contract, a microcircuit technique has been developed and used to suitably package a beam-lead version of the dual differential amplifier chip (CA 3049L) to obtain a better pin-out for transconductance multiplier applications. Details of this work are given in Appendix B. Approximately 40 of the devices were produced which could be used later for retrofit of the cascaded array, or for other applications, if desired. Success of this phase of the development effort is demonstrated by the measured multiplier characteristics of Figure IV-1 which show almost ideal multiplier performance over a dynamic range exceeding 70 dB for both x and y inputs. The basic multiplier circuit used in obtaining these measured characteristics is given in Figure IV-2. The test frequencies used

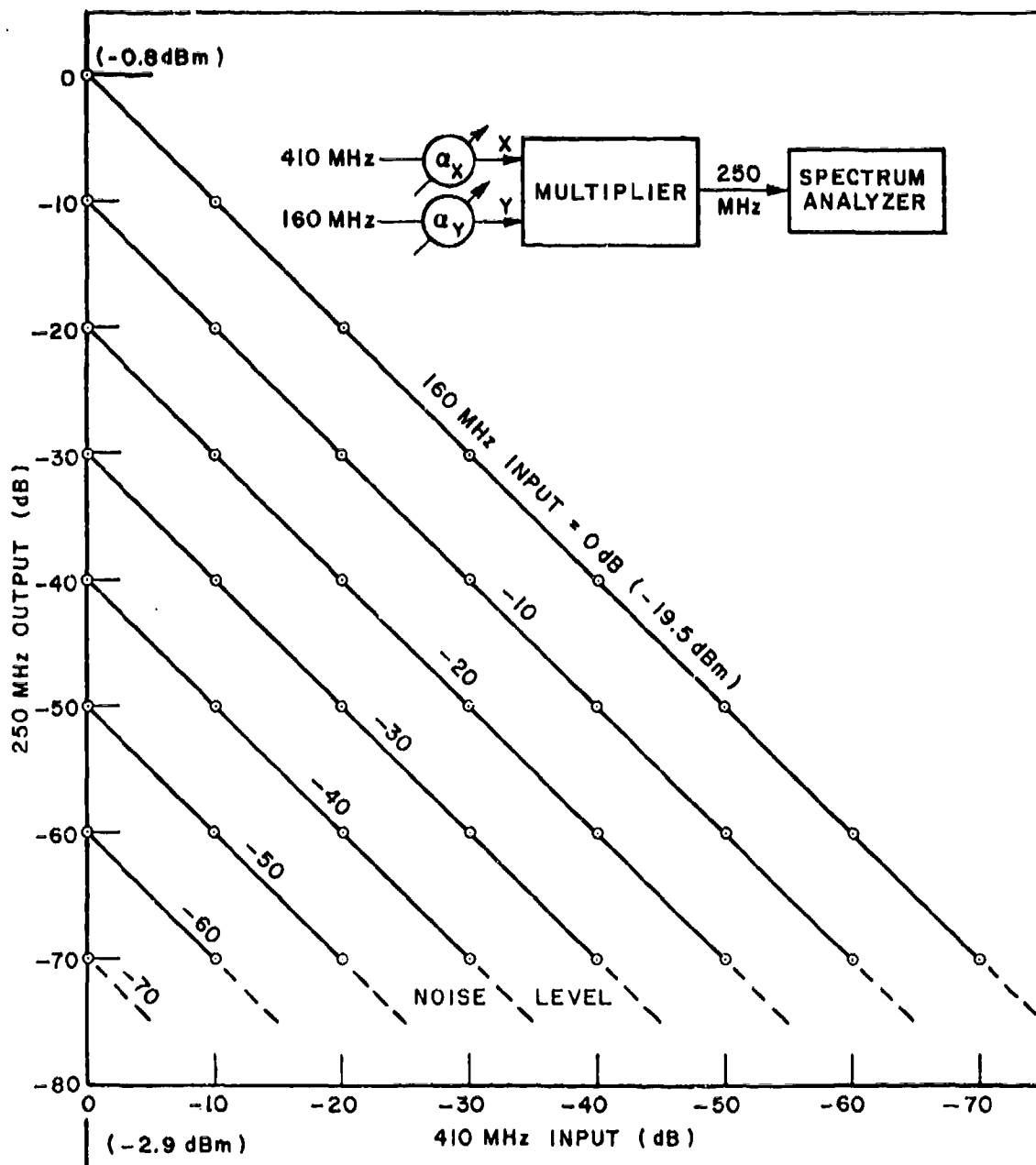


Figure IV-1. Microcircuit multiplier measured characteristics.

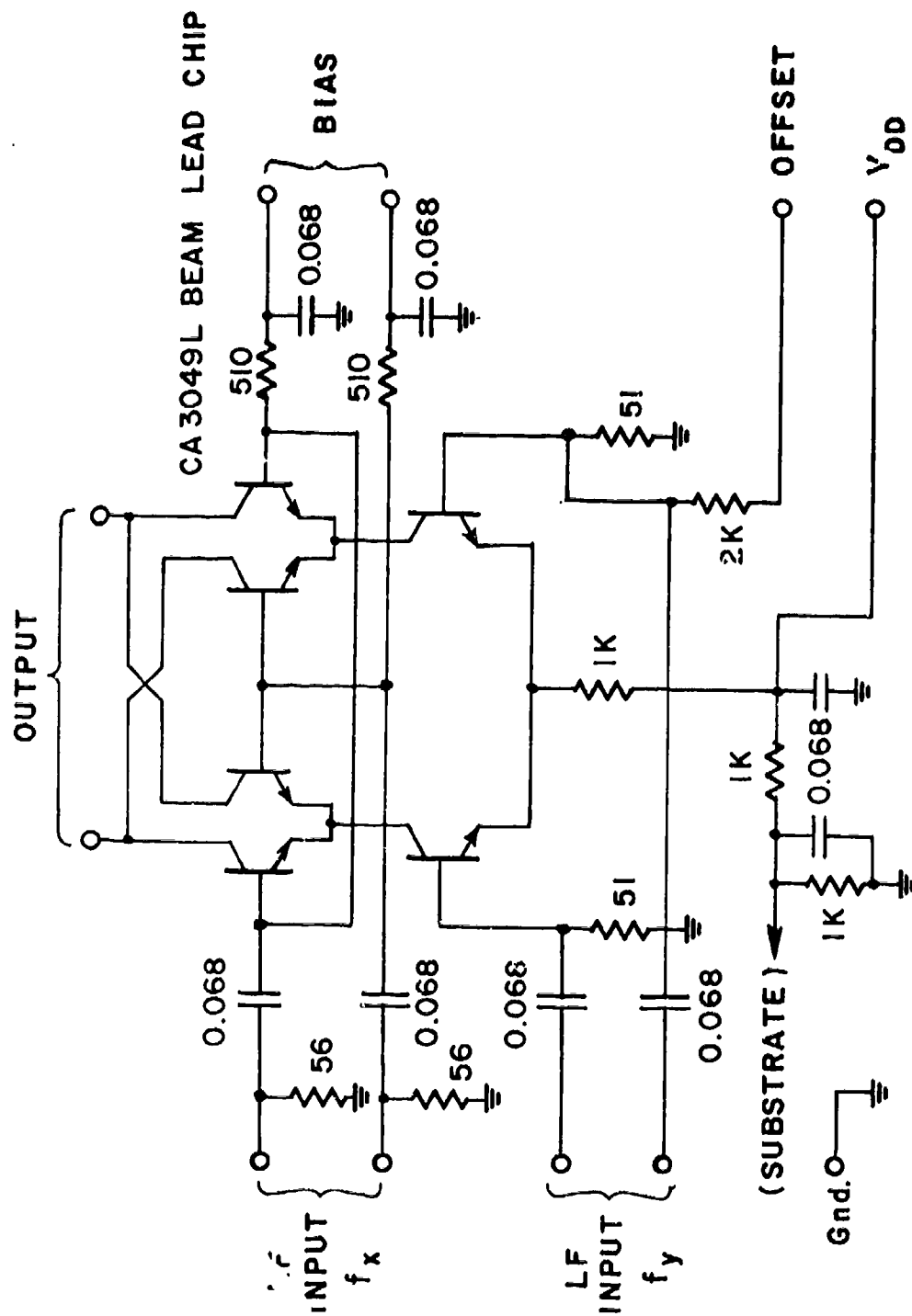


Figure IV-2. Developmental microcircuit active multiplier.

(i.e., input frequencies of 160 MHz and 410 MHz, with the output taken at 250 MHz) are those used for the PI array weighting multipliers of the current cascaded adaptive array.

For further development, the passive components of Figure IV-2 are to be included on the microcircuit substrate (as a thin-film hybrid device) resulting in a practical multiplier useful to approximately 500 MHz which will require a minimum of external circuitry; and eventually, advanced versions, either monolithic or hybrid, using a similar arrangement of FET active devices fabricated directly upon a silicon or gallium arsenide substrate are planned. These advanced devices should be useful to approximately 2 GHz.

SECTION V
A KALMAN PREDICTOR SAMPLED DATA DELAY
LOCK LOOP EXPERIMENT

An essential aspect of the implementation of time ordered relay communication systems is the capability to synchronize a locally generated pseudonoise (PN) code with the PN code of the received signal. This synchronization permits the correct detection of the pseudonoise coded signals and permits the proper operation of the adaptive array used for interference suppression. The Sampled Data Delay Lock Loop (SDDLL) has been developed [11,12] to accomplish this task. This circuit works extremely well for low PN code rates. However, for higher code rates (especially with maneuvering terminals) the code tracking performance of the current SDDLL is not adequate. Two theoretical studies have been completed [4,13] which show that the tracking performance of the SDDLL can be substantially improved by incorporating a Kalman estimator into the SDDLL.

In order to experimentally verify that a Kalman estimator could be interfaced with the SDDLL, some testing was done by using an existing TDMA modem (which contains a SDDLL) and an external Hewlett-Packard 2116 computer (to do the Kalman algorithm). This section documents this testing.

A. EXPERIMENTAL HARDWARE

A block diagram of the SDDL as used in the modem is shown in Figure V-1. The input to the circuit is a pulsed envelope biphase coded pseudo-noise (PN) signal and noise. The SDDL generates a local replica (the "Local Clock signal") of the incoming code. Advanced and delayed versions of the Local Clock Signal are correlated with the incoming code in the upper and lower mixer-bandpass filter-envelope detector circuits, respectively. The difference between the advanced and delayed correlations is sampled. The samples (labelled E_s in Figure V-1) are processed in a discrete (i.e., computer) algorithm and the processed output is used to correct the timing of the local PN code generator. The timing corrections are done digitally, with the period of the

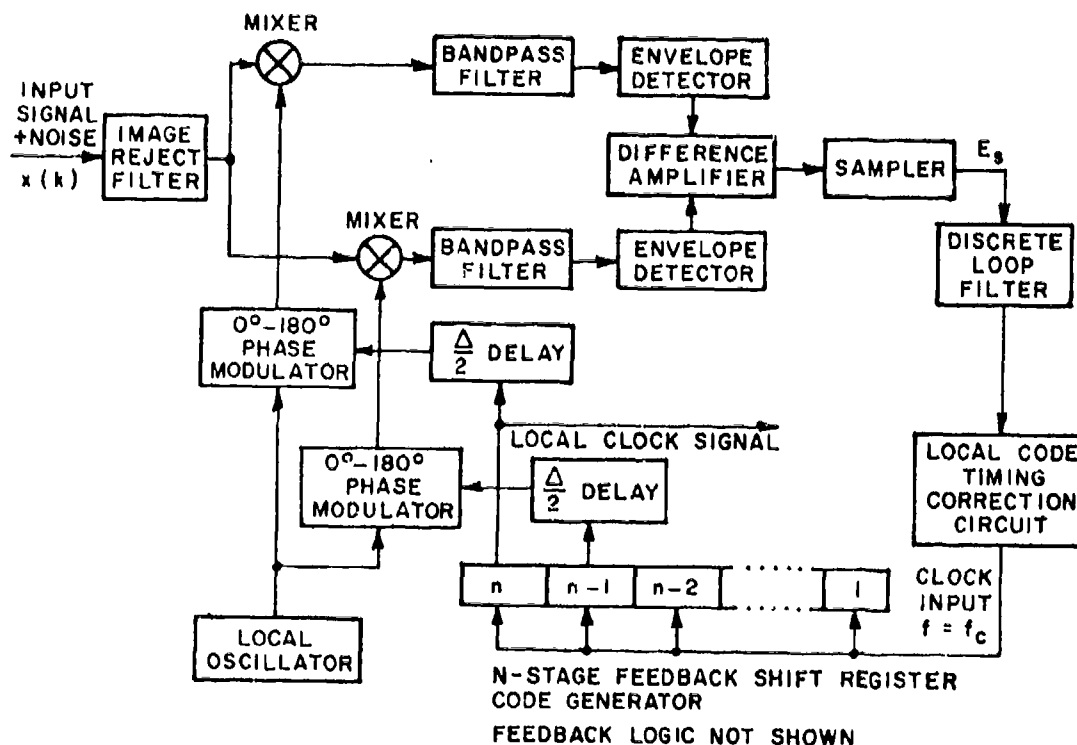


Figure V-1. Block diagram of the sampled dealy lock loop (SDDL).

clocking signal being modified in increments of $\Delta/48$, where Δ is the duration of a code chip. This digital correction method introduces quantization errors into the local clock timing. The jitter due to the quantization error is

$$\frac{\sigma_e}{\Delta} = .0104 \quad (5-1)$$

where σ_e is the rms timing jitter. This was computed based upon a uniform timing error distribution between $-\Delta/96$ and $+\Delta/96$.

Modifications were made to the circuit of Figure V-1 to accommodate the Kalman experiment. Specifically, the sampled correlation differences, E_s , were fed to an outboard computer for processing via the Kalman one step prediction algorithm. The algorithm generated the clock corrections. These were fed back to the modem to be carried out by the discrete correction circuitry.

A block diagram of the experimental hardware is shown in Figure V-2. Instead of measuring the error in code tracking, the quantity that was used in the tests to evaluate the code tracking accuracy was bit error rate. This was done because

1. Actual tracking error measurements would require elaborate hardware and circuit modifications to the modems.
2. A direct relationship of bit error rate degradations to code tracking errors exists [10] and can be used to convert from one to the other.

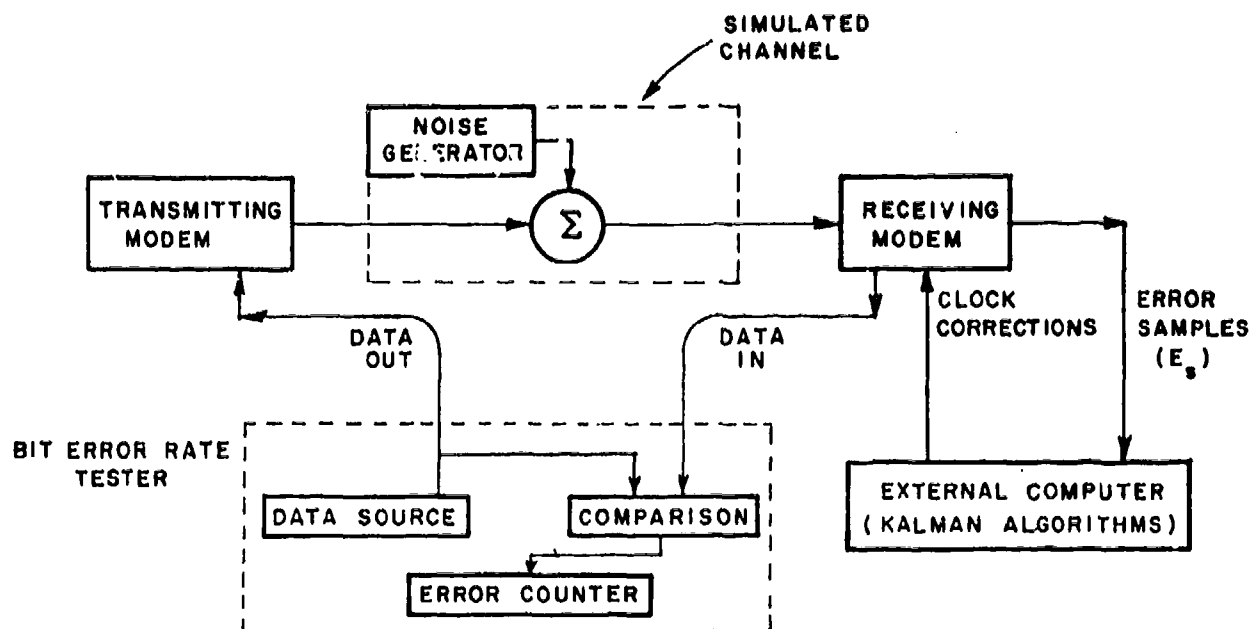


Figure V-2. Experimental hardware.

3. The objective of the experiment was limited to showing that Kalman processing could be used to improve the performance of the SDDL. Bit error rate testing is adequate for this.

Two modems were used for the testing. One was used as a transmitter to send a PN coded data stream. The other, with the modified tracking loop, was used as a receiver. External noise was added so that the channel signal to noise ratio could be adjusted. The external computer was programmed with four different Kalman predictor algorithms. The algorithms were selected based upon the data in [4] to give differing timing jitters. The standard four sample average was also programmed so that comparisons with the existing algorithm could easily be made. Four different Kalman predictors were used so that the effects of filter bandwidth changes could be observed.

B. RESULTS

Bit error rate testing was performed with the channel noise adjusted to give E_b/N_0 of 5.6 (numeric) at the receiver. E_b is the total energy in one bit and N_0 is the (one sided) noise spectral density. Figure V-3 shows the "measured" and the theoretical jitter for the given signal to noise ratio. The "measured" data was obtained by measuring the bit error rate and computing the jitter from Equation (A1) in Appendix C. The theoretical values include the effects of clock loop jitter and quantization noise in the clock correction circuitry (rms addition). The theoretical clock loop jitter for the 4 sample average was obtained from Equation (A4) of Appendix C. The gain (A_c) was unity and the pulse energy to noise ratio E_c/N_0 was 50.4

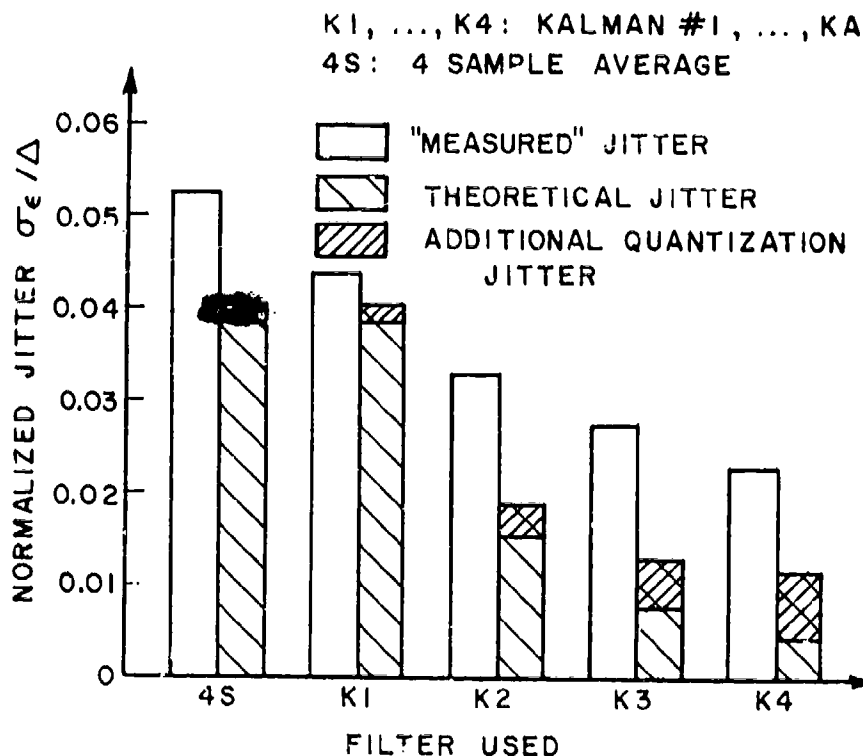


Figure V-3. Experimental and theoretical performance of the Kalman SDDL.

(the clock pulse duration is 9 times a single bit duration, thus $E_c = 9 \cdot E_b$). The theoretical jitter values for the respective Kalman predictors were obtained from Figure C.1 (Appendix C). The data in Figure C.1 is normalized to the open loop measurement jitter. The open loop jitter required to interpret Figure C.1 was obtained from Equation (A-3) (Appendix C). Quantization jitter was obtained from Equation (V-1) of this section and added in an RMS sense. The quantization jitter forms a more significant part of the total for the cases where the theoretical jitter is small.

Generally, the "measured" data of Figure V-3 agree very well with the theoretical data. The first Kalman algorithm tested (K1) was chosen to have a theoretical jitter equal to that of the 4 sample averager (theoretical). As seen in the graph, it performs significantly better than the 4 sample averages. This could be due to the Kalman algorithm's ability to "track" the incoming clock frequency. Differences between the incoming signal's clock frequency and the local clock frequency are considered to be doppler induced by the Kalman algorithm and are compensated for with appropriate clock corrections. The 4 sample averager does not compensate for clock frequency offsets. The remaining Kalman predictors (K2,K3,K4) each show the improvements predicted by theory, although they do not approach the theoretical values as well as the first Kalman predictor (K1). This is most likely due to errors in measuring the signal to noise ratios and/or some misadjustment in the modem detectors.

C. CONCLUSIONS AND RECOMMENDATIONS

We have demonstrated that a Kalman predictor can be interfaced with a sampled data delay lock loop to provide improved jitter performance. This evaluation was done with the existing (175 KHz code rate) modems mainly because of convenience. However, a Kalman processor is not needed until the code rate becomes high enough so that maneuvers (i.e., doppler effects) are a significant problem. In such cases, the selection of the Kalman processor parameters involves trade-offs between maneuver tracking and jitter performance. These trade-offs could not be evaluated here. Furthermore, the circuit techniques necessary for high code rates (>100 MHz) are not trivial. In order to properly evaluate the Kalman SDDL, a high code rate (320 MHz) tracking loop has been proposed, along with related circuitry to fully test it. Tracking performance will be evaluated by actual measurements of the tracking errors. Maneuvers will be simulated by varying the timing of the code source. Such an experiment will simultaneously satisfy two objectives. First, experimental verification of our previous theoretical work will be provided. Secondly, techniques for processing high rate PN signals will be developed. Both of these are needed for the development of high data rate anti-jam communications.

D. REFERENCES

- [1] H.S. Eilts, "The SINR Performance of Cascaded Adaptive Arrays", Technical Report 711679-9, May 1982, The Ohio State University ElectroScience Laboratory, Department of Electrical Engineering; prepared under Contract F30602-79-C-0068 for Rome Air Development Center.
- [2] T.W. Miller, "The Transient Response of Adaptive Arrays in TDMA Systems", Technical Report 4116-1, June 1976, The Ohio State University ElectroScience Laboratory, Department of Electrical Engineering; prepared under Contract F30602-75-C-0061 for Rome Air Development Center.
- [3] C.A. Baird, Jr., and C.L. Zahm, "Performance Criteria for Narrowband Array Processing", 1971 IEEE Conference on Decision and Control, Miami Beach, Florida, December 15-17.
- [4] H.S. Eilts, "The Performance of a Sampled Data Delay Lock Loop Implemented with a Kalman Loop Filter", Technical Report 711679-1, March 1979, The Ohio State University ElectroScience Laboratory, Department of Electrical Engineering; prepared under Contract F30602-79-C-0068 for Rome Air Development Center.
- [5] H.S. Eilts and W.G. Swarner, "A Weight Storage and Recall System for Use in an Experimental Adaptive Array", Technical Report 711679-3, March 1981, The Ohio State University ElectroScience Laboratory, Department of Electrical Engineering; prepared under Contract F30602-79-C-0068 for Rome Air Development Center.

- [6] T.W. Miller, R. Caldecott, and R.J. Huff, "A Satellite Simulator with a TDMA-System Compatible Adaptive Array", Technical Report 3364-4, January 1976, The Ohio State University ElectroScience Laboratory, Department of Electrical Engineering; prepared under Contract F30602-72-C-0162 for Rome Air Development Center.

- [7] B.V. Andersson, "Angle of Arrival Estimation", Technical Report 711679-4, April 1981, The Ohio State University ElectroScience Laboratory, Department of Electrical Engineering; prepared under Contract F30602-79-C-0068 for Rome Air Development Center.

- [8] H.S. Eilts, "The Performance of a Sampled Data Delay Lock Loop Implemented with a Kalman Loop Filter", M.S. Thesis, The Ohio State University, March 1979.

- [9] H.S. Eilts, "A Sampled Data Delay Lock Loop Implemented as a Kalman Predictor", IEEE Trans AES, Vol. AES-16, No. 6, November 1980, pp. 800-810.

- [10] R.J. Huff, "The Imperfectly-timed Demodulation of Differential Phase Shift Keyed Signals", Technical Report 2738-1, June 1969, The Ohio State University ElectroScience Laboratory, Department of Electrical Engineering; prepared under Contract F30602-69-C-0112 for Rome Air Development Center.

- [11] R.J. Huff, Kenneth L. Reinhard, and Daniel C. Upp, "The Synchronization of Time Division Multiple Access Systems - An Analytical and Experimental Study", Technical Report 2358-9, June 1969, The Ohio State University ElectroScience Laboratory, Department of Electrical Engineering; prepared under Contract F30602-67-C-0119 for Rome Air Development Center.
- [12] R.J. Huff and K.L. Reinhard, "A Delay Lock Loop for Tracking Pulsed-Envelope Signals", IEEE Trans. on Aerospace and Electronic Systems, Vol. AES-7, No. 3, May 1971, pp. 478-485.
- [13] W.G. Swarner, C.W. Chuang, R.J. Huff, and H.S. Eilts, "TDMA Timing Loops for High Data Rate Systems", Technical Report 710300-1, May 1978, The Ohio State University ElectroScience Laboratory, Department of Electrical Engineering; prepared under Contract F30502-75-C-0061 for Rome Air Development Center.

SECTION VI

THE MODIFIED-LMS FEEDBACK LOOP

A. INTRODUCTION

Adaptive arrays based on the least mean square (LMS) algorithm [1] have been extensively studied as a means of protecting communication systems from interference. These arrays can automatically point a beam toward a desired signal and simultaneously null interfering signals.

An important problem with the LMS adaptive arrays is their limited dynamic range. Two factors restrict the dynamic range of the adaptive array. First, the circuitry in the LMS feedback loop operates properly only in a certain range of signal power. As in other systems these hardware limitations are very real, but they are not due to the LMS feedback concept itself.

The second factor is inherent in the LMS algorithm itself. The speed of response in an LMS array is proportional to the powers of the input signals. In mathematical terms, the speed of response is determined by the eigenvalues of the covariance matrix. The covariance matrix is the matrix of the cross products between the array element signals. The LMS algorithm responds slowly to a weak signal and rapidly to a strong signal. When both strong and weak signals are present, the weight transients include both fast and slow terms, whose speeds are in the ratio of the eigenvalues of the covariance matrix. This is the so-called eigenvalue spread problem. This characteristic of the LMS

algorithm makes it difficult to accomodate a wide range of signal powers. For most applications of adaptive arrays, system requirements limit both the minimum and maximum speed of response of the array. The minimum speed is usually set by the slowest permitted adaption to a desired signal, while the maximum speed of response is set by the modulation rate of the desired signal. If the speed of response approaches the modulation rate of the desired signal, undesirable signal distortions will occur. As a result of these characteristics, the array can handle only a limited range of signal powers without exceeding the speed of response bounds.

To overcome this susceptibility of the LMS algorithm to the eigenvalue spread in the input covariance matrix, an improved feedback loop for adaptive arrays has recently been proposed by Compton [2]. We will refer this improved feedback loop as the "Modified-LMS feedback loop". The Modified-LMS feedback loop is based on an "ideal" control law [2] in which the eigenvalues of the input covariance matrix do not influence the speed of the transient response.

To assess the feasibility of using the Modified-LMS feedback loop in communications systems, modifications were made to an existing LMS array to implement the Modified-LMS algorithm. In this report the Modified-LMS transient response and overall performance are compared with those of the original LMS array. To quantitatively assess the performance of both the original and Modified-LMS algorithms, bit error rate testing was used. Here a simulated communications link employing the adaptive array was used for the transmission of binary data. The bit error rates over the simulated channel provide a good measure of the array performance.

In Section B, the Modified-LMS feedback loop is discussed briefly. Section C presents experimental results showing the improvement obtained by the Modified-LMS array over the original array. Hardware and implementation topics are studied in Section D.

B. MODIFIED-LMS FEEDBACK LOOP

The weights in the LMS array shown in Figure VI-1 satisfy the system of differential equations

$$dW/dt + 2k_0 XX^T W = 2k_0 XR(t) \quad (6.1)$$

where the superscript T denotes transpose, k_0 is a gain constant, $R(t)$ is a reference signal supplied to the array, and W and X are weight and input signal vectors, respectively

$$W = (W_1, W_2, W_3, \dots, W_M)^T \quad (6.2a)$$

$$X = (X_1, X_2, X_3, \dots, X_M)^T \quad (6.2b)$$

Here, M is the number of antenna elements. By replacing XX^T and $XR(t)$ by their time average values, Equation (6.1) can be solved approximately. Let Φ and S denote these averages:

$$\Phi = \overline{XX^T} \quad (6.3a)$$

$$S = \overline{XR(t)} \quad (6.3b)$$

With these substitution, the system in Equation (6.1) becomes

$$dW/dt + 2k_0 \Phi W = 2k_0 S \quad (6.4)$$

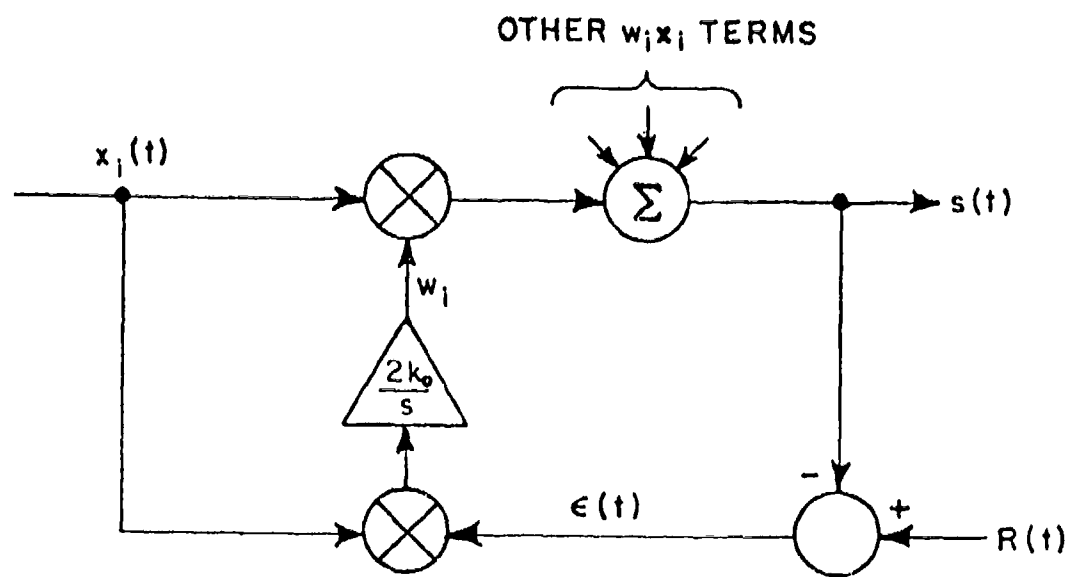


Figure 1. The LMS feedback loop.

Figure VI-1. The LMS feedback loop.

By diagonalizing Φ , the solution for the i -th weight is

$$w_i = A_{i1}\exp(-2k_0\lambda_1 t) + A_{i2}\exp(-2k_0\lambda_2 t) + \dots + A_{i2M}\exp(-2k_0\lambda_{2M} t) + C_i \quad (6.5)$$

where $A_{i1}, A_{i2}, \dots, A_{i2M}$ are constants determined by initial conditions, $\lambda_1, \lambda_2, \dots, \lambda_{2M}$ are the eigenvalues of Φ , and C_i is the steady state value of w_i . The time constant of the j -th exponential term is

$$\tau_j = \frac{1}{2k_0\lambda_j} \quad (6.6)$$

A strong signal produces a large eigenvalue and a weak signal produces a small eigenvalue. In a typical situation where the strongest signal is interference and the weakest signal is thermal noise, the ratio of maximum to minimum eigenvalues, the eigenvalue spread, is approximately

$$\text{Eigenvalue Spread} = \frac{\lambda_{\max}}{\lambda_{\min}} \approx M \frac{I}{N} \quad (6.7)$$

where I is the interference power and N is the thermal noise power. From Equation (6.6), there is a corresponding spread in the time constants of the weight response. This we will call the "time constant spread" (TCS).

The Modified-LMS feedback loop shown in Figure VI-2 satisfies the control law

$$dw_i/dt = 2k_m A \{ x_i(t) [R(t) - \sum_{j=1}^{2M} x_j(t) w_j - c \sum_{j=1}^{2M} x_j(t) dw_j/dt] \} \quad (6.8)$$

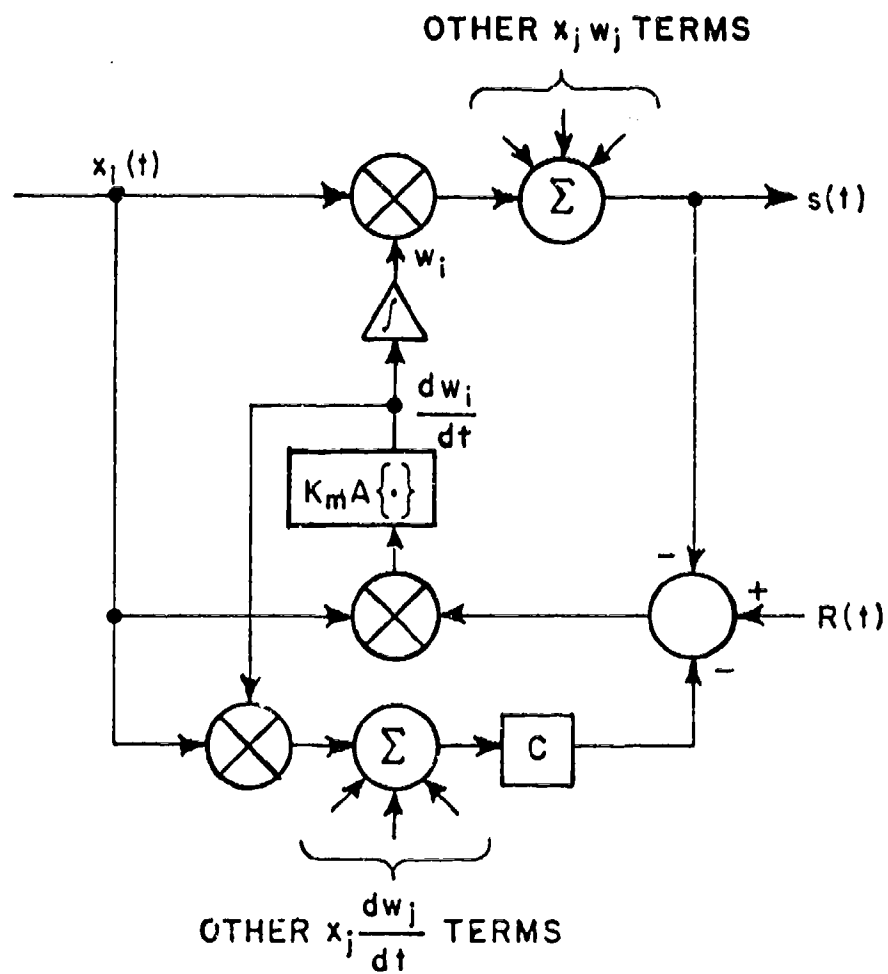


Figure VI-2. The modified feedback loop.

where $A\{\cdot\}$ is a finite time averaging operation and k_m is a gain constant for the Modified-LMS loop. The Modified-LMS loop is similar to the original LMS feedback loop except for the inclusion of the averaging operation $A\{\cdot\}$ and the additional feedback channel to form

$$c \sum_{j=1}^{2M} x_j(t) dw_j/dt$$

and subtract it from the reference signal. The added feedback channel will be called the weight derivative feedback channel hereafter. If we assume that the weights are slowly varying in comparison to the signals $x_i(t)$ and $R(t)$, and that the averaging operation is good enough so that $A\{XX^T\} = \Phi$ and $A\{XR(t)\} = S$, then we have

$$[I + 2k_m c \Phi] dW/dt + 2k_m \Phi W = 2k_m S \quad (6.9)$$

Note that Equation (6.9) has the same steady-state solution as for the original LMS array (Equation (6.4)) regardless of the value of c . A typical weight has the solution

$$\begin{aligned} w_i(t) = & A_{i1} \exp\{-[2k_m \lambda_1 t / (1 + 2k_m c \lambda_1)]\} \\ & + A_{i2} \exp\{-[2k_m \lambda_2 t / (1 + 2k_m c \lambda_2)]\} \\ & + \dots + A_{i2M} \exp\{-[2k_m \lambda_{2M} t / (1 + 2k_m c \lambda_{2M})]\} + C_i \end{aligned} \quad (6.10)$$

The j -th time constant in this transient response is

$$\tau_j = (1 + 2k_m c \lambda_j) / 2k_m \lambda_j \quad (6.11)$$

which may be compared with Equation (6.6) for the LMS algorithm. Note that as λ_j becomes large, τ_j does not become arbitrarily small as in Equation (6.6) but is bounded by c . By choosing c properly, we can limit the fast response speed of the array without limiting the maximum permitted input power to the array.

In the Modified-LMS loop, all of the time constants converge to c if $2k_m c \lambda_{\min} \gg 1$. To see the effects of k_m and c on the time constant spread the maximum and minimum time constants of the Modified-LMS loop can be normalized to the maximum time constant of the original LMS array:

$$\frac{1+2k_m c \lambda_{\min}}{2k_m \lambda_{\min}} / \frac{1}{2k_o \lambda_{\min}} = 1/k' + c \quad (6.12a)$$

$$\frac{1+2k_m c \lambda_{\max}}{2k_m \lambda_{\max}} / \frac{1}{2k_o \lambda_{\min}} = c' \quad (6.12b)$$

where $k' = k_m/k_o$ and $c' = c/(1/2k_o \lambda_{\min})$. In Equation (6.12b), $2k_m c \lambda_{\max} \gg 1$ is assumed. As explained below, k_m should be chosen so that this assumption is valid. The other normalized time constants of the Modified-LMS loop lie between $1/k'+c'$ and c' . As shown in Figures VI-3 and VI-4, the time constant spread ($TCS = 1 + 1/k'c'$) decreases as k' increases.

In the design phase, c should be chosen equal to the desired time constant and k_m chosen large enough so that c is the dominant term in Equation (6.11) for the weakest input signal (i.e., the smallest eigenvalue).

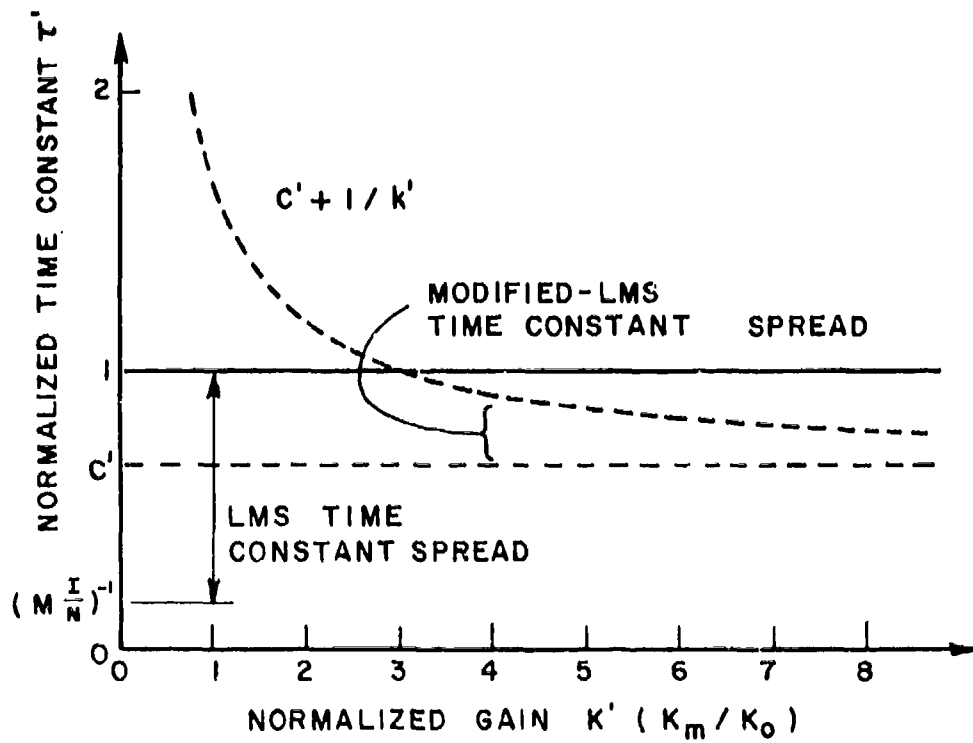


Figure VI-3. The normalized time constants for the modified-LMS loop.

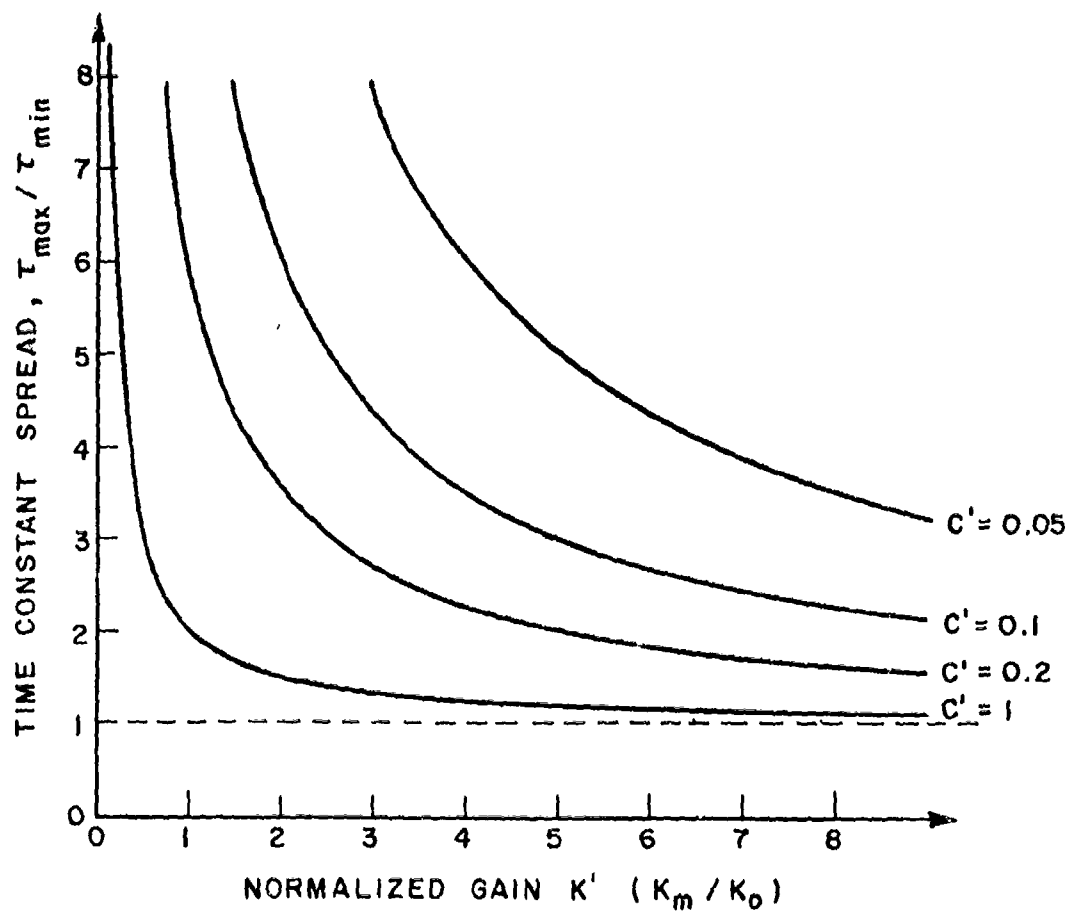


Figure VI-4. The time constant spread of the modified-LMS loop for several values of c' .

The finite time average in the loop of Figure VI-2 can be replaced with a single pole lowpass filter (LPF) [4]. The Modified-LMS feedback loop with a LPF transfer function $H(s)=1/(Ts+1)$ satisfies the differential equation

$$T \frac{d^2W}{dt^2} + [I + 2k_m c XX^T] \frac{dW}{dt} + 2k_m XX^T W = 2k_m XR(t) \quad (6.13)$$

where T is the time constant of the lowpass filter.

The transient behavior of the weights may then be found by replacing XX^T and $XR(t)$ by their average values (see Equations (6.3a,b)). With these substitutions the system in (13) becomes

$$T \frac{d^2W}{dt^2} + [I + 2k_m c \Phi] \frac{dW}{dt} + 2k_m \Phi W = 2k_m S \quad (6.14)$$

By making a coordinate rotation

$$W = RV \quad (6.15)$$

with R such that $R^{-1}\Phi R$ is diagonal, we find that v_i , the i -th component of V satisfies

$$T \frac{d^2v_i}{dt^2} + [I + 2k_m c \lambda_i] \frac{dv_i}{dt} + 2k_m \lambda_i v_i = 2k_m q_i \quad (6.16)$$

where q_i is the i -th component of the vector $R^{-1}S$.

As long as $2k_m c \lambda_i \gg 1$ and $c \gg T$, v_i has the solution

$$v_i(t) = \frac{K_i}{K_i - 1} [v_i(0) - \frac{q_i}{\lambda_i}] e^{-t/c} - \frac{1}{K_i - 1} [v_i(0) - \frac{q_i}{\lambda_i}] e^{-K_i t/c} + \frac{q_i}{\lambda_i} \quad (6.17)$$

where $K_1 = -\frac{c}{t} (1+2k_m c \lambda_1) - 1$.

For $K_1 \gg 1$ (which is usually the case), only the $e^{-t/c}$ term will be significant in $v_1(t)$ and hence the system will have the desired transient characteristics.

C. IMPLEMENTATION AND PERFORMANCE

As shown in Figure VI-2, the Modified-LMS Feedback Loop is an LMS array augmented with an additional feedback channel driven by the product of the derivative of the weight and the input signal. These modifications were implemented in the existing Satellite Simulator/Adaptive Null Steering Array [6] (SS/ANSA) by adding an additional feedback channel and inserting a lowpass filter (for averaging) into the baseband loop. Descriptions of the original LMS loop are given in [5] and [6].

Figure VI-5 shows a block diagram of the Modified-LMS loop as it was implemented. The components connected by the broken lines are the circuits for the weight-derivative feedback channel. The weight derivatives are amplified to match the input range of the weight-derivative multiplier.

The output of each in-phase weight-derivative multiplier is added to the three other in-phase weight-derivative multiplier outputs. Similarly, the outputs of the four quadrature weight-derivative multipliers are added. These sums are applied to a quadrature hybrid followed by a wideband amplifier stage, and a phase shifter. To

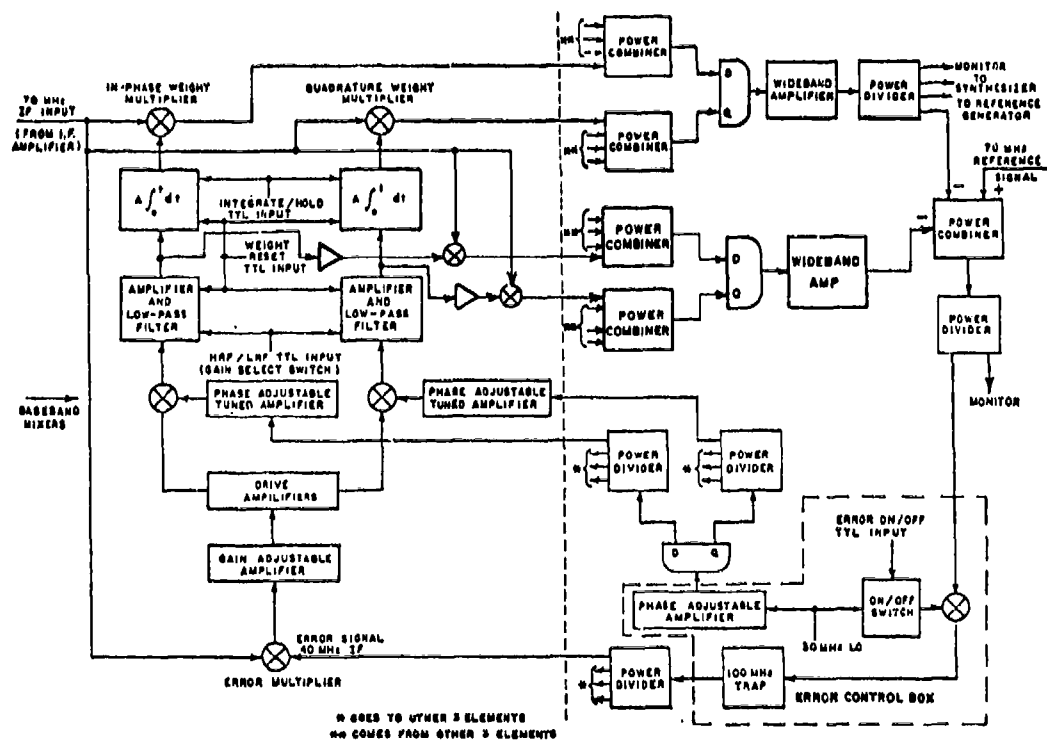


Figure VI-5. A block diagram of the modified-LMS loop implementation.

determine the effect of the weight-derivative feedback gain "c" a variable attenuator is placed before the error junction. The system can be returned to the original LMS configuration by bypassing the lowpass filter and disconnecting the weight-derivative feedback channel.

The lowpass filter was implemented with a resistor and a capacitor. The time constant T of the lowpass filter was chosen according to the formula

$$T = 2M/B \quad (6.18)$$

where B is the input signal bandwidth in Hz. and M is the number of antenna elements [2].

Figure VI-6(a,b) shows the weight behaviors of the original LMS and the Modified-LMS loops, respectively. The desired signal is generated by a single TDMA modem [7] operating in the low-rate format*. The desired signal level is approximately 4 mV p-p at each weight multiplier input. The thermal noise and the CW interference signal powers relative to the desired signal are 0 dB and 32 dB, respectively. The "flat-spots" which appear on the waveforms are due to an error-off function of the SS/ANSA. At the beginning of each data bit the error signal is gated off for a short interval. This is to compensate for a time delay problem in the SS/ANSA which causes the error signal to become large at the beginning of each bit. As shown in Figure VI-6a, the unmodified LMS algorithm exhibits very noisy weight behavior. This

*In the low-rate format data is sent as a Pseudo-Noise coded biphase constant envelope signal. The code and data rates are 175.2 KHz. and 10.95 KHz., respectively.

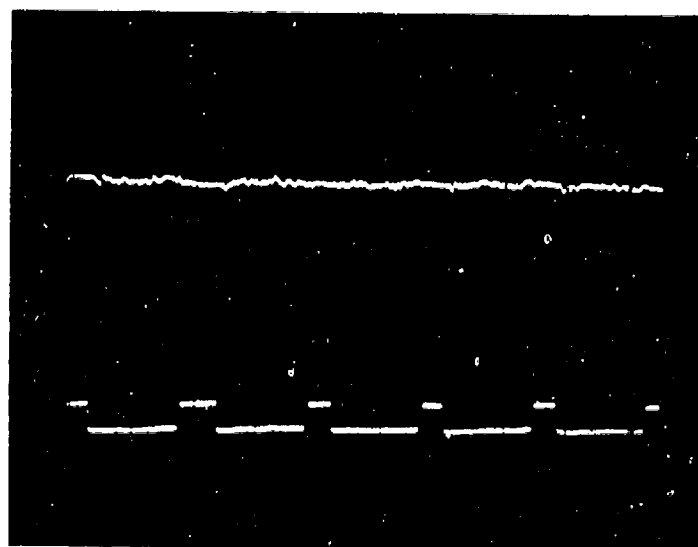
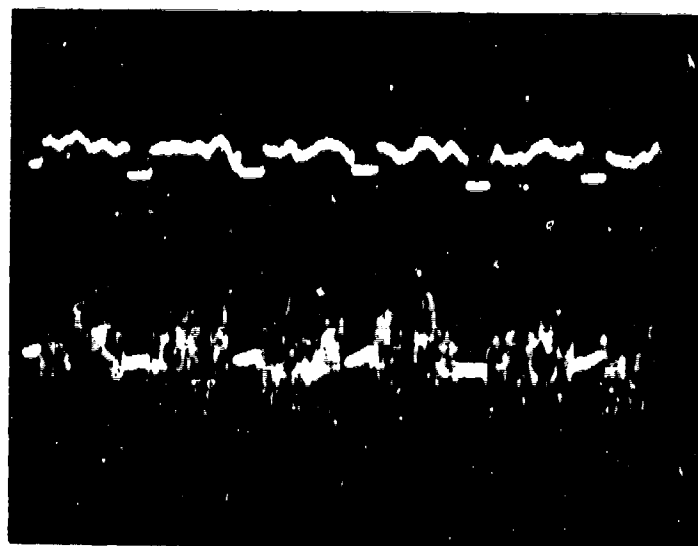


Figure VI-6. Waveforms of weights (lower trace) and their derivatives (upper trace). Horizontal: 50 μ sec/div.
(a) LMS array (b) Modified-LMS array.

is caused by the high power signal (the jammer) causing the speed of response to become very high. This, in turn, causes the weights to jitter excessively in response to noise on the input. In the Modified-LMS array, the weights are very well behaved. This is due to the limits placed upon the speed of response by the derivative feedback.

Figures VI-7(a) and VI-7(b) show the output spectra for the original and Modified-LMS arrays. The input signal strengths are the same as the case considered above. Figure VI-7(a) shows the biphase coded desired signal spectrum (the $\sin(x)/x$ pattern) with the jammer sticking out of the top. Although it may not be visible in the reproduction, the original photograph shows that the spectrum of the jammer is also somewhat spread. This is caused by a modulation of the CW jammer by the weights. When the weight response is too fast, the weights may impress the reference signal upon the jammer, so that the array can no longer distinguish between the desired signal and the interference. This situation, sometimes called the catastrophic failure mode, is being approached in Figure VI-7(a). Figure VI-7(b) shows the same signal scenario with the Modified-LMS array. Notice that the jammer is no longer visible in the output spectrum. This is the result of limiting the speed of response of the weights.

In order to evaluate the performance of the Modified-LMS array in a practical sense, a simulated satellite communications link was set up using the adaptive array for uplink protection. Bit error rate measurements were made over the simulated link for four different array configurations. These are:

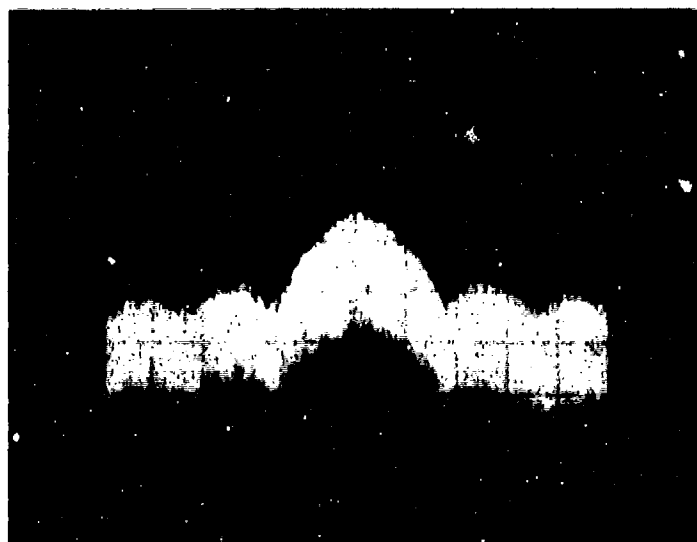
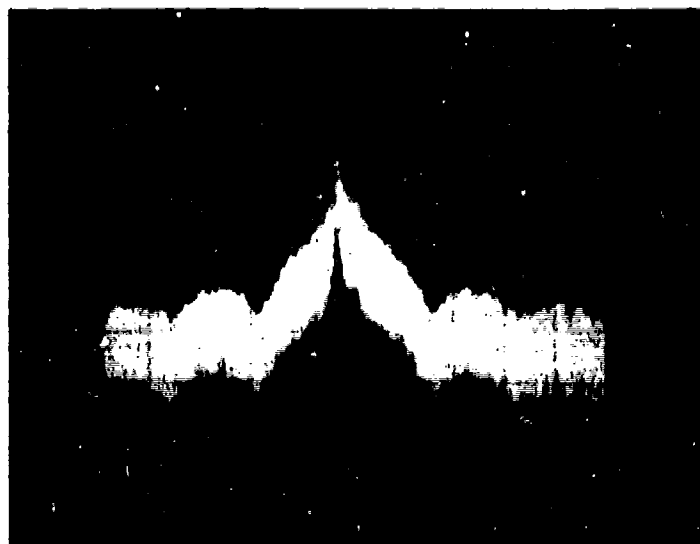


Figure VI-7. Spectrum of the array output. Horizontal: 100 KHz/div.
Vertical: 10 dB/div.
(a) LMS array (b) Modified-LMS array.

- 1) Original LMS loop without LPF (Average) in the baseband loop
- 2) Original LMS loop with LPF in the baseband loop
- 3) Modified-LMS loop without LPF
- 4) Modified-LMS loop with LPF

Testing was done both with and without the LPF because the unmodified LMS array sometimes exhibits a damped oscillatory weight behavior with the additional LPF. This phenomenon has been observed previously [5]. The Modified-LMS does not exhibit this property.

Figures VI-8 and VI-9 show the measured bit error rates as a function of the uplink jamming power. Here the uplink signal to noise ratio was set at 0 dB. Enough downlink noise was added to insure a moderately high bit error rate. Figure VI-8 was obtained with a continuously transmitted desired signal whereas Figure VI-9 was obtained for a pulsed desired signal. Both figures show very similar data. For high jammer powers, the Modified-LMS shows at least a 4 dB improvement. It is believed that the improvement would have been much greater had the testing been carried out for even larger jammers. However, testing was limited to the jammer powers shown because the amplifiers in the front end of the SS/ANSA were beginning to saturate. Notice also that the Modified-LMS array shows no degradation in performance when compared to the unmodified array for lesser jamming powers. This is equally important, since the power level of a jamming signal cannot be anticipated.

During the course of these experiments, it was observed that the Modified-LMS array was somewhat sensitive to the alignment of the derivative weight multipliers. These multipliers are implemented with the four quadrant transconductance multipliers described in [8]

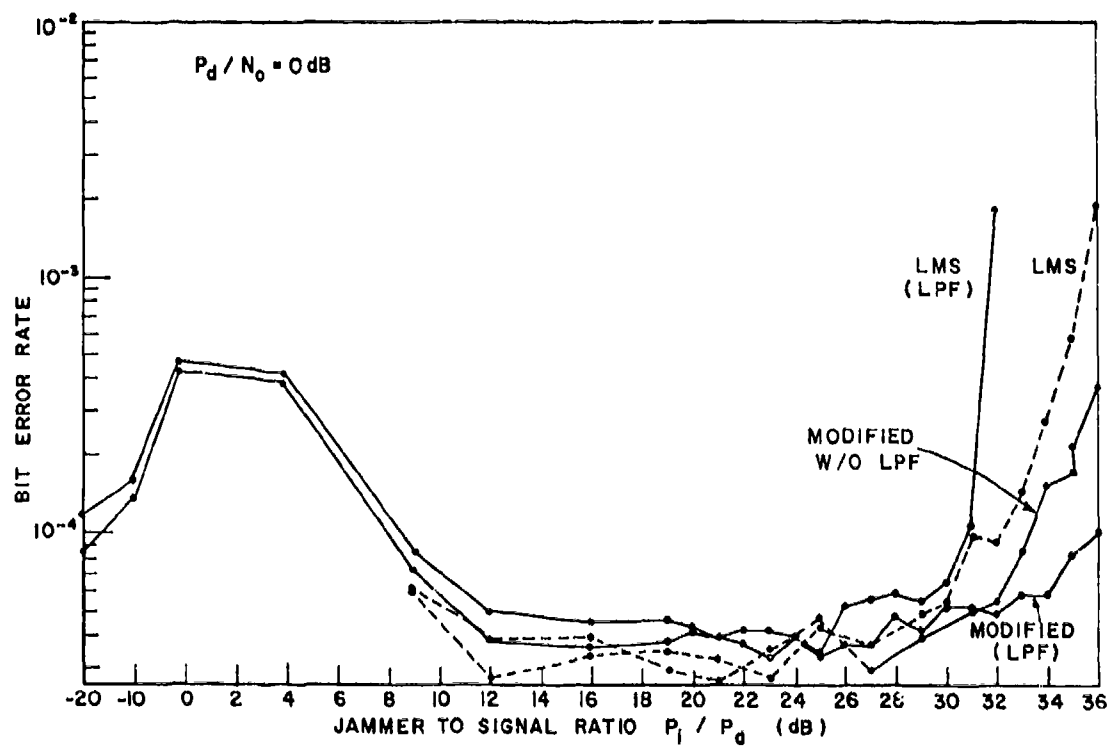


Figure VI-8. Bit error rate vs jammer to signal ratio for four different adaptive array configurations with pulse desired signal.

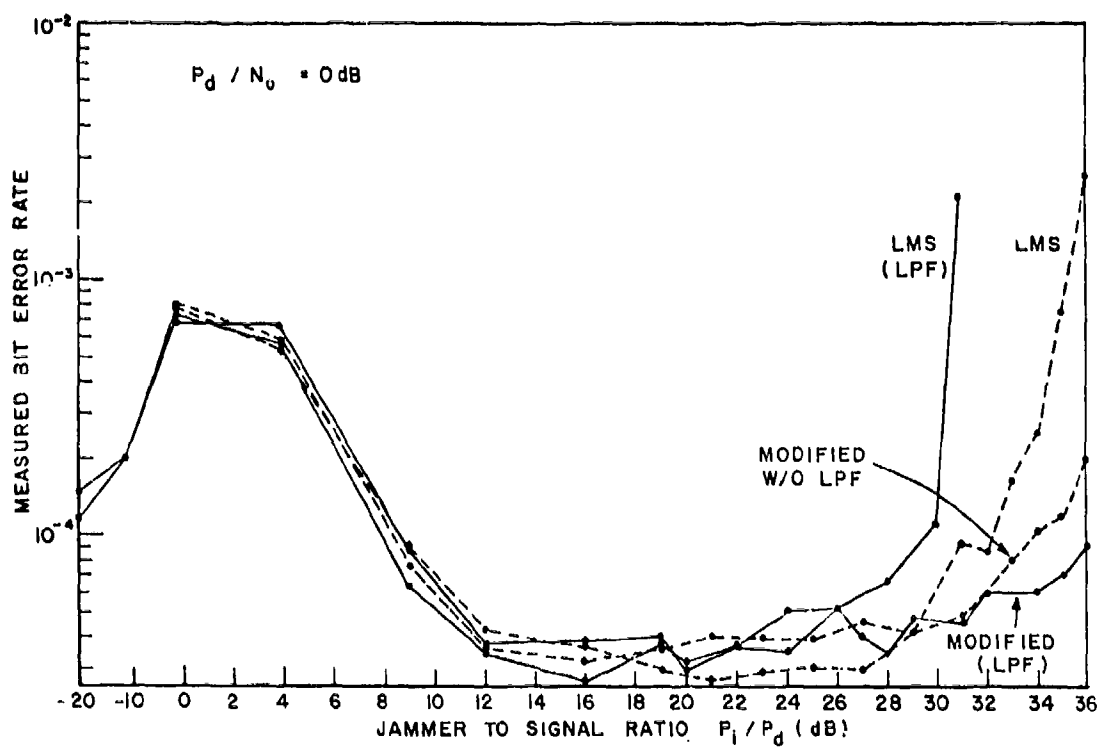


Figure VI-9. Bit error rate vs jammer to signal ratio for four different adaptive array configurations with continuous desired signal.

and require periodic alignment to counteract thermal drift. If misaligned, it was found that the speed of response could still be adjusted by changing the gain constant c , but these changes were accompanied by undesirable changes in the steady state values of the weights. From Equation (6.13) one might conclude that the steady state values of the weights are independent of the value of c . When properly aligned, this is so (at least very nearly so). When misaligned, this is not the case. The cause of this problem is feedthrough through or around the multiplier. Figure VI-10 shows a comparison between an "ideal" multiplier and an actual multiplier. Ideally, when the weight voltage is zero the multiplier output should also be zero. Feedthrough allows the output to be non-zero even with zero weight voltage. Since this seems to be a potential problem, the effects of feedthrough on the Modified-LMS array are analysed below. As a practical note, it was found experimentally that even though some feedthrough was always present the cumulative effect on the steady state weights could be minimized by balancing the feedthrough from one multiplier with opposite feedthrough from another channel.

D. MULTIPLIER FEEDTHROUGH

Feedthrough is the amount of "leakage" between the multiplier IF input and IF output ports caused by circuit mismatches and stray capacitances. With the multiplier feedthrough, the Modified-LMS loop can be modeled as in Figure VI-11. The parameters f_i and g_i are leakage terms around the weight and derivative multipliers, respectively. These are assumed constant for a given input signal scenario.

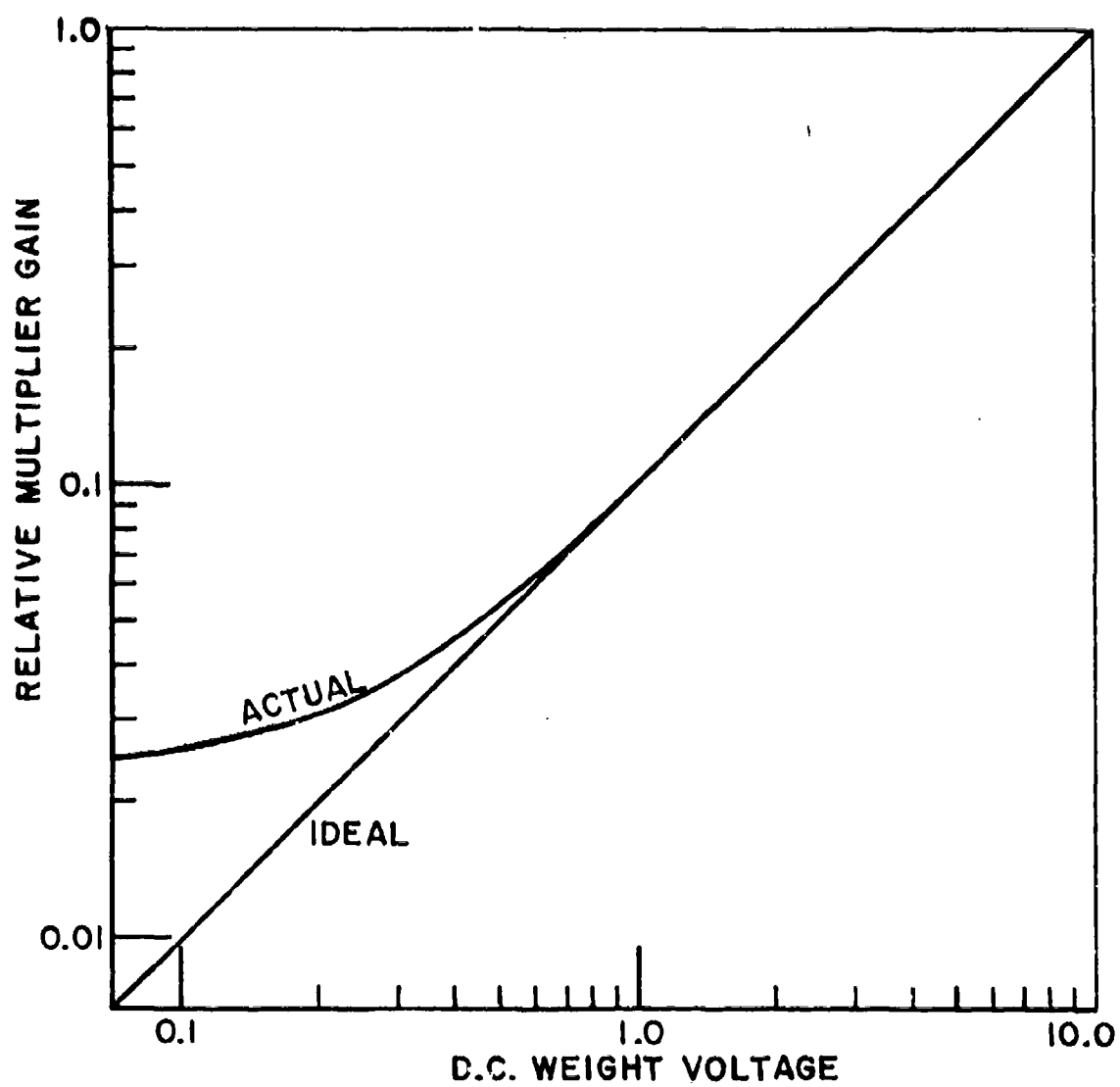
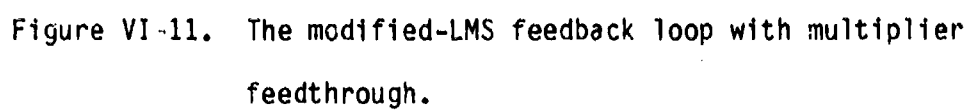


Figure VI-10. Weight multiplier characteristics.



The array output and the weight-derivative feedback signal can be expressed as follows:

$$s(t) = \sum_{j=1}^{2M} x_j(t)[w_j(t) + f_j] \quad (6.24)$$

$$\gamma(t) = \sum_{j=1}^{2M} x_j(t) \left[\frac{dw_j(t)}{dt} + g_j \right] \quad (6.25)$$

The differential equation governing the array modeled in Figure III-11 is then given by

$$T \frac{d^2 W}{dt^2} + [I + 2kc] \frac{dW}{dt} + 2k\phi W = 2kS - 2k\phi F - 2kc\phi G \quad (6.26)$$

where

$$F = \begin{bmatrix} f_1 \\ f_2 \\ \vdots \\ f_{2M} \end{bmatrix} \quad G = \begin{bmatrix} g_1 \\ g_2 \\ \vdots \\ g_{2M} \end{bmatrix} \quad .$$

The weight vector has the steady state solution

$$W(t) = \phi^{-1} S - F - G \quad (6.27)$$

The steady-state array output signal, obtained from Equations (6.24) and (6.27), is given by

$$\begin{aligned} S(t) &= \sum_{j=1}^{2M} x_j(t)[w_j(t) + f_j] = X^T W + X^T F \\ &= X^T W_{opt} - X^T G \end{aligned} \quad (6.28)$$

where $W_{opt} = \phi^{-1} S$ is the weight needed for optimizing the output signal to noise ratio [9]. Thus, the multiplier feedthru not only biases the steady-state weight vector, but also affects the output signal-to-noise ratio. Note that although both f and g affect the steady state weights, only the feedthrough in the weight-derivative feedback channel (g) affects the output signal.

E. CONCLUSION

An improved feedback loop for adaptive arrays proposed by Compton [2] has been demonstrated experimentally. This Modified-LMS feedback loop reduces weight jitter and undesirable modulation effects by limiting the fast time constants to reasonable values. In the unmodified LMS array these time constants are proportional to the input signal powers and for large signals can become too fast. By limiting the speed of response of the array, these larger signals no longer cause problems and the dynamic range of the array can be extended. Both the speed of response properties and the dynamic range extension of the adaptive array were observed in these experiments.

Although the concept of the Modified-LMS array has been experimentally verified, the experiments performed indicate some areas which require further research. First, the problem of multiplier feedthrough should be resolved. Perhaps processing at an intermediate frequency could be used to advantage. This technique is being used successfully in the cascaded array for similar problems. Alternately, better multipliers can be developed. Secondly, the problem of limiting with high powered signals needs to be addressed. In the present experiments limiting in the front end amplifiers prevented more

dramatic improvements. Since the algorithm no longer limits the dynamic range, all of the hardware should be examined to maximize the dynamic range properties of the array. Finally, although the Modified-LMS algorithm provides a method of controlling the speed of response of the weights, it is not clear what the optimal speed of response is. Obviously, one would want to null a jammer as quickly as possible, but the adaptive array cannot be made arbitrarily fast without deleterious effects from weight modulation. How fast an array should be is at present a subject for future research.

F. REFERENCES

- [1] B. Widrow, P.E. Mantey, L.J. Griffiths, and B.B. Goode, "Adaptive Antenna Systems," Proc. IEEE, vol.55, p. 2143, December, 1967
- [2] R. T. Compton, Jr., "Improved Feedback Loop for Adaptive Arrays," IEEE Trans. Aerospace and Electronic Systems, vol. AES-16, p.159, Mar. 1980.
- [3] K. Suen, "A Study of Eigenvalue Behavior in Adaptive Arrays," Technical Report 713603-2, Aug. 1981, The Ohio State University ElectroScience Laboratory, Department of Electrical Engineering; prepared under contract No. N00019-81-c-0093 for Naval Air Systems Command.

- [4] R. T. Compton, Jr., "Adaptive Antennas," To be published.
- [5] T. W. Miller, "The Transient Response of Adaptive Arrays in TDMA Systems," Technical Report 4116-1, June 1976, The Ohio State University ElectroScience Laboratory, Department of Electrical Engineering; prepared under Contract F30602-75-C-0061 for Rome Air Development Center.
- [6] T. W. Miller, R. Caldecott, and R. J. Huff, "A Satellite Simulator with a TDMA-System Compatible Adaptive Array," Report 3364-4, January 1976, The Ohio State University ElectroScience Laboratory, Department of Electrical Engineering; prepared under Contract F30602-72-C-0162 for Rome Air Development Center.
- [7] R. C. Taylor and R. J. Huff, "A Modem/Controller For TDMA Communication Systems," Technical Report 3364-5, August 1976, The Ohio State University ElectroScience Laboratory, Department of Electrical Engineering; prepared under Contract F30602-75-C-0061 for Rome Air Development Center.
- [8] W.G. Swarner, "Advanced TDMA Techniques and Bit Synchronous Design and Array Component Evaluation," Final Report 710300-5, April 1979, The Ohio State University ElectroScience Laboratory, Department of Electrical Engineering; prepared under Contract F30602-75-C-0061 for Rome Air Development Center.
- [9] C.A. Baird and C.L. Zahm, "Performance Criteria for Narrow Band Array Processing", 1971 IEEE Conference on Decision and Control, Miami Beach, Florida, December 15-17, 1971.

SECTION VII

COMMUNICATION SYSTEM APPLICATIONS STUDY

The effort under this heading involved a review of the pertinent literature with the objective of assessing promising technologies for DAMA applications in a predominantly TDMA context. The most prominent development observed was that of Packet Switching [1] which seems to be very successful in computer communication and is drawing increasing interest for general purpose satellite communication [2] and possibly military applications [3]. In fact, the original introduction of the packet switching idea by Baran [4] in 1964 was for survivability of a communication network in a hostile environment. As the name of the above work "On Distributed Communication" implies, the "distributed" aspect was the key element in the survivability feature of the proposed approach. The fact that the information flow is not constrained to follow a unique path, but has a number of optional paths through nodes dispersed over a wide spatial range, increases significantly the likelihood of the information reaching its destination--eventually. Another appealing aspect of packet switching is the resource sharing feature which permits a very large number of low duty factor users to use rather limited resources. This again is of importance to the military that must provide means of communication to a very large number of small (often mobile) terminals that most often, however, require only slow data rates and rather infrequently. Thus, in principle, packets transmitted by the various terminals would distribute themselves such

as to use efficiently the available communication links rather than hold captive dedicated circuits or links which would be idle most of the time. The various packet switching schemes have been well documented including a special issue of the Proceedings of the IEEE which thoroughly examines various aspects of the subject from the original conception to recent applications and implementations [1]. Therefore, no attempt will be made here to review this voluminous literature. Certain concerns, however, regarding the use of packet switching for Air Force communication needs will be discussed and possible approaches to alleviate them somewhat will be proposed.

First, consider the random aspect of the communication link in a packet switching system. It is this aspect which contributes to the survivability feature of the system in that each packet can travel various alternate routes with the actual route taken dependent on the traffic and equipment available at the time. It is, however, this unpredictability which makes the communication link risky for the user. Indeed, reliability which is directly related to predictability may be of paramount importance in certain situations. Measures of performance such as efficiency and throughput are very important in general, but in an emergency situation it is response time that is critical. It is not very helpful to know that on the average, the response time of the system is a fraction of a second but at the specific time of need, a link cannot be established for a long time. It was in recognition of this problem, as well as the attempt to accommodate voice which requires a fixed minimum sampling rate, that the the Priority Oriented Demand Assignment (PODA) protocol was proposed [2]. In TDMA channelization,

this involves the centralized assignment of time slots for high priority users and distributed assignments of slots to others. This assignment refers to a control subframe where the high priority users have fixed slots through which they can request time in the information subframe, they thus have continuous access to the satellite--this protocol is termed Fixed Priority Oriented Demand Assignment (FPODA) and is equivalent to a fixed slot in the order wire of a regular TDMA circuit switched system.

The PODA system recognizes the variety of priority levels and is a hybrid system including circuit switching for cases where access must be guaranteed and lower priority levels for users with varying requirements which are put in the proper place of a packet switched queue in accordance to an ordering algorithm.

In contrast with the above hybrid approach, pure packet switching systems have been proposed for military networks which appear to have the required guarantees of access. An example is described in a recent paper by Mowafi and Kelly [3] which proposes a "virtual circuit" which sets up a "fixed path through the network for the duration of a transaction." The method involves sending a trailblazer packet establishing the path through the various nodes of the network. The problem with the approach is that in the case of an emergency there would be numerous trailblazing packets that will most likely collide and destroy each other with no circuit established at all. Pure packet switching moreover, is normally designed for average and not peak traffic. But during emergencies which military communication must accommodate, the traffic is likely to reach a peak, and thus cause a failure at the worst time.

A packet switching scheme which may provide at least a partial solution to the above problem was described in a paper by Derosa and Ozarow [5], whose objective was to improve efficiency of packet switching satellite communication [6]. The proposed approach involves a digital processing satellite with multiple uplink (FDMA) channels and a TDM downlink. The availability of multiple uplink channels drastically reduces packet contention and permits the efficient utilization of the main resource, the downlink. This approach could provide a much more reliable communication system even at peak traffic periods, unless of course the downlink is saturated. Sudden bursts of traffic can be accommodated if an appropriately large buffer is provided on board, which could then channel the buildup in an orderly fashion on the downlink with close to 100% efficiency. The cost of a few additional uplink channels seems to be rather small compared to the expansion of the whole net to provide a dedicated circuit to each user.

As mentioned above, packet switching is particularly suitable for distributed control schemes. And, distributed control appears to provide better survivability in the sense that the communication net does not depend on one controller. Some of the disadvantages of the distributed control are high response time, indeed unpredictable, and low allocation flexibility. It appears, however, that survivability in a hostile, i.e., heavily jammed environment is also questionable. Since each terminal acts on its own depending on the information available to it, there is a high probability of improper transmissions by some terminals due to incomplete or erroneous information, particularly in times of stress. And once some of the terminals transmit in the wrong time, the system is very likely to break down

since the traffic will quickly back up, considering that an emergency exists and more urgent traffic is generated. It is thus felt that at least hybrid control should be used, with apportionment between central and distributed controls kept flexible and adapting to the situation. The last but, unfortunately not least disadvantage of the packet switching approach is in connection with the adaptive array which is most likely to be used for the uplink protection of military communication satellites. Each packet would have to include in its header, a preamble with the proper code that would allow its entry into the receiver. This would be rather time consuming since the adaptive array must respond with proper weight adjustments which would be rather slow since the signal level is usually low, especially from mobile users such as aircraft. A similar problem of course, would be present in a circuit switched system utilizing beam hopping. The difference, however, is that in the circuit switched beam hopping system, the beam returns to the same terminal at a predictable time in the multiplexing sequence and the adaptive array weights can be stored and recalled after the first acquisition period. Thus, the first time slot can be completely devoted to the acquisition process with the following ones requiring only minor adjustments. In the packet switching case, however, each packet arrives from an unpredictable direction requiring the whole acquisition process to repeat. Here again, centralized control could be helpful in assigning slots in the frame on a periodic, predictable basis.

The general conclusion reached from this study into packet switching is that it is a very attractive approach for commercial uses and can obtain high efficiencies by dynamic resource sharing and would

be particularly effective with the introduction of processing satellites. Its promise for military uses, though, especially in hostile and jammed environments, appears to be rather limited.

A. REFERENCES

- [1] Special Issue on Packet Communication Networks, Proceedings of the Institute of Electrical and Electronic Engineers, Vol. 66, No. 11, November 1978.
- [2] "General Purpose Packet Satellite Networks", Jacobs, I.M., et al., Proceedings IEEE, Vol. 66, No. 11, pp. 1448-1467, November 1978.
- [3] "Integrated Voice/Data Packet Switching Techniques for Future Military Networks", Mowafi, O.A., and W.J. Kelly, IEEE Transactions on Communications, Vol. COM-28, No. 9, pp. 1655-1661, Sept. 1980.
- [4] "On Distributed Communication", P. Baran, et al., Vols. I-XI RAND Corporation Research Documents, August 1964.
- [5] "Packet Switching in a Processing Satellite", Derosa, J.K. and L.H. Ozarow, Proceedings of IEEE, Vol. 66, No. 1, pp. 100-102, January 1978.
- [6] "Efficient Packet Satellite Communications", J.K. Derosa, et al., IEEE Transactions on Communications, Vol. COM-27, No. 10, pp. 1416-1422, October 1979.

SECTION VIII

CONFORMAL ARRAYS ON C-135 AIRCRAFT FOR SATELLITE COMMUNICATION

A. INTRODUCTION

The design of a conformal array antenna for an aircraft requires the overall aircraft structure such as the tail and wing surfaces to be included in the analysis. The reflection and diffraction effects caused by these surfaces and effects of diffraction around the curvature of the fuselage must be included.

The objectives of this investigation include an analysis of the performance of a large conformal array or a set of subarrays mounted on a KC-135 aircraft. The pattern performance and array design optimization will be studied.

The following assumptions concerning the conformal array will be used.

1. The array is to be used for communication with a geostationary satellite at 135 degrees west longitude.
2. Circular polarization will be used, but polarization diversity (one data channel with RHC and one with LHC), will not. Cross polarization properties of the antenna, therefore, will contribute to loss of signal, but not to cross channel interference.
3. A maximum of 4096 array elements will be used on each large array.

The geometrical theory of diffraction (GTD) was used to model KC135 aircraft fuselage, tail, and wing effects. A mathematical model of the fuselage (prolate spheroid) tail, and wings (4 cornered plates) was used. This model was incorporated into a computer program which allowed an antenna element to be mounted on the structure and which used the GTD to compute the electromagnetic radiation patterns from the antenna element [1].

The accuracy of the GTD solution approach is well documented. Numerous comparisons with experimental aircraft measurements have established the applicability of the GTD at UHF frequencies and above. In fact, one of the first major evaluations of the GTD approach was performed on a KC-135 aircraft [2].

The initial phase of this study concerned the blockage that the aircraft structures introduced in the desired coverage region. It was soon discovered that the problem of blockage was not a major problem. If the antenna is mounted on the fuselage forward of the wings and centered at 45 degrees from the top of the fuselage, the tail blockage can be shown to be not in the hemisphere of interest, and in any case less than one degree wide. Also, the tail structure is so small that it is unable to block more than a small percentage of the elements of a large conformal array. The major blockage is due to the wing area, and that blockage is in the lower hemisphere with respect to the aircraft. Since the requirement is for the aircraft to communicate with a geostationary satellite while flying over the central United States, wing blockage is of low probability, as will be shown.

The study next focused on gain degradation due to polarization mismatch as well as wing reflection nulling of particular groups of antenna elements. These effects produce reduced gain in the region of interest. The study of this problem involved the mapping of the upper hemisphere (left side of aircraft for left array, and right side of the aircraft for the right array) signal strength from a selected group of individual circularly polarized antenna elements. These element pattern maps were then combined to give a picture of the directive gain of the array as a function of boresite direction.

Discussions of these results will be given below.

B. BLOCKAGE EFFECTS

The initial stage of this research involved a study of the effects of blockage and techniques for mitigating blockage. In order to study the extent of the blockage problem, the GID computer program [1] was used to make plots of the far field signal from circularly polarized antenna elements located at selected positions on the fuselage of the KC135.

1. The Aircraft Model

The model of the KC135 which was used here is described in Table VIII-1 and in Figure VIII-1. Note that the computer program which is used to compute the antenna element pattern [1] requires that the structure be described using a prolate spheroid for the fuselage and flat plates for the wings and vertical stabilizer. The coordinates of

TABLE VIII-1

PARAMETERS OF MODEL OF THE KC135 AIRCRAFT

(SEE REFERENCE 1)

PROLATE SPHEROID MODEL HAS THE FOLLOWING DIMENSIONS IN INCHES:						
MINOR AXIS = 3.000, RADIUS = 3.0, MAJOR AXIS RADIUS = 80.0						
THE PATTERN ORIGIN LOCATION IN INCHES IS GIVEN BY THE FOLLOWING						
DIMENSIONS: X = 0.000, Y = 0.000, Z = 0.000						
WINGS (1:25 SCALE) PLATES ARE ATTACHED TO FUSELAGE BY PROGRAM						
RIGHT WING			LEFT WING			
INPUT LOCATION IN INCHES			INPUT LOCATION IN INCHES			
X	Y	Z	X	Y	Z	
-1.000	3.000	12.310	-1.000	-3.000	24.610	
-1.000	28.500	36.410	-1.000	-28.500	40.410	
-1.000	28.500	40.41	-1.000	-28.500	36.410	
-1.000	3.000	24.610	-1.000	-28.500	36.410	
VERTICAL STABILIZER - PLATES ARE ATTACHED TO FUSELAGE BY PROGRAM						
LEFT STABILIZER			RIGHT STABILIZER			
INPUT LOCATION IN INCHES			INPUT LOCATION IN INCHES			
X	Y	Z	X	Y	Z	
2.946	0.500	55.672	2.946	0.000	49.492	
14.076	0.500	64.205	14.076	0.000	58.025	
14.076	0.000	58.025	14.976	-0.500	64.205	
2.946	0.000	49.492	2.946	-0.500	55.672	
CROSSED SLOT (RHC) (1/2 X 1/10 LAMBDA)						
THERE ARE 2 SOURCES IN THIS COMPUTATION						
PHASE CENTER: ROLL ANGLE = 65.0°; Z AXIS DISPLACEMENTS = 10.950"						
SOURCE	TYPE	BETA	LENGTH	EXCITATION MAG	PHASE	
1	SLOT	0.00	0.01, 0.03	1.00	0.00	
2	SLOT	-90.00	0.01, 0.03	1.00	90.00	
FQ: 7.57 GHz = T/R MID FREQ (1:25 SCALE)						
THE FOLLOWING FREQUENCY DIMENSIONS ARE IN GIGAHERTZ:						
NFREQ = 1	FREQI = 189.250	DFREQ = 1.000				

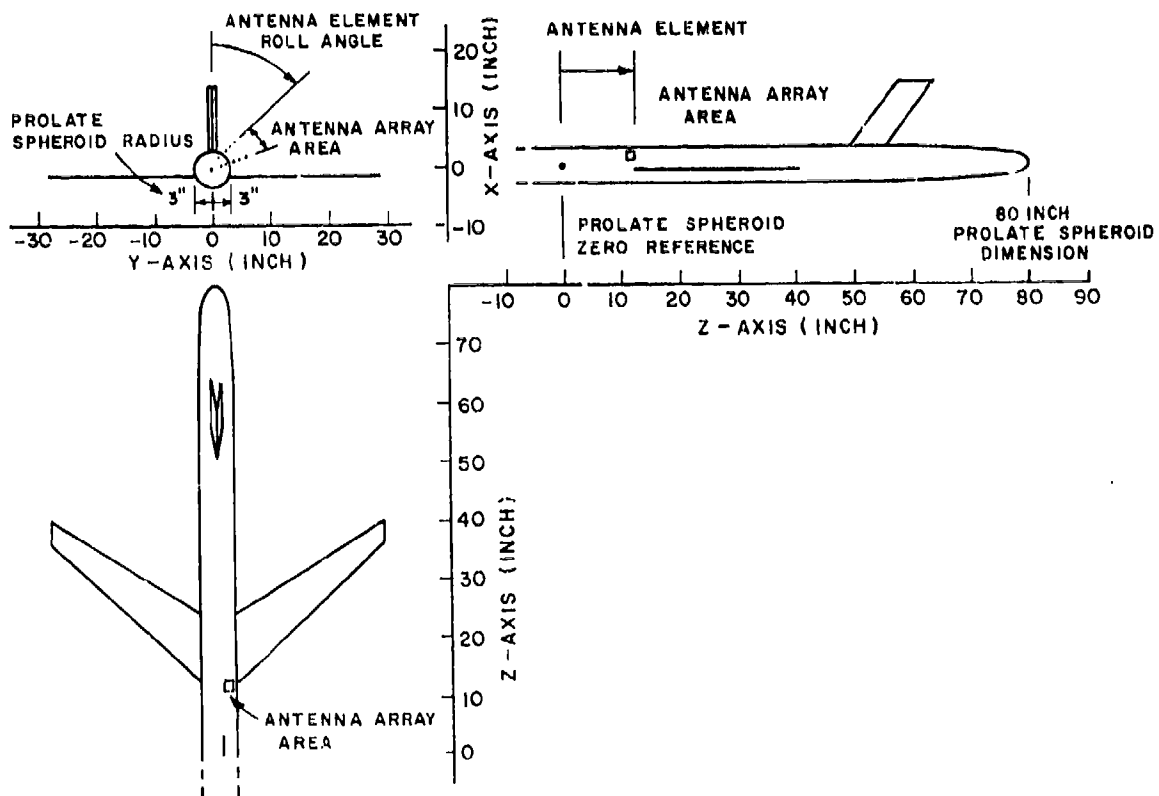


Figure VIII-1. Prolate spheroid model of KC135 with attached plates.

the corners of the plates are used to describe the plates in this computer program. For this task, the units used in the model are inches and the aircraft size has been scaled by a factor of 25. The origin of the coordinate system is chosen to be the center of the prolate spheroid. The nose section of the aircraft is thus not very well modeled. The nose section is in the shadow region of the fuselage mounted antenna elements, however, and the nose section discrepancies will not cause significant errors.

2. Example Far Field Plot

An example of a particular field plot is shown in Figure VIII-2. In this plot, the signal level (far field) for a conical scan is shown. The scan is 38 degrees off the fuselage axis. This conical scan was chosen because it passes through the wing of the aircraft, a direction which produces maximum scattering variation.

As can be seen in the plot, the effect of the wing is to produce rapid scintillation of the pattern in the neighborhood of 90 degrees. These scintillations are nearly 10 DB in magnitude.

The study of the blockage effects involved a large number of such antenna patterns. In general, it was seen that the tail of the aircraft was not a significant blockage contributor, and that the wing could block only below the aircraft upper hemisphere. The significance of such blockage depends on the application of the conformal array. In this case the purpose of the conformal array is to provide communication with a geostationary satellite at 135 degrees west longitude. A plot of

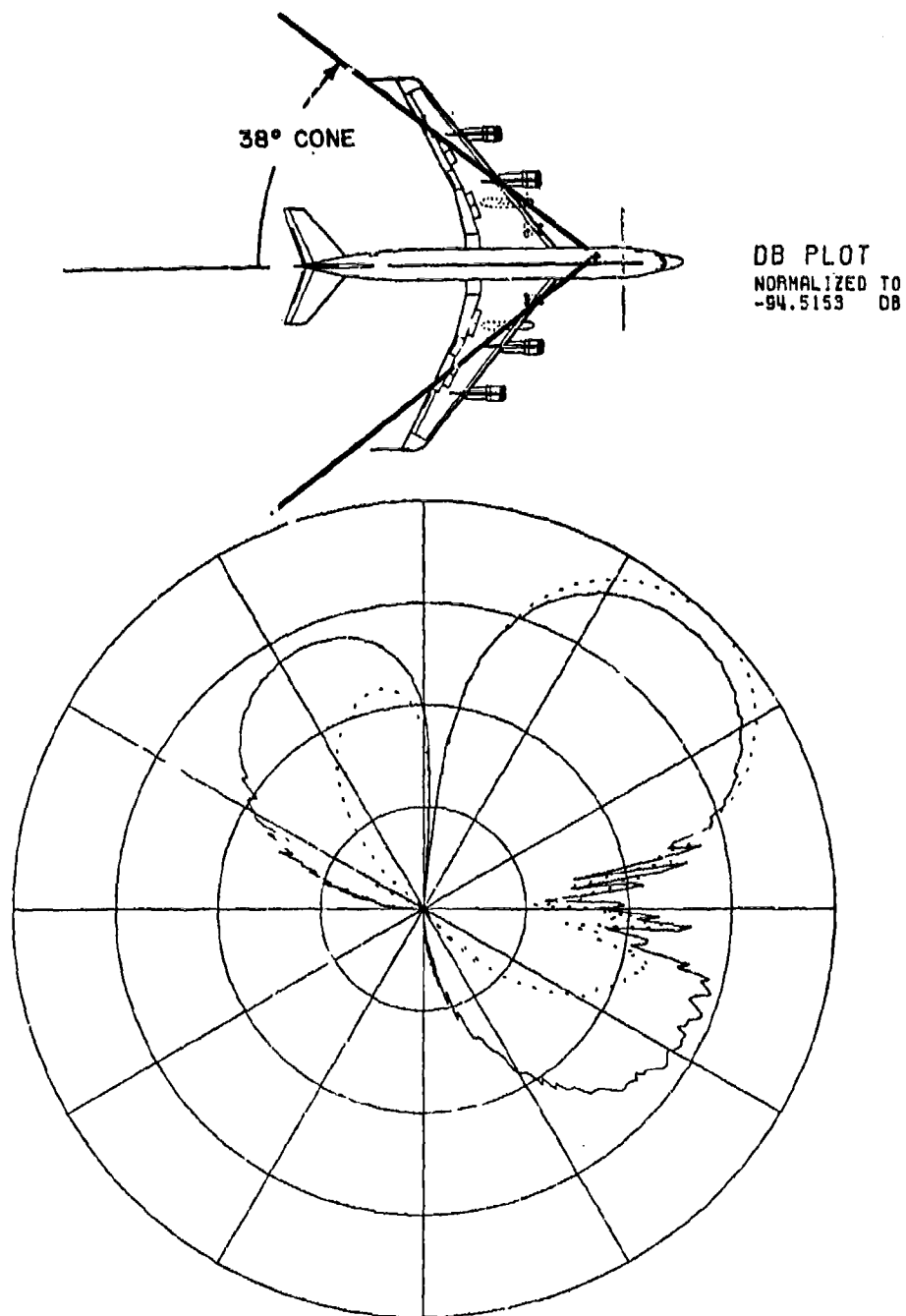


Figure VIII-2. Field plot for single antenna element. Scan angle is 38° off fuselage axis.

the elevation angle of this satellite as a function of geographic location is shown in Figure VIII-3. If the operational area of the aircraft is restricted as shown, it is clear that the necessary performance of the antenna is as shown in Figure VIII-4.

Figure VIII-4 also shows the required coverage of the aircraft antenna if the aircraft is allowed to bank by as much as 40 degrees. The figure was derived by considering the angle from the zenith to the satellite when the aircraft is flying straight and level. Then, if the maximum aircraft angle of bank is 40 degrees, and the pitch excursions are restricted to be much less than the angle of bank, the curve in the middle of the figure moves to the right or to the left by 40 degrees. (Pitch angle variations are quite small during operation of a transport aircraft of this type at operational altitudes.) It is interesting to note that there is an area near vertical (with respect to the aircraft frame of reference) where the satellite is not found. It can also be seen that there is a low probability that the direction to the satellite is off the aircraft nose or tail. This is particularly fortunate since the nose and tail regions are intrinsically difficult regions in which to form a beam with a conformal phased array.

C. SINGLE ELEMENT PATTERNS

In order to describe the behavior of a particular antenna element, it was decided to create a map of the upper hemisphere far field pattern. We are considering a left fuselage and a right fuselage array, and thus this map need only cover the half of the upper hemisphere which is of interest to a particular array. If the line of sight to the satellite is left of the aircraft, the left array will be activated,

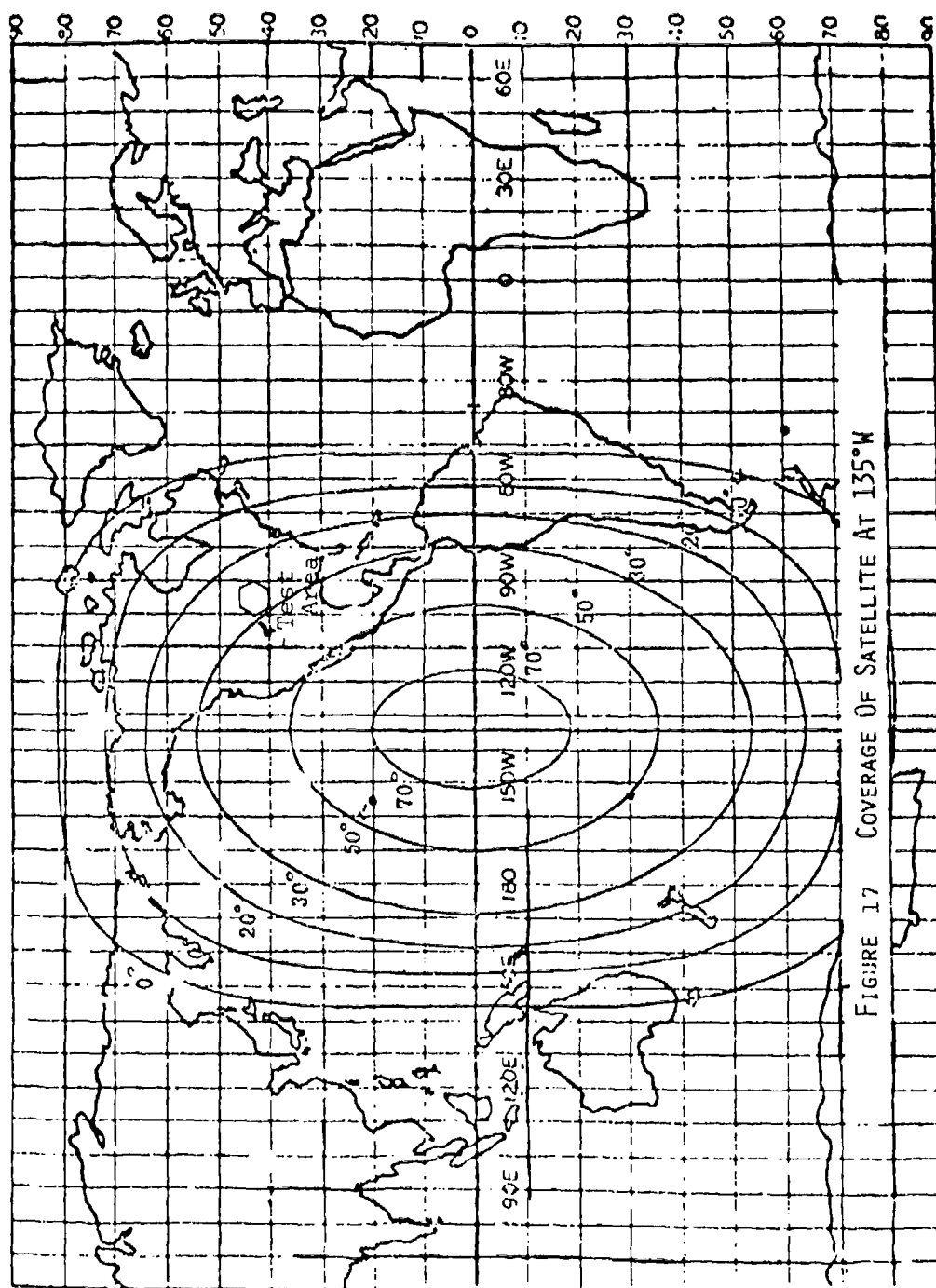


Figure VIII-3. Elevation angle to geostationary satellite located at 135° west longitude as a function of geographic location.

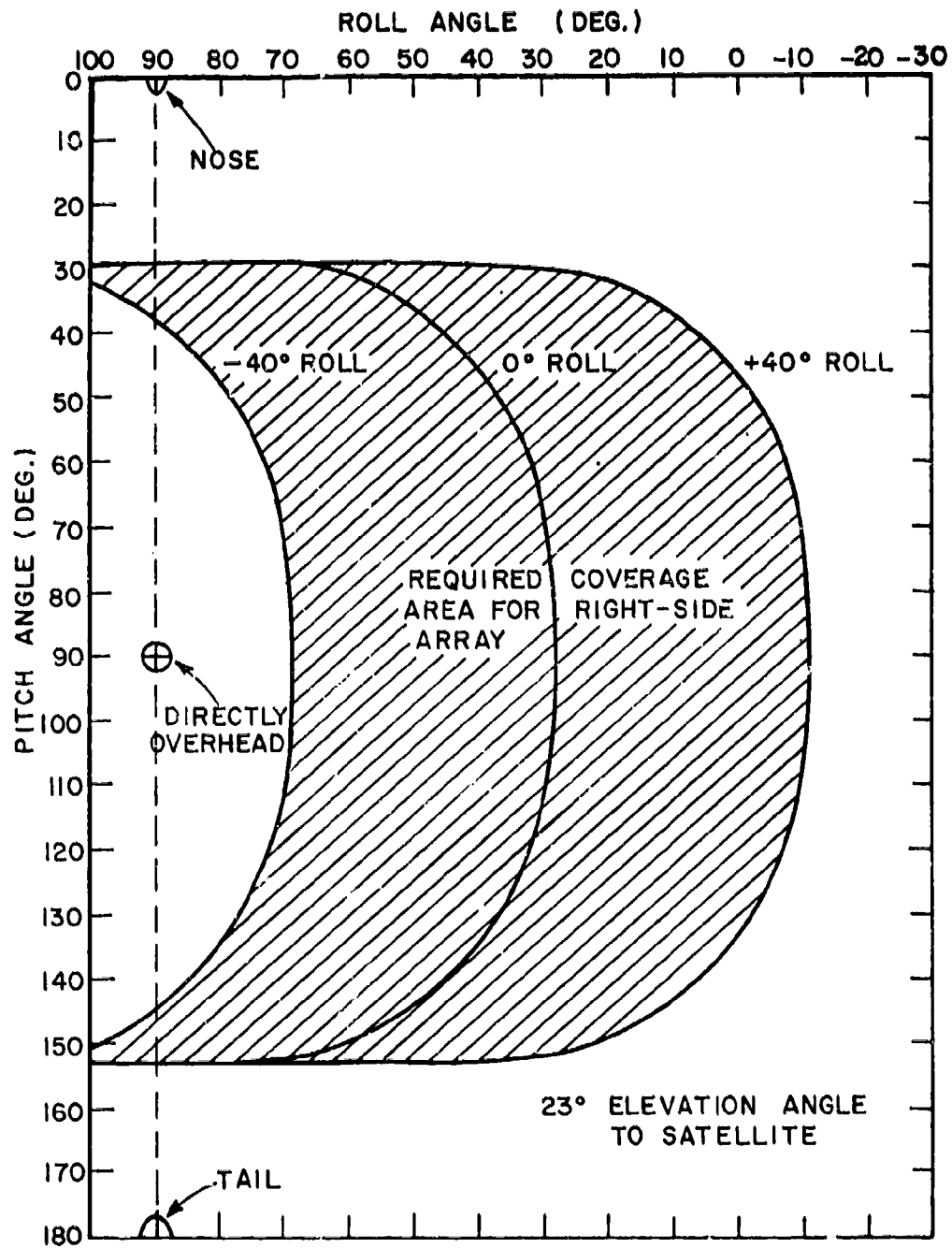


Figure VIII-4. Operational performance envelope of array based on Figure VIII-3.

otherwise, the right array will be activated. In order to prevent rapid left/right switching when the line of sight is on the switching boundary, an overlap in the coverage of the left and right arrays can be exploited. As the line of sight to the satellite moves from left to right (or vice versa), array switching from left array to right array can be delayed until one is well past the center point. Reswitching (back to the left array) will not occur until the line of sight has moved well past the center point in the opposite direction.

1. Mapping Procedure

Mappings of the right hand polarized (or left hand polarized) far field pattern due to a right hand circularly polarized antenna element have been generated. The scheme for choosing the observation directions of interest was based on the fact that if nose-to-tail scans are made in equal increments, there will be significant "crowding" of the observation directions in the nose and tail directions. The observation directions were chosen to be close enough together so that no significant variation in the element radiation pattern would occur between samples (see section C-3). In this case, the beam maximum will likewise not change abruptly between observation directions, as will be shown. The final arrangement of the observation directions chosen for the mapping scheme is shown in Figure VIII-5.

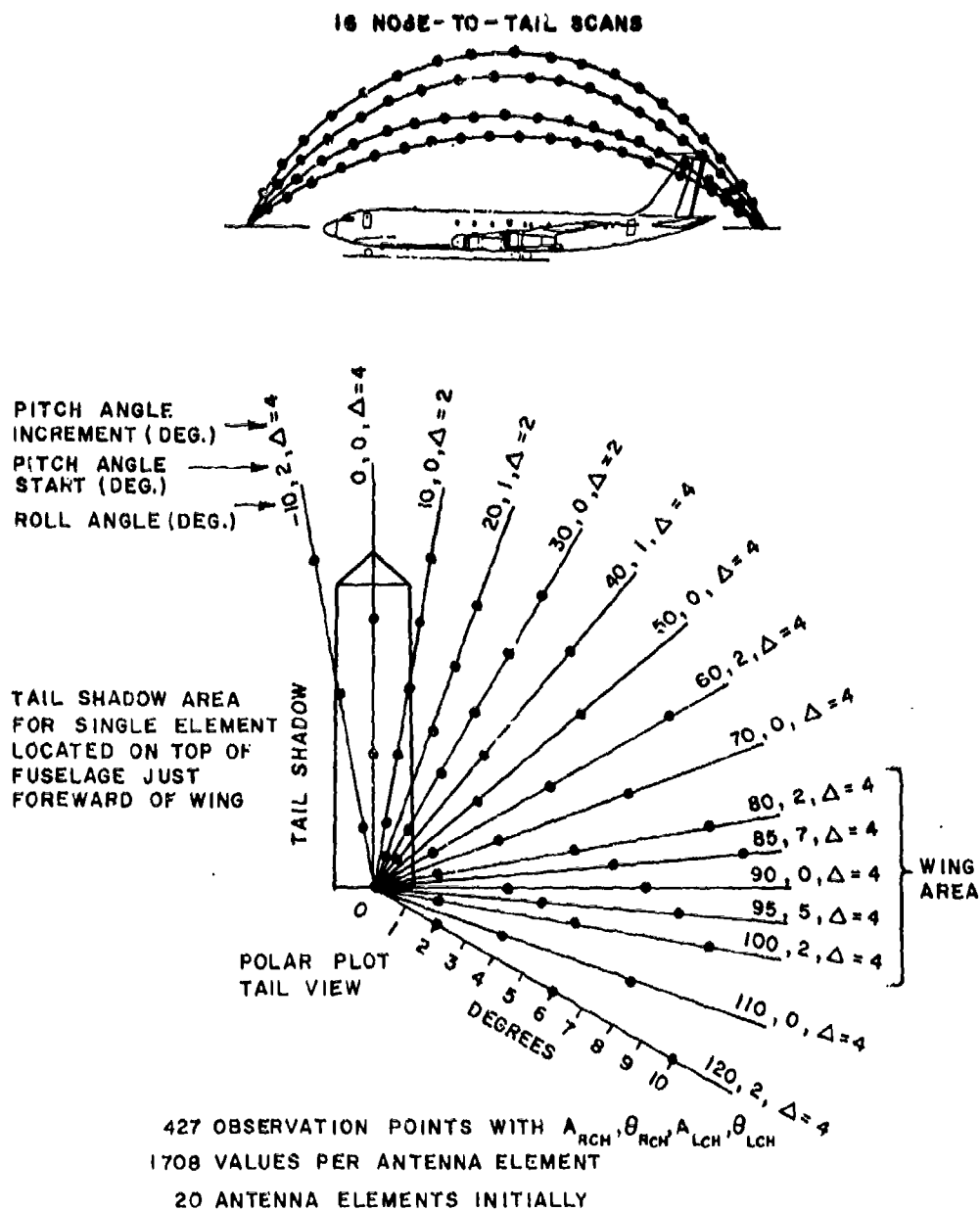


Figure VIII-5. Observation point mapping scheme.

As can be seen from Figure VIII-5, all scans were taken from nose to tail. The starting point, ending point and increment (given in degrees) are listed on the figure. A region of tail shadowing (or blockage) is shown. This tail shadow region corresponds to an antenna element located on top of the fuselage just forward of the wings. Any observation direction located in this shadow region will be blocked from a direct line of sight to the element. The signal from the particular element in such a direction would be very low. It was seen, however, that a small position change in the element on the fuselage can place this tail shadow out of the region of interest. For example, if the array is on the left side of the fuselage, the tail shadow would only block directions toward the right of the aircraft. In any such case, then, the active array would be switched from the left side to the right side before the tail shadowing effect becomes significant.

2. Computer Program Descriptions

A number of computer programs were used to create the far field maps which will be discussed here. A flowchart of the linkages of the programs is shown in figure VIII-6. Below is a description of the computer programs and data files shown in the figure.

1. FILE.DAT

A data file giving the parameters of the antenna element, the aircraft structure, and the desired far field scanning directions for each antenna element.

THIS IS THE FLOWCHART OF THE
OPERATION OF THE KC135 ANTENNA PROGRAMS

```

      FILE.DAT
      :
      :
      $SUBMIT/PARA=FILE RUANT.....(NEWMAIN)
      :
      :
      FILE.BIN      FILE.OUT
      :
      :
      @CCOMP FILE.....(COMP2)
      :
      :
      FILE.CMP      FILE.BUG
      :
      :
      @MAPPER FILE.....(MAPP)
      :
      :
      FILE.MAP
  
```

Figure VIII-6. Flowchart of computer program linkages.

2. RUANT

A file which invokes NEWMAIN -the GTD program described in reference 1.

- * FILE.BIN A binary file written as output from RUANT.

Contains the far field signal level data.

- * FILE.OUT

A file which describes the performance of RUANT to the user.

3. @CCOMP FILE

A procedure which invokes COMP2 -a program which compacts the data in FILE.BIN for efficient data storage.

- * FILE.BUG

A file which contains parameters from the data conversion for use in debugging problems.

- * FILE.CMP

The compressed output file from @CCOMP

4. @MAPPER FILE

A procedure which invokes MAPP -a computer program which used FILE.CMP to create the final mapping of the fields from the original antenna element.

- * FILE.MAP

The file containing the image of the far field map created by @MAPPER

3. Single Element Mappings

Three examples of maps of the far field pattern of specified antenna elements are given in Figures VIII-7, VIII-8, and VIII-9. In these figures, the RHP or LHP component of the signal (given in dB) is printed at the roll angle versus pitch angle point for the associated observation direction. The effect of the element pattern (crossed slots operated in the turnstile mode) and their interaction with the aircraft structure as seen in these maps, also the effects due to the depolarization of the signal at angles off broadside to the antenna elements will be discussed.

The pattern of the individual elements will be shown to contain a number of nulls. In the next section, however, it will be shown that when these element patterns are combined into an array (with as few as 20 elements), the nulls shown here will be averaged out.

a. Antenna Element On Fuselage (25 deg. Roll -12.525 Inches Tailward Of Reference Point).

Figure VIII-7 shows a map of the right hand polarized signal strength in the far field for a right hand polarized (RHC) crossed slot antenna element located on the fuselage of the KC135 at 25 degrees off vertical, and 12.525 inches (full scale) tailward from the z axis zero point (see Figure VIII-1). On the full scale aircraft, this places the antenna 5.4 inches rearward of the fuselage attachment point of the wing leading edge. In the figure, the far field amplitude (in dB below the (given) maximum value) is printed. The values are printed at a location which corresponds to the associated observation direction given

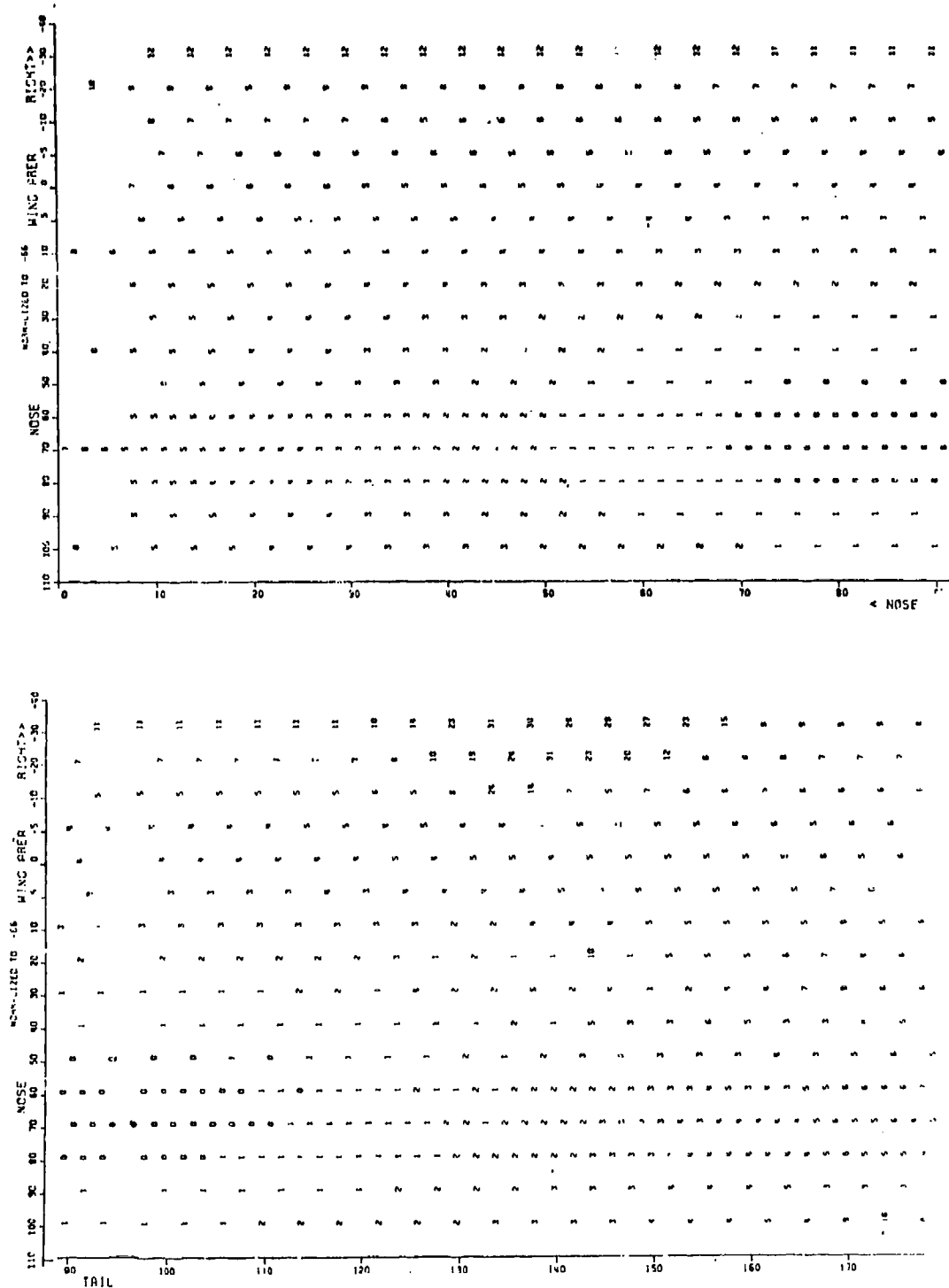


Figure VIII-7. Signal strength map due to single antenna element.
(Location - 25° x 12.5 in.).

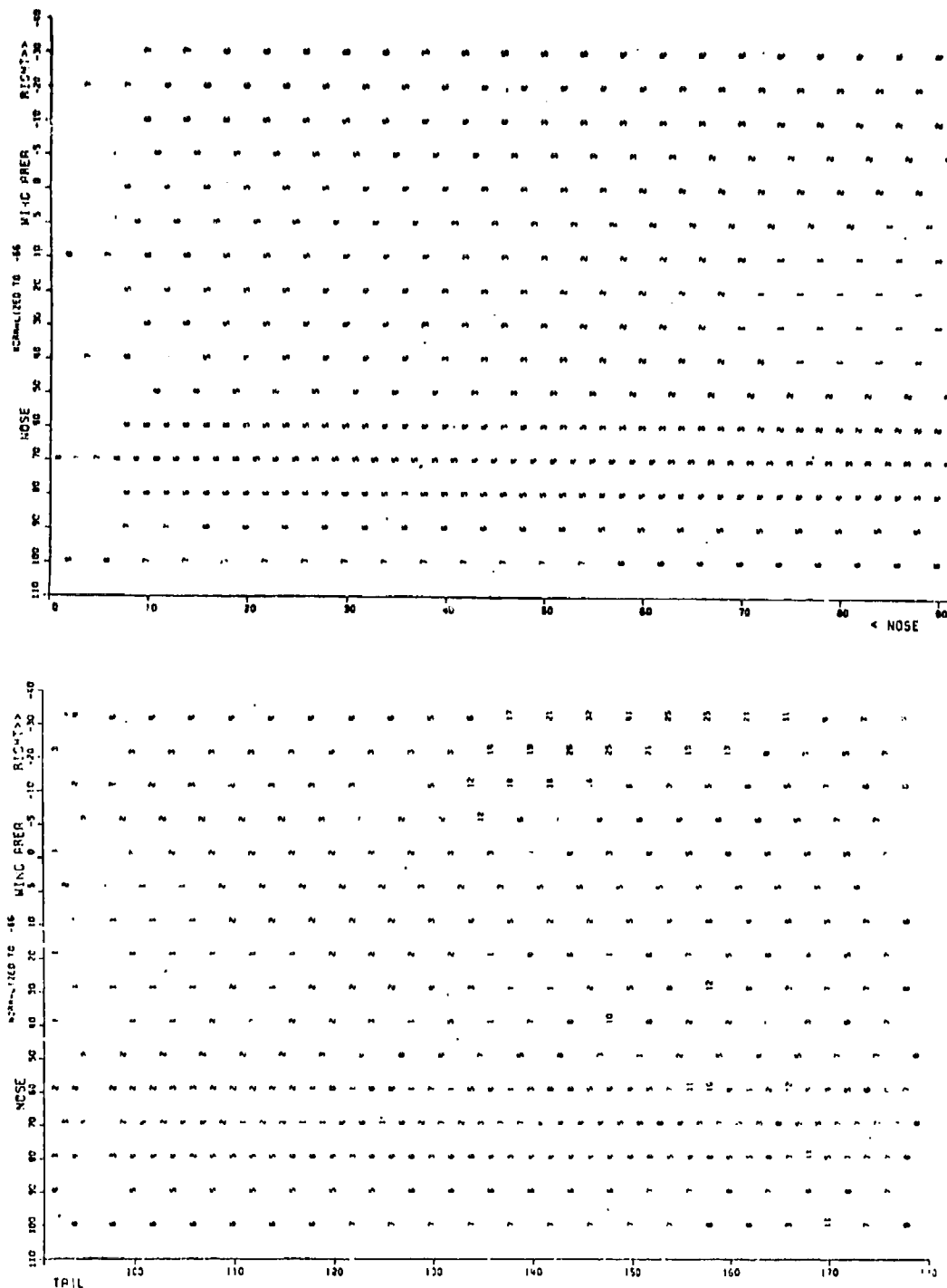


Figure VIII-8. Signal strength map (RHP) due to single antenna element.
(Location - 65° x 12.5 in.).

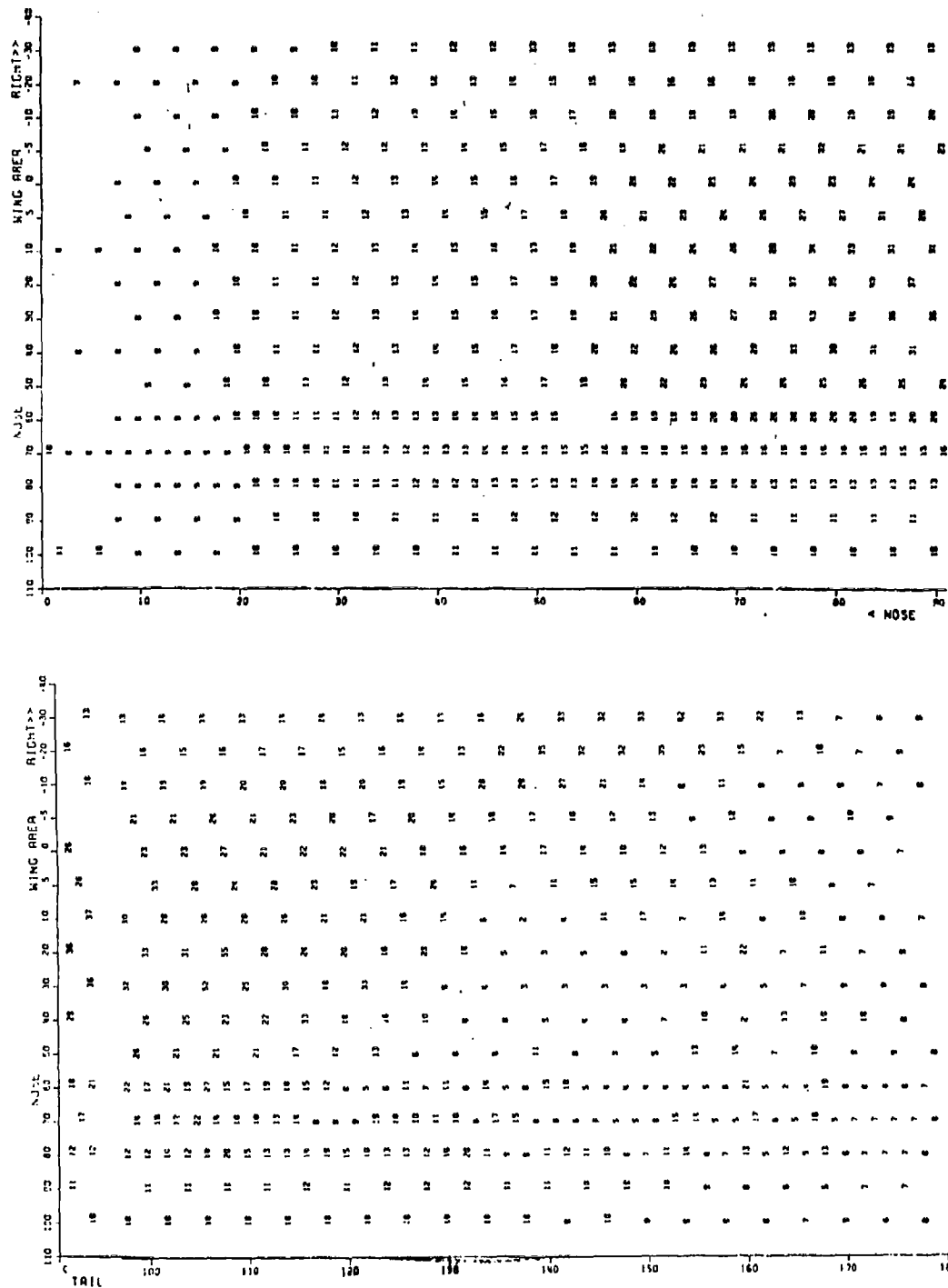


Figure VIII-9. Signal strength map (LHP) due to single antenna element.
(Location - 65° x 12.5 in.).

by the roll angle scale and the pitch angle scale. The roll angle increments are smaller in the neighborhood of the wing blockage effect, so that this effect can be observed more accurately.

It can be seen that the pattern of the RHC element falls off rather gradually, but that there are several localized low amplitude directions. The blockage of the pattern due to the wing can be seen in the region between 130 and 160 degrees pitch and -10 to -40 degrees roll. The effect of tail blockage at 100 degrees roll and 170 and 174 degrees pitch can also be seen. A localized region of small signal is also found at 144 degrees pitch and 20 degrees roll. This appears to be due to cancellation of the signal by the effect of the image of the antenna element in the wing surface.

b. Antenna Element On Fuselage (65 deg. Roll-12.525 Inch Tailward of Reference point) -RHP -

Another map of the the RHC signal pattern is given in Figure VIII-8. This map is in the same format as the last map, but is for an antenna element located at 65 degrees from the top of the aircraft fuselage. This element is the same distance along the fuselage as the previous element. It can be seen that the blockage areas and localized nulls of this antenna element are in different areas from the previous element.

Note that the large broad maximum is located broadside to the antenna. (The map has been normalized to a slightly larger value than the previous map due to the existence of some localized peaks.) Wing blockage is still visible in the map from 145 to 170 deg pitch. Rapid signal variations can also be seen in the tail region of the aircraft (145 to 170 degrees pitch).

c. Antenna Element On fuselage (65 deg. Roll -12.525 Inch Tailward of Reference Point) -LHP-

The map shown in Figure VIII-9 is given in the same format as the previous maps. This map is of the left hand circular component (LHP) radiated by the right hand circular antenna element. It can be seen that the signal is quite weak near the broadside of the element. As the observation direction moves off broadside, the polarization approaches linear, and the LHP component grows in signal strength even though the element pattern is falling off in total signal power radiated. The wing blockage effects can still be seen in this map, as well as the effects of the wing scattering and tail scattering. Study of individual numbers will reveal observation directions near the wing and tail region where the LHP component actually dominates.

D. ARRAY PATTERN

The individual element patterns were next combined into an array. An array of 4096 elements with half wavelength spacing is to be considered.

1. Array Pattern Computation

Fortunately, it is not necessary to compute the antenna pattern from each of 4096 elements to estimate the far field pattern of the conformal array. Let the voltage magnitude in the far field in the direction θ, ϕ due to element p , be $V_p(\theta, \phi)$. Then the total far field voltage for the 4096 element array is

$$V_T = \sum_{p=1}^{4096} V_p(\theta, \phi). \quad (8.1)$$

if the individual source voltage phases are adjusted so that the signal arrives at the far field point in phase. We can divide the 4096 element array into 20 subarrays (all approximately the same size). Then dropping the θ, ϕ notation here

$$V_T = \sum_{i=1}^{20} (V_{i,1} + V_{i,2} + V_{i,3} + V_{i,4} + \dots). \quad (8.2)$$

Now each subset of V has (1) a fairly constant part which varies only due to fuselage curvature effects, blockage effects, etc., and (2) a rapidly varying part which varies due to reflection and diffraction effects.

Thus,

$$V_{i,j} = V_i^C + V_{i,j}^r \quad (8.3)$$

where

V_i^C is the fairly constant component

and

$V_{i,j}^r$ is the rapidly varying component.

So, over each subarray

$$\sum_{j=1}^N V_{i,j} = NV_i^C + \sum_{j=1}^N V_{i,j}^r \doteq NV_i^C \quad (8.4)$$

since $\sum_{j=1}^N V_{i,j}^r \doteq 0$.

Therefore,

$$V_T = N \sum_{i=1}^{20} V_i^c. \quad (8.5)$$

Now, what we know is the voltage due to a representative element in each subarray, $V_{i,1}$, $i=1\dots 20$. So we know $V_{i,1} = V_i^c + V_{i,1}^r$ $i = 1\dots 20$ and we can find

$$N \sum_{i=1}^{20} (V_{i,1}) = N \sum_{i=1}^{20} (V_i^c + V_{i,1}^r) \doteq N \sum_{i=1}^{20} V_i^c \doteq V_T \quad (8.6)$$

since

$$\sum_{i=1}^{20} V_{i,1}^r \doteq 0.$$

Below, we will use

$$V_T \doteq N \sum_{i=1}^{20} V_i^c. \quad (8.7)$$

The array gain is defined as

$$DG(\theta, \phi) = \frac{P_{\max}(\theta, \phi)}{P_{\text{ave}}(\theta, \phi)} \quad (8.8)$$

where:

1. $DG(\theta, \phi)$ is the maximum array directive gain which can be obtained in the θ, ϕ direction.
2. $P_{\max}(\theta, \phi)$ is the power per unit solid angle transmitted in the θ, ϕ direction when individual element electrical phases are adjusted to form a beam in the θ, ϕ direction.
3. $P_{\text{ave}}(\theta, \phi)$ is the average power per unit solid angle radiated (i.e., isotropic power) when the electrical phases are defined as in 2 above.

In this case, $P_{\max}(\theta, \phi)$ is proportional to V_T^2 or $(\sum_{i=1}^{20} V_i^c)^2$; the square of the sum of the voltage fields from each of the 20 elements,

$V_T \propto \sum_{i=1}^{20} V_i^c$ was shown above.

The variation of P_{ave} can be estimated by setting the behavior of $(1/P_{\text{ave}})$ proportional to the behavior of the large aperture array maximum gain factor. This factor falls off as a cosine from the array broadside to 77 degrees, and then remains constant to 90 degrees (endfire case) (See references 3 and 4).

For this initial study, the elements representing the 20 subarrays were located as shown in Figure VIII-10. Note that the aperture represented by this set of elements is defined by the 4096 element constraint. Thus we must model an array of 64×64 elements spaced $1/2\lambda$ apart. The result is an array of size $32 \times 32\lambda$.

INITIAL DISTRIBUTION OF ARRAY ELEMENTS

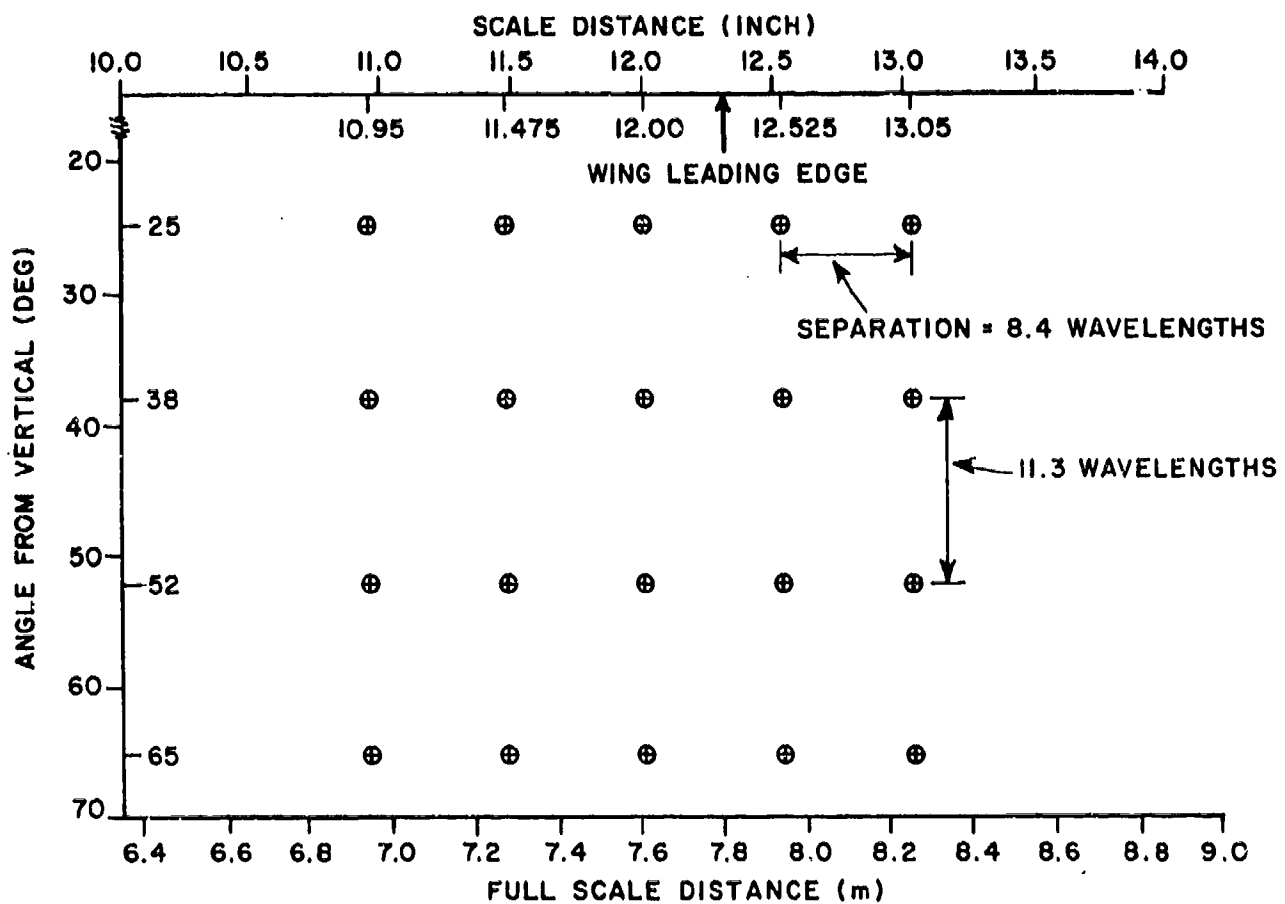


Figure VIII-10. Initial distribution of array elements.

An array of this size (32 x 32 wavelengths) should be capable of a broadside directive gain of approximately 41 dB. A more practical value is 38 dB gain for a real array. The 38 dB value for the gain in the array broadside direction will be used here.

2. Mapping Of Array Gain Coverage

Figure VIII-11 is the resulting map of the array gain available from the fully populated array as a function of beam pointing direction. It is given in the same format as the element maps shown earlier, except that it shows the gain at each observation direction when the array is maximized (or pointing) in that direction.

A number of comments concerning Figure VIII-11 are in order.

1. Remember that this is a mapping of the maximum available gain at each observation direction. The array beam must be directed in each of the given directions by proper element phasing.
2. The broadside region, which is centered at 90 degrees pitch and 45 degrees roll is quite smooth. The variations seen previously for the individual element patterns have been averaged out over the 20 elements included here.
3. The -5 dB region (33 dB gain) is quite large, extending from roughly 33 degrees to 146 degrees pitch and from greater than 100 degrees roll to -12 degrees roll.

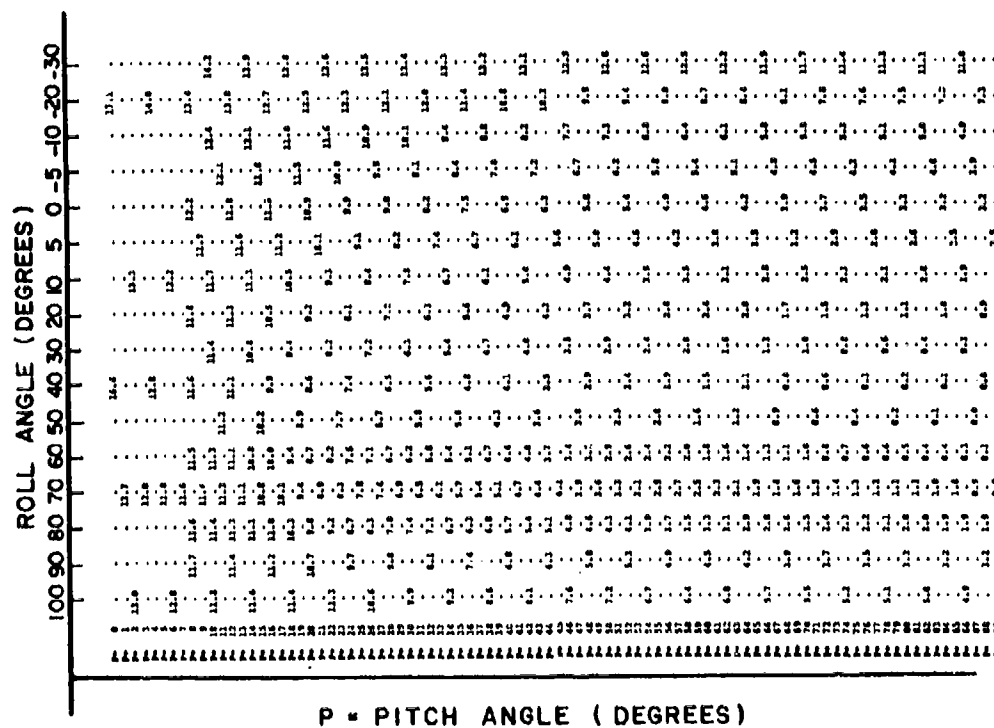
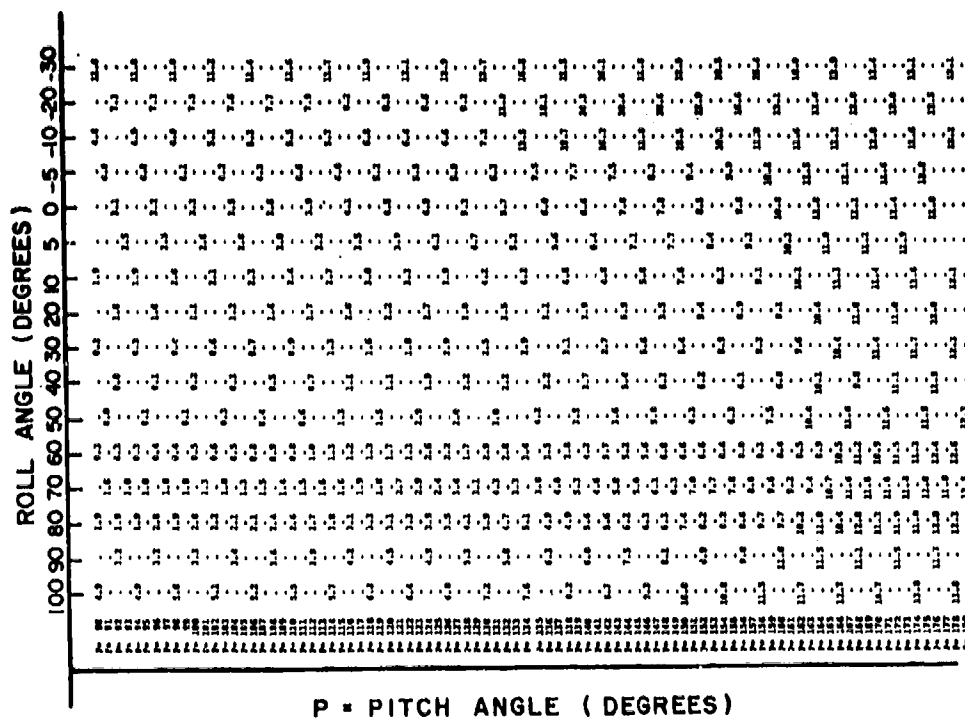


Figure VIII-11. Signal strength map due to sum of the signal amplitude of each of the 20 elements.

4. Even the -10 dB region (28 dB gain) is quite smooth and large in coverage. There is a small "dent" in the -10 dB coverage pattern at 140 degrees pitch below the horizon line, due to the wing effect, but otherwise, the -10 dB pattern is quite well behaved.

3. Directional Gain vs. Satellite Direction

A comparison between the available coverage of the particular conformal array configuration discussed here and a communications satellite with a 28 degree elevation angle is also shown in Figure VIII-12. Note that for roll angles less than 40 degrees, no regions of directive gain degradation greater than 10 dB are experienced. (Remember that it is assumed that there are two arrays used to obtain hemispherical coverage, one on the right side of the aircraft and one on the left.)

E. CONCLUSIONS

A technique has been developed and demonstrated for predicting the performance of a contiguous conformal array on the surface of a specific aircraft. Questions concerning the blockage region and scattering nulls in the pattern have been studied for a KC135 and for a number of specific elements mounted on the fuselage.

The important conclusions are summarized below.

1. Blockage due to the tail is not a serious problem because the tail blockage is in the opposite hemisphere from the array, and only a small percentage of the elements from the array for any particular look angle will be blocked.

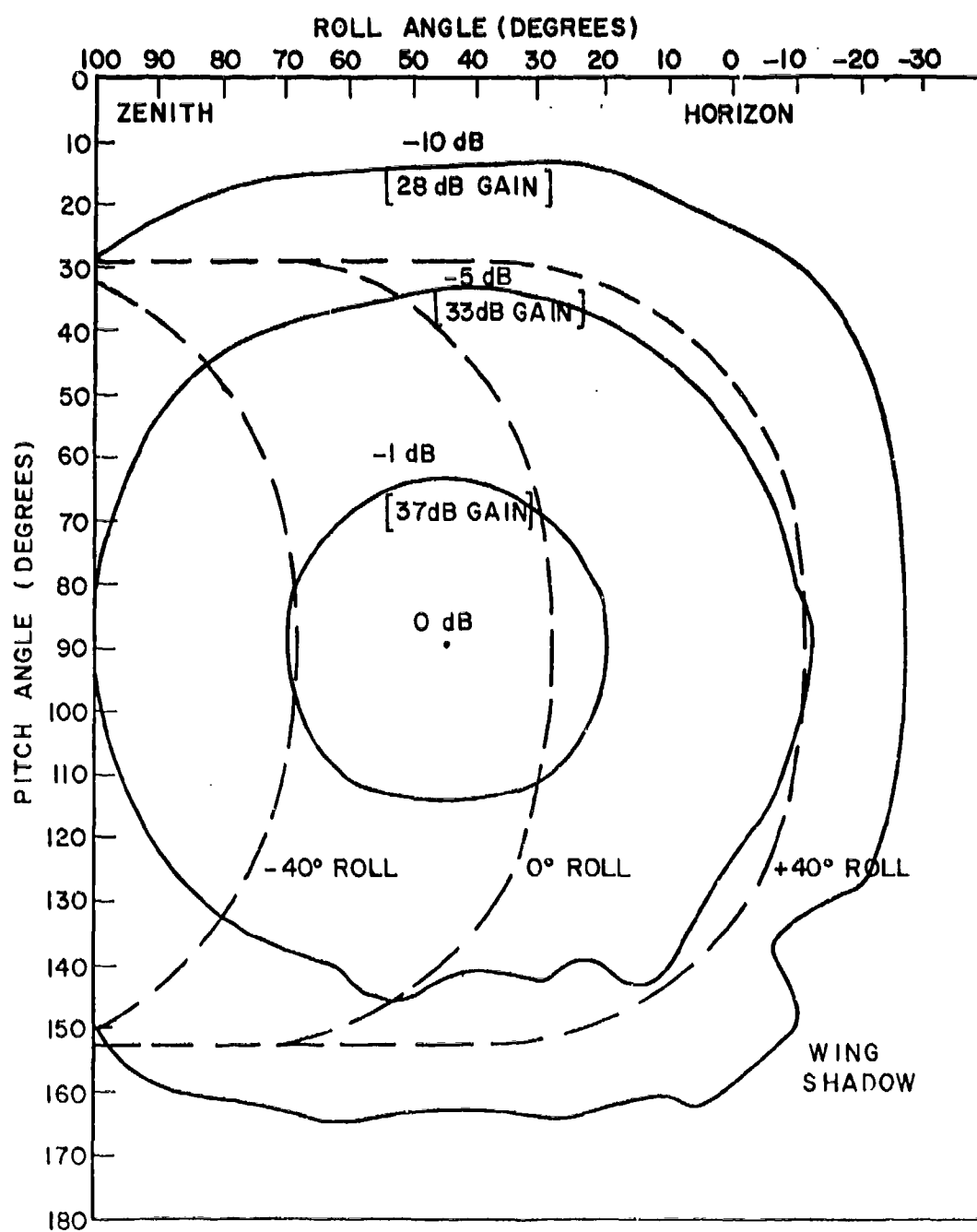


Figure VIII-12. Plot of array gain and operational performance map for conformal array.

2. Wing blockage is not likely to be serious. A realistic look at possible geostationary communication satellite acquisition angles, indicates that the aircraft must roll beyond 40 degrees for the wing to significantly block a satellite with a 28 degree elevation angle.
3. The use of a limited number of representatively placed array elements (20 in this case) to study the reflection, blockage and diffraction effects for the entire array has been shown to be an effective tool. In particular, it has been shown that nulls in the patterns of individual array elements caused by scattering effects will be averaged out when a number of elements are considered. Nulls in the pattern of individual elements due to blockage will only be important to the array pattern if the blockage affects the majority of the elements of the array.
4. The nose and tail areas are regions of low gain, while the roll angle coverage is quite good. Below are two methods of improving this coverage restriction with the existing arrays.
 - a. The array studied here was square, but if the same number of elements were used in an elongated rectangular shape (elongated in the direction of the fuselage), the gain in the nose and tail regions would be improved in exchange for a small acceptable loss in gain coverage in the roll axis.

- b. Both the left and right arrays could be activated for the nose and tail regions where both arrays can "see" in the direction of interest.
- c. It must be remembered that the satellite acquisition curves do not extend into the nose and tail regions, and it may be decided that such extended coverage is not warranted.

F. REFERENCES

- [1] W.D. Burnside and T. Chu, "Airborne Antenna Pattern Code User's Manual", Technical Report 711679-2, March 1980, The Ohio State University ElectroScience Laboratory, Department of Electrical Engineering; prepared under Contract F30602-79-C-0068 for Rome Air Development Center.
- [2] W.D. Burnside, et al., "A Study of KC-135 Aircraft Antenna Patterns", IEEE Trans. on Antennas and Prop., Vol. AP-23, No. 3, May 1975, pp. 309-306.
- [3] B.A. Munk and R.J. Luebbers, "Gain of Arrays of Dipoles with a Ground Plane", IEEE Trans. on Antennas and Propagation, AP-20, September 1972, pp. 641-642.
- [4] B.A. Munk, R.J. Luebbers and R.C. Hansen, "Comments on 'Comparison of Square Array Directivity Formulas'", IEEE Trans. on Antennas and Prop., AP-20, pp. 676-677.

SECTION IX

DEGREES OF FREEDOM OF AN ADAPTIVE ARRAY

In this section, a definition is formulated for the number of degrees of freedom of an adaptive array and a method is given to ensure that a distribution of antenna elements provides enough degrees of freedom in a specified field of view. It will be shown that one can find the number of degrees of freedom of an adaptive array in an arbitrary conical cut by projecting the array elements onto a planar cut. A conical cut is not the most general cut, but is one that is most often used as an observation subspace and, as will be shown later, is a generalized representation of a planar cut. The performance of adaptive arrays in a specified cut for an arbitrarily distribution of jammers will be studied.

In Subsection A, the number of degrees of freedom of an adaptive array is defined. A method to find the number of degrees of freedom of an adaptive array is given in Subsections B and C. In Subsection D, the effect of arbitrarily located jammers on the performance of an adaptive array in a specified cut is studied.

A. DEGREES OF FREEDOM OF AN ADAPTIVE ARRAY

It is well known that a conventional array of N elements has $N-1$ degrees of freedom, in that it can point $N-1$ independent nulls. When this array is operated in an adaptive mode, the weight vector is automatically chosen such that the adapted pattern has nulls along the jammer directions (assuming that the jammers are much stronger than the

receiver thermal noise). An adaptive array, therefore, can null $N-1$ jammers. In a communication or radar system, the adaptive array should point its main beam towards the desired signal to provide a useful signal at the array output. If, due to the nulling of the jammers, the main beam of the array is moved away from the desired signal or is suppressed significantly, the system may not perform satisfactorily. The number of degrees of freedom of an adaptive array, therefore, should be redefined so as to take into account the desired signal as well. An appropriate definition to accomplish this objective is proposed as follows:

'The maximum number of independent jammers that an adaptive array can null without significantly suppressing the desired signal located within a specified field of view gives the number of degrees of freedom of the array.'

Since an adaptive array cannot receive a desired signal while suppressing an undesired one if the two are incident from the same direction (and are similarly polarized if polarization diversity is available) a certain minimum angular separation between desired and undesired signal must be specified. That separation must be consistent with the array beamwidth or resolution to prevent excessive suppression of the desired signal. This angular separation should be taken into account when specifying the "field of view" stated in the above definition.

A key parameter in evaluating the performance of a communication or radar system in the presence of jammers is the Signal to Interference plus Noise Ratio (SINR) and consequently it is this parameter that will be used as a performance criterion in the study of the number of degrees of freedom of adaptive arrays.

B. DEGREES OF FREEDOM OF AN ADAPTIVE ARRAY IN A CONICAL CUT

Consider a linear array of N isotropic elements as shown in Figure IX-1. The output SINR of the array in the presence of a single jammer will be given by [1]

$$\text{SINR} = \epsilon_d \left(N - \frac{|U_i^T U_d|^2}{N} \right) \quad (9.1)$$

where,

$$U_d = \begin{bmatrix} e^{j 2\pi/\lambda z_1 \cos \theta_d} \\ e^{j 2\pi/\lambda z_2 \cos \theta_d} \\ \vdots \\ e^{j 2\pi/\lambda z_N \cos \theta_d} \end{bmatrix} \quad (9.2)$$

and

$$U_i = \begin{bmatrix} e^{j 2\pi/\lambda z_1 \cos \theta_i} \\ e^{j 2\pi/\lambda z_2 \cos \theta_i} \\ \vdots \\ e^{j 2\pi/\lambda z_N \cos \theta_i} \end{bmatrix} \quad (9.3)$$

where (θ_d, ϕ_d) and (θ_i, ϕ_i) give the direction of desired signal and jammer, respectively. If the two signals (desired and jammer) are incident from the same direction, the array can not discriminate between

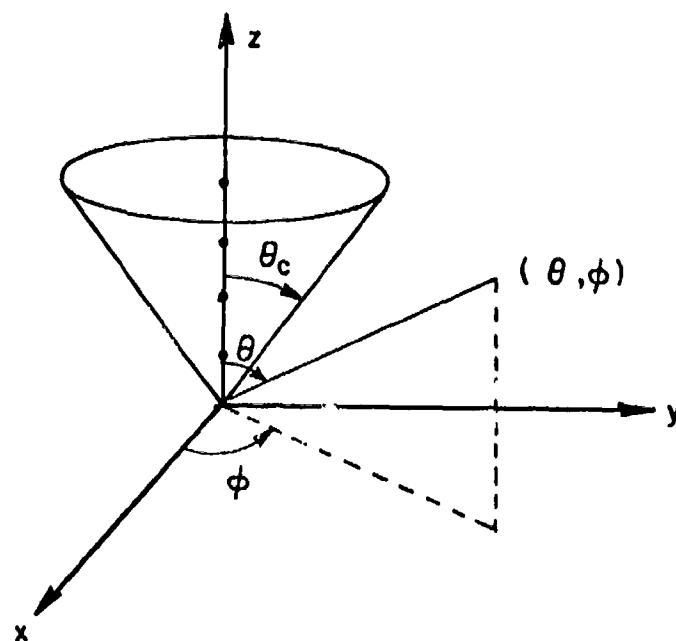


Figure IX-1. A linear array in a 3-dimensional space.

the two and the array output SINR will be zero. Let the two signals be incident from two different directions but lie on a cone as shown in the figure. (The cone axis coincides with the z axis and the cone angle is θ_c). Then the two signal directions will be given by (θ_c, ϕ_d) and (θ_c, ϕ_i) , respectively. The desired signal vector, U_d , and the interference signal vector, U_i , for these two directions becomes

$$U_d = \begin{bmatrix} e^{j 2\pi/\lambda z_1 \cos \theta_c} \\ e^{j 2\pi/\lambda z_2 \cos \theta_c} \\ \vdots \\ e^{j 2\pi/\lambda z_N \cos \theta_c} \end{bmatrix} \quad (9.4)$$

and

$$U_i = \begin{bmatrix} e^{j 2\pi/\lambda z_1 \cos \theta_c} \\ e^{j 2\pi/\lambda z_2 \cos \theta_c} \\ \vdots \\ e^{j 2\pi/\lambda z_N \cos \theta_c} \end{bmatrix} \quad (9.5)$$

Substituting (9.4) and (9.5) into Equation (9.1), one gets

$$\text{SINR} = 0 \quad (9.6)$$

or the array cannot discriminate between the two signals. Thus, the array has zero degrees of freedom in the conical cut. In this section, the number of degrees of freedom of an adaptive array in any conical

cut will be found. In later sections, it will be shown that an adaptive array has its minimum degrees of freedom in a conical cut. Thus, the knowledge of the number of degrees of freedom of an array in a conical cut can be used to evaluate the lower bound of the array performance.

Any conical cut (cone apex coinciding with the origin of the coordinates) in a three dimensional space can be defined by a cone axis and the cone angle as illustrated in Figure IX-2. The cone axis is defined by the spherical angles (θ_r, ϕ_r) . Using these spherical angles, one can set up a new coordinates system in relation to the original coordinates. The new cartesian coordinates (x', y', z') are found by first rotating about the z' -axis, the angle ϕ_r , and then by rotating about the y' -axis, the angle θ_r . The cone angle is then defined in the new coordinates (x', y', z') in terms of the spherical angle $\theta' = \theta_c$. Note that $\theta_c = 90^\circ$ will lead to a planar cut given by the $x'y'$ plane. The relation between the two sets of cartesian coordinates is given by:

$$\begin{bmatrix} x' \\ y' \\ z' \end{bmatrix} = \begin{bmatrix} \cos \theta_r \cos \phi_r & \cos \theta_r \sin \phi_r & -\sin \theta_r \\ -\sin \theta_r & \cos \theta_r & 0 \\ \sin \theta_r \cos \phi_r & \sin \theta_r \sin \phi_r & \cos \theta_r \end{bmatrix} \begin{bmatrix} x \\ y \\ z \end{bmatrix} \quad (9.7)$$

Let a signal be incident on an array of N isotropic elements. Assume that the signal lies in a conical cut defined by $(\theta_r, \phi_r, \theta_c)$. The signal vector for the array will be given by

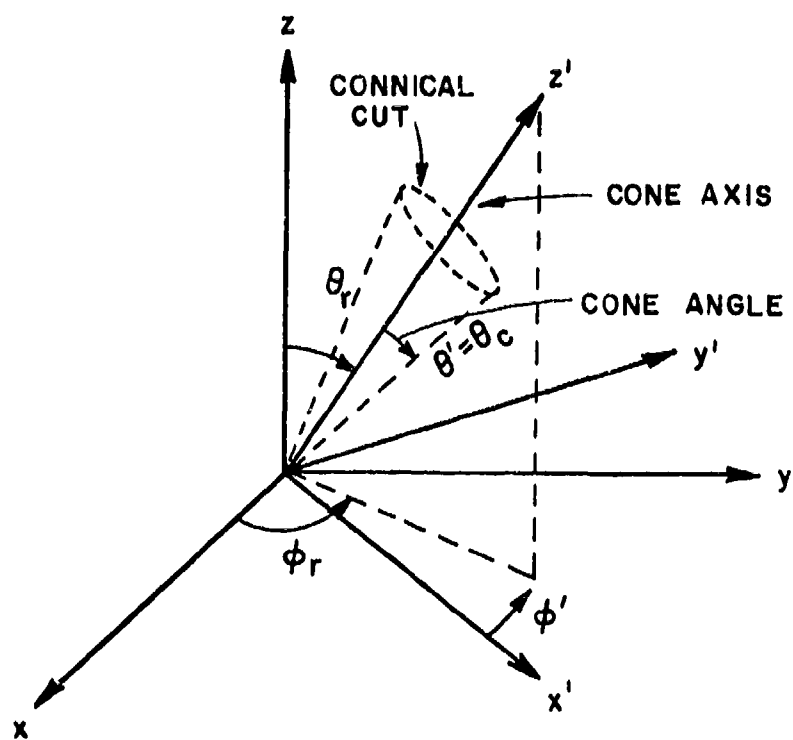


Figure IX-2. An arbitrary conical cut in a 3-dimensional space.

$$U = \begin{bmatrix} e^{j\rho_1} \\ e^{j\rho_2} \\ \vdots \\ \vdots \\ \vdots \\ e^{j\rho_N} \end{bmatrix} \quad (9.8)$$

where

$$\rho_k = \frac{2\pi}{\lambda} (x'_k \sin\theta_c \cos\phi' + y'_k \sin\theta_c \sin\phi' + z'_k \cos\theta_c) , \quad (9.9)$$

(x'_k, y'_k, z'_k) in Equation (9.9) defines the location of the k^{th} element in the new coordinate system and (θ_c, ϕ') gives the direction of the signal.

If

$$W = (w_1, w_2, \dots, w_N)^T \quad (9.10)$$

is the weight vector for the array, then the signal at the array output will be

$$F = U^T W ,$$

or,

$$F = U^T W' \quad (9.11)$$

where

$$u_k' = u_k e^{-j 2\pi/\lambda z' \cos \theta_c} \quad (9.12)$$

$$w_k' = w_k e^{j 2\pi/\lambda z' \cos \theta_c} \quad (9.13)$$

and T denotes transpose.

In the new coordinate system, some of the elements may have the same x', y' coordinates. For example, elements 2 and 3, and 4 and 5 in Figure IX-3 have the same x', y' coordinates when $(\theta_r, \phi_r) = (90^\circ, 0^\circ)$.

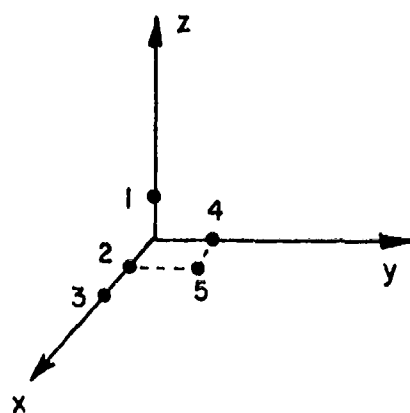
Let

$$\begin{aligned} (x_1', y_1') &= (x_2', y_2') = (x_3', y_3') = (x_1'', y_1'') \\ (x_4', y_4') &= (x_2'', y_2'') \\ &\cdot \quad = \quad \cdot \\ &\cdot \quad = \quad \cdot \\ &\cdot \quad = \quad \cdot \\ &\cdot \quad = \quad \cdot \\ (x_{N-1}', y_{N-1}') &= (x_N', y_N') = (x_M'', y_M'') \end{aligned} \quad (9.14)$$

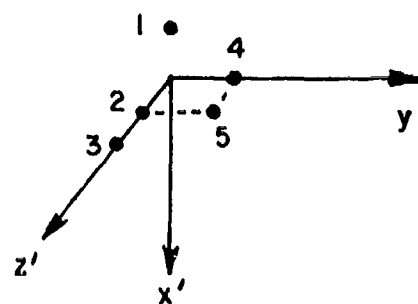
$$M < N$$

and

$$\begin{aligned} (x_i'', y_i'') &\neq (x_j'', y_j'') \\ i &\neq j \\ i, j &= 1, 2, \dots, M \end{aligned} \quad (9.15)$$



(a) ORIGINAL COORDINATE SYSTEM



(b) NEW COORDINATE SYSTEM $(\theta_r, \phi_r) = (90^\circ, 0^\circ)$

Figure IX-3. A five element array in a 3-dimensional space.

Then Equation (9.11) yields

$$\begin{aligned}
 F = & (w_1^i + w_2^i + w_3^i) e^{j 2\pi/\lambda (x_1'' \sin\theta_c \cos\phi^i + y_1'' \sin\theta_c \sin\phi^i)} \\
 & + w_4^i e^{j 2\pi/\lambda (x_2'' \sin\theta_c \cos\phi^i + y_2'' \sin\theta_c \sin\phi^i)} \\
 & + \dots + (w_{N-1}^i + w_N^i) e^{j 2\pi/\lambda (x_M'' \sin\theta_c \cos\phi^i + y_M'' \sin\theta_c \sin\phi^i)}.
 \end{aligned} \tag{9.16}$$

Let

$$\begin{aligned}
 w_1^i + w_2^i + w_3^i &= w_1'' \\
 w_4^i &= w_2'' \\
 \cdot &= \cdot \\
 \cdot &= \cdot \\
 \cdot &= \cdot \\
 \cdot &= \cdot \\
 w_{N-1}^i + w_N^i &= w_M''
 \end{aligned} \tag{9.17}$$

Then from Equation (2.16)

$$F = U^T W'' \tag{9.18}$$

where

$$W'' = (w_1'', w_2'' \dots \dots \dots w_N'') , \tag{9.19}$$

$$U'' = \begin{bmatrix} e^{j\rho_1''} \\ e^{j\rho_2''} \\ \vdots \\ e^{j\rho_M''} \end{bmatrix} \quad (9.20)$$

and

$$\rho_k'' = \frac{2\pi}{\lambda} (x_k'' \sin\theta_c \cos\phi' + y_k'' \sin\theta_c \sin\phi') \quad (9.21)$$

From Equation (9.18) it is clear that F will be zero for all ϕ' if, and only if, $W'' = 0$. Let m independent jammers be incident on the array in the conical cut. Then the array will choose a weight vector W'' such that

$$F_{ik} = U_{ik}''^T W'' = 0 \quad (9.22)$$

$$k = 1, 2, \dots, m$$

where

$$U_{ik}'' = \begin{bmatrix} e^{j\rho_{ik1}''} \\ e^{j\rho_{ik2}''} \\ \vdots \\ e^{j\rho_{ikM}''} \end{bmatrix} \quad (9.23)$$

and

$$\rho_{1kj}'' = \frac{2\pi}{\lambda} (x_j'' \sin \theta_c \cos \phi_{1k}' + y_j'' \sin \theta_c \sin \phi_{1k}') \quad (9.24)$$

In Equation (9.24), (θ_c, ϕ_{1k}') gives the direction of the k^{th} jammer. The m simultaneous equation (Equation (9.22)) will have a non-zero solution for the weight vector as long as $m < M$. Thus, the array will respond to the signal, i.e., $F \neq 0$ (Equation (9.18)), if the signal direction does not coincide with one of the jammers. In case of an adaptive array, the array will try to maximize F while satisfying Equation (9.22). For $m > M$, the only possible solution for the weight vector is

$$W'' = (0., 0., \dots, 0.)^T \quad (9.25)$$

and the response of the array to a signal from any direction in the conical cut will be zero. The maximum number of degrees of freedom of an adaptive array in a conical cut is, therefore, $M-1$. Now, M is the number of elements with different (x', y') value. Thus, to find the degrees of freedom of an array in a conical cut, project the array elements in the $x'y'$ plane. The maximum number of degrees of freedom of the array will then be given by the number of elements with different locations in the plane. One important point to be observed here is that the number of projected elements in the $x'y'$ plane is independent of the cone angle. Thus, the number of degrees of freedom of the array is the same in all conical cuts with the same cone axis. The planar cuts ($\theta_c = 90^\circ$), therefore, will be chosen in further discussions.

Consider a linear array of five isotropic elements as shown in Figure IX-4. Let the field of view be the upper half space, i.e., $0 < \theta < \pi$ and $0 < \phi < \pi$. Figure IX-5 shows the output SINR of the array in the xy plane ($(0^\circ, 0^\circ, 90^\circ)$ conical cut) in the absence of any jammer (dotted line) and in the presence of one jammer (solid line). The jammer is incident from $(90^\circ, 90^\circ)$ and is 20 dB stronger than the desired signal. The SINR is plotted as a function of the desired signal direction $(90^\circ, \phi_d)$. Note that the output SINR in the presence of the jammer is the minimum $(\sim \xi_d/\xi_j)$ for all directions of incidence of the desired signal. Therefore, the array has zero degrees of freedom in the xy plane. The projection of the array elements in the xy plane is also shown in the figure. Note that all array elements project to one point in the xy plane, or, $M=1$ in the xy plane for the array. The array, therefore, should have zero degree of freedom in the xy plane, which is true.

Figure IX-6 shows the output SINR of the array in the yz plane in the presence of four (solid line) and five (dotted line) independent jammers. All the jammers are in the yz plane and are 20 dB stronger than the desired signal. The projection of the array elements in the yz plane is also shown in the figure. Note that the total number of projected elements in this plane is five, or $M=5$. Thus the array has a maximum of four degrees of freedom in the cut. From the SINR plots we see that, in the presence of five jammers, the output SINR is at its minimum $(\sim \xi_d/\xi_j)$ for all desired signal directions. Thus, the array has a maximum of four degrees in the yz plane. In the presence of four jammers, the array responds to the desired signal and reaches its maximum value (~ 7 dB) at 90° . The array, therefore, has four degrees

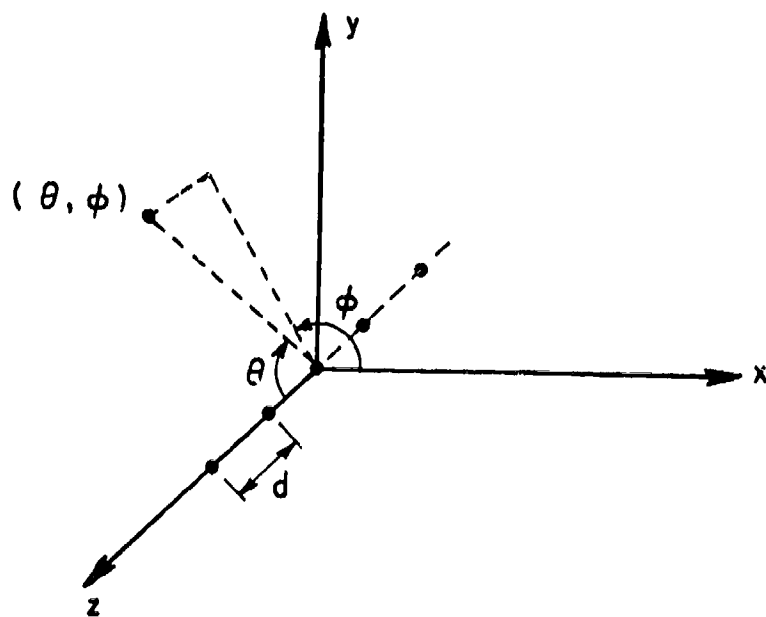


Figure IX-4. A linear array of five isotropic elements. Field of view
 $0 < \theta < \pi$, $0 < \phi < \pi$, $d = 0.5\lambda$.

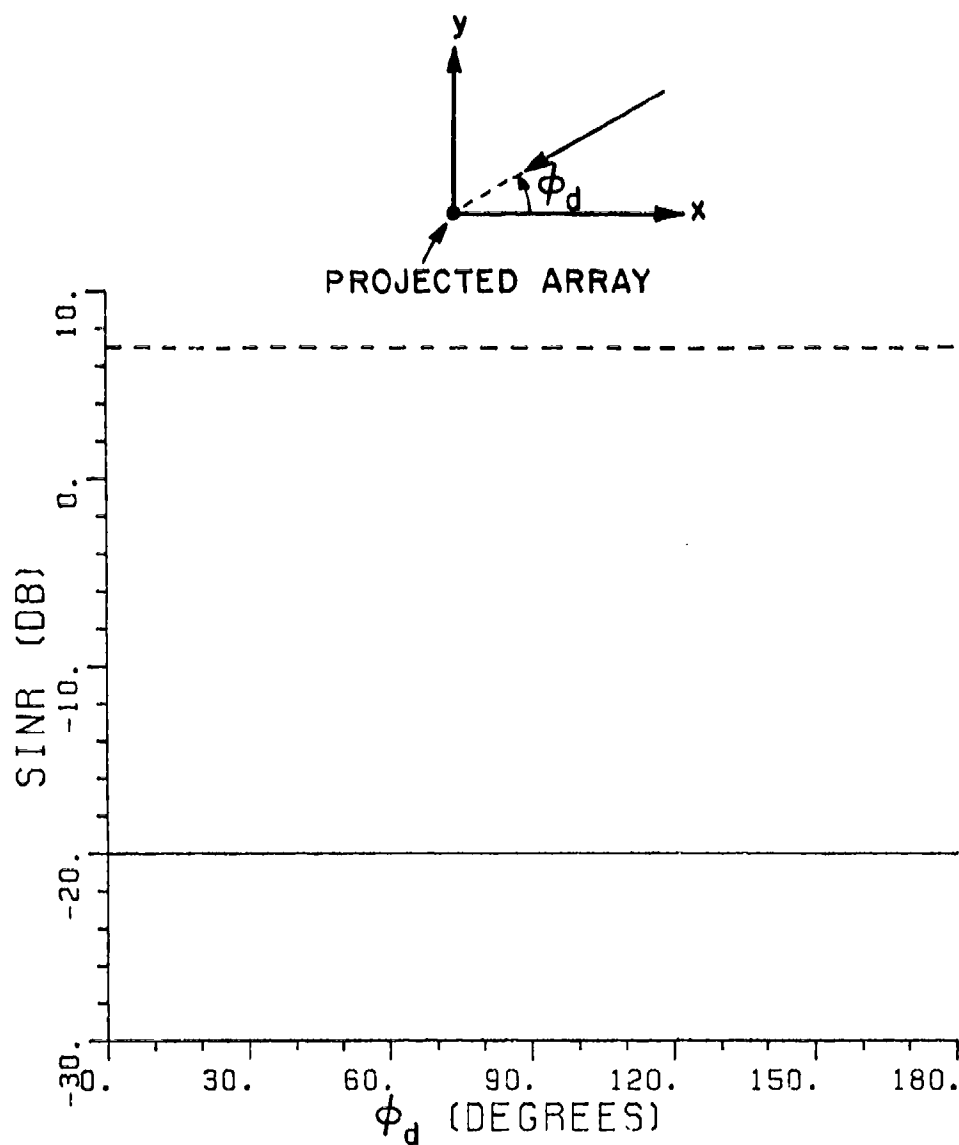


Figure IX-5. Output SINR of the linear array of five isotropic elements in the xy plane. (—) one jammer, (----) no jammer. $(\theta_j, \phi_j) = (90^\circ, 90^\circ)$, $\xi_d = 1$, $\xi_j = 100$.

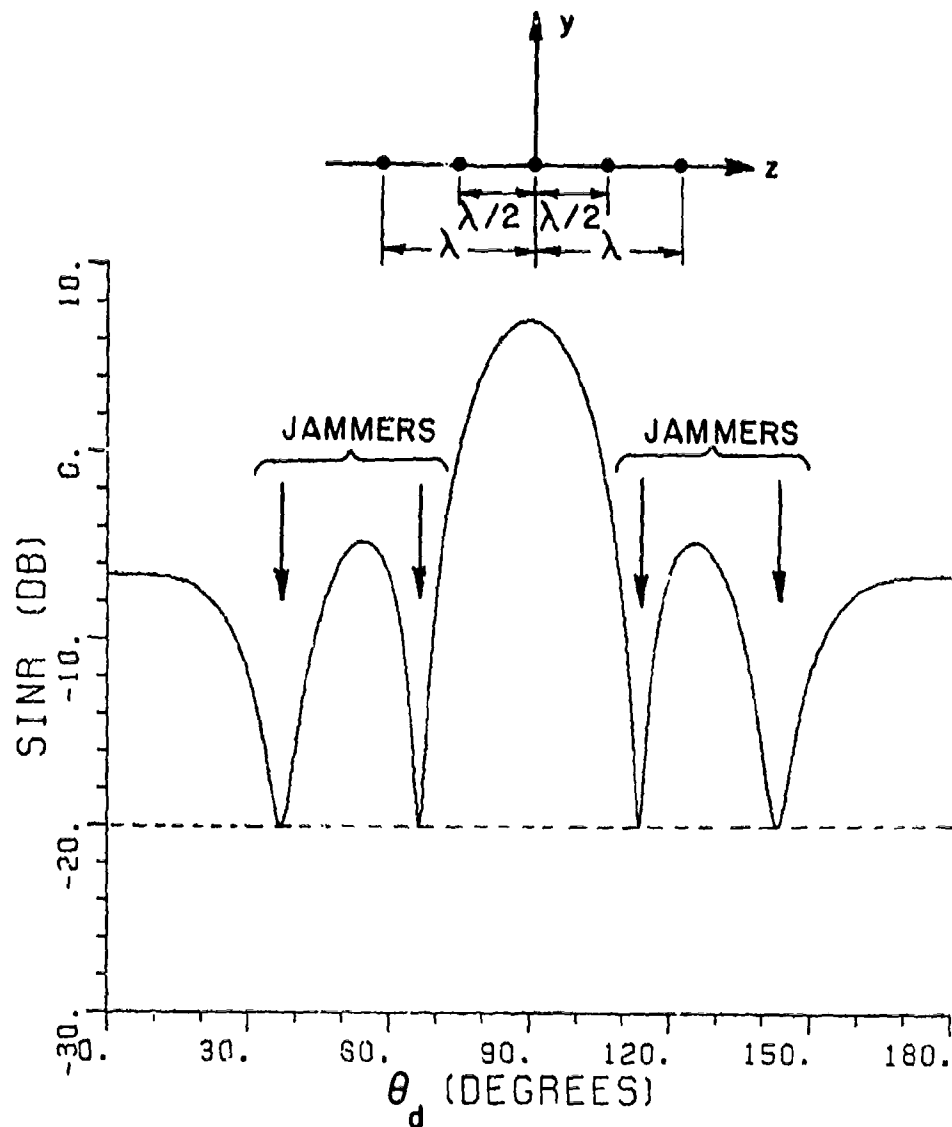
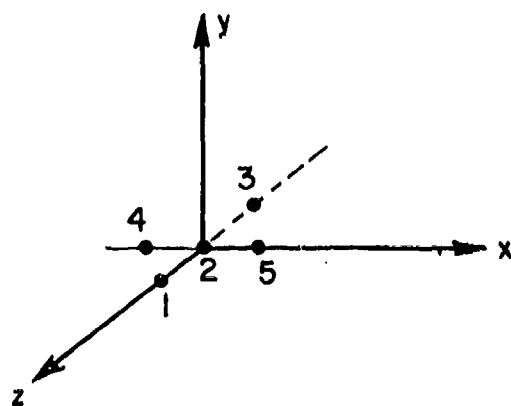


Figure IX-6. Output SINR of the linear array of five isotropic elements in the yz plane in the presence of four (—) and five (----) jammers. $\xi_d = 1$, $\xi_{i1} = \xi_{i2} = \xi_{i3} = \xi_{i4} = 100$.

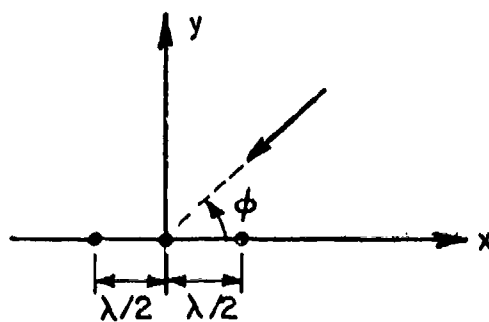
of freedom in the cut. Thus, the projection of the array elements gives the maximum number of degrees of freedom of an adaptive array in a conical cut.

As an example of a planar array, consider the crossed array shown in Figure IX-7a. The spacing between the elements is $\lambda/2$. The projection of the array elements in the xy plane is also shown in the Figure IX-7b. Note that the total number of projected elements in this cut is three, i.e., $M=3$. The array, therefore, should have a maximum of two degrees of freedom in the cut. Figure IX-8 shows the output SINR of the array in the xy plane in the presence of two (solid line) and three (dotted line) jammers. All of the jammers are in the xy plane and are 20 dB stronger than the desired signal. Note that the array is responding to the desired signal in the presence of two jammers and the output SINR reaches its optimum value (~ 7 dB) at 109° . The output SINR is minimum ($\sim \xi_d/\xi_j$) for all desired signal direction in the presence of three jammers. Thus, the array has two degrees of freedom in the xy plane.

Next, consider the array performance in a θ_r cut ($(\theta_r, 0^\circ, 90^\circ)$ conical cut) as shown in Figure IX-9. Projection of the array elements in a θ_r cut is also shown in the figure. Note that the planar array reduces to a linear array in the θ_r cut. Figure IX-10 shows the output SINR of the array in $\theta_r = 60^\circ$ cut in the presence of three jammers (solid line) and four (dotted line) jammers. All the jammers are incident in the $\theta_r = 60^\circ$ cut and are 20 dB stronger than the desired signal. The projection of the array elements in the cut is also shown in the figure. Note that the total number of projected elements in the cut is five. The array can, therefore, have a maximum of four degrees



(a)



(b)

Figure IX-7. a) Crossed array of five isotropic elements,
b) Projection of array in the xy plane.

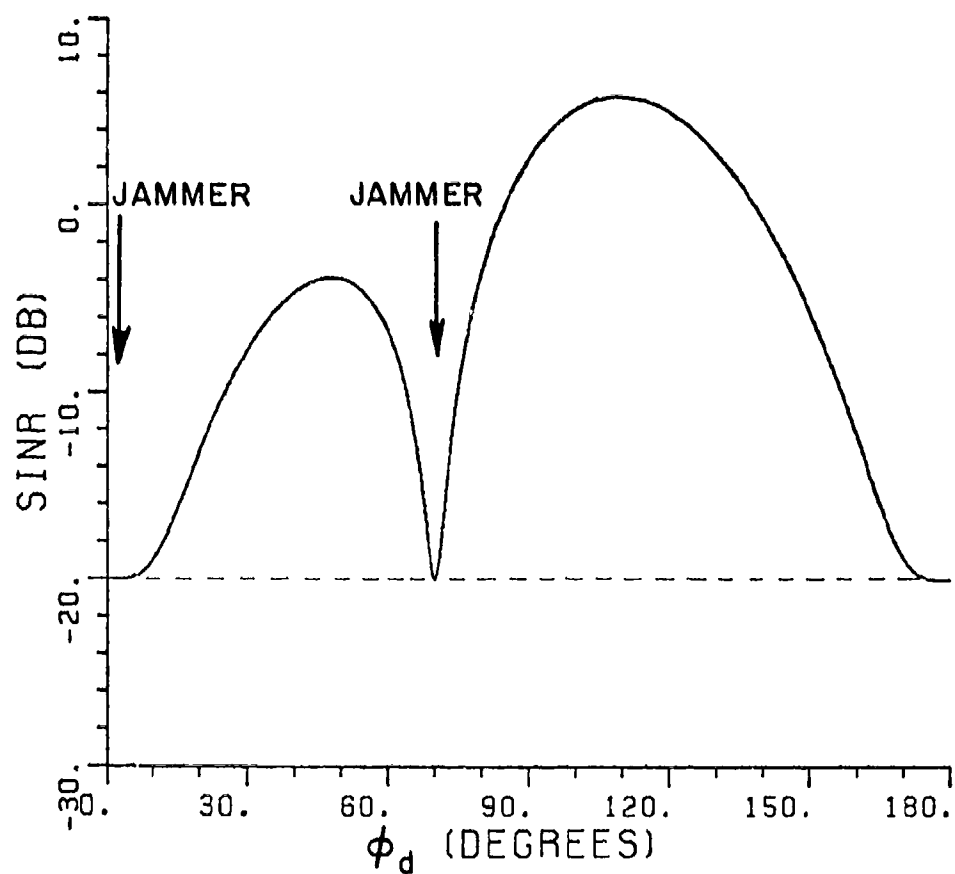
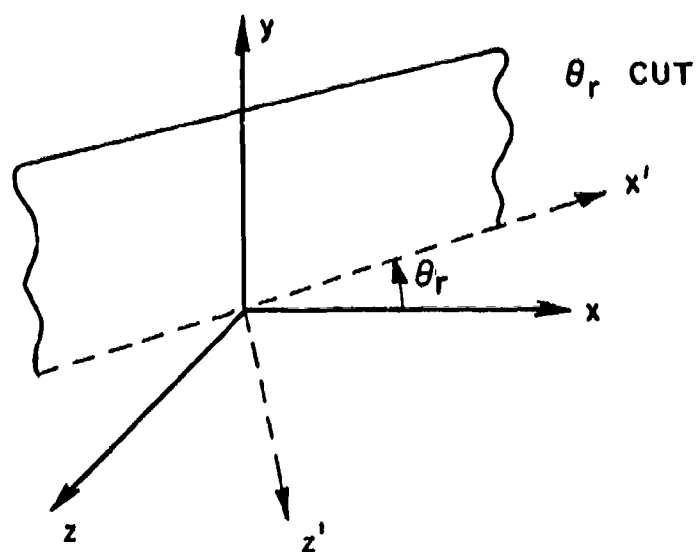
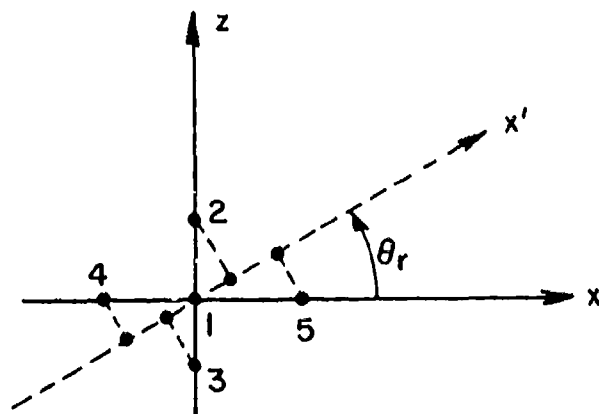


Figure IX-8. Output SINR of the crossed array in the xy plane in the presence of two (—) and three (----) jammers. $\xi_d = 1$, $\xi_{i1} = \xi_{i2} = \xi_{i3} = 100$, $\phi_{i1} = 0^\circ$, $\phi_{i2} = 70^\circ$, $\phi_{i3} = 109^\circ$.



(a)



(b)

Figure IX-9. a) θ_r cut in the coordinate system,
b) Projection of the array elements in the θ_r cut.

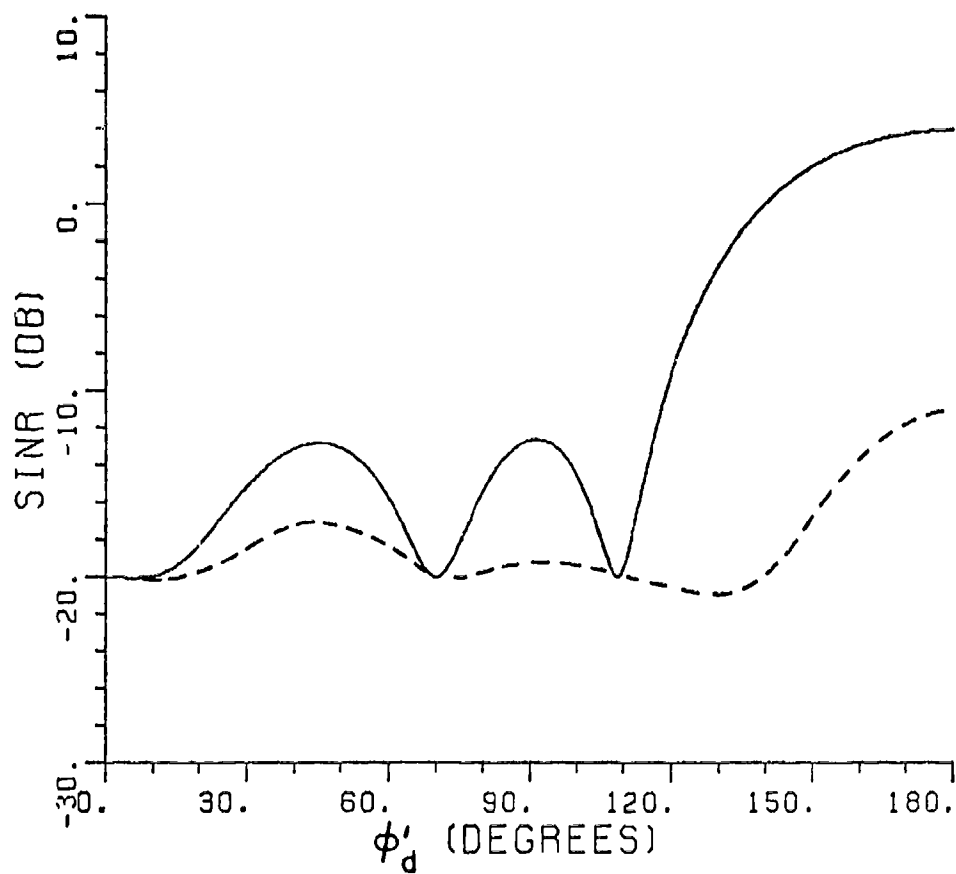


Figure IX-10. Output SINR of the crossed array in $\theta_r = 60^\circ$ cut in the presence of (—) three jammers, (----) four jammers.

$\phi'_{i1} = 0^\circ$, $\phi'_{i2} = 70^\circ$, $\phi'_{i3} = 109^\circ$, $\phi'_{i4} = 140^\circ$, $\xi_d = 1$,
 $\xi_{i1} = \xi_{i2} = \xi_{i3} = \xi_{i4} = 100$.

of freedom in the cut. From the output SINR plots it is clear that the array responds to the desired signal in the presence of three and four jammers but the output SINR never reaches its optimum value (~ 7 dB). Thus, although the array is able to null four jammers, the array does not have four degrees of freedom according to the definition proposed in this study. The reason for this will be discussed next where it will be shown that interelement spacings of the projected elements directly affect the number of degrees of freedom of an adaptive array in a cut.

C. EFFECT OF THE DISTRIBUTION OF PROJECTED ELEMENTS IN A CUT ON THE NUMBER OF DEGREES OF FREEDOM AN ADAPTIVE ARRAY

In the last section, it was shown that the maximum number of degrees of freedom of an adaptive array in a conical cut is given by the projection of the array elements in the $x'y'$ plane. In this section, the affect of the interelement spacings of the projected elements on the number of degrees of freedom of an adaptive array in the conical cut will be studied.

Figure IX-11 shows the output SINR of a linear array of four isotropic elements in the presence of three jammers. Interelement spacing is half a wavelength and the jammers are incident from orthogonal directions [1]. Note that the array is responding to the desired signal and the output SINR reaches its maximum (5 dB) at $\theta_d = 0^\circ$ and 180° . Thus, the array has three degrees of freedom. Figure IX-12 shows the output SINR of the array when the interelement spacing is reduced to 0.3λ . Again the jammers are incident from orthogonal directions. Note that the array is responding to the desired signal

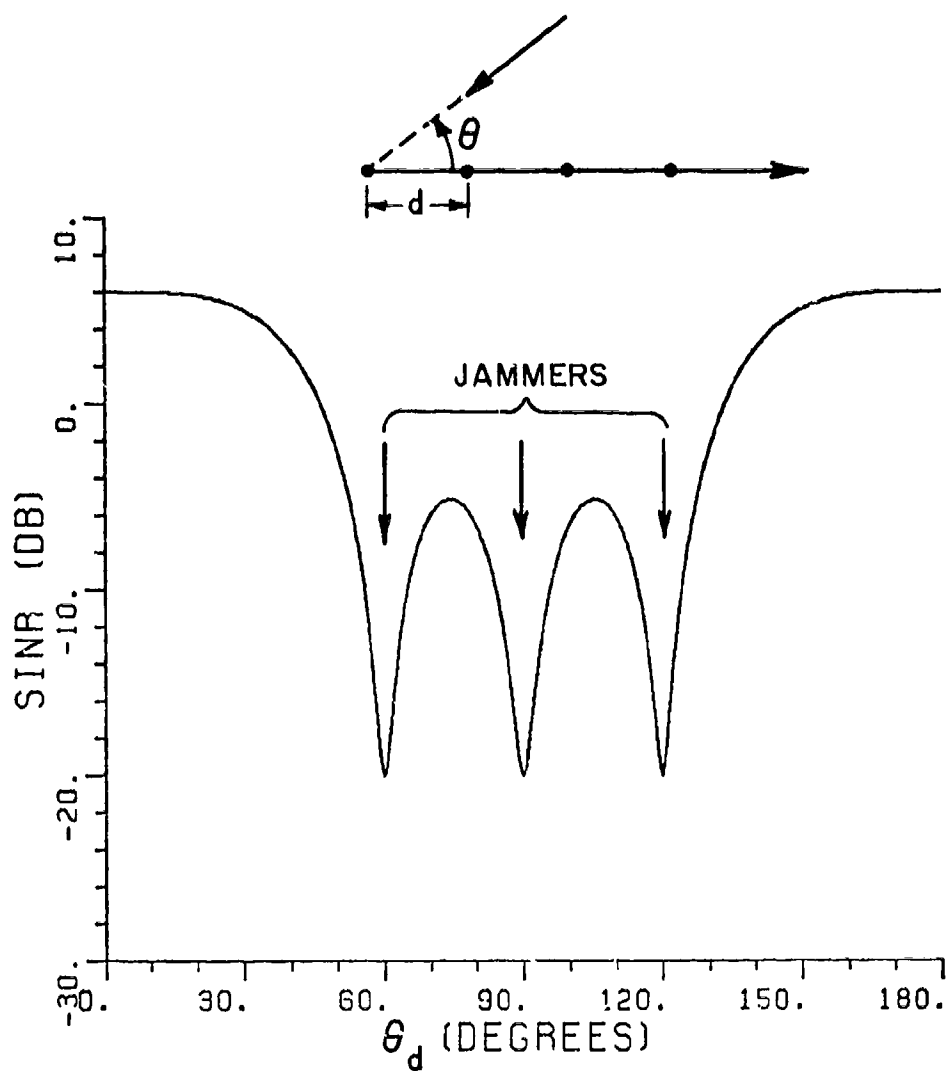


Figure IX-11. Output SINR of a linear array of four isotropic elements in the presence of three jammers. $d = 0.5\lambda$, $\theta_{j1} = 60^\circ$, $\theta_{j2} = 90^\circ$, $\theta_{j3} = 120^\circ$, $\xi_d = 1$, $\xi_{j1} = \xi_{j2} = \xi_{j3} = 100$.

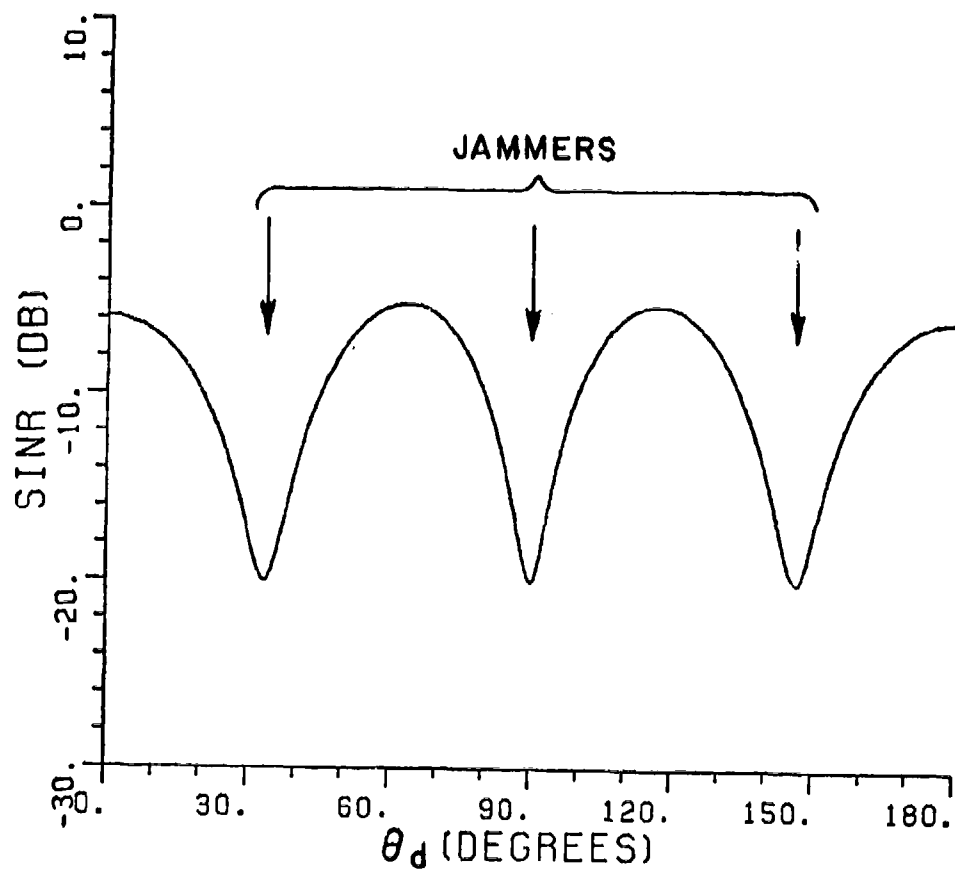


Figure IX-12. Output SINR of a linear array of four isotropic elements in the presence of three jammers. $d=0.3\lambda$, $\theta_{j1}=33.5^\circ$, $\theta_{j2}=90^\circ$, $\theta_{j3}=146.5^\circ$, $\xi_d=1$, $\xi_{j1}=\xi_{j2}=\xi_{j3}=100$.

but the output SINR never reaches its maximum value. The main beam of the array is, therefore, suppressed and the array does not have three degrees of freedom.

For a given aperture of length 'L', the maximum number of independent space samples one can have is $\frac{2L \sin \psi_{\max}}{\lambda} + 1$, where ψ_{\max} defines the field of view on either side of broadside, and the minimum separation between the samples should be approximately $\frac{\lambda}{2 \sin \psi_{\max}}$. The number of independent samples is related to the number of independent beams the antenna can point and thus to the number of degrees of freedom of the antenna. An antenna with N independent samples can point N-1 independent beams and, therefore, has N-1 degrees of freedom. Thus an antenna of length L has $\frac{2L \sin \psi_{\max}}{\lambda}$ degrees of freedom. In this study $\psi_{\max} = 90^\circ$ and, therefore, the number of degrees of freedom of the antenna is $\frac{2L}{\lambda}$.

In the case of an adaptive array, the continuous aperture is replaced by discrete elements. If the interelement spacing is approximately $\frac{\lambda}{2}$ and the total length of the array is L, the array will yield $\frac{2L}{\lambda} + 1$ independent samples and the number of degrees of freedom of the array will be $\frac{2L}{\lambda}$. If the array elements are densely packed so that the total number of elements exceeds $\frac{2L}{\lambda} + 1$, the number of degrees of freedom of the array would not exceed $\frac{2L}{\lambda}$. The array may be able to point more than $\frac{2L}{\lambda}$ independent nulls, but in the process, the gain of the array may drop, depending on the distribution of jammers. In the above example, when the interelement spacing was reduced to 0.3λ , the array was not able to achieve the maximum SINR for any desired signal direction though it was able to null three jammers. The reason was that the array does not have three degrees of freedom. The total aperture

of the array is 0.9λ . Thus, the array has a maximum of two degrees of freedom.

Another interesting point to be observed is that by increasing the interelement spacing so that it is more than $\lambda/2$, one can not increase the number of degrees of freedom of the array, since the maximum number of degrees of freedom of an array is given by $N-1$ (Section B), where N is the number of elements in the array. Increasing the interelement spacing will increase the total aperture and thus the resolution of the array, but the number of degrees of freedom of the array will remain fixed. An array with large interelement spacings may be able to null more than $N-1$ jammers, but the jammers would not be independent of each other from the array point of view. An illustration of this situation is discussed next.

Figure IX-13 shows the output SINR of a linear array of four isotropic elements in the presence of four jammers. The interelement spacing is one wavelength. Note that the array is responding to the desired signal and the output SINR reaches its maximum value (~ 6 dB) at 75.5° and 139.5° . Does this mean that the array has four degrees of freedom? The answer is no because the jammers incident from 0° and 90° are parallel jammers [1]. But the array certainly has three degrees of freedom: the jammers at 0° , 41.5° and 60° are orthogonal jammers. Figure IX-14 shows the output SINR of the array when the jammer incident at 90° changes its direction of incidence. Note that, with a change in the jammer direction, the output SINR decreases and drops to its minimum value for all desired signal direction when $\theta_{j4} = 75^\circ$. Thus, the number of degrees of freedom of the array is three. For large interelement

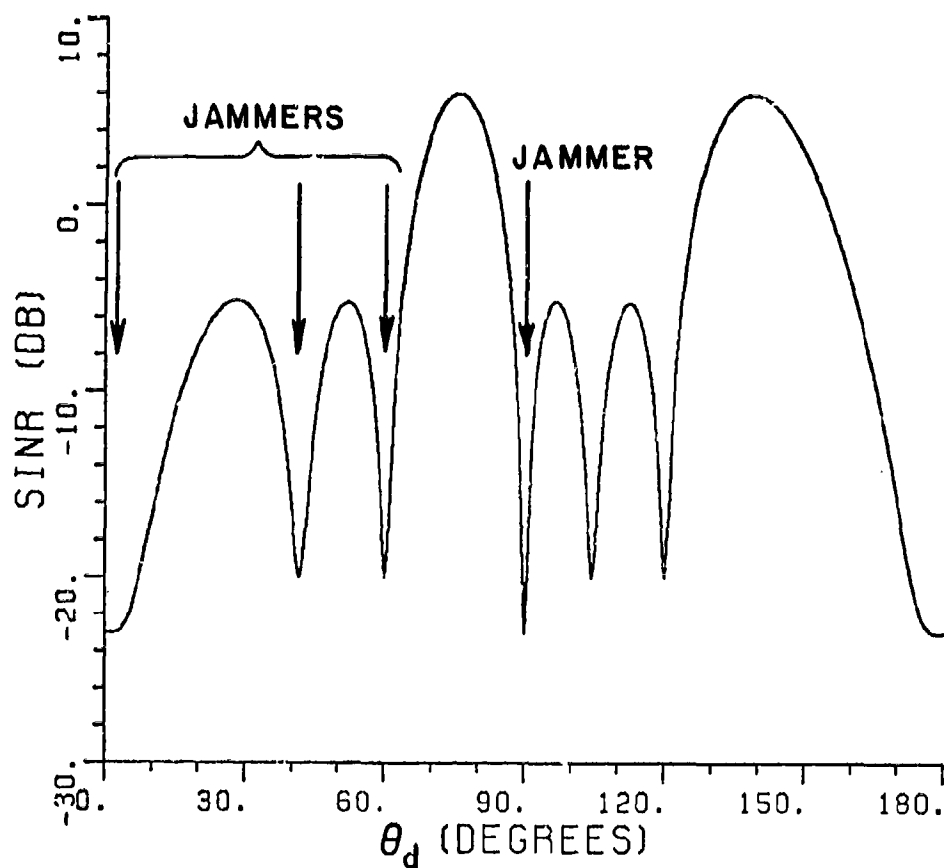


Figure IX-13. Output SINR of a linear array of four isotropic elements in the presence of four jammers. $d = \lambda$, $\theta_{j1} = 0^\circ$, $\theta_{j2} = 41.5^\circ$, $\theta_{j3} = 60^\circ$, $\theta_{j4} = 90^\circ$, $\xi_d = 1$, $\xi_{j1} = \xi_{j2} = \xi_{j3} = \xi_{j4} = 100$.

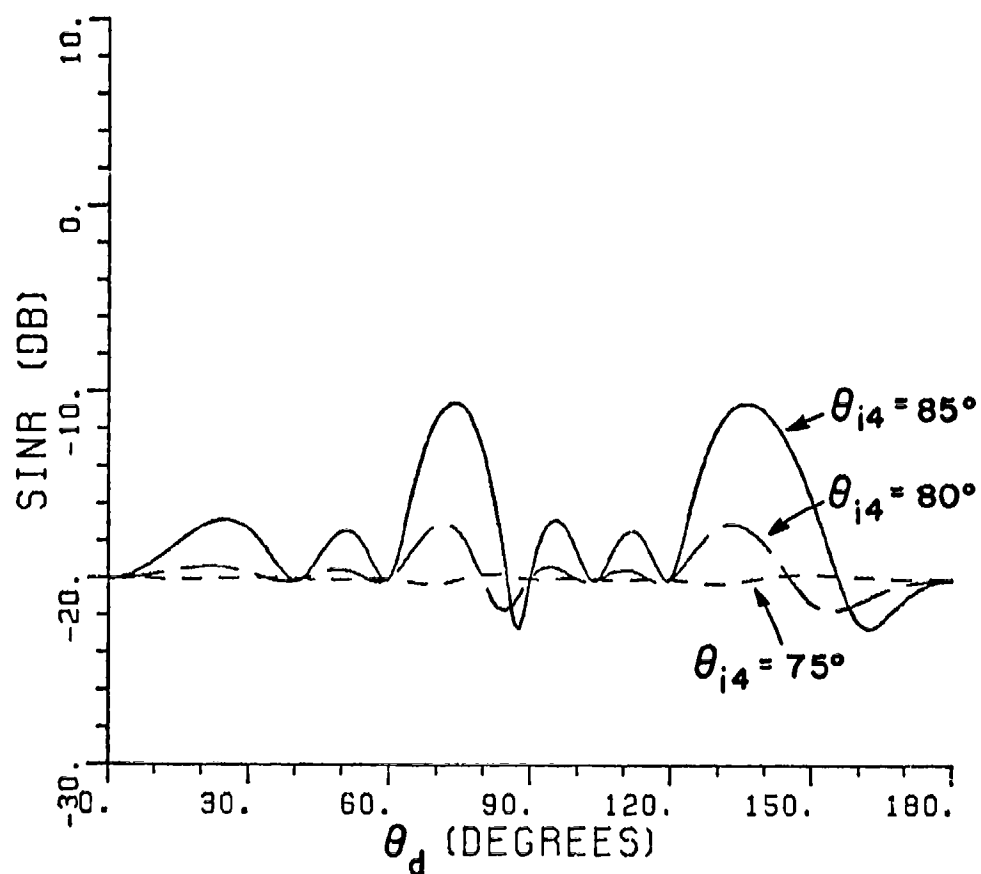


Figure IX-14. Output SINR of a linear array of four isotropic elements in the presence of four jammers for different θ_{i4} .

$$d = \lambda, \theta_{i1} = 0^\circ, \theta_{i2} = 41.5^\circ, \theta_{i3} = 60^\circ, \xi_d = 1,$$

$$\xi_{i1} = \xi_{i2} = \xi_{i3} = \xi_{i4} = 100.$$

spacings the total number of degrees of freedom of an adaptive array is, therefore, given by the total number of projected elements.

In this section, the effect of the distribution of projected elements on the number of degrees of freedom of an adaptive array in a conical cut was discussed. It was found that for large interelement spacings ($> \lambda/2$) the number of degrees of freedom will be given by $M-1$, where M is the total number of projected elements. If the elements are densely packed, the number of degrees of freedom is given by the aperture size measured in half wavelengths.

In the above discussion, all jammers were incident in the same planar cut. It was found that, for that case, the array has a maximum of $M-1$ degrees of freedom in the cut. The case when all the jammers are not in the same planar cut will be discussed in the next section, where it will be shown that the array may be able to null more than $M-1$ jammers.

D. ADAPTIVE ARRAY PERFORMANCE WHEN ALL JAMMERS ARE NOT IN THE SAME CUT

To find the number of degrees of freedom of an adaptive array in a planar cut when all jammers are not in the same cut, the crossed array (Figure IX-7) will be considered again. If the desired signal is in the xy plane, then the array response to the desired signal will be

$$F_d = (w_1 + w_2 + w_3) + w_4 e^{j 2\pi/\lambda x_4 \cos \phi_d} + w_5 e^{j 2\pi/\lambda x_5 \cos \phi_d} \quad (9.26)$$

where $(90^\circ, \phi_d)$ gives the desired signal direction and

$$w = (w_1 \ w_2 \ w_3 \ w_4 \ w_5)^T \quad (9.27)$$

is the weight vector of the array. The array response to the desired signal for all ϕ_d will be zero if, and only if,

$$\begin{aligned} w_1 + w_2 + w_3 &= 0 \\ w_4 &= 0 \\ w_5 &= 0 \end{aligned} \quad (9.28)$$

Let m independent jammers be incident on the array. Then

$$\begin{aligned} F_{ik} &= w_1 + w_2 e^{j 2\pi/\lambda z_2 \cos \theta_{ik}} + w_3 e^{j 2\pi/\lambda z_3 \cos \theta_{ik}} \\ &+ w_4 e^{j 2\pi/\lambda x_4 \sin \theta_{ik} \cos \phi_{ik}} + w_5 e^{j 2\pi/\lambda x_5 \sin \theta_{ik} \cos \phi_{ik}} \\ k &= 1, 2, \dots, m \end{aligned} \quad (9.29)$$

F_{ik} is the response of the array to the k^{th} jammer. In Equation (9.29), (θ_{ik}, ϕ_{ik}) defines the direction of the k^{th} jammer. Assuming that the jammers are much stronger than the thermal noise, then

$$\begin{aligned} F_{ik} &= 0 \\ k &= 1, 2, \dots, m \end{aligned} \quad (9.30)$$

For $m > 5$, the only possible solution to Equation (9.30) is

$$w_1 = w_2 = w_3 = w_4 = w_5 = 0 \quad (9.31)$$

Thus, the array response to the desired signal in the xy plane will be zero, or the array has, at most, four degrees of freedom. It was shown in Section B that if all the jammers are in the xy plane, then, at the most, the array can null two independent jammers. Let three jammers be incident on the array and let two of the jammers be in the xy plane.

Then

$$w_1 + w_2 + w_3 + w_4 e^{j 2\pi/\lambda x_4 \cos \phi_{11}} + w_5 e^{j 2\pi/\lambda x_5 \cos \phi_{11}} = 0 \quad (9.32)$$

$$w_1 + w_2 + w_3 + w_4 e^{j 2\pi/\lambda x_4 \cos \phi_{12}} + w_5 e^{j 2\pi/\lambda x_5 \cos \phi_{12}} = 0 \quad (9.33)$$

and

$$w_1 + w_2 e^{j 2\pi/\lambda z_2 \cos \theta_{13}} + w_3 e^{j 2\pi/\lambda z_3 \cos \theta_{13}} \quad (9.34)$$

$$+ w_4 e^{j 2\pi/\lambda x_4 \cos \theta_{13} \cos \phi_{13}} + w_5 e^{j 2\pi/\lambda x_5 \cos \theta_{13} \cos \phi_{13}} = 0.$$

From Equations (9.32) and (9.33)

$$w_4 (e^{j 2\pi/\lambda x_4 \cos \phi_{11}} - e^{j 2\pi/\lambda x_4 \cos \phi_{12}}) = \quad (9.35)$$

$$w_5 (e^{j 2\pi/\lambda x_5 \cos \phi_{12}} - e^{j 2\pi/\lambda x_4 \cos \phi_{12}})$$

and

$$w_1 + w_2 + w_3 = -w_4 e^{j 2\pi/\lambda x_4 \cos \phi_{11}} - w_5 e^{j 2\pi/\lambda x_5 \cos \phi_{12}}. \quad (9.36)$$

From Equations (9.28), (9.35), and (9.36), it is clear that the response of the array to the desired signal is zero if w_4 or $w_5=0$. But this is not the only possible solution for Equations (9.32) - (9.34). Hence,

the array will respond to the desired signal. In fact, in the case of an adaptive array, the weights will be chosen such that F_d in Equation (9.26) is maximized while satisfying Equations (9.32) - (9.34). Thus, the array can null more than two jammers. The jammers outside the cut are, therefore, not as effective as jammers inside the cut.

Figure IX-15 shows the output SINR of the array in the xy plane in the presence of four jammers (solid line) and five jammers (dotted line) respectively. The jammers are randomly distributed in the given field of view (upper half space) and are 20 dB stronger than the desired signal. Note that the array is responding to the desired signal in the presence of four jammers and the output SINR reaches its maximum value for some desired signal directions. In the presence of five jammers, the output SINR is very low (~ 20 dB) for all desired signal directions. Thus, the array has four degrees of freedom for the given distribution of jammers.

One important thing to be observed from the SINR plot is that the jammers closer to the planar cut (xy plane) have a stronger effect on the performance of the array in the cut. The angular separation between the planar cut and the jammer direction before the jammer starts causing nulls in the output SINR of the array in the cut depends upon the beam width or resolution of the array in the other principal cut (for xy plane the other principal cut will be yz plane). Figure IX-16 shows the output SINR of the crossed array in the xy plane in the presence of one jammer. The jammer is incident in the yz plane. Curves are drawn for different jammer directions. Note that when the jammer is 15° away from the xy plane, a null starts appearing in the output SINR of the array.

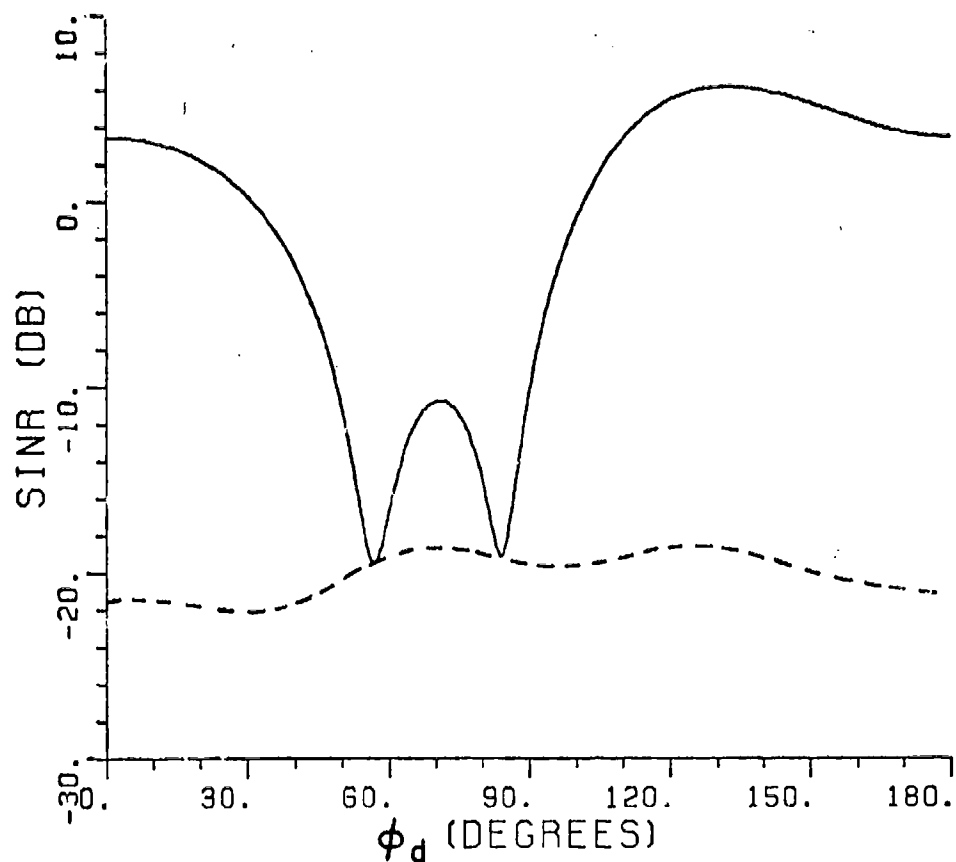


Figure IX-15. Output SINR of the crossed array in the presence of
 (—) four jammers, (----) five jammers vs desired
 signal in the xy plane. $(\theta_{i1}, \phi_{i1}) = (60^\circ, 0^\circ)$,
 $(\theta_{i2}, \phi_{i2}) = (80^\circ, 90^\circ)$, $(\theta_{i3}, \phi_{i3}) = (120^\circ, 40^\circ)$,
 $(\theta_{i4}, \phi_{i4}) = (150^\circ, 120^\circ)$, $(\theta_{i5}, \phi_{i5}) = (90^\circ, 150^\circ)$,
 $\xi_d = 1$, $\xi_{i1} = \xi_{i2} = \xi_{i3} = \xi_{i4} = \xi_{i5} = 100$.

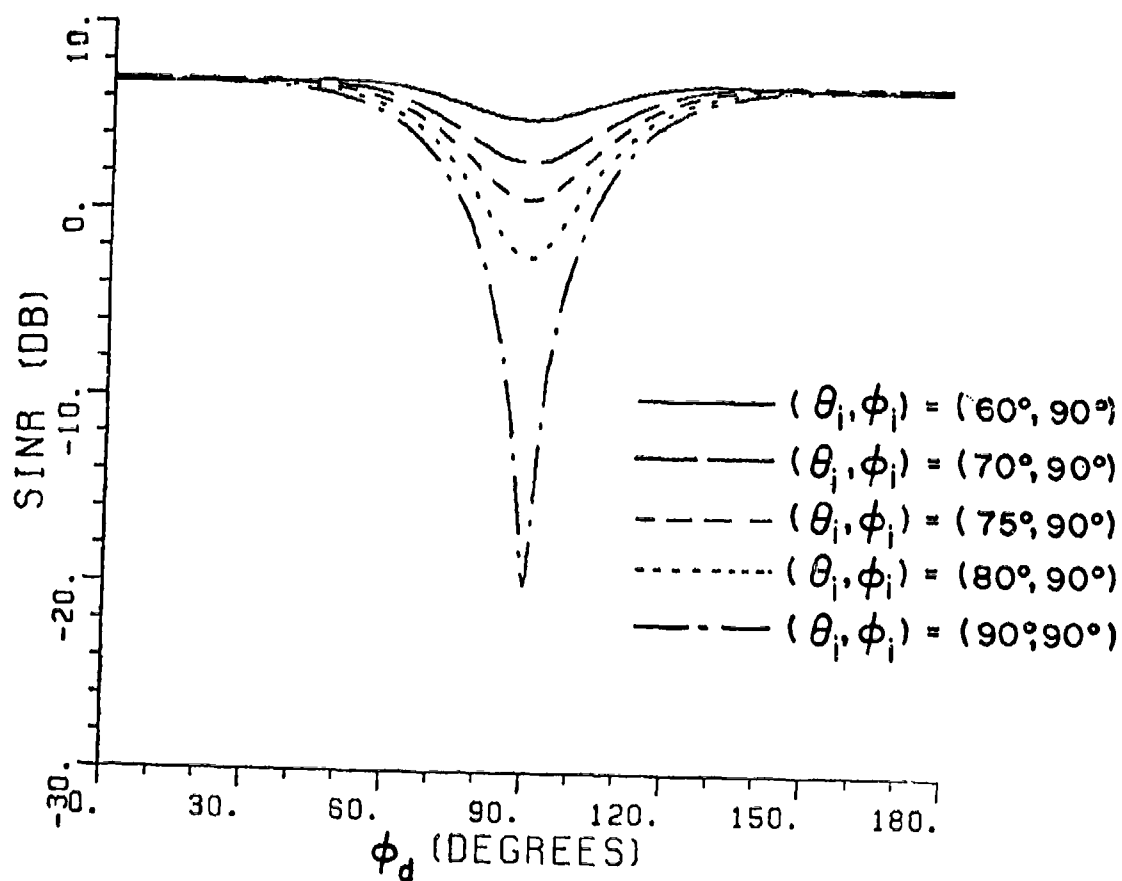


Figure IX-16. Output SINR of the crossed array of five elements in the xy plane in the presence of one jammer in the yz plane.
 $\xi_d = 1$, $\xi_j = 100$.

Figure IX-17 shows the output SINR of a seven element crossed array in the xy plane. The distribution of the array elements is also shown in the figure. The spacing between the elements is half a wavelength. From the element distribution, it is clear that the array has a narrower beam in the yz plane as compared to the 5-element array (Figure IX-7). The jammer is incident in the yz plane. Curves are drawn for different jammer directions. Note that now the jammer has to be within 10° of the xy plane before a null starts appearing in the output SINR of the array. Thus the resolution of the array in the yz plane indicates the minimum angular separation permitted between the jammer and the cut.

Figures IX-16 and IX-19 show the output SINR of the two arrays in the xy plane when the jammer is incident in $\theta_p=60^\circ$ cut. Again, note that the seven element array has more protection against the jammer outside the xy plane.

In this section, the number of degrees of freedom of an adaptive array in a cut for arbitrarily distributed jammers were studied. It was shown that the jammers incident in the cut are more effective than the jammers outside the cut. Further it was shown that jammers displaced from the cut cause degradation of the output SINR in proportion to their displacement from the cut and the angular resolution of the array in the orthogonal principal cut.

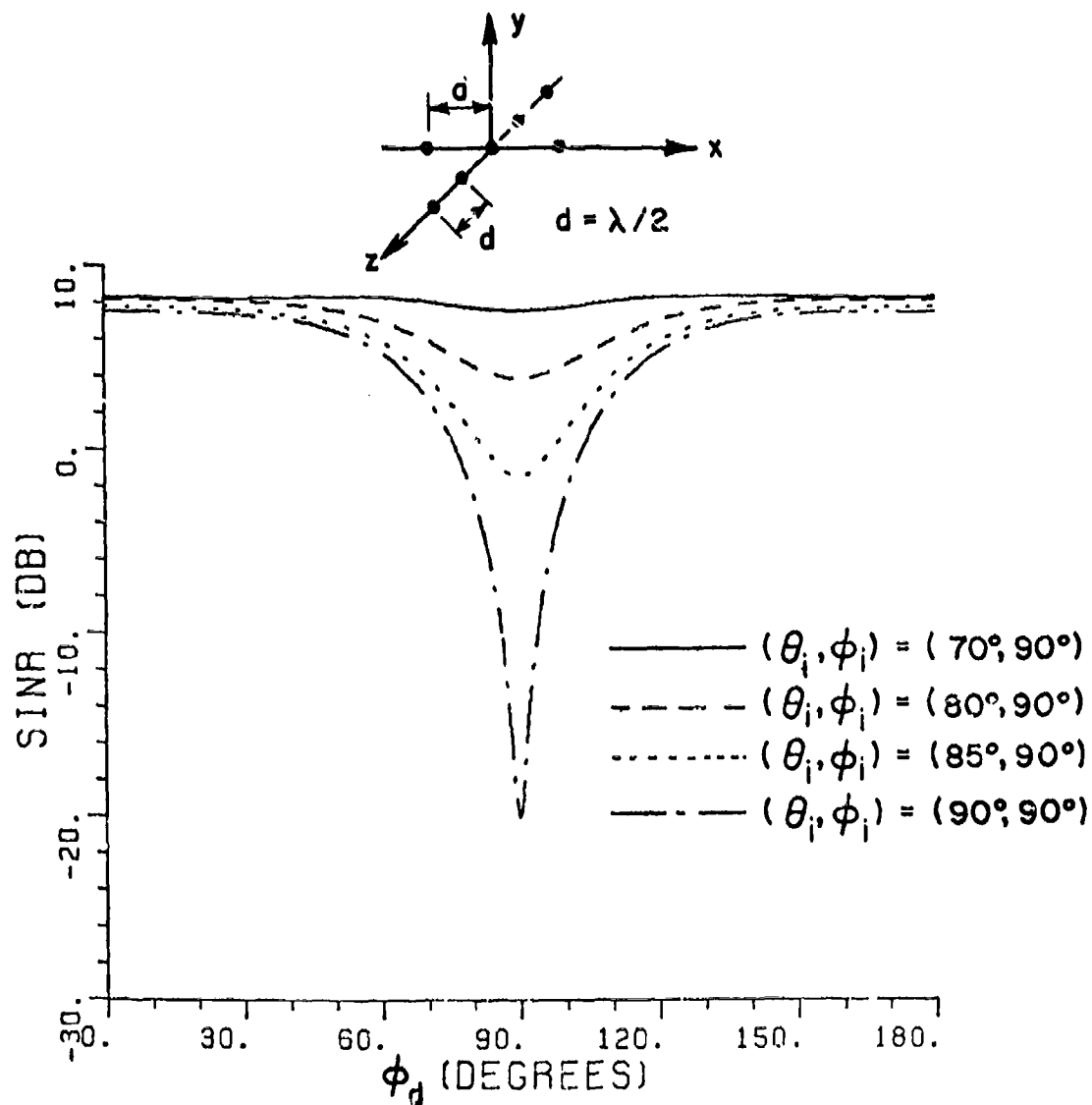


Figure IX-17. Output SINR of the crossed array of seven elements in the xy plane in the presence of one jammer in the yz plane.

$$\xi_d = 1, \xi_j = 100.$$

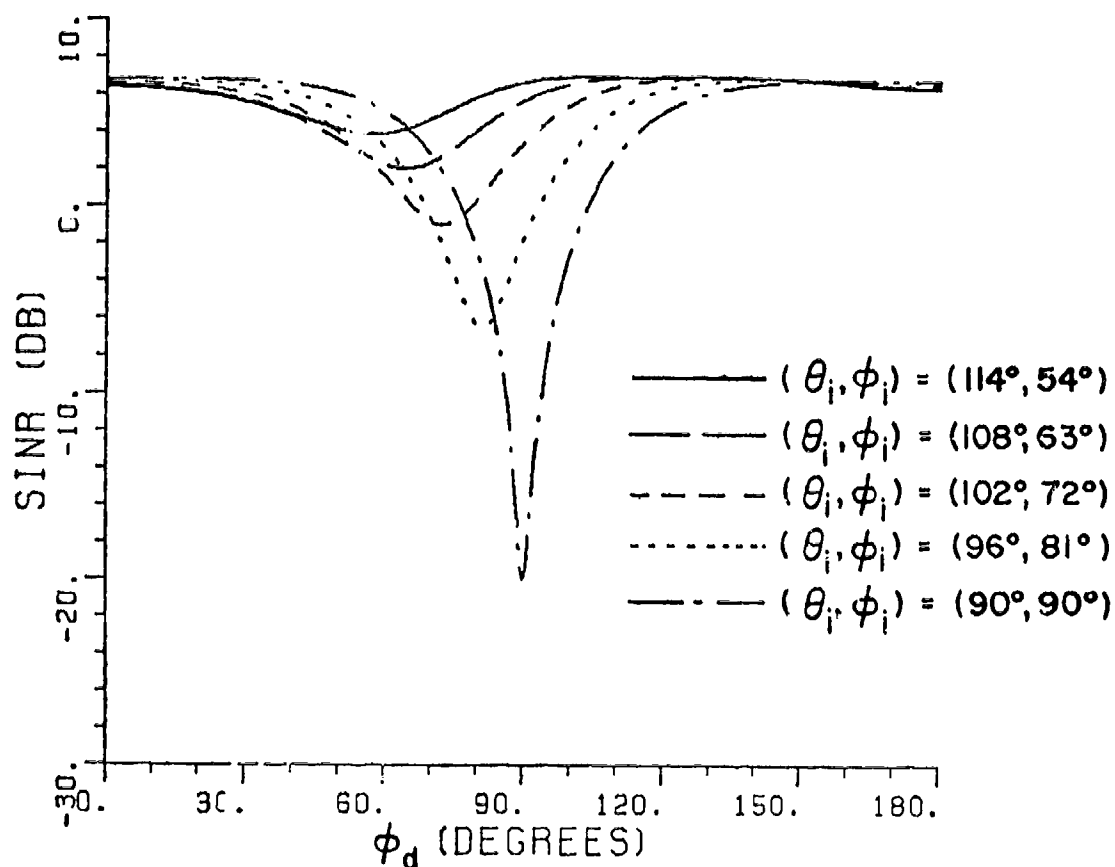


Figure IX-18. Output SINR of the crossed array of five elements in the xy plane in the presence of one jammer in $\theta_r = 60^\circ$ cut. $\xi_d = 1$, $\xi_i = 100$.

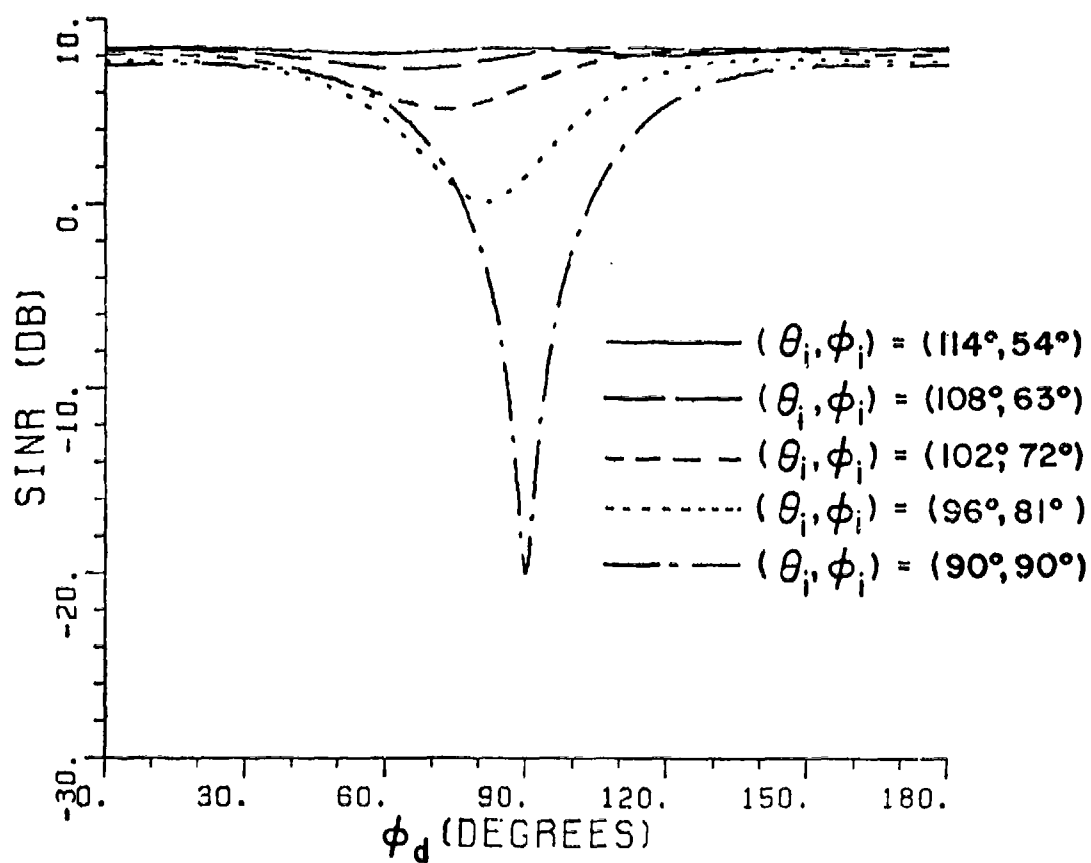


Figure IX-19. Output SINR of the crossed array of seven elements in the xy plane in the presence of one jammer in $\theta_r = 60^\circ$ cut.
 $\xi_d = 1$, $\xi_i = 100$.

E. CONCLUSIONS

In this section, the number of degrees of freedom of an adaptive array was studied. It was found that an adaptive array has the smallest number of degrees of freedom in a planar cut. The number of degrees of freedom of an adaptive array in a planar cut can be found by projecting the array of elements in the plane. For large interelement spacings, the number of degrees of freedom is given by the number of projected elements with different locations in the plane. If the elements are densely packed, the number of degrees of freedom will be dictated by the size of the aperture formed by the projected elements.

F. REFERENCES

- [1] I.J. Gupta and A.A. Ksienski, "Prediction of Adaptive Array Performance in a Multiple Jammer Environment," Technical Report 711679-8, December 1981. The Ohio State University ElectroScience Laboratory, Department of Electrical Engineering; prepared under Contract F30602-79-C-0068 for Rome Air Development Center.

SECTION X

ELEMENT PLACEMENT FOR ADAPTIVE ANTENNA ARRAYS

A. INTRODUCTION

One of the results obtained in previous work [1,2] was that the conventional design goals of antenna arrays, namely low sidelobes and a narrow beam, are essential to the adequate performance of an array in an adaptive mode. One can meet these design goals in a planar array by distributing the array elements at a spacing of $d = \frac{\lambda}{2 \sin \psi_{\max}}$, where ψ_{\max} defines the field of view measured from the broadside direction. The array so obtained will completely fill the available aperture and may require a large number of antenna elements. The larger the number of antenna elements, the larger will be the number of feedback loops which in turn will add to the cost and complexity of the system. Thus, the total number of antenna elements should be kept to a minimum. Also, in some applications, for example, airborne radar systems, the whole aperture may not be available for the distribution of array elements. More restricted distributions with fewer antenna elements, therefore, should be considered.

In this section, the direct relationship between the conventional array characteristics and the array performance in an adaptive mode is used to find element locations of an adaptive array. It is shown that the number of array elements can be reduced by a significant factor. First, an algorithm to select element location of a linear array is developed. The algorithm leads to a one dimensional thinned array which provides the required performance in a two dimensional field of view. The linear array is then used to develop planar arrays which provide required performance levels in a three dimensional field of view.

The design algorithm is described in subsection B. The interelement spacing of a linear array in the presence of a single incident jammer are given in subsection C. In subsection D, the algorithm is used to find interelement spacing in the presence of multiple jammers. Planar arrays are discussed in subsection E.

B. THE ELEMENT PLACEMENT ALGORITHM

In the presence of m independent jammers, an antenna array to be used in an adaptive mode needs at least $m+1$ elements (the array should have at least m degrees of freedom). To provide good resolution the array elements should have large interelement spacings. But interelement spacings at or above $\frac{\lambda}{2}$ may result in high sidelobes which in turn will cause dips¹ in the output SINR. In order to avoid these

¹Whenever the output SINR of an adaptive array drops below a certain threshold (except when the jammer direction approaches the desired signal direction), it will be called a dip in the output SINR. Depending upon the system requirements one can choose any threshold. In this work the input desired signal-power-to-thermal noise ratio (E_d) is chosen as the threshold.

dips one should either decrease interelement spacing or add extra elements to the antenna such that the total aperture remains unchanged. Decreasing interelement spacing will decrease the total antenna aperture resulting in poorer resolution. Therefore, in the design procedure given below it is assumed that the array has more than $m+1$ elements. Further, the antenna elements are distributed to achieve the maximum resolution in the presence of the maximum expected number of jammers.

For large angular separations (of the order of half a null to null beamwidth of the array) between jammers, the output SINR of an array of N isotropic elements is [2]

$$\text{SINR} = \xi_d \left(N - \sum_{k=1}^m \frac{|g_k|^2}{N} \right) \quad (10.1)$$

where g_k is the value of the unperturbed pattern in the k th jammer direction. The degradation in the output SINR will reach a maximum when all the jammers are incident from directions in which the unperturbed pattern has sidelobe peaks.² Let s be the largest sidelobe level, then

$$(\text{SINR})_{\min} > \xi_d \left(N - \frac{ms^2}{N} \right) \quad (10.2)$$

The equality in Equation (10.2) will hold if and only if all the sidelobes are of the same level. Assuming that all sidelobes are of the

²As pointed out in [2], jammers at small angular separations can cause more degradation. But as the total number of antenna elements is assumed to be more than the expected number of jammers the total degradation will not differ much from the one given in Equation (10.2). Further, we will see that the element distribution is accomplished using the worst situation, therefore, jammers at small angular separations should not cause problems.

same level³ and the minimum desirable output SINR (threshold) is chosen to be ϵ_d , we obtain from Equation (10.2)

$$s = \sqrt{\frac{N^2 - N}{m}}. \quad (10.3)$$

Thus knowing the total number of antenna elements and the expected number of jammers, the maximum permissible sidelobe level can be calculated. The antenna elements should be distributed such that all the sidelobe peaks are lower than the maximum permissible sidelobe levels. Further, for a good resolution, the antenna should have the minimum beamwidth. It is well known that an antenna with uniform sidelobes has the narrowest mainbeam. The antenna elements, therefore, should be distributed such that all sidelobes are uniform and are at a level s . For a large number of antenna elements, one can use the theory of random arrays [3] to distribute the array elements. The sidelobe levels of the distribution of elements thus obtained will be less than s and the output SINR will not have any dips. The array will provide the maximum resolution in the presence of the maximum expected number of jammers. Dynamic programming [4] can also be used to select optimum element locations.

A new algorithm to select element locations of an adaptive array is given below. The algorithm is useful for small arrays (total number of antenna elements is 10-15). The algorithm distributes the antenna elements such that all the sidelobes are below the level given by

³This is a pessimistic assumption, but is safe.

Equation (10.3) and thus guarantees no dips in the output SINR. The algorithm is applicable to linear arrays and leads to a thinned array. The algorithm is based on dividing the total number of array elements into two parts.

a) The Constraint Elements: If m interference signals are expected to be incident on the array then $m+1$ elements will be needed in this part of the array. These elements will be referred to as the constraint elements. The constraint elements are uniformly spaced to ensure

(i) The maximum sidelobe level to be less than the one given by Equation (10.3) when $N=m+1$.

(ii) The required number of degrees of freedom.

Since the constraint elements are equally spaced the constraint part of the array would have grating lobes for excessive interelement spacings. To avoid grating lobes, one should choose spacing between the constraint elements, d_c , such that

$$d_c < \frac{\lambda}{2 \sin \psi_{\max}} \quad , \quad (10.4)$$

where ψ_{\max} is the maximum field of view on either side of the broadside direction (Figure X-1). Next, the constraint elements are distributed to ensure m degrees of freedom. This requirement asks for a minimum of m natural nulls⁴ in the given

⁴Nulls obtained by the uniform illumination of an antenna.

field of view. For a linear array of N equally spaced isotropic elements, the minimum interelement spacing for $N-1$ natural nulls in the given field of view is

$$\frac{d}{\lambda} = \frac{N-1}{2N \sin \psi_{\max}} \quad (10.5)$$

Therefore, for m incident jammers

$$\frac{m}{2(m+1) \sin \psi_{\max}} < \frac{d_c}{\lambda} < \frac{1}{2 \sin \psi_{\max}} \quad (10.6)$$

If the field of view extends to the whole visible space, i.e., $\psi_{\max} = \pi/2$ then from Equation (10.6)

$$\frac{m}{2(m+1)} < \frac{d_c}{\lambda} < \frac{1}{2} \quad (10.7)$$

- b) The Resolution Elements: Since the constraint elements have an interelement spacing $d_c < \frac{\lambda}{2 \sin \psi_{\max}}$, the constraint part of the array may not provide the required resolution. As a result, additional elements will be needed to ensure the required resolution. These elements are placed at relative large distances and constitute the "resolution" part of the array. These elements will be called the "resolution elements".

The constraint elements are specified first. Once the spacing of the constraint element is decided, one adds resolution elements until the required resolution is achieved.

We will develop the algorithm for a single incident jammer and then the algorithm will be extended to multiple jammers.

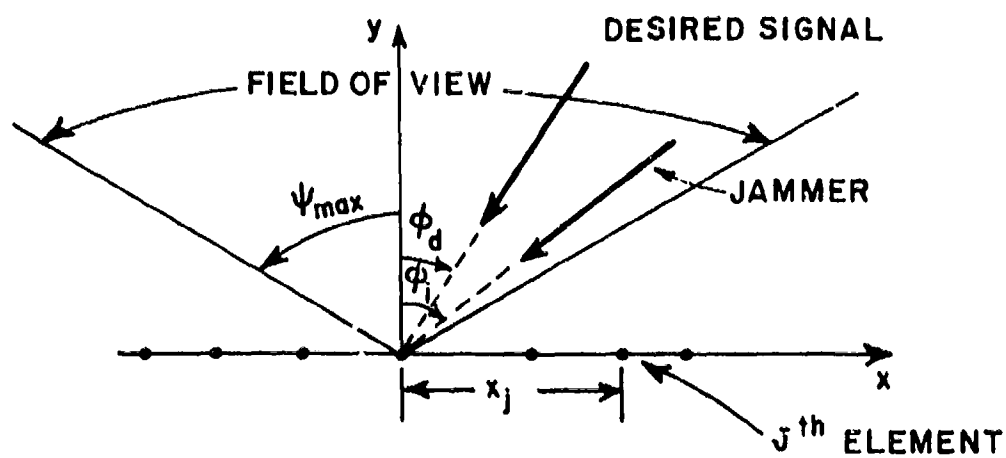


Figure X-1. A linear of N isotropic elements with one incident jammer and a desired signal.

3. ELEMENT LOCATIONS OF A LINEAR ARRAY IN THE PRESENCE OF ONE JAMMER

a) Constraint Element Placement

In the presence of one jammer, the constraint part of the array consists of two elements. From Equation (10.3) the maximum permissible sidelobe level for the constraint part of the array, therefore, is $\sqrt{2}$ volts (V). From Equation (10.7)

$$0.25 < \frac{d_c}{\lambda} < 0.5 \quad (10.8)$$

Let us choose $d_c = 0.375\lambda$. It is the maximum allowable spacing between the constraint elements to limit the sidelobe levels within $\sqrt{2}$ V. Figure X-2 shows the unperturbed pattern of the two element array (constraint part). The spacing between the two elements is 0.375λ and the desired signal is incident from $\phi = -90^\circ$. Note that the sidelobe level is less than $\sqrt{2}$ V, but the array has a very wide mainbeam. The array operating in an adaptive mode, therefore, will not have any dips but the resolution of the array will be poor. Figure X-3 shows the output SINR of the array in the presence of one jammer. The desired signal is incident from $\phi = -90^\circ$ while the jammer is swept across the whole visible space. $\xi_d = 1$ and $\xi_j = 100$ in the plot. The output SINR is plotted as a function of the jammer direction. Note that there are no dips in the

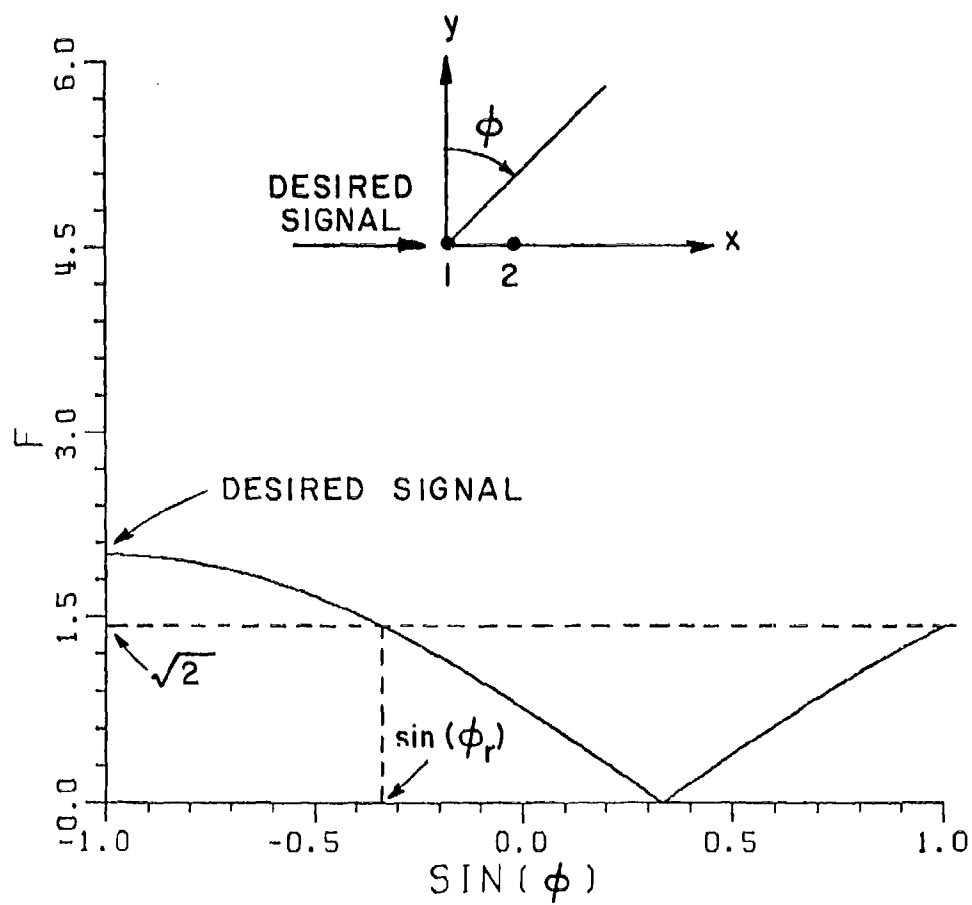


Figure X-2. Unperturbed pattern (F) of a linear array of two elements (constraint elements). $x_1=0.$, $x_2=0.375\lambda$, $\phi_D=-90^\circ$.

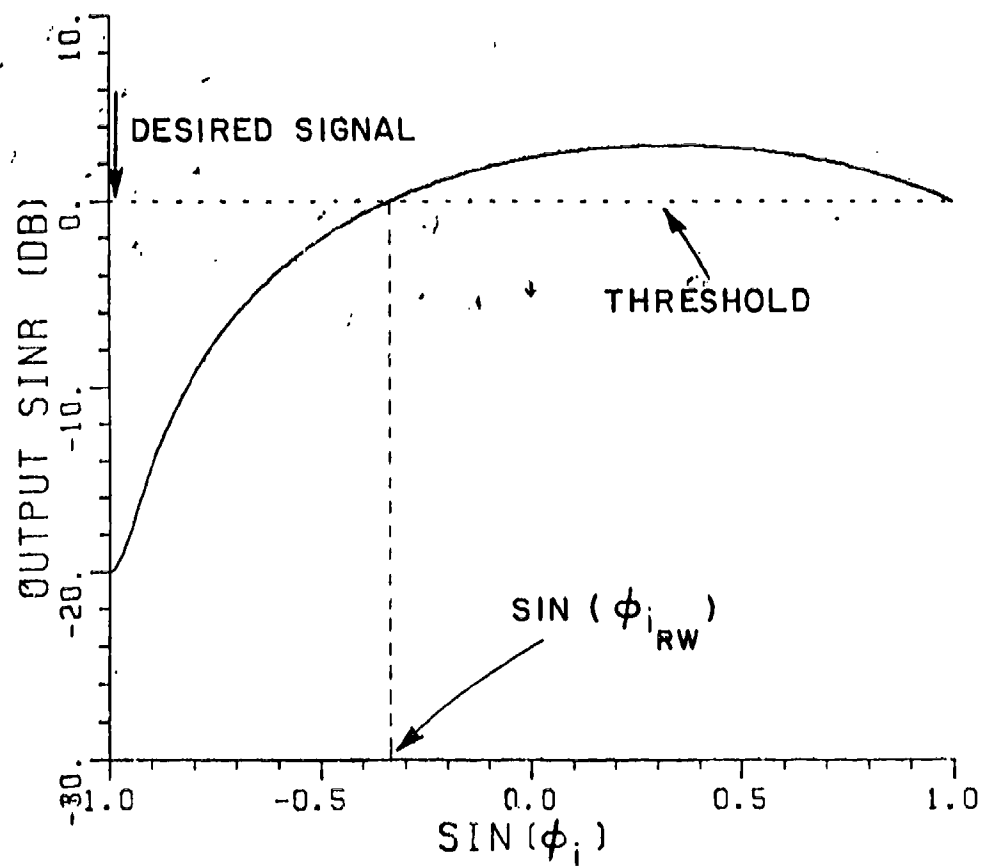


Figure X-3. Output SINR of a two element (constraint elements) array in the presence of one jammer vs. the jammer direction. $x_1=0$, $x_2=0.375\lambda$, $\phi_d=-90^\circ$, $\xi_d=1$, $\xi_i=100$.

output SINR, i.e., for large angular separation between the two signals the output SINR never goes below threshold (ξ_d in this study). On the other hand, the resolution of the array is relatively poor. The minimum angular separation (between a jammer and a desired signal) required to bring the output SINR from a null (when the two signals coincide) to the threshold will be called the resolution of the array, and is defined as

$$R = | \sin \phi_d - \sin \phi_{j_{RW}} | \quad , \quad (10.9)$$

where $\phi_{j_{RW}}$ is the jammer direction at which the output SINR reaches the threshold. For example, in Figure X-3, $\sin \phi_d = -1$, $\sin \phi_{j_{RW}} = -0.333$ and, therefore, $R = 0.667$.

In order to improve the resolution one must add resolution elements which will complete the design.

- b) Resolution Element Placement: Since the maximum resolution of a linear array is dependent on its total length, or distance between the end elements, one must add resolution elements to increase the maximum aperture. With the addition of the first resolution element the unperturbed pattern of the array will change and the amplitude of the unperturbed pattern of the new array will be within $\pm 1V$ of the amplitude of the unperturbed pattern of the constraint elements. From Equation (10.3), the maximum permissible sidelobe level of a three element array in the presence of one jammer is 2.45V. Thus, if the new element

is added such that the sidelobes of the new array are lower than 2.45V, the array performance in the adaptive mode will be satisfactory. Since the sidelobes due to the constraint part are less than 1.4V, the amplitude of the unperturbed pattern of the new array in this region will be less than 2.4V and the array performance for a jammer in this angular region will meet the required performance level. The new sidelobes generated in the mainbeam region of the constraint part, however, may have higher amplitude than 2.45V which in turn will cause dips in the output SINR. The new sidelobes will be generated due to the interferometric effect produced by the end elements. One way to keep the sidelobe levels lower than 2.45V is to add the resolution element such that the first grating lobe of the interferometer falls outside the angular region at which the mainbeam drops down to the 1.45V level. Let this angle be ϕ_r . The length of the interferometer that produces the first grating lobe at ϕ_r is given by

$$\frac{1}{\lambda} = \frac{1}{|\sin \phi_m - \sin \phi_r|} \quad , \quad (10.10)$$

where ϕ_m defines the direction of the mainbeam. From Figure X-2, $\sin \phi_m = -1$ and $\sin \phi_r = -0.333$. Substituting these values in Equation (10.10), we get

$$\frac{1}{\lambda} = 1.5 \quad .$$

Or, the first resolution element should be added such that the total length of the array is 1.5λ . One should note that the resolution element can be added on either side of the original array. Figure X-4 shows the unperturbed pattern of the new array. The element distribution is also shown in the figure. Note that all the sidelobe peaks are less than $2.45V$ and the array has a narrower mainbeam than the original array (Figure X-2). The array operating in an adaptive mode, therefore, should have better resolution. Figure X-5 shows the output SINR of the array in the presence of one jammer as a function of the jammer direction. Note that the resolution of the array has improved and there are no dips in the output SINR.

If one wishes to improve the resolution further, a second resolution element may be added. From Equation (10.3) the maximum permissible sidelobe level of a four element array in the presence of one jammer is $3.465V$. Therefore, the next resolution element should be added such that the first grating lobe of the new interferometer falls outside the angular region at which the main lobe drops down to $2.465V$ level. From Figure X-4, $\sin \phi_r = -0.844$. Using Equation (10.10),

$$\frac{1}{\lambda} = 6.4$$

or, the second resolution element should be added such that the total length of the array is 6.4λ . Figure X-6 shows

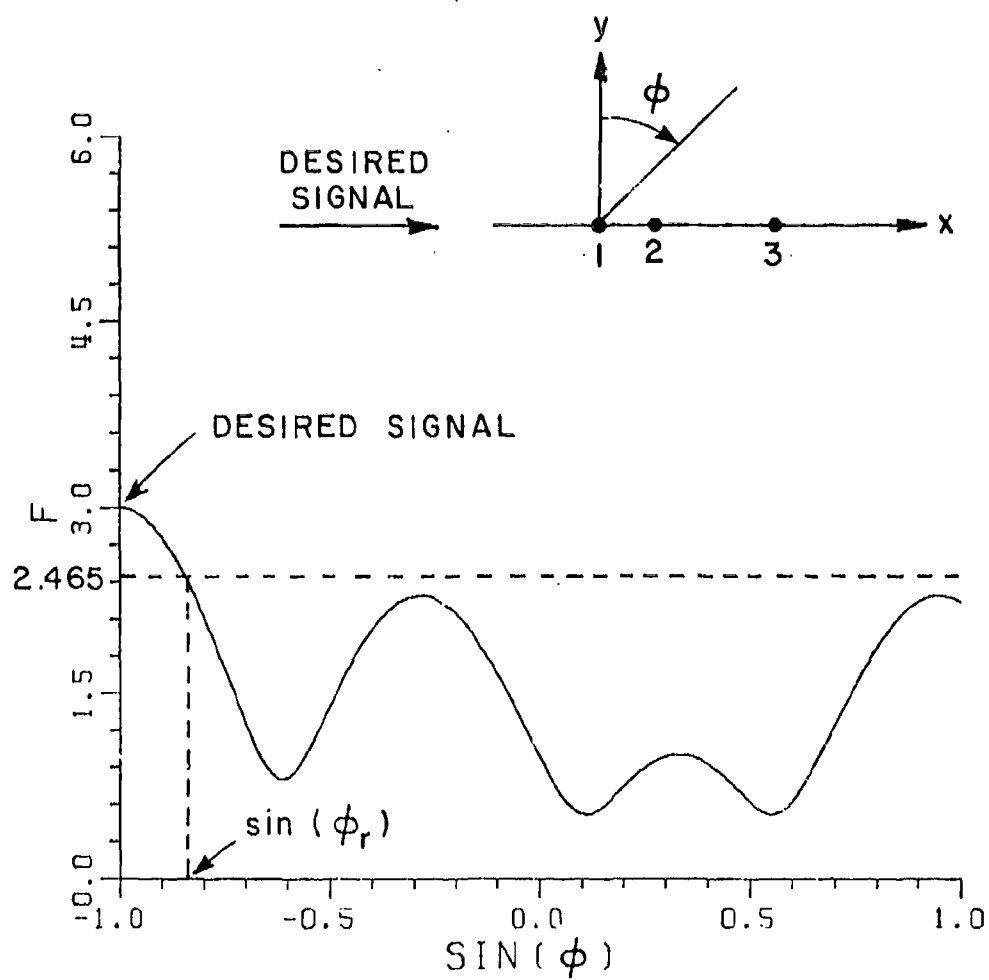


Figure X-4. Unperturbed pattern (F) of a three element array
 (constraint elements plus one resolution element). $x_1=0.$,
 $x_2=0.375\lambda$, $x_3=1.5\lambda$, $\phi_d=-90^\circ$.

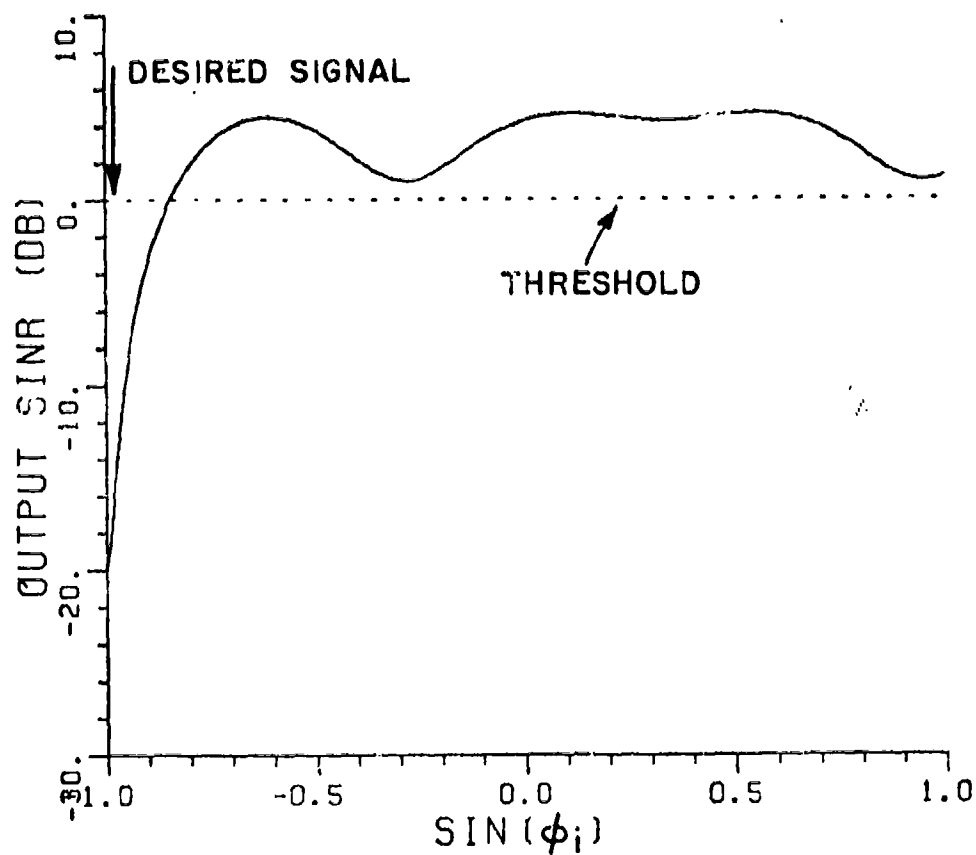


Figure X-5. Output SINR of a three element array (constraint elements plus one resolution element) in the presence of one jammer vs. the jammer direction. $x_1=0.$, $x_2=0.375\lambda$, $x_3=1.5\lambda$, $\phi_d=-90^\circ$, $\epsilon_d=1$, $\epsilon_f=100$.

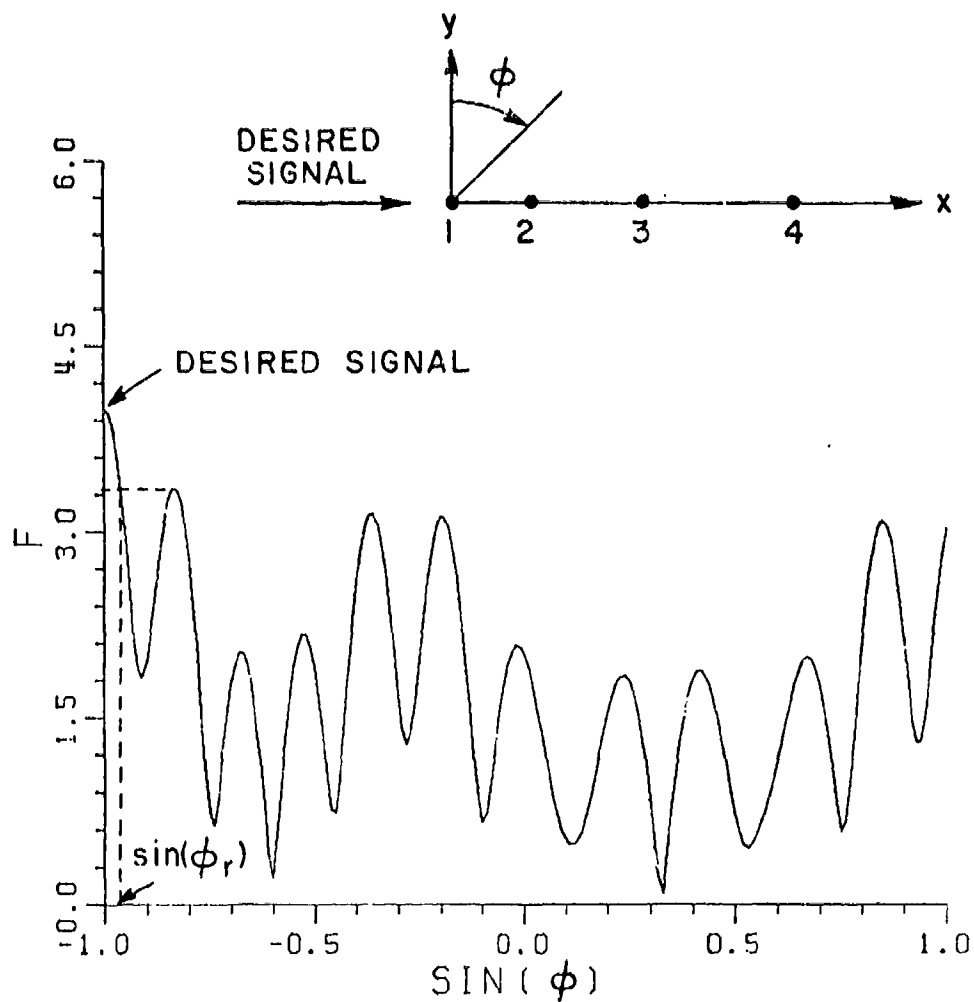


Figure X-6. Unperturbed pattern (F) of a four element array
(constraint elements plus two resolution elements).
 $x_1=0.$, $x_2=0.375\lambda$, $x_3=1.5\lambda$, $x_4=6.4\lambda$, $\phi_d=-90^\circ$.

the unperturbed pattern of the new array. The element distribution is also shown in the figure. Note that all the sidelobe peaks are less than 3.465V and the array has a narrower mainbeam than the three element array (Figure X-4). The array operating in an adaptive mode, therefore, should have better resolution. Figure X-7 shows the output SINR of the array in the presence of one jammer as a function of the jammer direction. Again there are no dips in the output SINR and the resolution has greatly improved. Thus, one can achieve as much resolution as one wishes provided that the number of elements does not exceed the specified number.

In the above discussion, Equation (10.3) was used to find the permissible sidelobe level of the new array and the sidelobe level was used to find the angle ϕ_r . Instead, one can use the peak of the largest sidelobe of the original array to find the angle ϕ_r . It leads to approximately the same distribution of antenna elements, but is a faster way to build the antenna. For example, using the peak of the largest sidelobe (Figure X-6), $\sin \phi_r = -0.967$ and thus the next resolution element should be added such that the total length of the array is 30λ (using Equation (10.10)), which is approximately the same as will be obtained by using Equation (10.3). Thus the different steps involved in the process are:

- (1) Find the spacing of the constraint elements.
- (2) Find the peak of the largest sidelobe of the array.

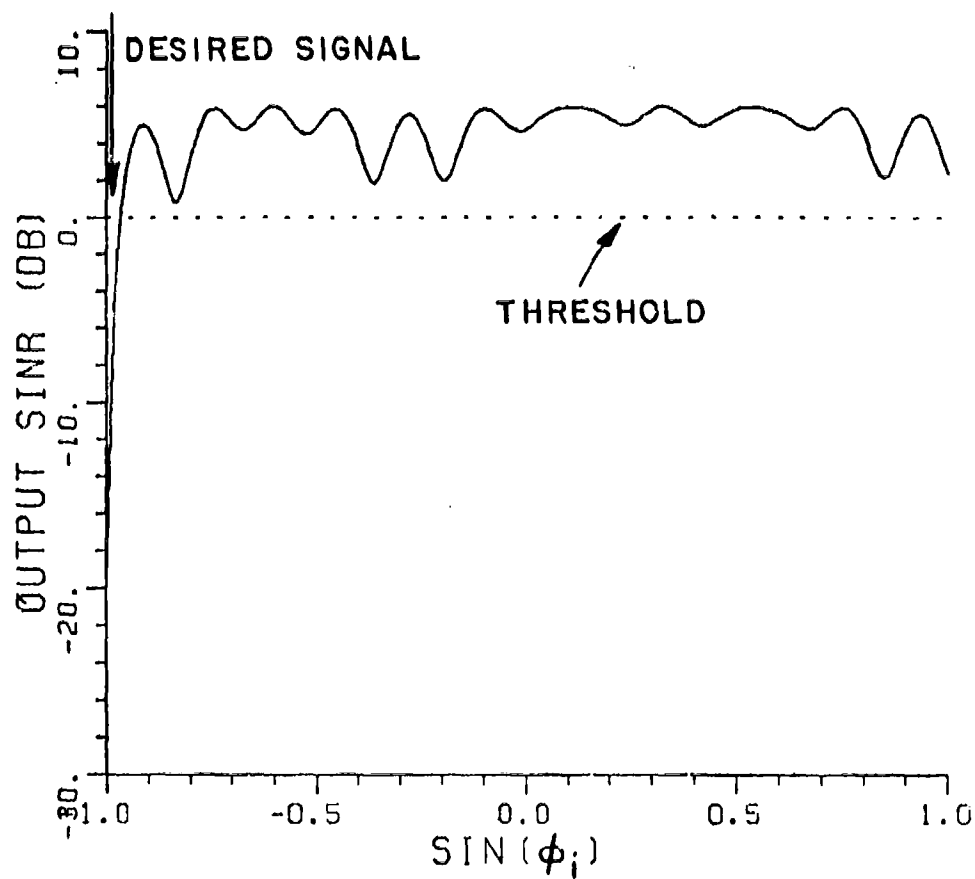


Figure X-7. Output SINR of a four element array (constraint elements plus two resolution elements) in the presence of one jammer vs. the jammer direction. $x_1=0.$, $x_2=0.375\lambda$, $x_3=1.5\lambda$, $x_4=6.4\lambda$, $\phi_d=-90^\circ$, $\xi_d=1$, $\xi_j=100.$

- (3) Find the angular location, ϕ_r , at which the mainbeam drops down to the level of the peak of the largest sidelobe.
- (4) Add a resolution element to the array such that the total length of the array becomes

$$\frac{1}{\lambda} = \frac{1}{|\sin \phi_m - \sin \phi_r|}$$

- (5) Repeat steps 2, 3 and 4 until the desired resolution is achieved or the total number of elements exceeds the specified number.

In this section the element locations of a linear array in the presence of one jammer were found. It is clear that, by using the prescribed algorithm, one can reduce the number of array elements by a significant factor, (a completely filled 6.4 wavelength aperture needs approximately 14 elements). In the next section, the algorithm is used to select element locations of a linear array in the presence of multiple jammers.

D. ELEMENT PLACEMENT OF A LINEAR ARRAY IN THE PRESENCE OF MULTIPLE JAMMERS

In the last section, an algorithm to select element locations of a linear array of isotropic elements for a single incident jammer was developed. The same algorithm can be used when the array is to be designed for multiple incident jammers. As an illustration, the algorithm is used to find element distributions of linear arrays when the total expected number of jammers is three and five, respectively. Again, we

will see that the number of antenna elements can be reduced by a significant factor and the thinned arrays meet the required performance level.

- a) Three Incident Jammers: In the presence of three jammers, the constraint part of the array contains four elements. From Equation (10.7)

$$0.375 < \frac{d_c}{\lambda} < 0.5 \quad . \quad (10.11)$$

Figure X-8 shows the unperturbed pattern of the constraint part of the array when $d_c = 0.4\lambda$ (this value of d_c gives approximately equal sidelobes and sidelobe levels are less than s). The desired signal is incident from $\phi = -90^\circ$. Note that the unperturbed pattern has low sidelobes. The maximum sidelobe level is $\sim 1.2V$. Using Equation (10.3), the maximum permissible sidelobe level for a four element array in the presence of three jammers is $2V$. The output SINR of the array, therefore, will not have any dips. The beamwidth of the array is quite large and thus the array operating in an adaptive mode will have poor resolution. To improve it, resolution elements should be added to the array.

Figures X-9, X-10 and X-11 show the unperturbed pattern of the array with the addition of one, two and three resolution elements, respectively. The resolution elements are added using the procedure outlined in the last section. Element distributions are also shown in the figures. Note that peaks

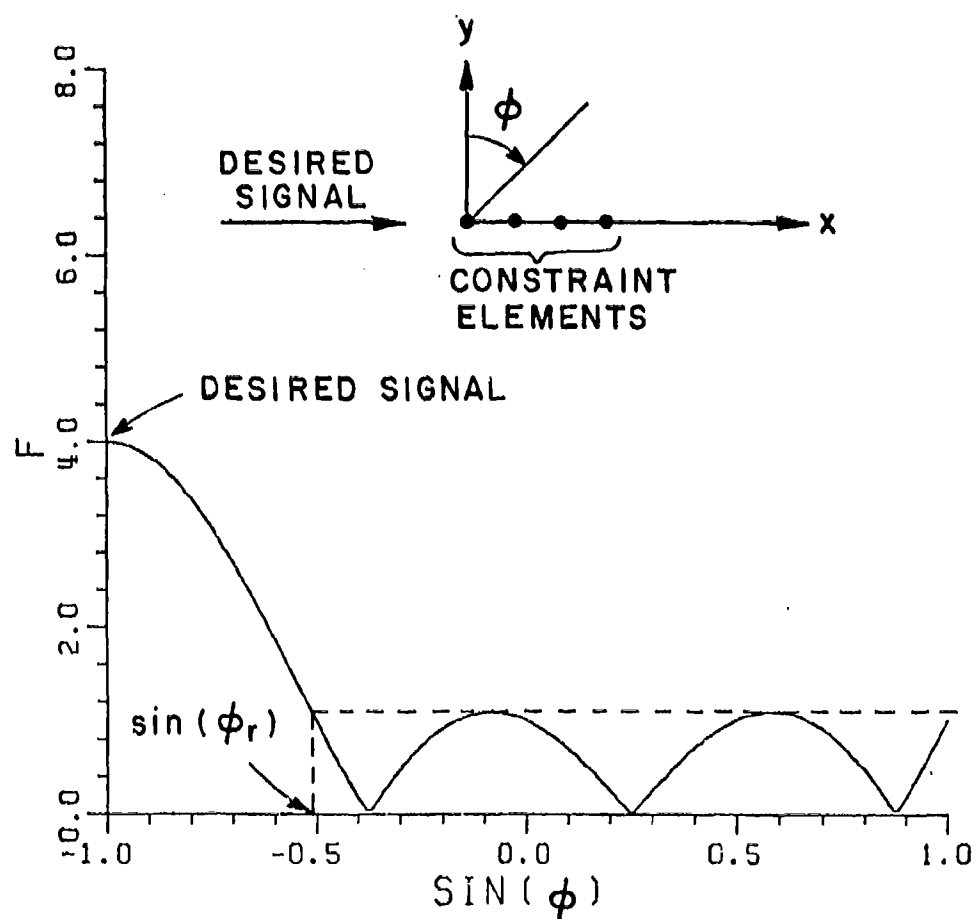


Figure X-8. Unperturbed pattern (F) of a linear array of four elements (constraint elements). $d_c = 0.4\lambda$, $\phi_d = -90^\circ$, $s = 2V$.

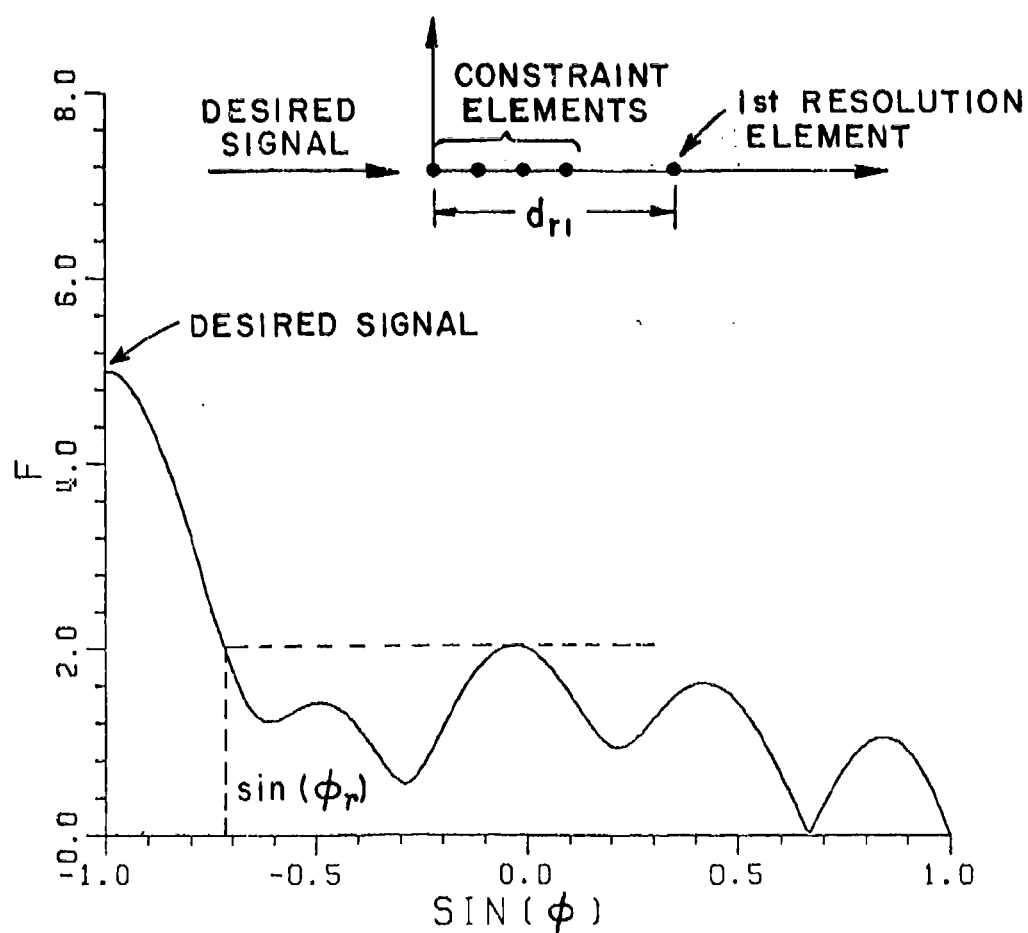


Figure X-9. Unperturbed pattern (F) of a linear array of five elements (constraint elements plus one resolution element). $d_c = 0.4\lambda$, $d_{r1} = 2.1\lambda$, $\phi_d = -90^\circ$, $s = 2.58V$.

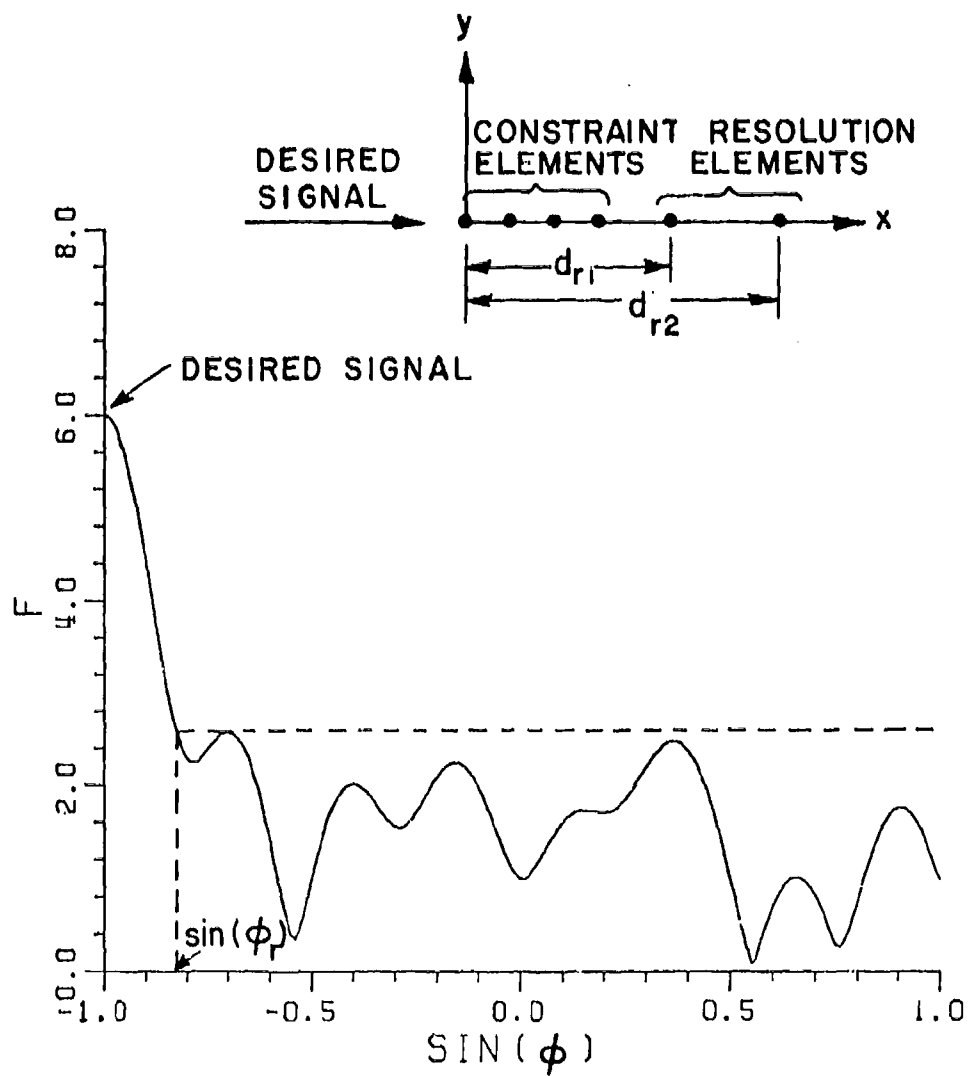


Figure X-10. Unperturbed pattern (F) of a linear array of six elements (constraint elements plus two resolution elements).

$$d_c = 0.4\lambda, d_{r1} = 2.1\lambda, d_{r2} = 3.6\lambda, \phi_d = -90^\circ, s = 3.16V.$$

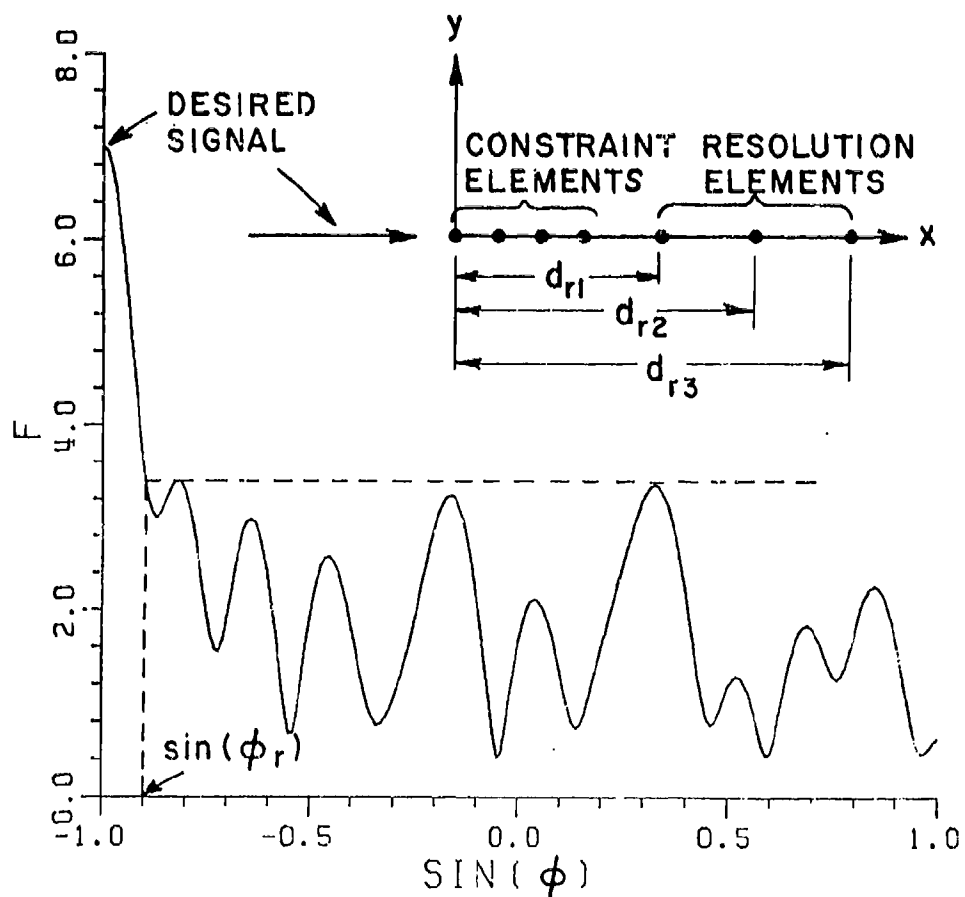


Figure X-11. Unperturbed pattern (F) of a linear array of seven elements (constraint elements plus three resolution elements).

$$d_c = 0.4\lambda, d_{r1} = 2.1\lambda, d_{r2} = 3.6\lambda, d_{r3} = 5.9\lambda, \phi_d = -90^\circ, s = 3.74V.$$

of the sidelobes for all element distributions are lower than the maximum permissible sidelobe level, s . The array operating in an adaptive mode, therefore, will not have any dips. The total aperture with the addition of three resolution is 5.9λ which will lead to an improved resolution. The array has seven elements. A completely filled array would contain approximately 13 elements. The array is, thus, significantly thinned.

Figure X-12 shows the unperturbed pattern of a 14 element array. The elements are uniformly spaced at a distance $d=0.47\lambda$. Comparing Figures X-11 and X-12 we see that the 3 dB beamwidth of the thinned array is smaller than that of the completely filled array. The thinned array will, therefore, provide good resolution in the presence of jammers.

- b) Five Incident Jammers: In the presence of five jammers, the constraint part of the array contains six elements. From Equation (10.7)

$$0.4167 < \frac{d_c}{\lambda} < 0.5 \quad (10.12)$$

Figure X-13 shows the unperturbed pattern of the constraint part of the array when $d_c=0.43\lambda$. Again d_c is chosen so that all the sidelobes are approximately equal and the sidelobe levels are less than the maximum permissible level given by Equation (10.3). The desired signal is incident from $\phi=-90^\circ$. Note that the unperturbed pattern has low sidelobes. The maximum

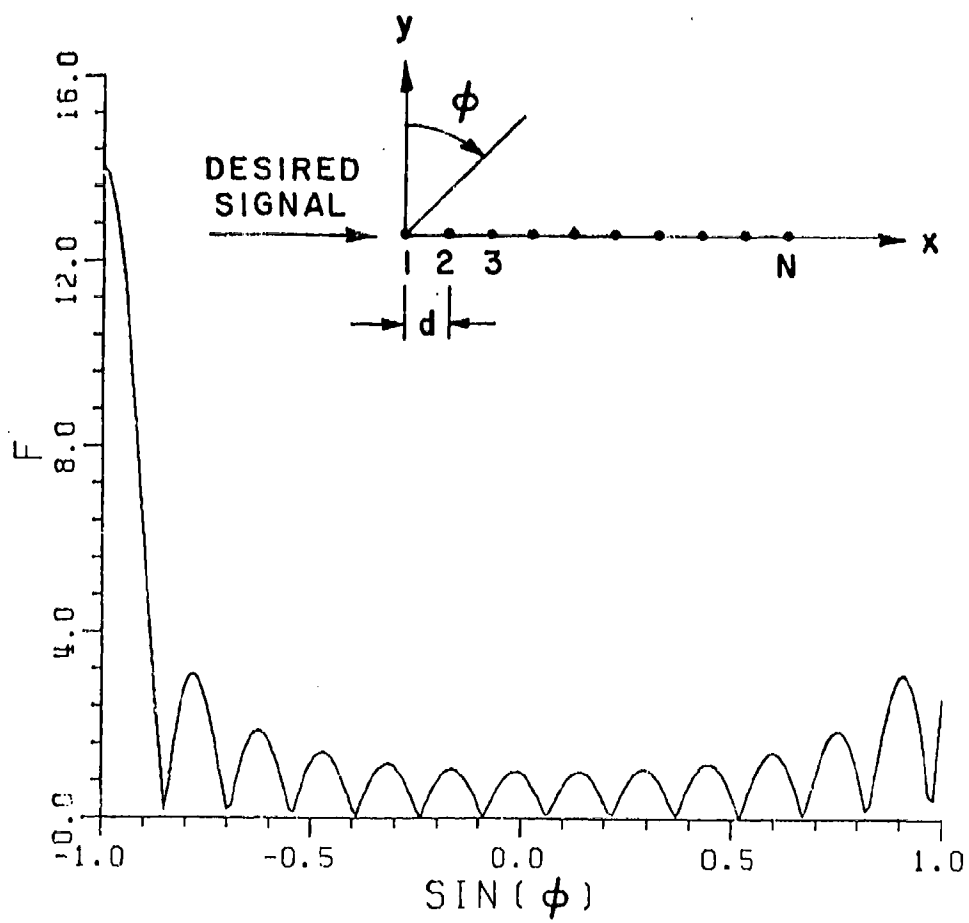


Figure X-12. Unperturbed pattern (F) of a completely filled linear array of fourteen elements. $d=0.47\lambda$, $\phi_d=-90^\circ$.

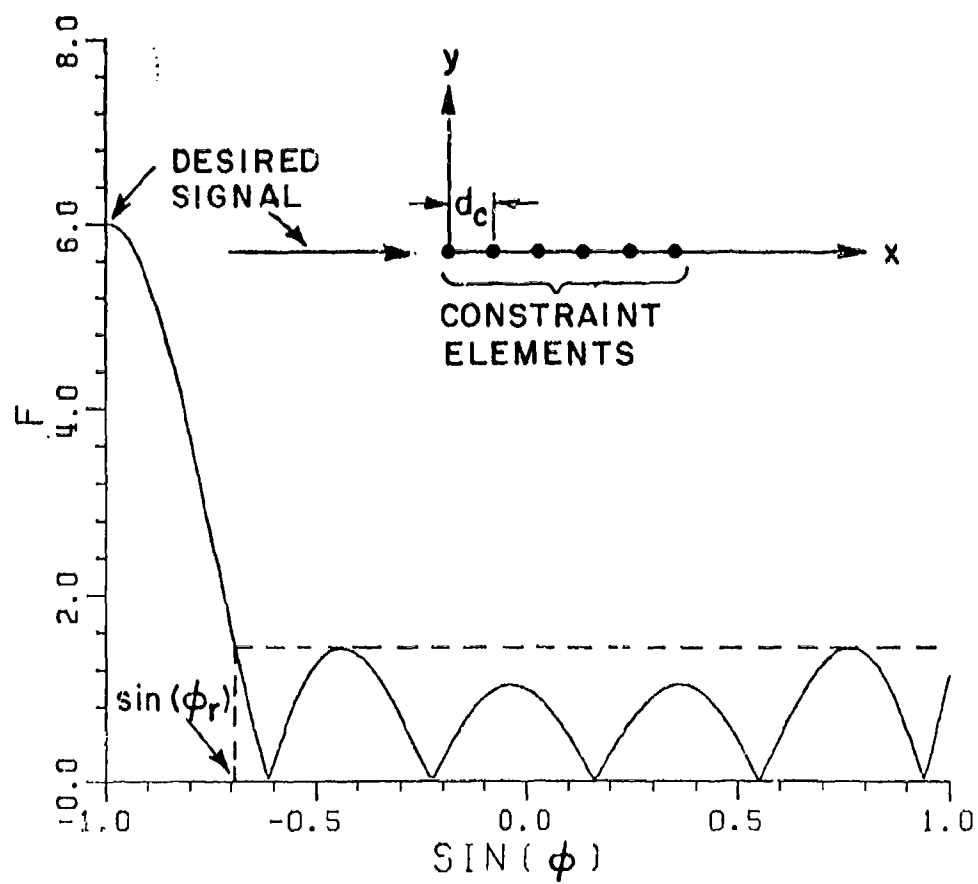


Figure X-13. Unperturbed pattern (F) of a linear array of six elements (constraint elements). $d_c = 0.43\lambda$, $\phi_d = -90^\circ$, $s = 2.45V$.

sidelobe is $\sim 1.35V$. Using Equation (10.3), the maximum permissible sidelobe level for a six element array in the presence of five jammers is $2.45V$. The output SINR of the array due to the constraint part, therefore, will not have any dips. If the beamwidth of the array is considered excessive, resolution elements should be added to the array.

Figures X-14, X-15 and X-16 show the unperturbed pattern of the array with the addition of one, two and three resolution elements, respectively. Element distributions are also shown in the figures. Note that the peaks of the sidelobes for all element distributions are lower than the maximum permissible sidelobe level, s . The total aperture with the addition of three resolution element is 6λ which will lead to improved resolution. The total number of antenna elements in the array is nine. A completely filled array would contain approximately 13 elements. The array, therefore, is a thinned array. Comparing Figures X-12 and X-16 we see that the 3 dB beamwidth of the thinned array (Figure X-16) is smaller than that of the completely filled array. The thinned array, therefore, will provide good resolution in the presence of jammers.

One thing to be noted from the above radiation pattern plots is that the sidelobes become unequal as the number of elements is increased. The unequal sidelobes imply that a better resolution could be attained from the array by changing the element distribution. The algorithm, therefore, though it

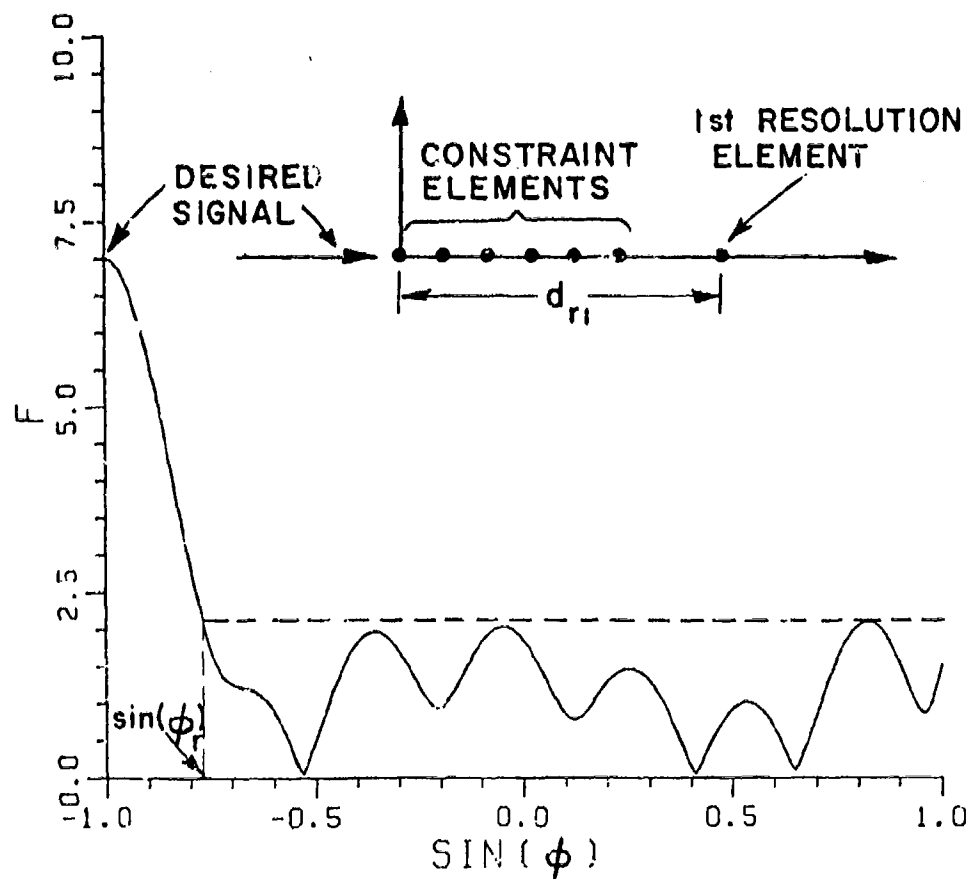


Figure X-14. Unperturbed pattern (F) of a linear array of seven elements (constraint elements plus one resolution element).

$$d_c = 0.43\lambda, d_{r1} = 3.2\lambda, \phi_d = -90^\circ, s = 2.9V.$$

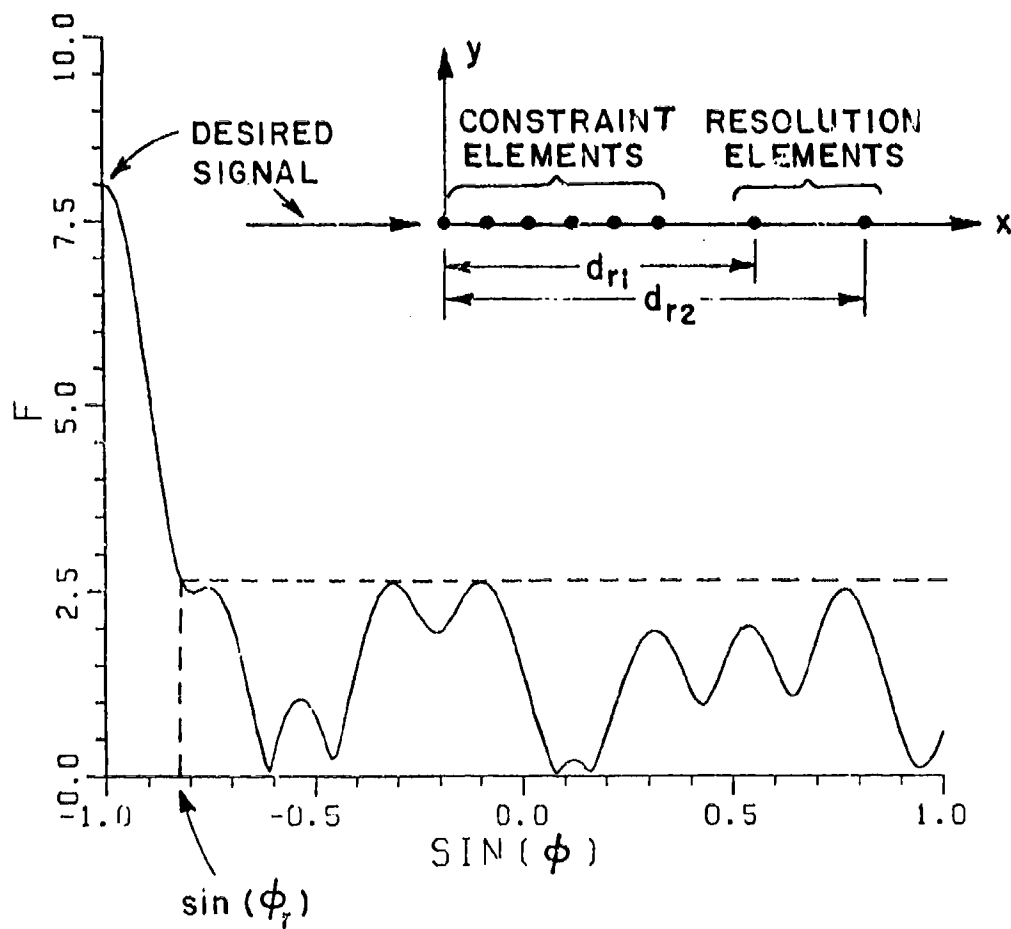


Figure X-15. Unperturbed pattern (F) of a linear array of eight elements (constraint elements plus two resolution elements).

$$d_c = 0.43\lambda, d_{r1} = 3.2\lambda, d_{r2} = 4.5\lambda, \phi_d = -90^\circ, s = 3.35V.$$

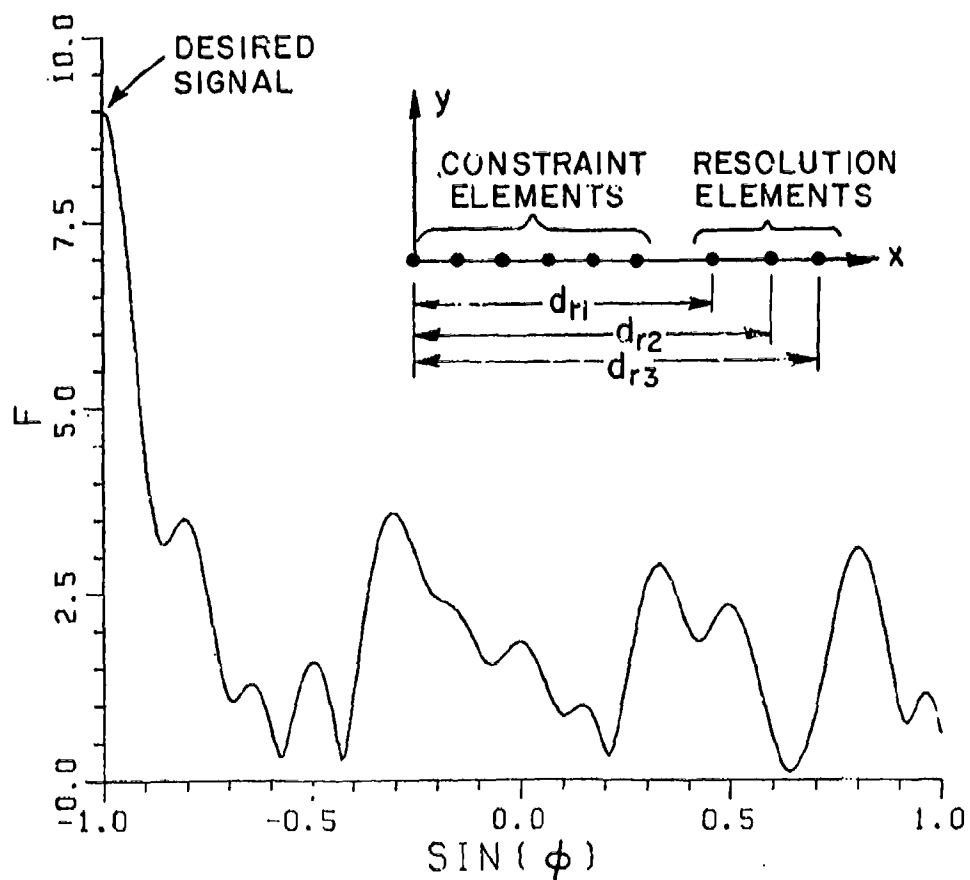


Figure X-16. Unperturbed pattern (F) of a linear array of nine elements (constraint elements plus three resolution elements).
 $d_c = 0.43\lambda$, $d_{r1} = 3.2\lambda$, $d_{r2} = 4.5\lambda$, $d_{r3} = 6\lambda$, $\phi_d = -90^\circ$, $s = 3.8V$.

guarantees the required performance, does not lead to the optimum distribution of antenna elements as the number of antenna elements become large. One can use the theory of random array [3] or dynamic programming [4] to find the optimum element distributions, for large arrays.

In this subsection an algorithm to select element locations of a linear array was developed. The algorithm leads to thinned linear arrays and guarantees the required performance in a two dimensional field of view. In practice, the field of view covers, of course, a three dimensional space. In the next subsection, various planar arrays that provide required coverage in a three dimensional field of view are discussed. The planar arrays can be obtained using the linear arrays discussed in this section, and thus would be thinned arrays.

E. PLANAR ARRAY TO PROVIDE COVERAGE IN A THREE DIMENSIONAL SPACE

In the last subsection, an algorithm to select element locations of a linear array was described. It was shown that by using the algorithm one can reduce the total number of antenna elements, and the thinned array so obtained provides satisfactory performance in a two dimensional field of view. In practice, the field of view extends to three dimensional space, and the array elements are distributed on a surface rather than along a line. In this subsection, performance of various planar arrays will be studied. The field of view will be the upper half space (Figure X-17), i.e., $0 \leq \theta \leq \pi$, $0 \leq \phi \leq \pi$. For the

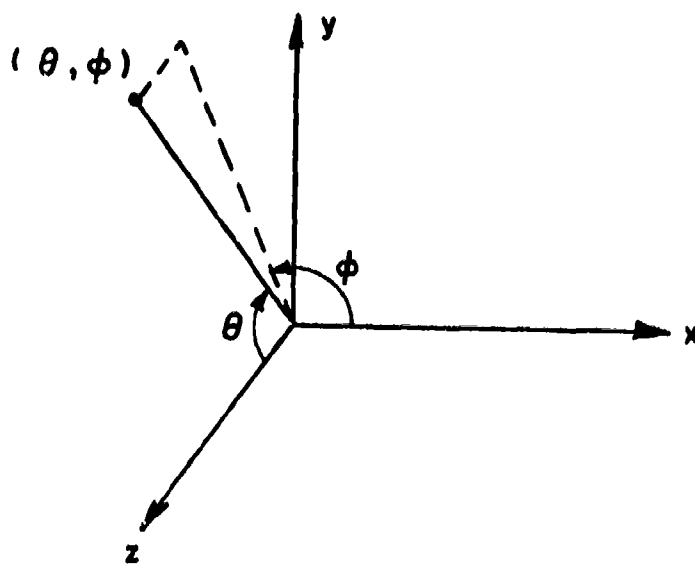


Figure X-17. Coordinate system for a three dimensional space.

Field of view $0 \leq \theta \leq \pi$, $0 \leq \phi \leq \pi$.

purpose of illustration, a jammer scenario consisting of three jammers of equal strength will be considered. A linear array will be studied first. It will be shown that a linear array is not suitable for the given field of view, and one needs to add elements in another dimension to achieve the required performance. Various planar distributions of array elements will then be considered.

- a) Linear Array: A linear array designed using the prescribed algorithm (subsection C) is shown in Figure X-18. The minimum output SINR for acceptable performance (threshold) is chosen to be 0 dB, which is equal to the input signal-power-to-thermal noise ratio (ξ_d). As the jammer scenario consists of three jammers, there are four constraint elements in the array which are spaced 0.4λ apart. There are three resolution elements in the array. The total length of the array is 5.9λ .

Figure X-19 shows the unperturbed pattern of the array when the desired signal is incident from the broadside direction, i.e., $(90^\circ, 90^\circ)$. The plot is a quantized linear representation of the voltage pattern with increment size, Δ , equal to 0.05. The various symbols and the corresponding radiation levels are given in Table X-1. Note that the array is incapable of resolution in any vertical cut (constant θ cut). Figure X-20 shows the output SINR (in dB) of the array in the presence of three jammers. Two of the jammers are incident from $(30^\circ, 45^\circ)$ and $(108^\circ, 145^\circ)$, respectively, and the third jammer is swept across the whole visible range. Note that the unperturbed pattern of the array has sidelobe peaks along

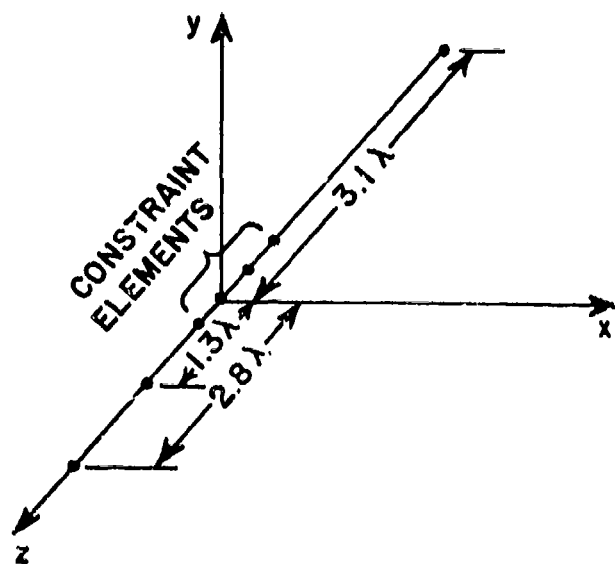


Figure X-18. A linear array for three incident jammers. $N=7$,
 $d_c=0.4\lambda$.

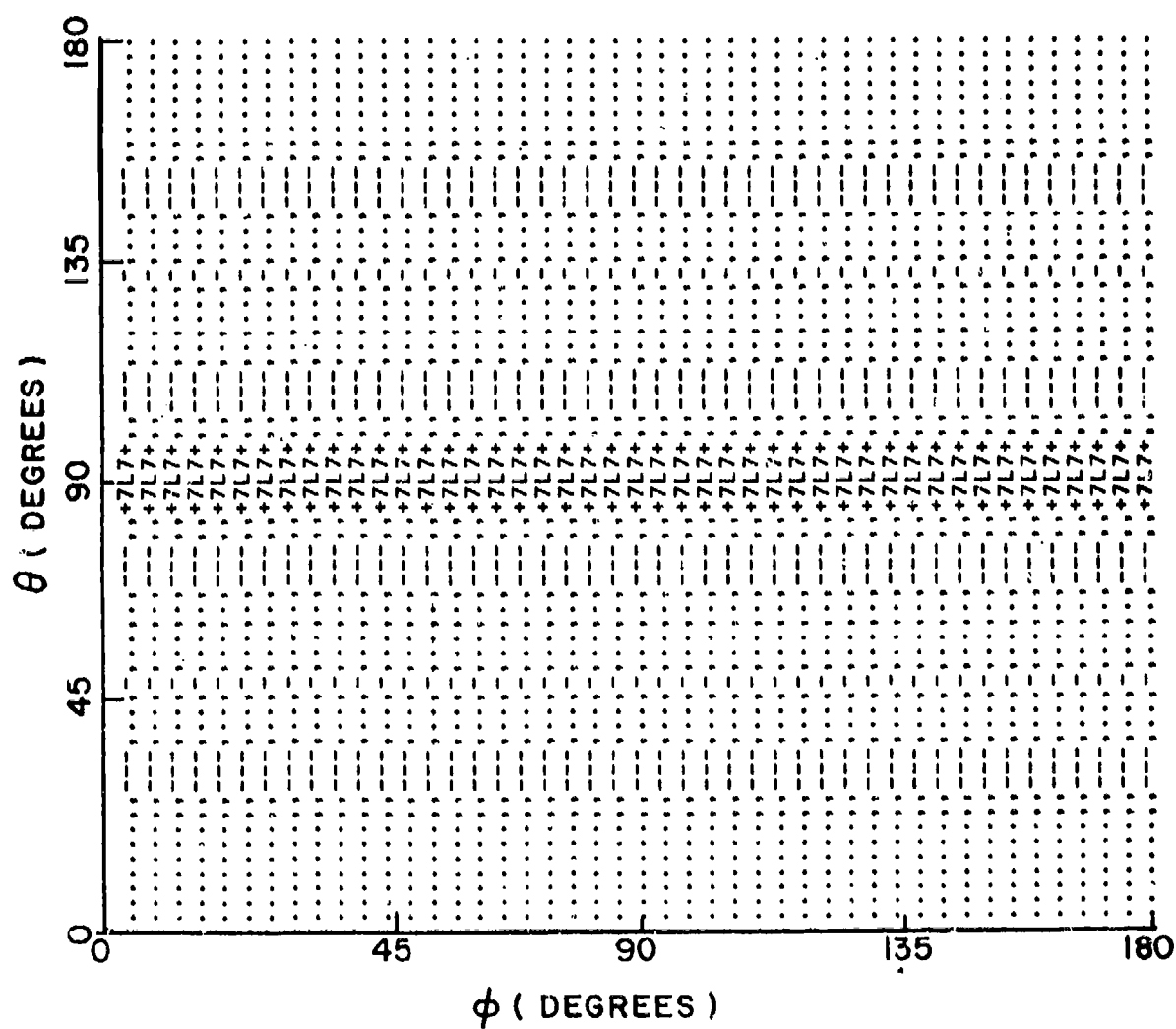


Figure X-19. Unperturbed pattern of the linear array.

$$(\theta_d, \phi_d) = (90^\circ, 90^\circ), \Delta = 1.$$

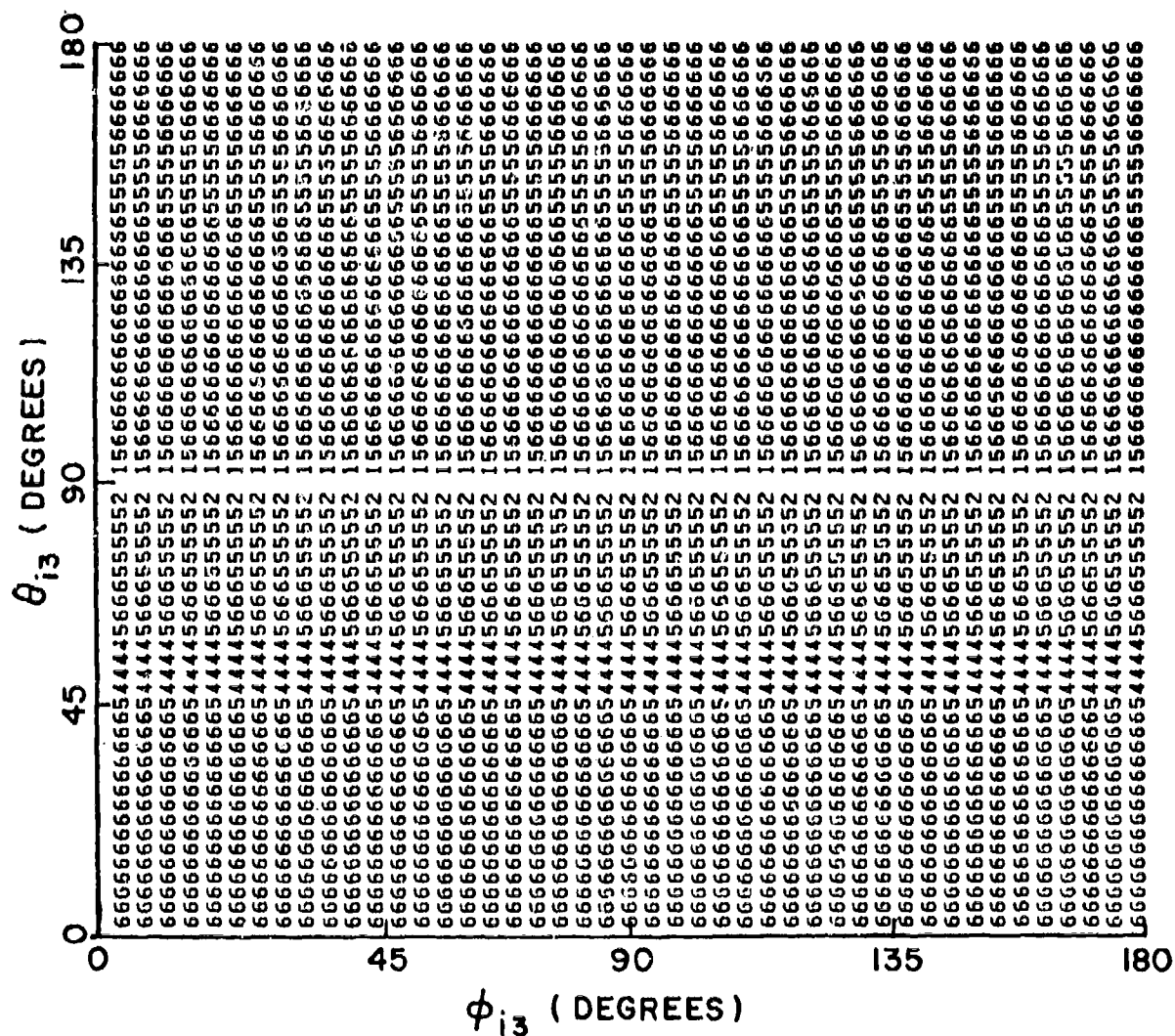


Figure X-20. Output SINR of the linear array in the presence of three jammers vs. the third jammer direction. $\xi_d=1$, $\xi_{ij}=100$, $(\theta_d, \phi_d)=(90^\circ, 90^\circ)$, $(\theta_{i1}, \phi_{i1})=(30^\circ, 45^\circ)$, $(\theta_{i2}, \phi_{i2})=(108^\circ, 145^\circ)$, threshold=0 dB.

TABLE X-1
VARIOUS SYMBOLS AND CORRESPONDING LEVELS

RADIATION LEVEL	SYMBOL
0 - 0.5 Δ	
0.5 Δ - 1.5 Δ	.
1.5 Δ - 2.5 Δ	,
2.5 Δ - 3.5 Δ	-
3.5 Δ - 4.5 Δ	+
4.5 Δ - 5.5 Δ	1
5.5 Δ - 6.5 Δ	7
6.5 Δ - 7.5 Δ	L
7.5 Δ - 8.5 Δ	ϕ
8.5 Δ - 9.5 Δ	8
9.5 Δ - 10.5 Δ	\$
10.5 Δ - 11.5 Δ	B
11.5 Δ - 12.5 Δ	C

Increment $\equiv \Delta$

(30°, 45°) and (108°, 145°). The output SINR is plotted as a function of the third jammer direction when the desired signal is incident from the broadside direction. The threshold is set at 0 dB and the plot shows the amount by which the output SINR exceeds the threshold. The blank portion of the plot corresponds to the angular region where the output SINR is below the threshold. From the plot, it is clear that the total degradation in the output SINR due to three jammers is approximately 3 dB (output SINR in the absence of all jammers is approximately 8 dB) if $\theta_1 \neq \theta_d = 90^\circ$. But the output SINR drops below threshold for $\theta_1 \approx 90^\circ$, since the array has no resolution in any vertical cut (constant θ cut). The drop in SINR can also be explained by projecting the array elements in the $\theta=90^\circ$ cut (xy plane). In the xy plane the array projects to a single element and, therefore, has no degrees of freedom in the cut. To improve the array performance, elements should be added to the array. The new elements should be added such that the array acquires enough degrees of freedom in all cuts and has low sidelobes and a narrow mainbeam. Various planar distributions of array elements will be considered next.

- b) Rectangular Array: In subsection C an algorithm to select element locations of a thinned one dimensional array was presented. The thinned array meets the required performance level in a two dimensional space but is not suitable when the field of view is extended to a three dimensional space. The

one dimensional array (linear array) can, however, be used as a building block to obtain various planar arrays for a three dimensional field of view. One such planar array is a rectangular array (Figure X-21). The total number of elements in the array will be $N \times N$, where N is the number of elements in the linear array. The rectangular array will have low sidelobes, a narrow mainbeam, and at least N projected elements in all planar cuts. The array, therefore, should provide the required performance in the three dimensional space. For three incident jammers, the total number of antenna elements in the array will be forty-nine.

Figure X-22 shows the unperturbed pattern of the array when the desired signal is incident from the broadside direction. $\Delta=5$ in the plot. Note that the unperturbed pattern has low sidelobes and a narrow mainbeam. The array performance in an adaptive mode, therefore, should be satisfactory.

Figure X-23 shows the output SINR of the array in the presence of three jammers. Two of the jammers are incident from $(30^\circ, 90^\circ)$ and $(90^\circ, 28^\circ)$, respectively, and the third jammer is swept across the whole visible region. The output SINR is plotted as a function of the third jammer direction when the desired signal is incident from the broadside direction. The threshold in the plot is set at 8 dB. The output SINR of the array is above threshold for all directions of incidence of the third jammer, except when the jammer

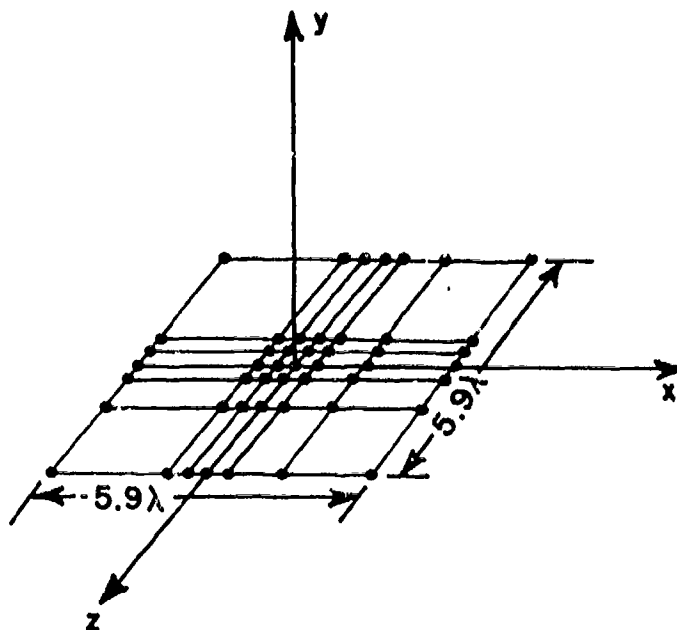


Figure X-21. A thinned rectangular array.

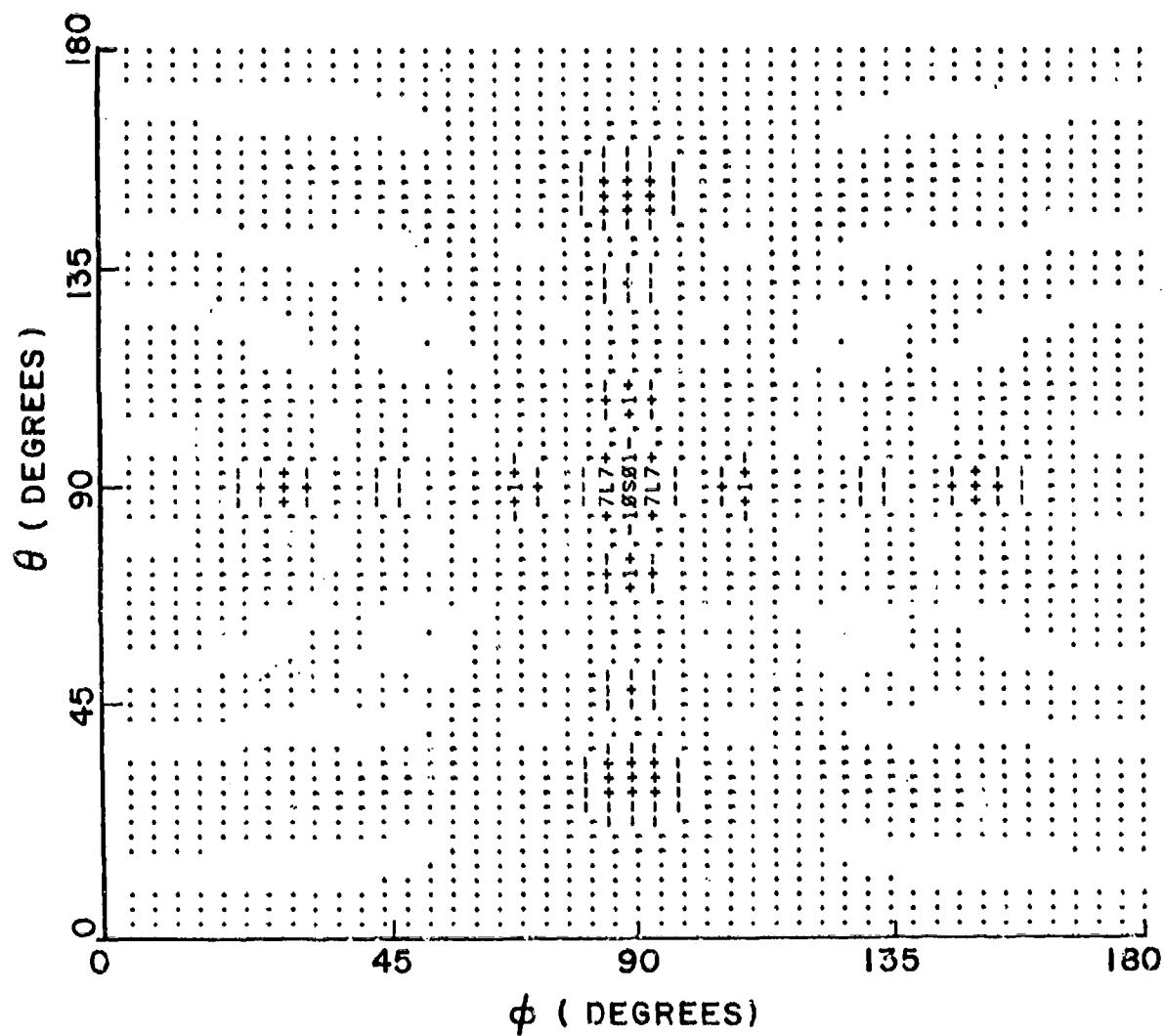


Figure X-22. Unperturbed pattern of the rectangular array.

$$(\theta_d, \phi_d) = (90^\circ, 90^\circ), \Delta = 5.$$

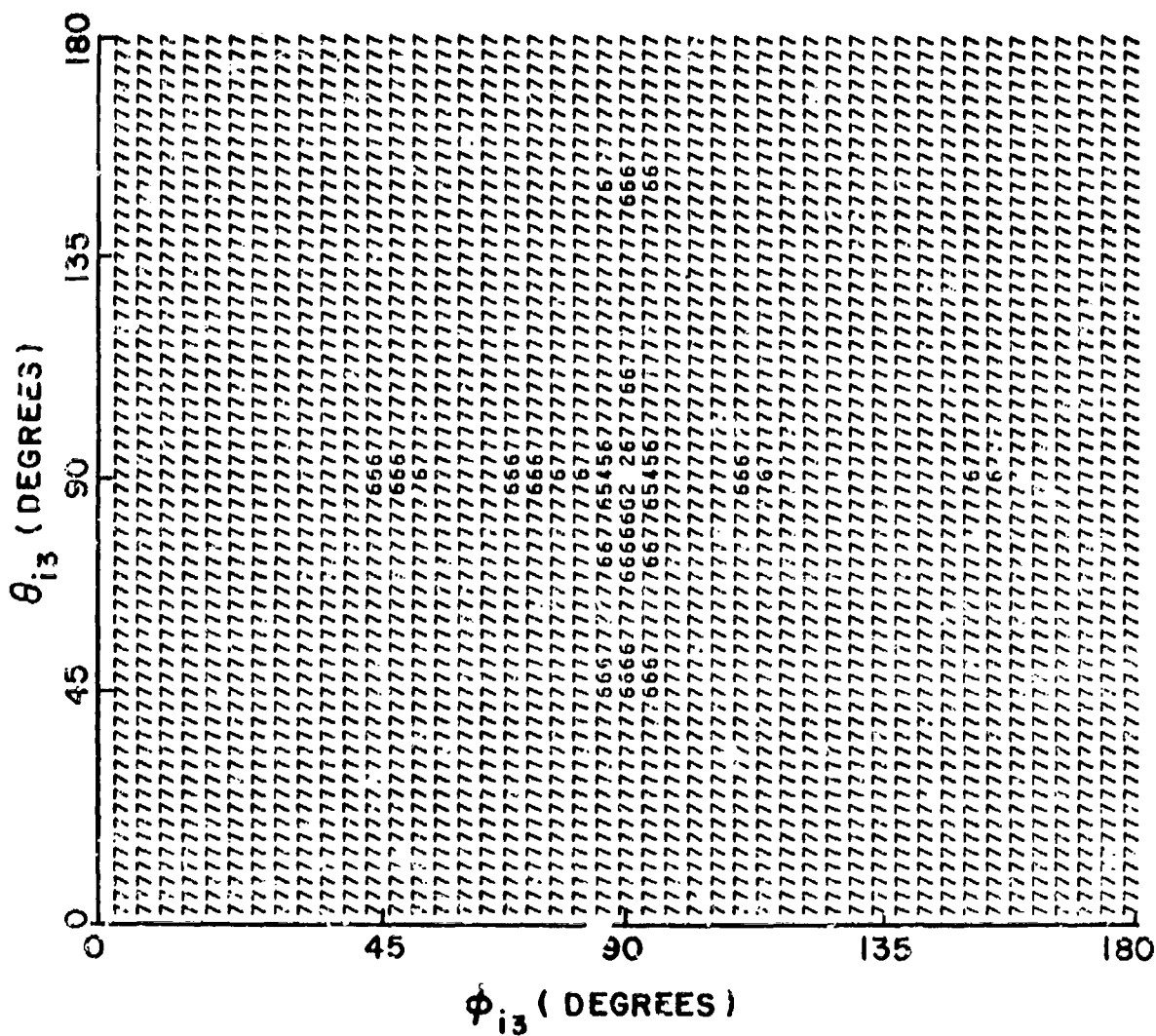


Figure X-23. Output SINR of the rectangular array in the presence of three jammers vs. the third jammer direction.

$(\theta_d, \phi_d) = (90^\circ, 90^\circ)$, $(\theta_{i1}, \phi_{i1}) = (40^\circ, 90^\circ)$, $(\theta_{i2}, \phi_{i2}) = (90^\circ, 40^\circ)$, $\xi_d = 1$, $\xi_{ij} = 100$, threshold = 8 dB.

direction coincides with the desired signal direction. The total degradation in the output SINR due to the three jammers is 3 dB (output SINR in the absence of all jammers is approximately 17 dB). The performance of the array is, therefore, quite satisfactory.

In the rectangular array discussed above, the total number of antenna elements is 49, which is quite large for three incident jammers. Moreover, as the number of jammers increases, the number of antenna elements will increase as N^2 (N is the number of elements in a linear array). Other distributions of array elements which need considerably fewer elements are discussed next.

- c) Crossed Array: A planar array which can be easily obtained using two linear arrays (designed for a two dimensional field of view) is a crossed array shown in Figure X-24. The total number of antenna elements in a crossed array is $2N-1$, where N is the number of elements in the linear array. For this arrangement of elements the minimum number of projected elements in any planar cut will be N and thus the array should have enough degrees of freedom. In the presence of three jammers, the total number of antenna elements will be thirteen and the distribution of elements is shown in Figure X-24.

Figure X-25 shows the unperturbed pattern of the array when the desired signal is incident from the broadside direction. $\Delta=1$ in the plot. Note that the beam width of the array is

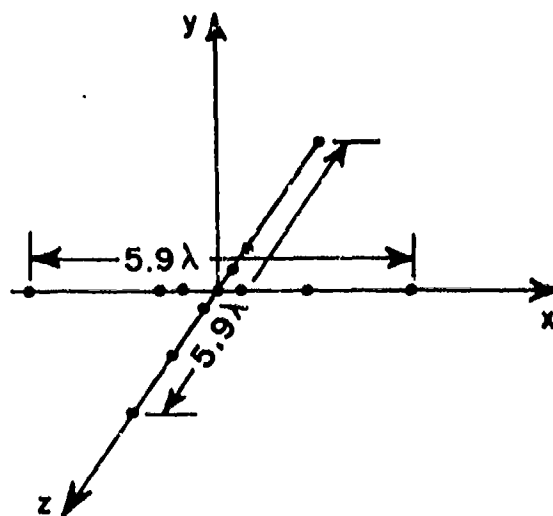


Figure X-24. The crossed array.

small in both principal cuts ($\theta=90^\circ$ and $\phi=90^\circ$ cuts), but the sidelobes are quite high. The sidelobes are much higher than those of the linear array (Figure X-19). Does this mean that the array performance will be worse than a linear array? The answer is no. This can be explained as follows.

The output SINR of an adaptive array of N isotropic elements in the presence of one jammer [1,2] is

$$\text{SINR} = \xi_d \frac{(N^2 - |g_1|^2)}{N} \quad (10.13)$$

where $|g_1|$ is the value of the unperturbed pattern of the array in the jammer direction.

$$\text{Let } |g_1| = \alpha N \quad (10.14)$$

Note that α corresponds to the value of the normalized unperturbed pattern in the jammer direction. Substituting Equation (10.14) in Equation (10.13) we get

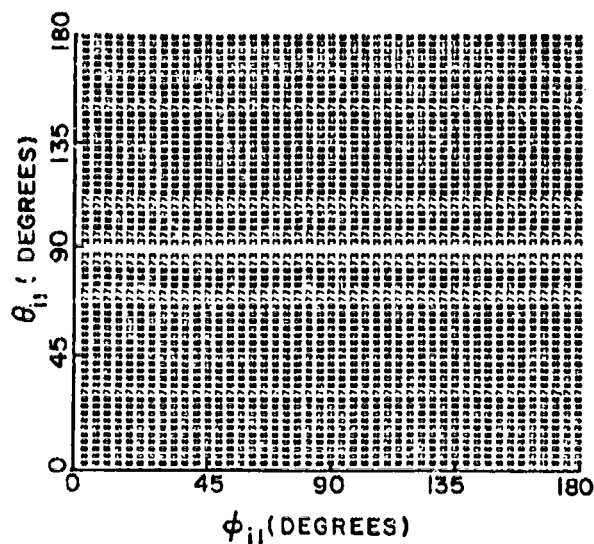
$$\text{SINR} = \xi_d N(1 - \alpha^2) \quad (10.15)$$

From Equation (10.15) it is clear that as N , the total number of array elements, is increased, α can be increased while maintaining the same output SINR. For example, if $\alpha=0.1$ (20 dB sidelobe) for a linear array then α can be as high as 0.7 (3 dB sidelobe) for a crossed array (the total number of antenna elements in the crossed array is twice the number of elements in the linear array) for the same output SINR.

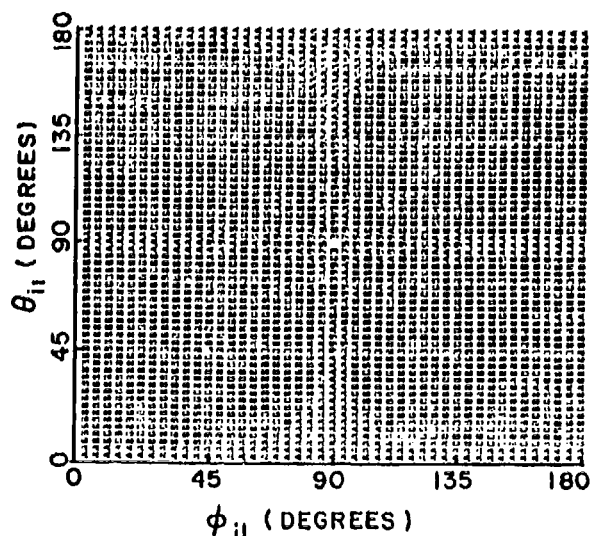
Figure X-26 shows the output SINR of the linear array (Figure X-19) and the crossed array (Figure X-24) in the presence of one jammer as a function of the jammer direction. The desired signal is incident from the broadside direction and the threshold is set at 0 dB. Symbols A and B in the plot correspond to 10 dB and 11 dB above the threshold. Note that the crossed array has a higher output SINR for all jammer directions.

Figure X-27 shows the output SINR of the crossed array in the presence of three jammers. Two of the jammers are incident from $(35^\circ, 90^\circ)$ and $(90^\circ, 45^\circ)$, respectively, and the third jammer is swept across the given field of view. The output SINR is plotted as a function of the third jammer location, when the desired signal is incident from the broadside direction. The threshold for the plot is set at 0 dB. The unperturbed pattern of the array (Figure X-25) has high sidelobes along $(35^\circ, 90^\circ)$ and $(90^\circ, 45^\circ)$. The cumulative effect of three jammers can, therefore, degrade the array performance significantly which is obvious from the SINR plot. The output SINR has dropped as much as 6 dB for some directions of incidence of the third jammer. (In the absence of all jammers the output SINR of the array is approximately 11 dB). But the output SINR is above threshold in all sectors. The system performance, therefore, will be satisfactory.

The crossed array discussed above, thus, provides the required performance in the given field of view. The total



(a) LINEAR ARRAY



(b) CROSSED ARRAY

Figure X-26. Output SINR in the presence of one jammer vs. the jammer direction. $(\theta_d, \phi_d) = (90^\circ, 90^\circ)$, $\xi_d = 1$, $\xi_j = 100$, threshold = 0 dB.

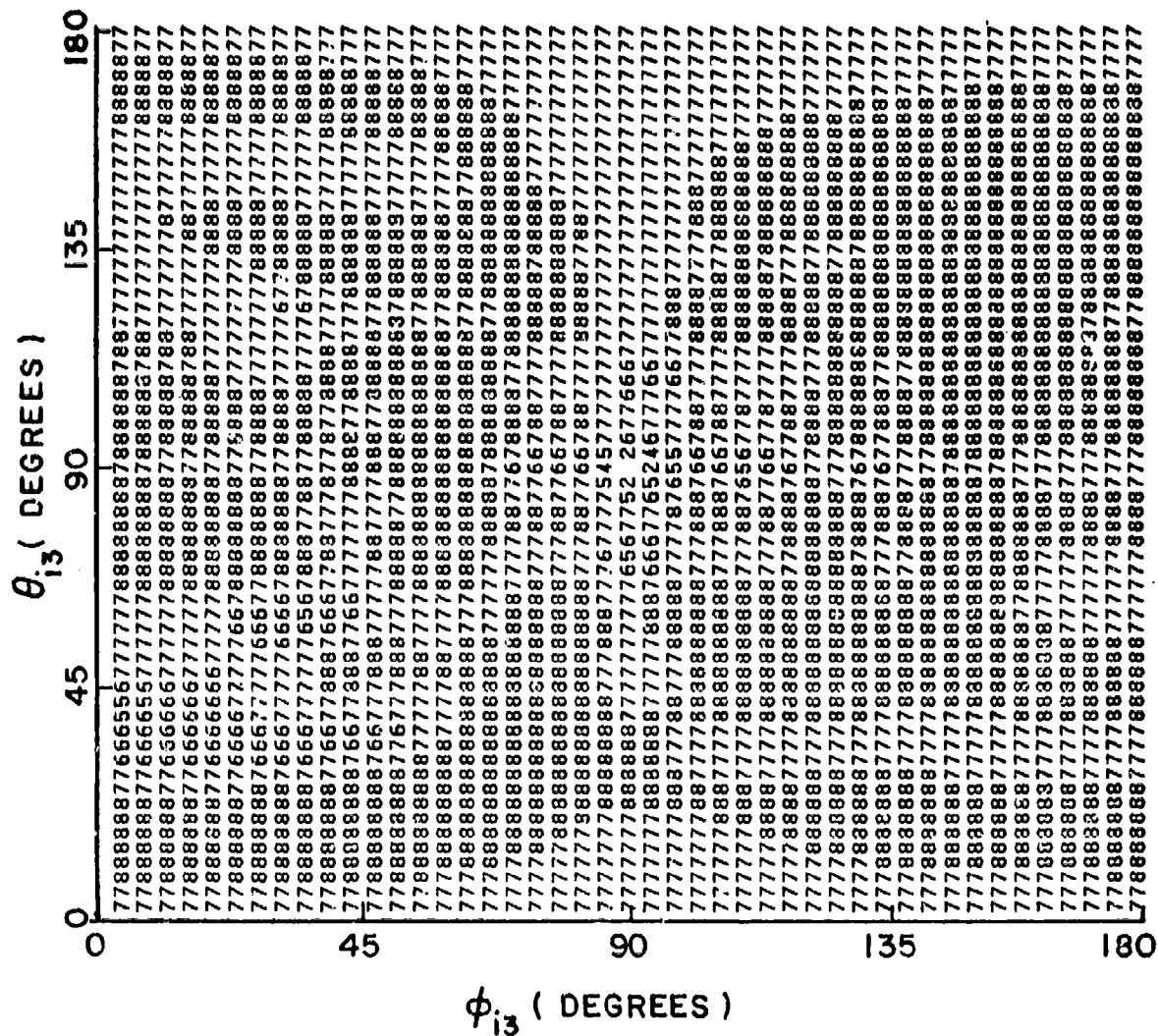
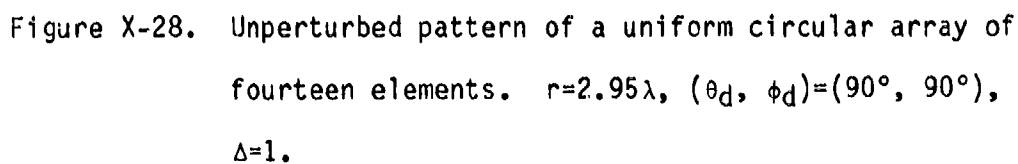


Figure X-27. Output SINR of the crossed array in the presence of three jammers vs. the third jammer direction. $(\theta_d, \phi_d) = (90^\circ, 90^\circ)$, $(\theta_{i1}, \phi_{i1}) = (35^\circ, 90^\circ)$, $(\theta_{i2}, \phi_{i2}) = (90^\circ, 45^\circ)$, $\epsilon_d = 1$, $\epsilon_{ij} = 100$, threshold = 0 dB.

number of array elements is reasonable and the array does not need the whole aperture for implementation. The crossed array, therefore, is suitable for adaptive array systems.

- e. Circular Arrays: Another planar array which provides coverage over a three dimensional space is a circular array. Using a circular distribution of elements, one can reduce the number of antenna elements by a significant factor. The diameter of the circle for a circular array is dictated by the resolution requirements. In this study, the diameter of the circle will be chosen as the length of a linear array for a two dimensional coverage. Thus the circular array will provide the same resolution as a linear array. If the elements are placed uniformly around a circle then the total number of elements will be $\frac{2\pi}{\psi_d}$, where ψ_d is the spacing between the elements in radians. With a uniform distribution of elements, the minimum number of projected elements in a cut will be approximately equal to $\frac{\pi}{\psi_d}$, and this will dictate the maximum spacing between the array elements.

In the presence of three jammers, the total length of the linear array for two dimensional coverage was 5.9λ and the array had seven elements. Thus, the circular array (with uniformly spaced elements) should have fourteen elements and the diameter of the circle should be 5.9λ . Figure X-28 shows the unperturbed pattern of a circular array of fourteen elements. The antenna elements lie in the xz plane and are uniformly



distributed around a circle of radius 2.95λ . The desired signal is incident from the broadside direction. $\Delta=1$ in the plot. Note that the unperturbed pattern has a narrow beam, but very high sidelobes. The array performance in an adaptive mode, therefore, may be unsatisfactory.

Figure X-29 shows the output SINR of the array in the presence of three jammers. Two of the jammers are fixed at $(28^\circ, 90^\circ)$ and $(78^\circ, 28^\circ)$ respectively and the third jammer is swept across the whole visible space. The output SINR is plotted as a function of the third jammer location when the desired signal is incident from the broadside direction. Again, the threshold is set at 0 dB. Note that the three jammers cause significant degradation in the output SINR and for some directions of incidence of the third jammer, the output SINR is below threshold. Thus, the array does not meet the required performance level.

The main reason for the unsatisfactory performance is the high sidelobe level. One way of avoiding high sidelobes is to alter the uniform element spacing. One can place elements such that the elements have an exponential taper, i.e., the spacing between the elements is given by

$$\psi_i = \frac{2\pi (e^{B \frac{i-1}{N}} - 1)}{(e^B - 1)} \quad (10.16)$$

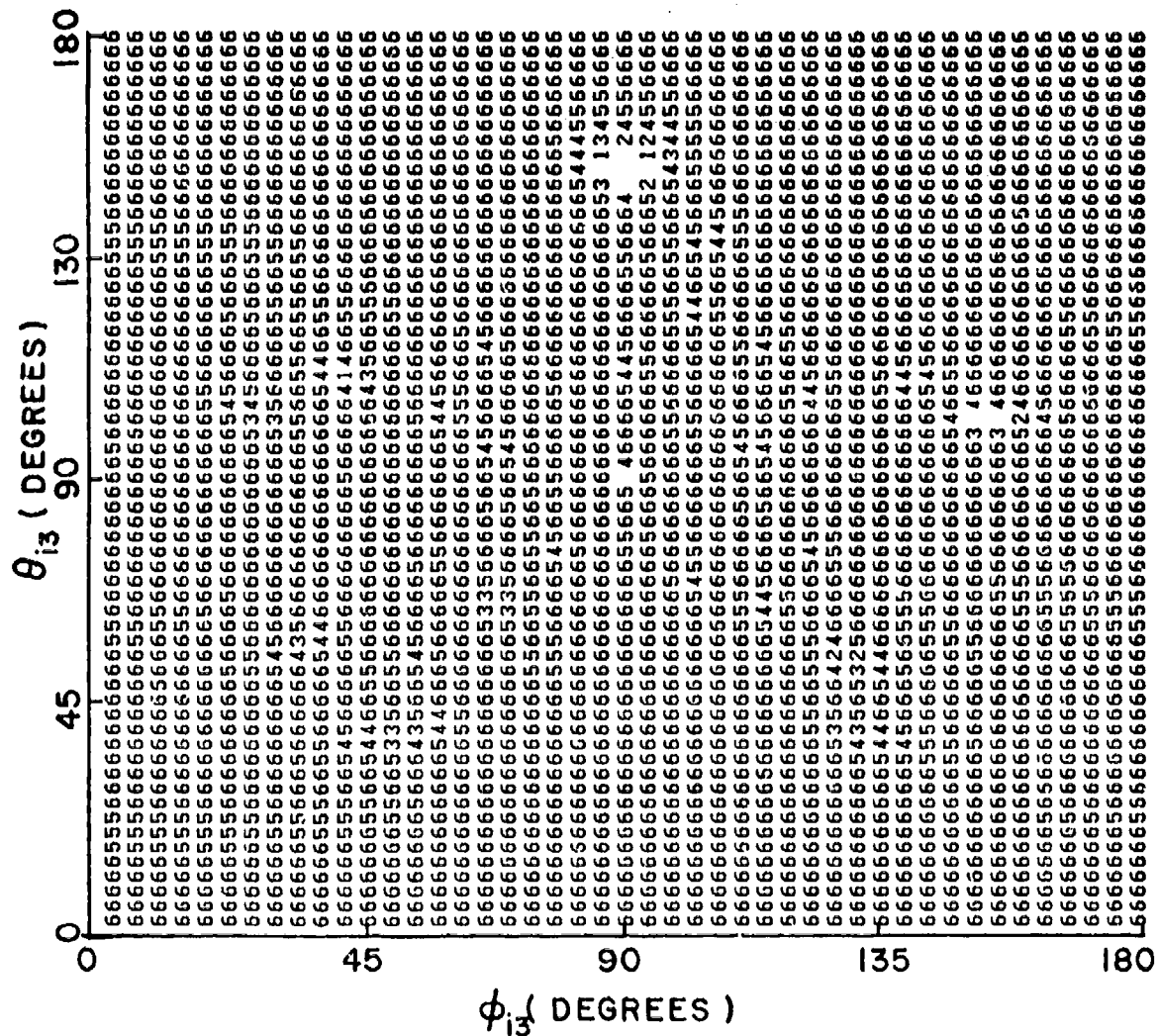


Figure X-29. Output SINR of a uniform circular array of fourteen elements in the presence of three jammers vs. the third jammer direction. $r=2.95\lambda$, $(\theta_d, \phi_d)=(90^\circ, 90^\circ)$, $(\theta_{i1}, \phi_{i1})=(28^\circ, 90^\circ)$, $(\theta_{i2}, \phi_{i2})=(78^\circ, 28^\circ)$, $\xi_d=1$, $\xi_{ij}=100$, threshold=0 dB.

where ψ_i is the angular location of the i^{th} element with respect to z-axis, B is a constant and N is the total number of elements in the array. Figure X-30 shows the unperturbed pattern of a circular array of fourteen elements. The spacing between the elements is chosen using Equation (10.16) with $B=1.5$. The antenna elements are distributed around a circle of radius 2.95λ . The desired signal is incident from the broadside direction and $\Delta=1$ in the plot. Note that the sidelobe level has decreased. Figure X-31 shows the output SINR of the array in the presence of three jammers. Two of the jammers are incident from the directions $(4^\circ, 4^\circ)$ and $(45^\circ, 40^\circ)$, and the third jammer is swept across the whole field of view. Note that the unperturbed pattern of the array (Figure X-30) has high sidelobes along $(4^\circ, 4^\circ)$ and $(45^\circ, 40^\circ)$. The desired signal is incident from the broadside direction and the output SINR is plotted as a function of the third jammer direction. Again the threshold is set at 0 dB. Note that though the output SINR has degraded significantly, it is still above threshold for all directions of incidence of the third jammer. Thus, the array performance is satisfactory.

In this subsection the performance of a circular array in an adaptive mode was studied. It was found that the circular array provides satisfactory performance in the three dimensional space. The total number of antenna elements in the circular array was about the same as that in the crossed array. Thus, the two distributions of elements should have the same

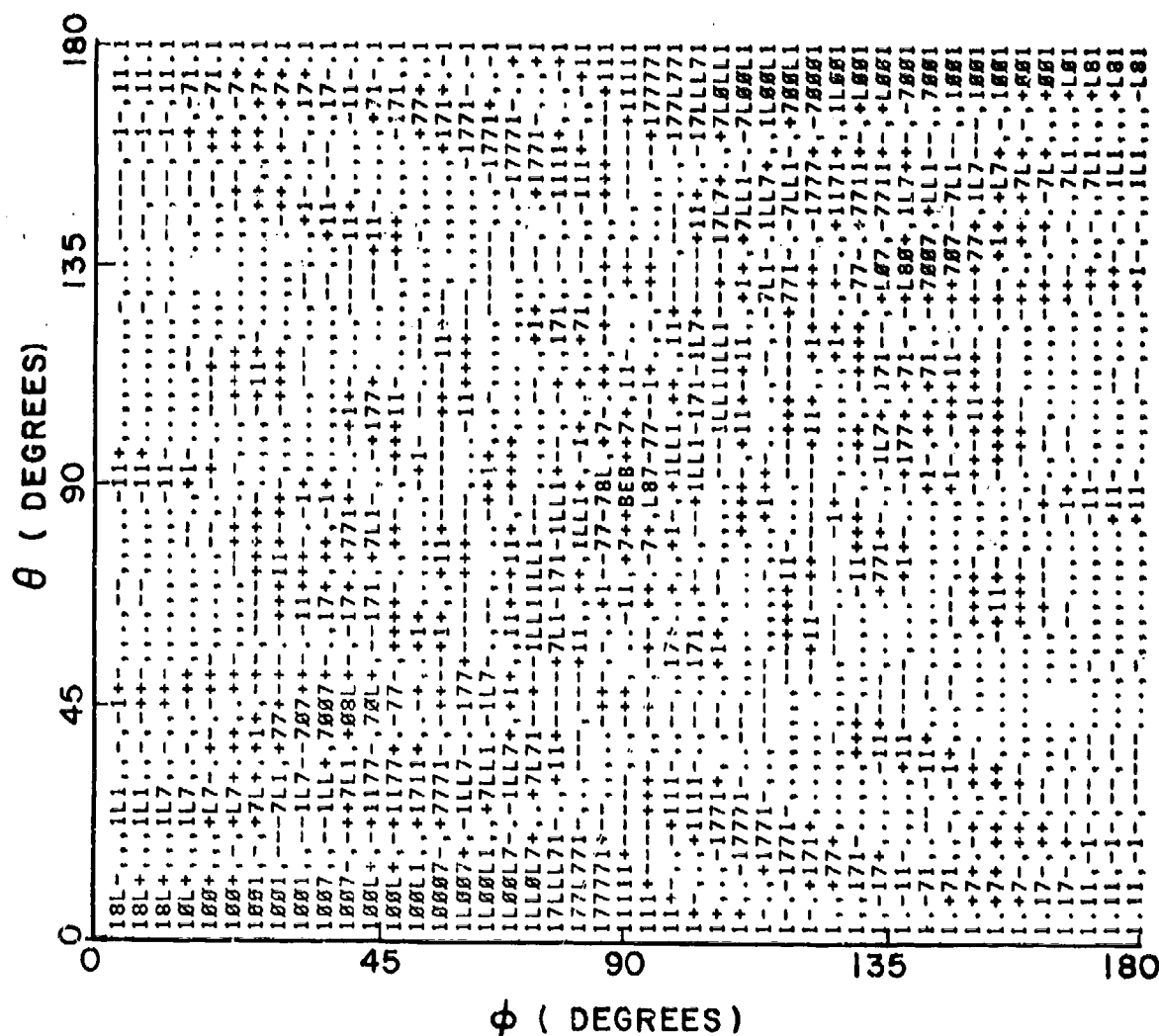


Figure X-30. Unperturbed pattern of a tapered circular array of fourteen elements. $r=2.95\lambda$, $(\theta_d, \phi_d)=(90^\circ, 90^\circ)$, $\Delta=1$.

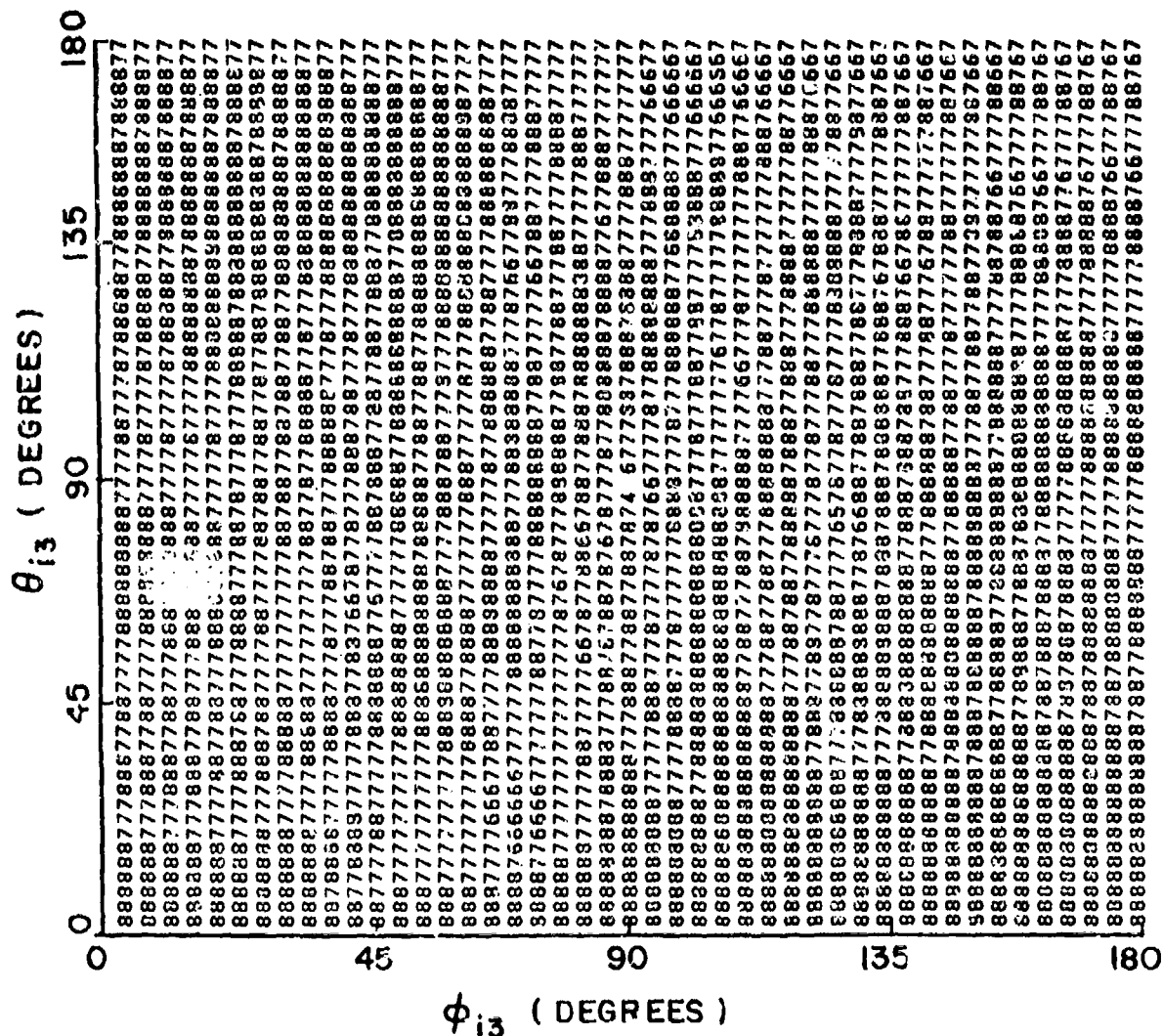


Figure X-31. Output SINR of a tapered circular array of fourteen elements in the presence of three jammers vs. the third jammer direction. $r=2.95\lambda$, $(\theta_d, \phi_d)=(90^\circ, 90^\circ)$, $(\theta_{i1}, \phi_{i1})=(4^\circ, 4^\circ)$, $(\theta_{i2}, \phi_{i2})=(45^\circ, 40^\circ)$, $\epsilon_d=1$, $\epsilon_{ij}=100$, threshold=0 dB.

cost effectiveness. The choice between the two depends on the particular application. For example, a crossed array is suitable for aircraft mounted UHF adaptive arrays: elements of one of the linear arrays can be distributed along the fuselage while the other linear array can be distributed at right angles to it, around the fuselage. Due to the symmetrical distribution, circular arrays may be preferred for satellite based communication systems.

In the above discussion, the desired signal was incident from the broadside direction. In practice, the desired signal can be incident from any direction in the given field of view. The array performance would not change with the direction of the desired signals as the unperturbed pattern of the array will just shift so that its mainbeam is in the desired signal direction. The sidelobe levels will not change. The array performance, therefore, will be satisfactory.

F. SUMMARY

In this section, an algorithm to select element locations of a linear array to be used in an adaptive mode was developed. Using the algorithm one can thin the array while assuring the required performance levels when the array is operating in an adaptive mode. It was shown that one can use the linear array (obtained using the algorithm) to develop various thinned planar arrays. The planar arrays provided the required performance when the field of view was extended to the upper half space.

G. REFERENCES

- [1] I.J. Gupta and A.A. Ksienski, "Dependence of Adaptive Array Performance on Conventional Array Design", Technical Report 711679-6, August 1981, The Ohio State University ElectroScience Laboratory, Department of Electrical Engineering; prepared under contract F30602-79-C-0068 for Rome Air Development Center.
- [2] I.J. Gupta and A.A. Ksienski, "Prediction of Adaptive Array Performance in a Multiple Jammer Environment", Technical Report 711679-8, December 1981, The Ohio State University ElectroScience Laboratory, Department of Electrical Engineering; prepared under contract F30602-79-C-0068 for Rome Air Development Center.
- [3] Y.T. Lo, "A Mathematical Theory of Antenna Array with Randomly Spaced Elements," IEEE Transactions on Antennas and Propagation, Vol. AP-12, No. 3, pp. 257-268, May 1964.
- [4] M.I. Skolnik, A. Neimhauser and J.W. Sherman, III, "Dynamic Programming Applied to Unequally Spaced Arrays", IEEE Transactions on Antennas and Propagation, Vol. AP-12, No. 1, pp. 35-43, January 1964.

SECTION XI

CONCLUSIONS AND RECOMMENDATIONS

One of the major accomplishments of this research effort was the establishment of a direct and explicit relationship between the electromagnetic properties of an antenna array and its performance in an adaptive mode. This permitted the adaptive performance prediction of an array without exhaustive tests and lead to an array synthesis procedure for both linear and two dimensional arrays. The synthesis procedure permits the design of both filled and thinned arrays to meet required SINR specifications over prescribed fields of view. The formulas developed are expected to hold for reasonable operating bandwidths but in a strict sense they apply to narrow band signals. It is recommended, therefore, that they be tested for wideband signals and be modified as appropriate. Also, the general problem of antenna element distribution to provide adequate performance in terms of SINR in the presence of jammers, treated in Section X in considerable detail, should be extended to include mutual coupling and multipath effects.

Another major accomplishment has been the extension of the dynamic range of adaptive arrays. Two approaches were attempted, one involves a cascaded array whose first stage consists of Power Inversion arrays and the second of an LMS adaptive array. The second approach utilized a

modified LMS loop which attempts to equalize the response times of the array to signals of all power levels. Both approaches were implemented experimentally and initial tests indicate significant improvement of dynamic range. It is recommended that both techniques be pursued to assess their performance limits and the dependence of those limits on equipment imperfections and limitations. The optimum approach, or possibly the combination of both approaches should be optimized to achieve maximum dynamic range. Also, an investigation of the broadband nulling capabilities of the arrays should be made, with further development as necessary to achieve a desired nulling bandwidth. It is also suggested that the performance of the arrays be tested in a communication context by measuring bit error rates. This is stressed since indirect tests of the output signal may be rather misleading. In fact, a general study of the signal degradation occurring while traversing the adaptive array is recommended. Such properties as coherence, spectral integrity and waveform fidelity should be studied and methods explored to overcome any degradations.

An investigation into waveforms jointly compatible with efficient digital communication and adaptive array processing lead to the development of a QPSK modulation that ensures rapid acquisition of desired signals and effective protection against both brute force and "smart" jammers. The technique was thoroughly analyzed and tested experimentally verifying its predicted effectiveness. The present implementation utilizes linear codes but nonlinear codes can be

accommodated by the system and a study of such codes to further enhance security is recommended.

An angle of arrival estimation technique was developed to provide accurately pointed high gain spot beams at both stationary and mobile terminals in a beam hopped TDMA system. The technique provides accurate angular positions of accessing terminals in the presence of high powered main beam and sidelobe jammers. The technique was successfully tested by computer simulation. It is recommended that the technique be experimentally tested which would give assurance that unexpected hardware problems would not compromise the proposed approach and also provide useful design data for eventual prototype implementation.

A study of conformal arrays on a C-135 aircraft to replace an existing reflector type antenna has been successfully completed showing that a single contiguous array of flush mounted antenna elements appropriately placed on the fuselage will perform adequately over the required field of view.

In order to carry out a reliable analysis of adaptive array performance for arrays located on a variety of airplanes including A-10, F-15, F-16 and C-141 aircraft, appropriate computer simulation codes have been developed using the Geometrical Theory of Diffraction. The computer simulated results were compared with measured data as they became available with excellent agreement. It is recommended that these studies be extended to include mutual coupling effects and applied to wideband signals to assess the impact on adaptive array performance.

Studies to develop techniques for implementing time ordered relay communication systems operating at very high data rates, yielded a Kalman loop filter approach for timing corrections. Effective corrections are critical for maintaining low bit error rates with maneuvering mobile terminals operating at high data rates. The technique was analyzed and tested by computer simulation with the results agreeing with analysis predictions. It is recommended that the technique be tested experimentally to assure that unforeseen difficulties do not develop in its eventual implementation.

One of the most critical components required for practical implementation of an adaptive array is the 4-quadrant multiplier needed for signal weighting and correlation in each feedback loop. In previous arrays, many types of devices have been used to perform these functions. They all have, unfortunately, various shortcomings. One of the best involves active transconductance multipliers which perform very well at the design frequency when properly aligned, but performance is seriously degraded at much higher frequencies due to stray circuit capacitance and inductance, and the resultant signal leakage paths caused by the relatively large physical sizes of components and their arrangement required for implementation. Consequently, a microcircuit technique has been developed which could be used to retrofit the present cascaded array, or for other applications, if desired. This circuit shows almost ideal multiplier performance over a dynamic range exceeding 70 dB for both x and y inputs. Further development is recommended which will

include either monolithic or hybrid circuits using FET active devices fabricated directly upon a silicon or gallium arsenide substrate. These advanced devices would be useful to approximately 2 GHz.

APPENDIX A

CASCADED ARRAY DIAGRAMS

Detailed block diagrams and schematics for the experimental cascaded adaptive array described in Section III of this report are collected in this Appendix for convenience. Descriptions and explanations of circuit operation relative to these diagrams are given in Section III-C-4.

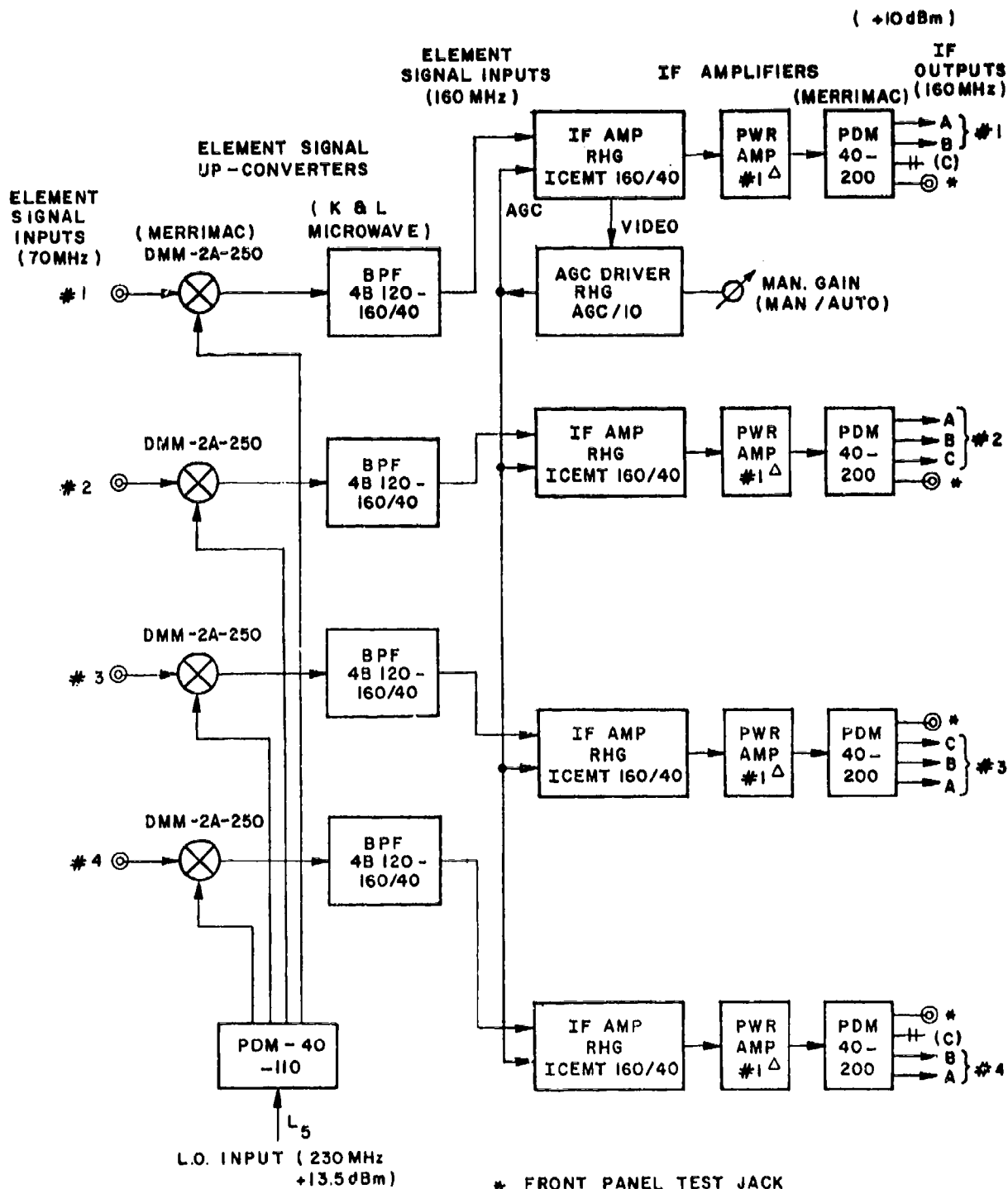


Figure A1. Cascaded adaptive array - converters and I-F amplifiers.

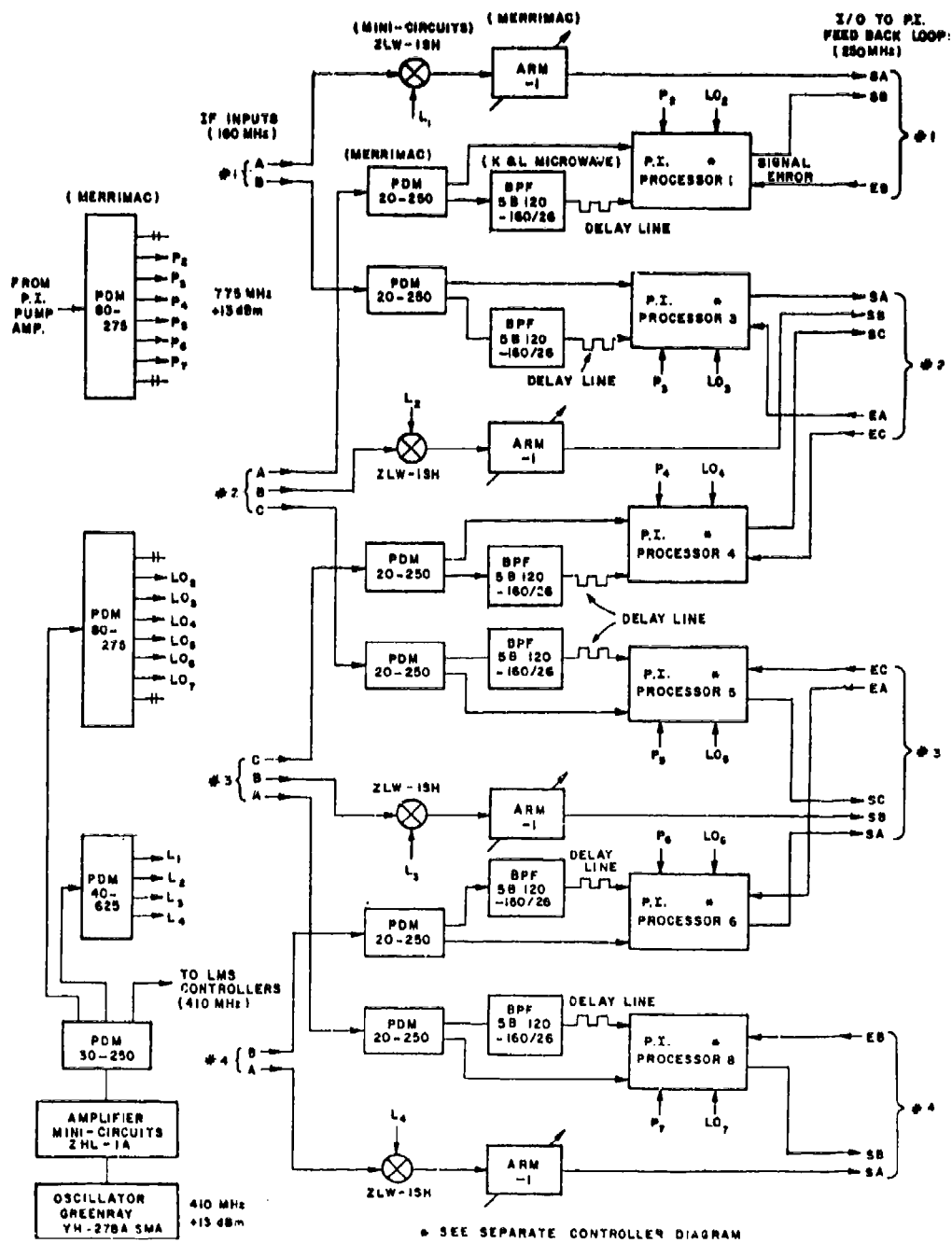


Figure A2. Cascaded adaptive array - power inversion controllers,
4 x (2,3,3,2) configuration.

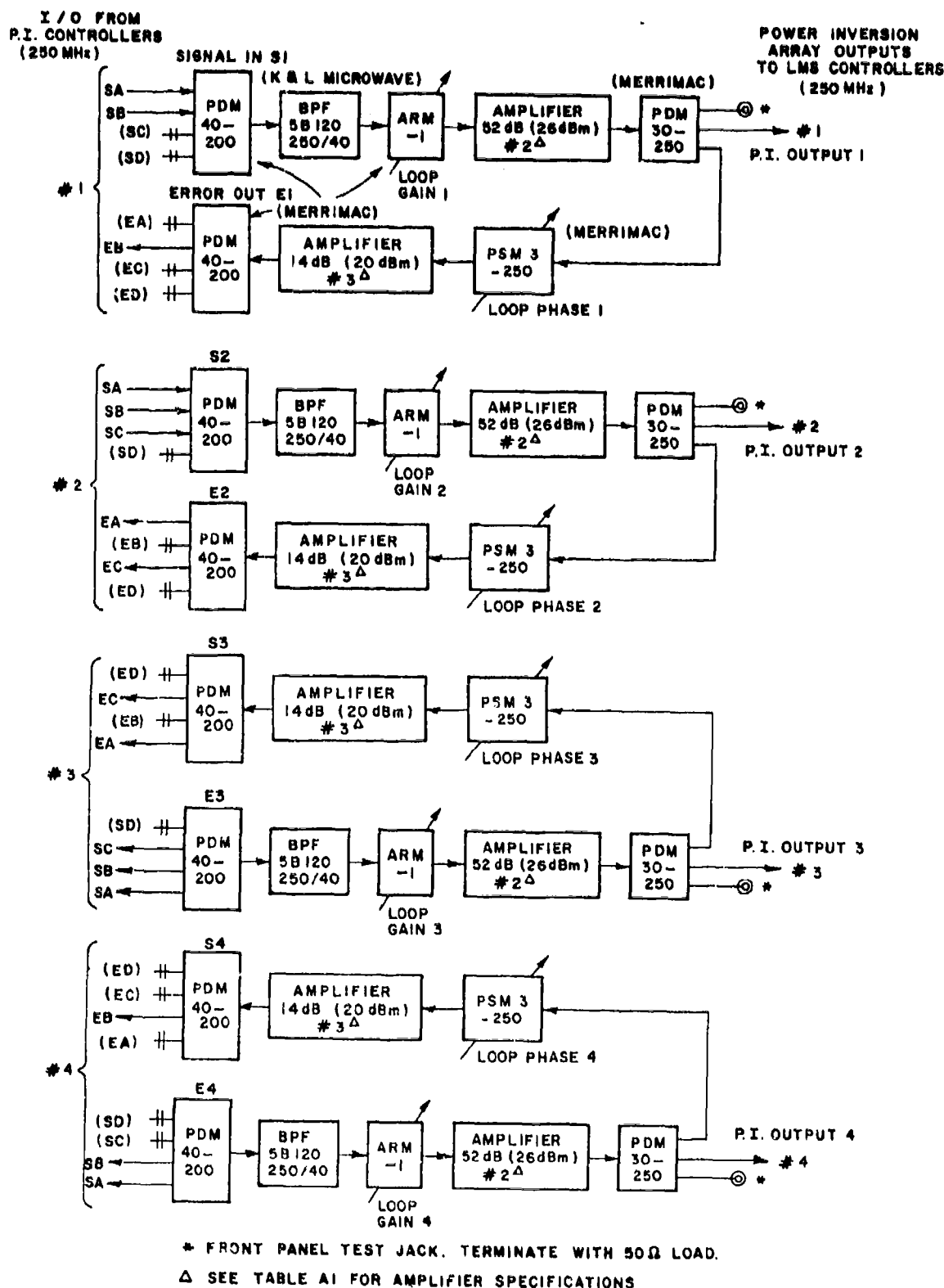
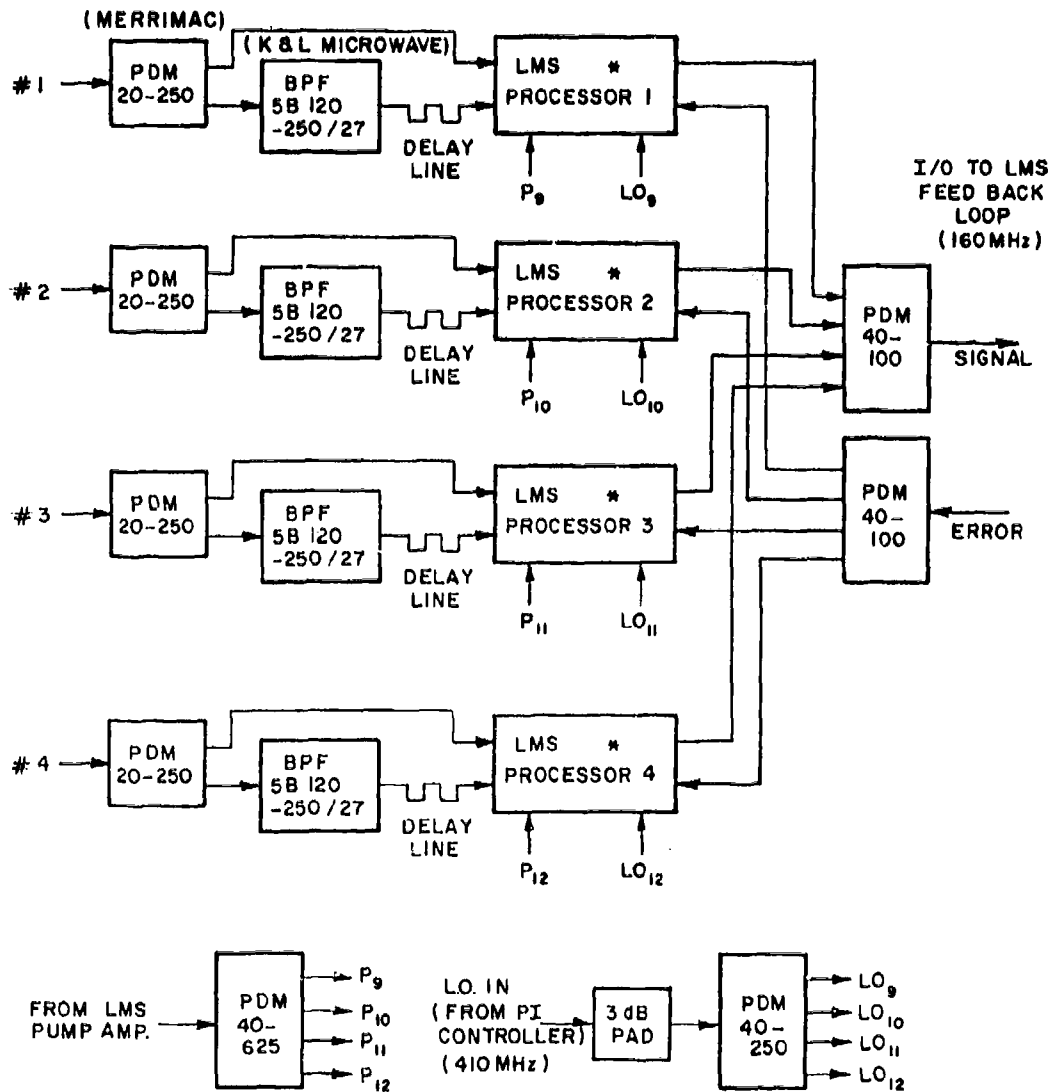


Figure A3. Cascaded adaptive array - power inversion feedback loops,
4 x (2,3,3,2) configuration.

INPUTS FROM
P.I. ARRAYS
(250 MHz)



* SEE SEPARATE CONTROLLER DIAGRAM

Figure A4. Cascaded adaptive array - LMS controllers.

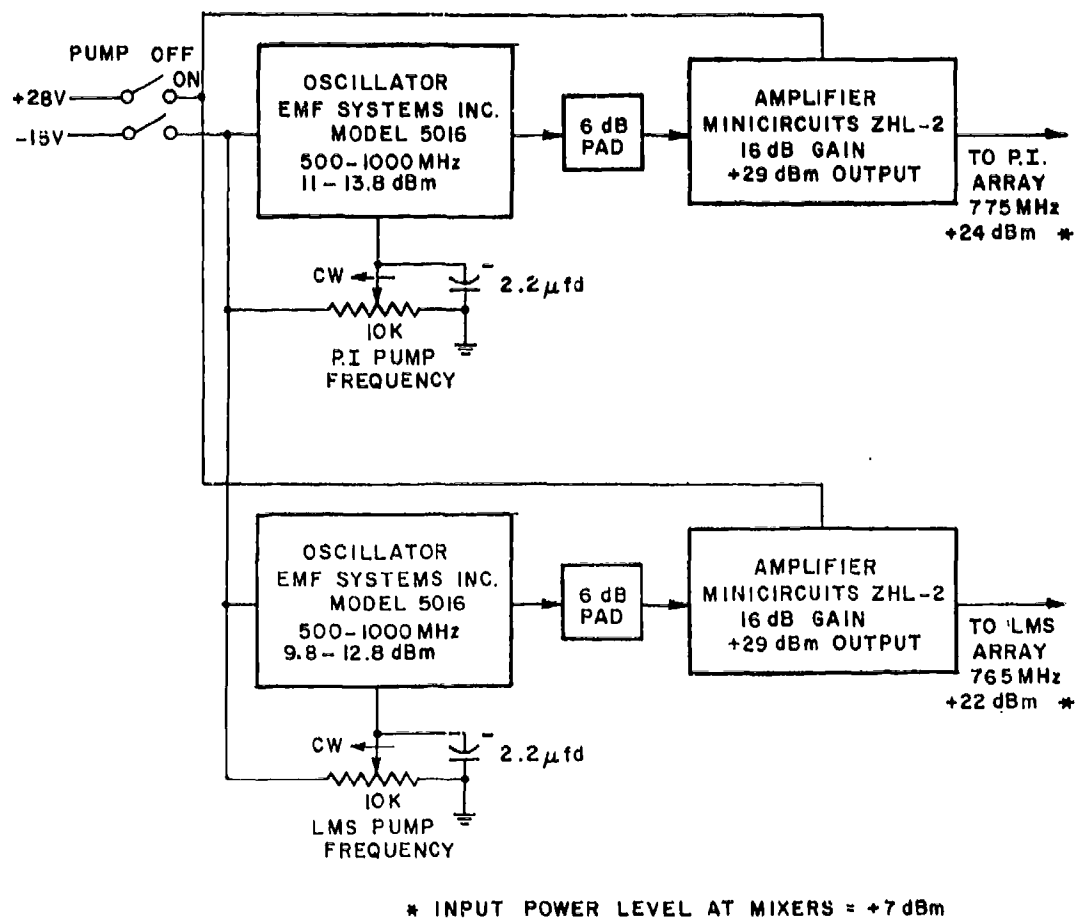


Figure A6. Cascaded adaptive array - pump oscillators and amplifiers.

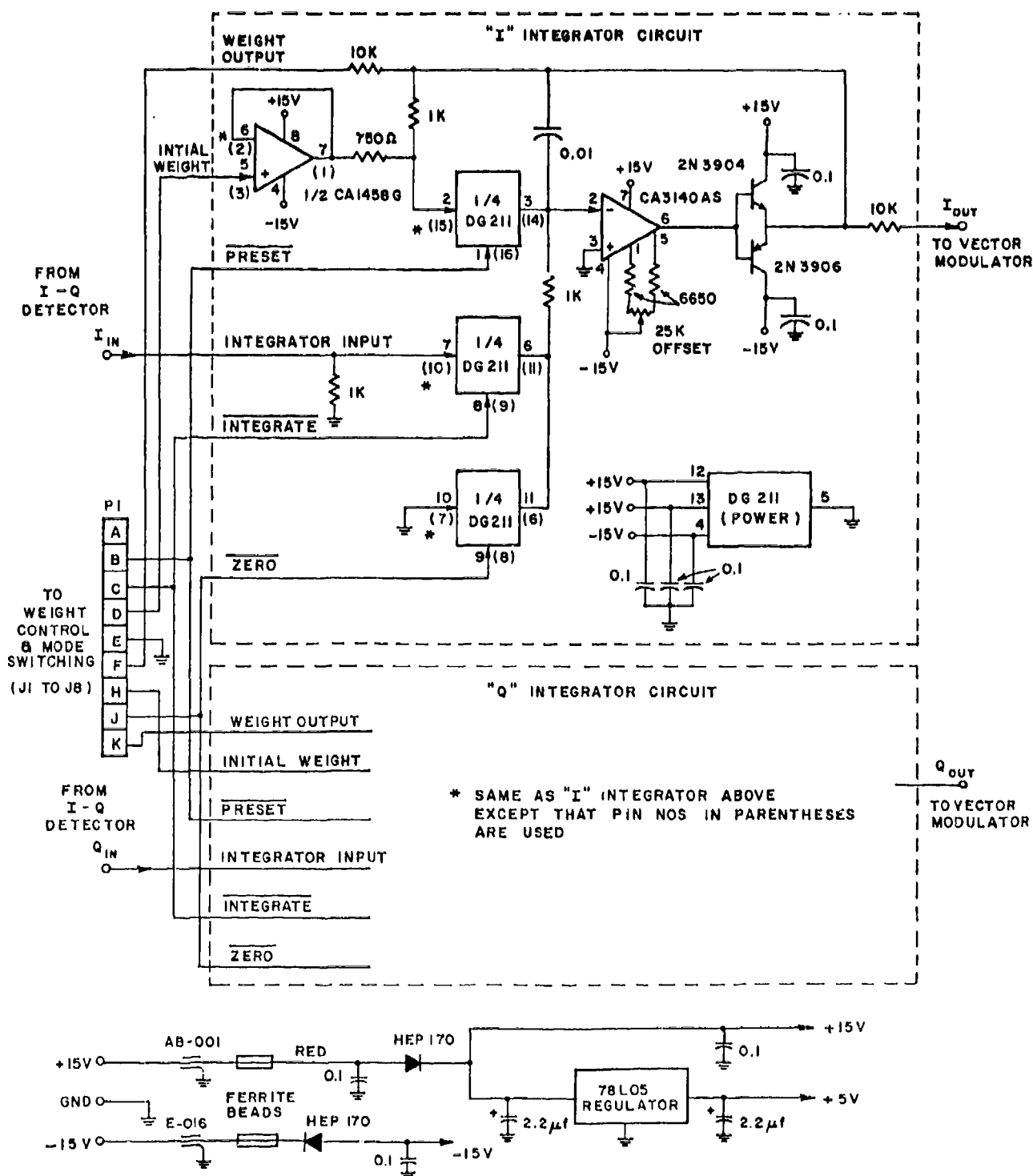
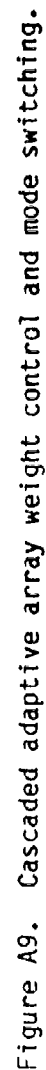


Figure A8. Cascaded adaptive array baseband integrators.



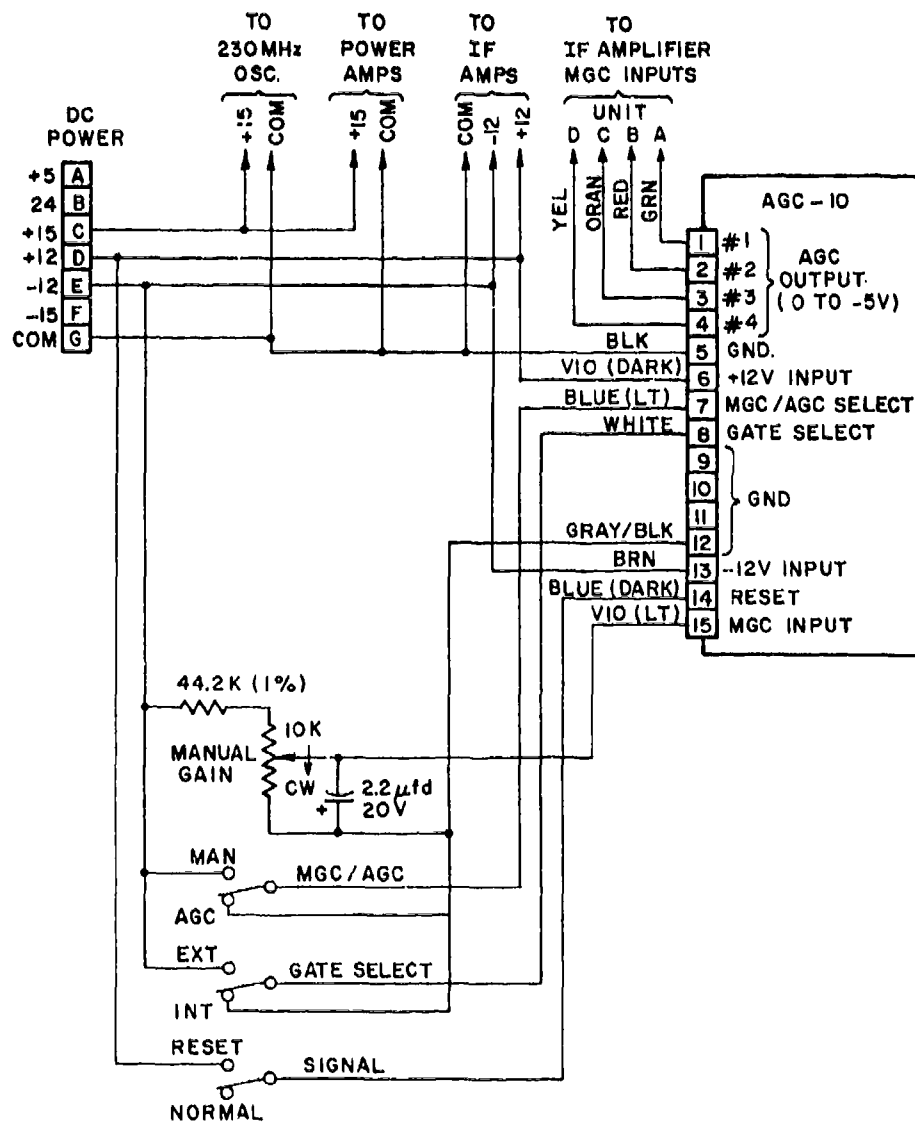


Figure A10. Cascaded adaptive array I-F amplifier gain control and power wiring.

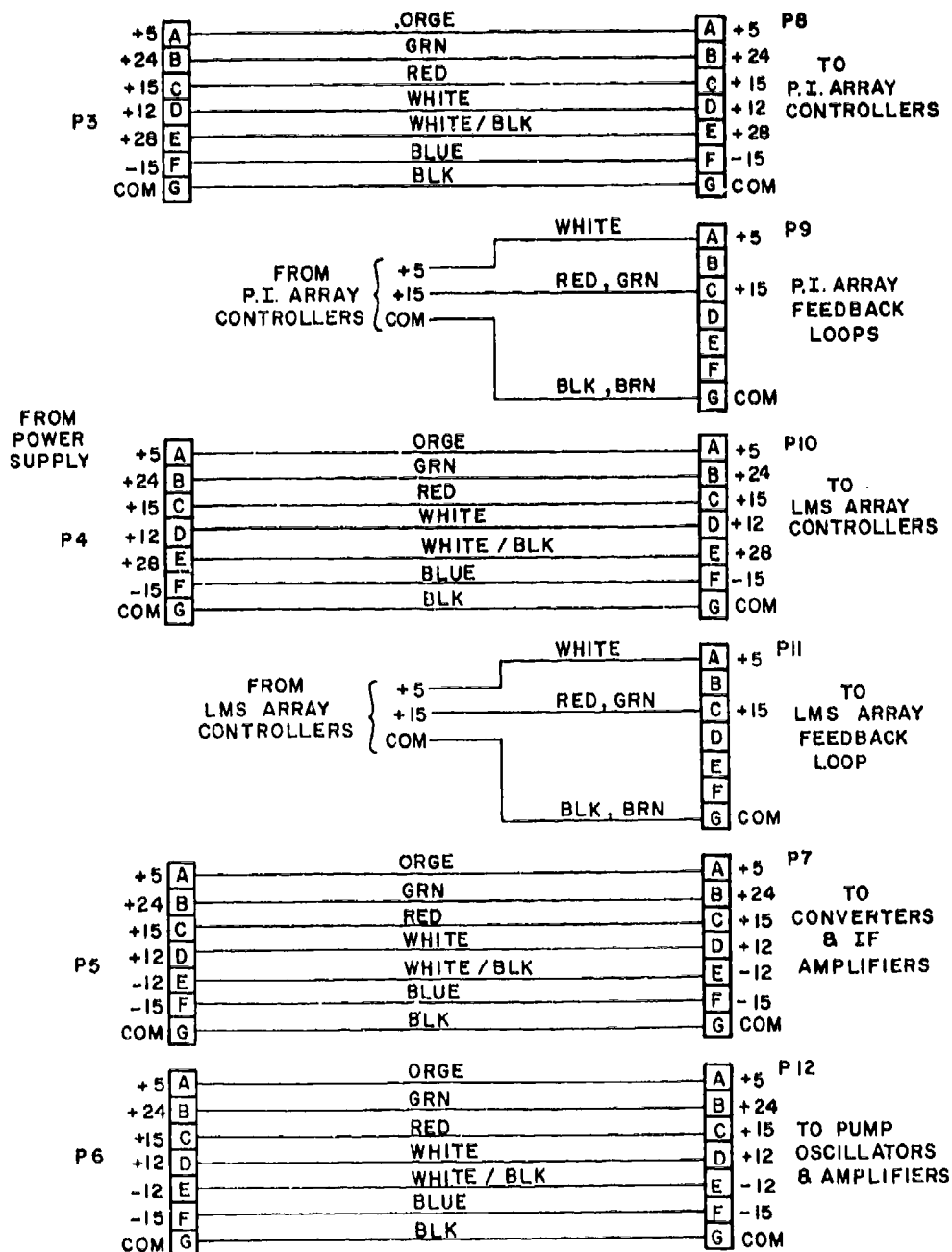


Figure A11. Cascaded adaptive array power distribution.

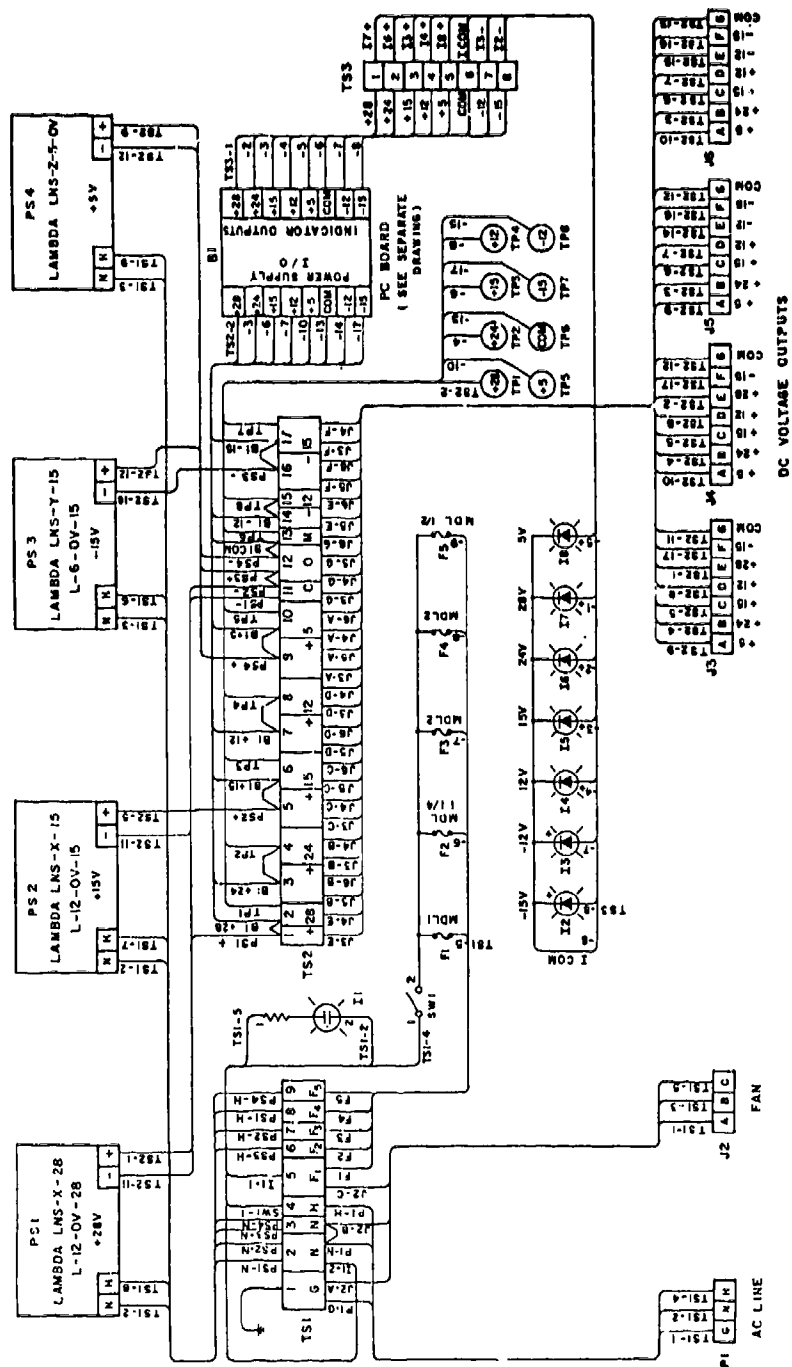
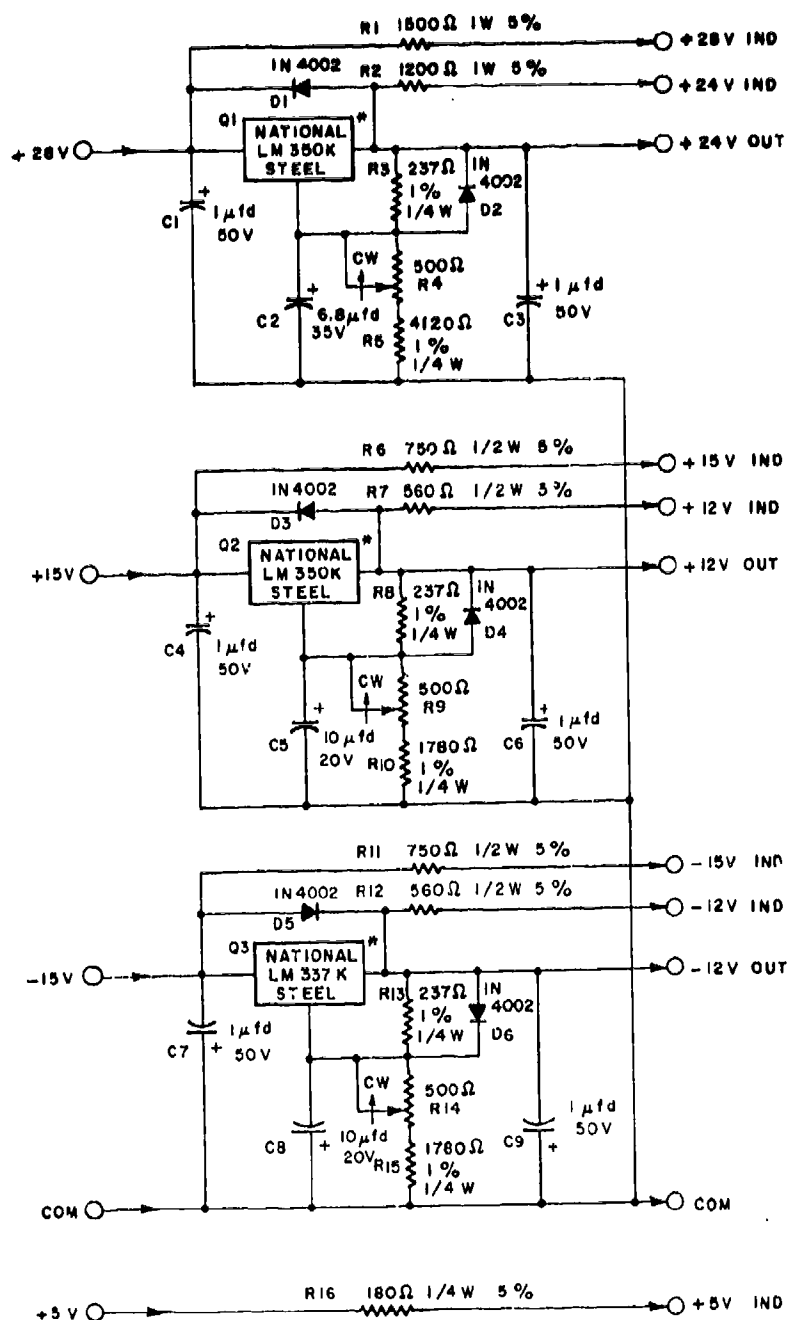
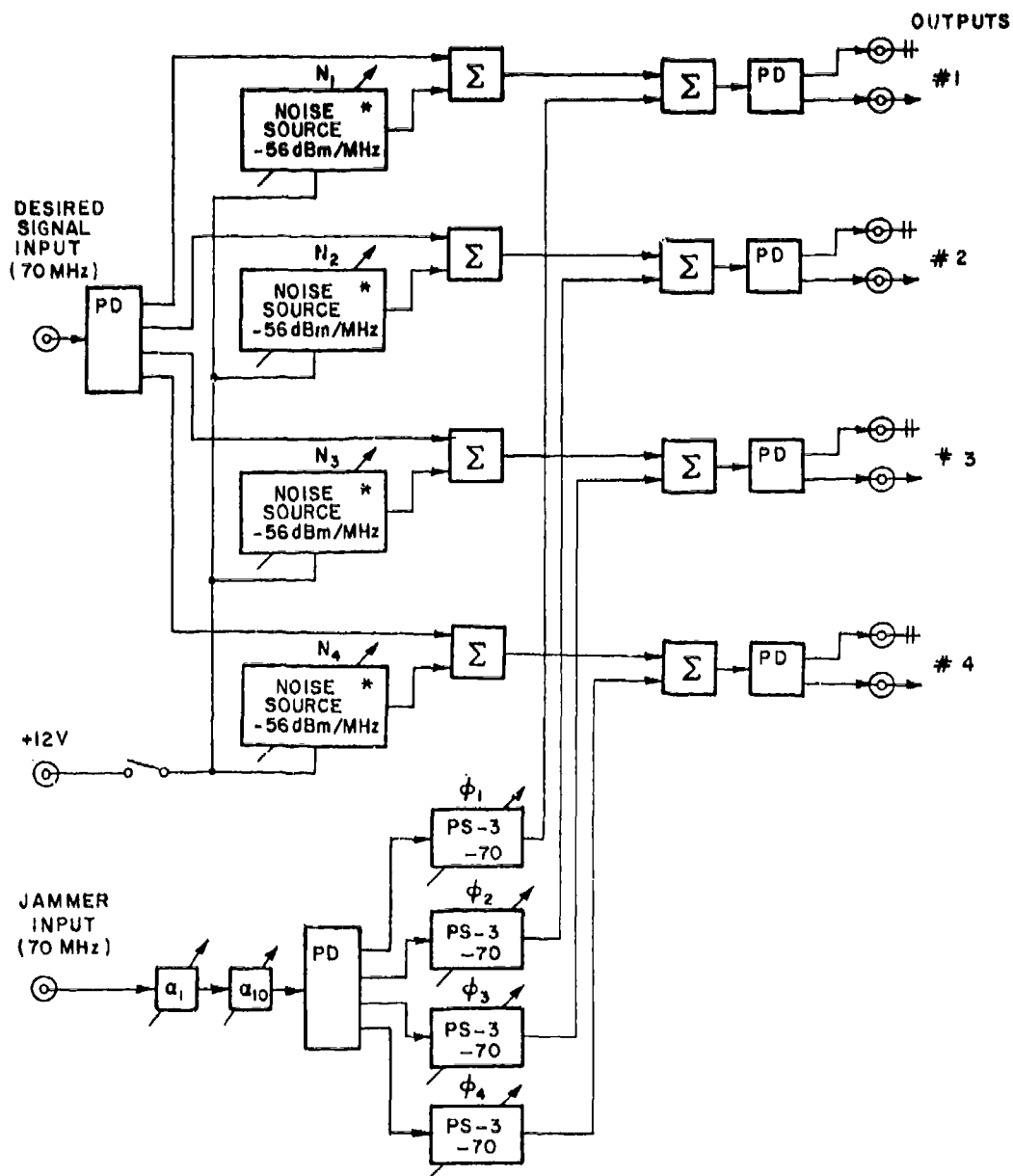


Figure A12. Cascaded array power supply APS-2.



* NOTE : REGULATORS ARE MOUNTED ON EXTERNAL
HEAT SINK : (WAKEFIELD 401-A)

Figure A13. Cascaded array power supply regulator circuit board.



* NOISE SOURCES ARE APPROXIMATELY 10MHz BANDWIDTH GAUSSIAN. TOTAL NOISE POWER IN 15MHz BANDWIDTH = -49 dBm. GAIN CONTROL PROVIDES BOTH HIGHER & LOWER NOISE POWER SETTINGS RELATIVE TO THOSE GIVEN.

Figure A14. Adaptive array element signal simulator (70 MHz).

TABLE AI
 CASCADED ADAPTIVE ARRAY
 AMPLIFIER SPECIFICATIONS

Δ AMPLIFIER SPECIFICATIONS							
No.	Gain, dB	Power Output dBm	Avantek Components	N.F.,dB	DC Power Volts Ma.		Number Required
#1	14	20	UT0-507,TB-1,TC-2	8.5	15	110	4
#2	52	26	UT0-501,502,507,561, TB-4,TC-4	4.2	15	333	4
#3	14	20	UT0-507,TB-1,TC-2	8.5	15	110	4
#4	10	12	UT0-544,TB-1,TC-2	3.0	15	35	1
#5	63	26	UT0-511,523,507,561, TB-4,TC-4	2.7	15	390	1
#6	11	26	UT0-561,TB-1,TC-2	9.0	15	190	1

APPENDIX B
MICROELECTRONICS LAB
ELECTRICAL ENGINEERING DEPARTMENT
THE OHIO STATE UNIVERSITY

HYBRID ELECTRONICS PROJECT
COMMUNICATION LABORATORY
ELECTROSCIENCE LABORATORY
THE OHIO STATE UNIVERSITY

Harold K. Brown
Supervisor

Ron Chaffee
Bill Stevens
Assistants

I. Introduction

The objectives of this project are to improve the frequency response of an active four quadrant multiplier from 80 MHz to the needed 400 MHz. Hybrid technology is utilized in order to reduce parasitic capacitance and inductance associated with the presently used circuit. Specifically an RCA CA 3049L beam lead differential amplifier (see Fig. 1) is mounted onto a ceramic substrate allowing the reconfiguration of the pin-out, thus minimizing the parasitics (see Fig. 2). This device is then used in an existing circuit to achieve the desired frequency response.

Procedures for the fabrication of the hybrid circuit are presented, explaining the techniques for aluminum pattern deposition, device mounting (CA 3049L) on through to packaging. Also suggestions for improving future fabrication techniques are presented.

In conclusion, 40 devices were delivered with the proper frequency response satisfying the contract needs.

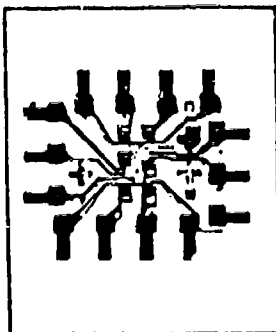
II. Design Specification

In this design several parameters are optimized, boosting the frequency response. First, parasitic inductance and capacitance are both kept to a minimum, by reconfiguring the pin-out of the CA 3049L (see Fig. 3), thus reducing the external wiring. Lead resistance is also kept small (less than 4Ω) by evaporating a minimum of 3 micro-

Linear Integrated Circuits

Monolithic Silicon

CA3049L



Beam-Lead Dual Independent Differential Amplifiers

For Low-Power Applications at Frequencies up to 500 MHz

Applications

- VHF amplifiers
- VHF mixers
- Multifunction combinations —
RF/Mixer/Oscillator; Converter/IF
- IF amplifiers (differential and/or cascade)
- Product detectors
- Doubly balanced modulators and demodulators
- Balanced quadrature detectors
- Cascade limiters
- Synchronous detectors
- Balanced mixers
- Synthesizers
- Balanced (push-pull) cascade amplifiers
- Sense amplifiers

CA3049L is the beam-lead version of the CA3049 and consists of two independent differential amplifiers with associated constant-current transistors on a common monolithic substrate. The six n-p-n transistors which comprise the amplifiers are general-purpose high frequency devices which exhibit a value of f_T in excess of 1000 MHz. These features make the CA3049L useful to 500 MHz. Bias and load resistors have been omitted to provide maximum application flexibility.

CA3049L is particularly suited for applications in hybrid circuits where hermetic packaging, low cost, and reliable operation are prime considerations.

The monolithic construction of the CA3049L provides close electrical and thermal matching of the amplifiers. This feature makes this device particularly useful in dual-channel applications where matched performance of the two channels is required.

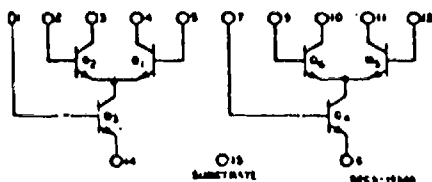
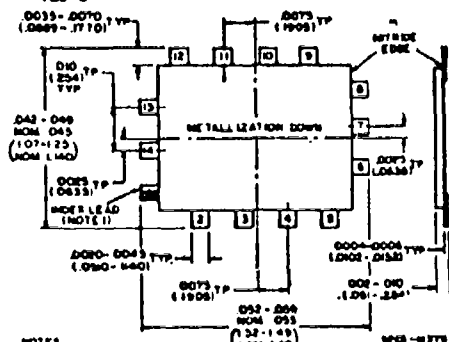


Fig. 7-1—Schematic diagram of CA3049L

Features

- Power Gain 23 dB (typ.) at 200 MHz
- Noise Figure 4.6 dB (typ.) at 200 MHz
- Two differential amplifiers on a common substrate
- Independently accessible inputs and outputs
- Full military temperature range capability — -55°C to $+125^{\circ}\text{C}$



NOTES

1. NOTE 3 CONTINUATION ON BEAM NO. 1. OPTIONAL PROVIDED LEAD MAX IS NOT INCREASED MORE THAN D08.
2. LEADS AT TRUE POSITION (TYP) WITHIN D08 TOTAL (REF. USAS YN. 8-1964).
3. SILICON MUST NOT EXTEND BEYOND WITHE OVER A BEAM.

Fig. 7-2—Terminal layout for CA3049L (14-lead configuration)

CAUTION: Substrate **MUST** be maintained negative with respect to all collector terminals of this device. Although RCA-CA3049L is electrically similar to CA3049, it is not a pin-for-pin replacement.

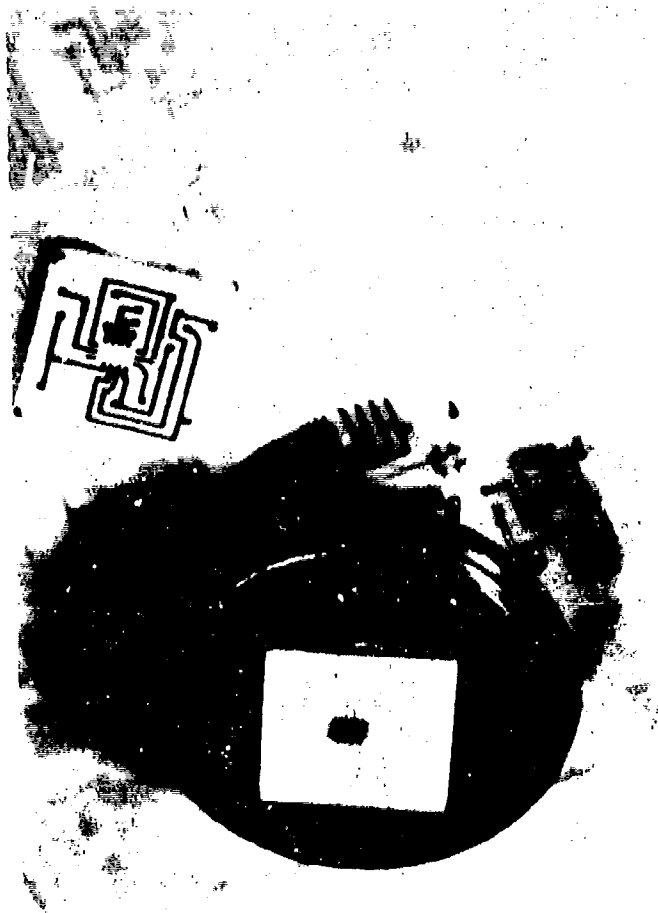


Figure 2 -- a) Illustrated in the background is a ceramic board with 20 circuit patterns. b) Illustrated in the middle right is the device substrate. c) Illustrated in the upper portion is the complete device before capping.

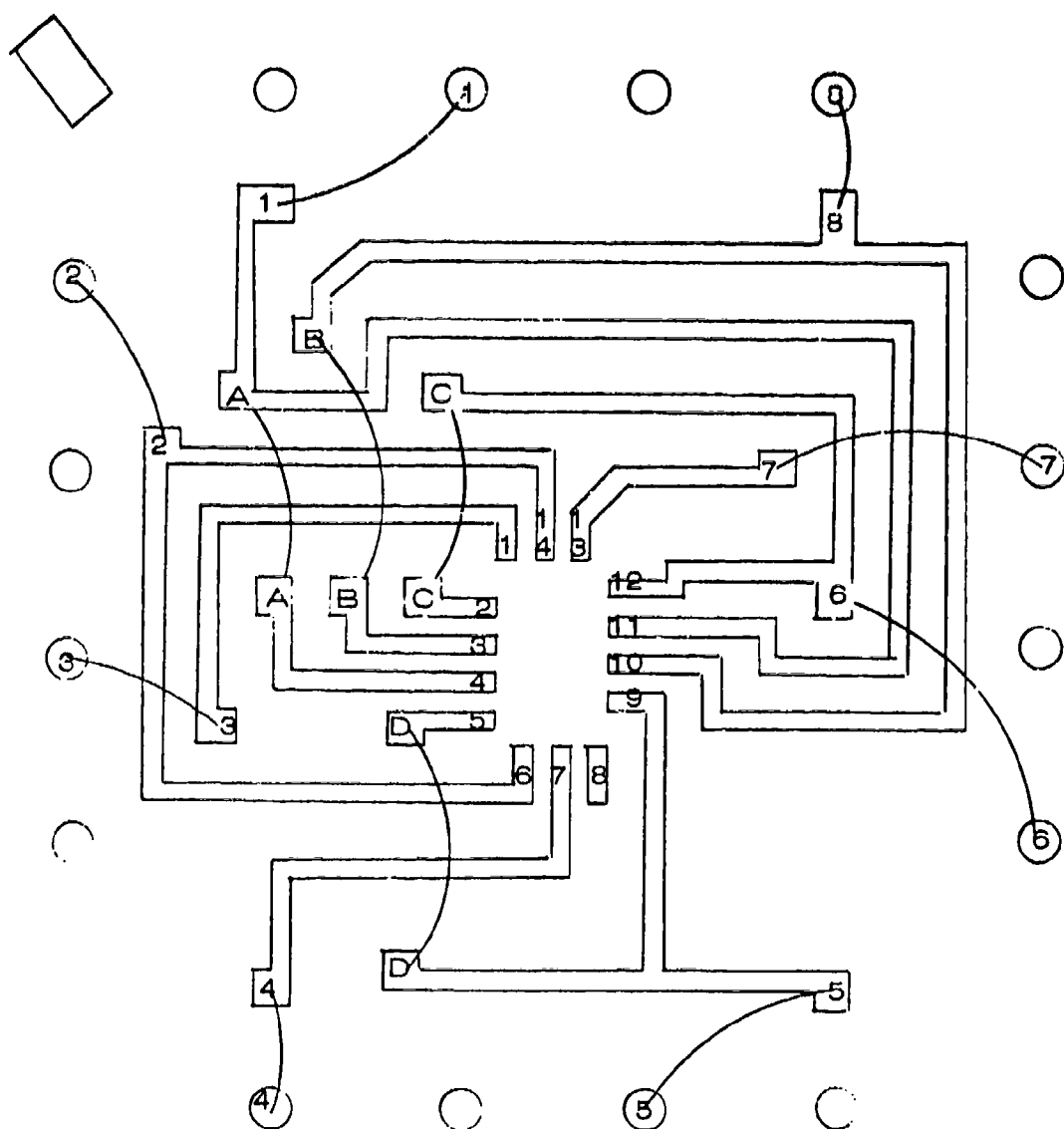


Figure 3 -- Conductor pattern and pinout configuration of the hybrid circuit.

meters of aluminum onto the ceramic substrate for the conductor paths. Finally, the overall size is minimized by fabricating the hybrid circuit so as to fit into a TO-8 16 pin header (see Fig. 4).

To minimize the cost of fabrication, 20 devices are fabricated at a time, thus allowing the use of a two inch square ceramic substrate. After aluminum deposition and photolithography, the ceramic substrate is sawed into 20 separate device substrates measuring .27 inches square. The device substrate is mounted onto a TO-8 header. Then the CA 3049L is then mounted onto the device substrate by thermally compressing the beam leads to the proper pads. Finally, gold wire is bonded between the header's posts and the device substrate which is then capped with a protective covering.

III. Procedure

To process twenty devices at a time, it is necessary to create a mask with 20 patterns.* To fabricate this mask two reductions are necessary. First the original 15 x 15 inch art work is reduced into 20 one-inch circuit patterns onto a 5 x 7 inch glass

* Due to the size of the ceramic board, a mask that would contain 20 devices was decided upon.

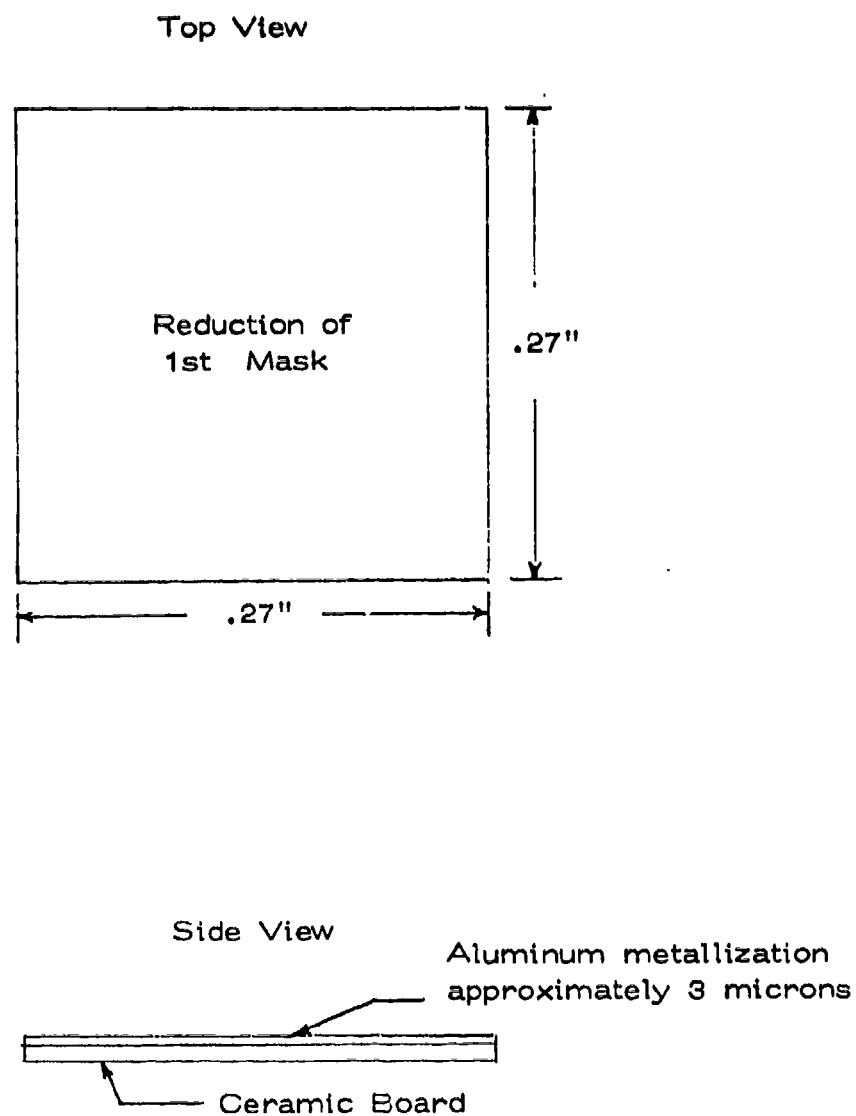


Figure 4 -- Mechanical drawing of metalized ceramic substrate.

plate. The one-inch patterns are then reduced into .27 inch circuit patterns on to a 4 x 4 inch glass plate to be used with a Cobill 400A mask aligner.

Once the mask is produced, the fabricating procedure for the hybrid circuit is as follows:

1. Clean thoroughly a 2 x 2 ceramic board, follow the 3 step cleaning procedure; TCE, Acetone, and Methyl Alcohol.
2. Evaporate aluminum onto the ceramic board, following the "Evaporation Procedures". Use 20 inches of aluminum wire for the NRC evaporator and 24 inches of aluminum wire for the Cooke evaporator.
3. Process the aluminized ceramic board following the "Photo-lithography Procedures".
4. Saw the Aluminized board into .27 x .27 inch squares creating 20 individual device substrates, following the "Sawing Procedures". (See Fig. 5)
5. Mount and bond the individual device substrated onto the headers.
6. Bond the active device onto the individual aluminized devices substrates following "Bonding Procedures".
7. Complete bonding from board to header posts, following the "Bonding Procedures". (See Fig. 6)

IV. Device Evaluation

The devices were tested by the Communications laboratory with inputs of 400 MHz and 160 MHz producing a product of 240 MHz. (see Fig. 7). The CA 3049L's originated from two different batches. By processing devices from each batch together, using the same fabrication techniques, a 20% yield was achieved



Figure 5 -- Twenty device substrates after sawing is complete.

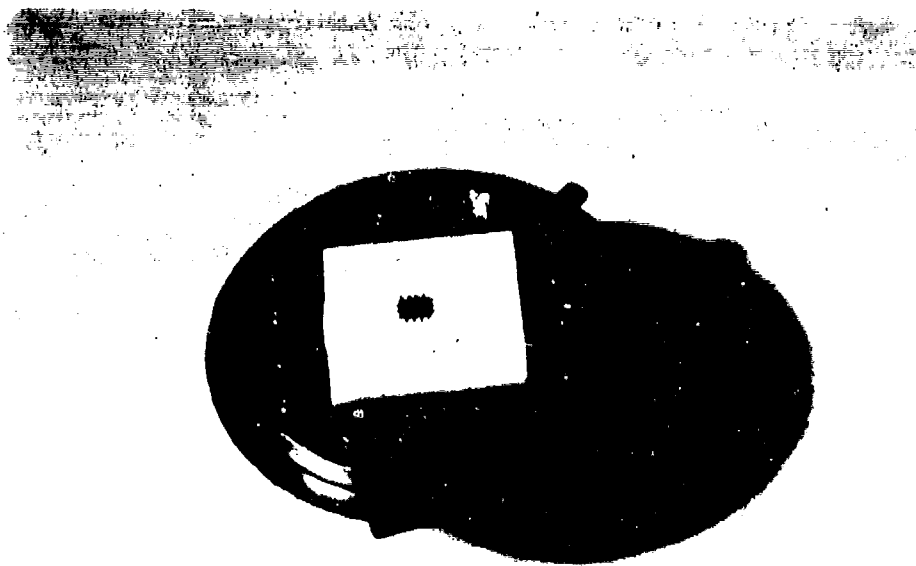


Figure 6 -- Complete device before capping.

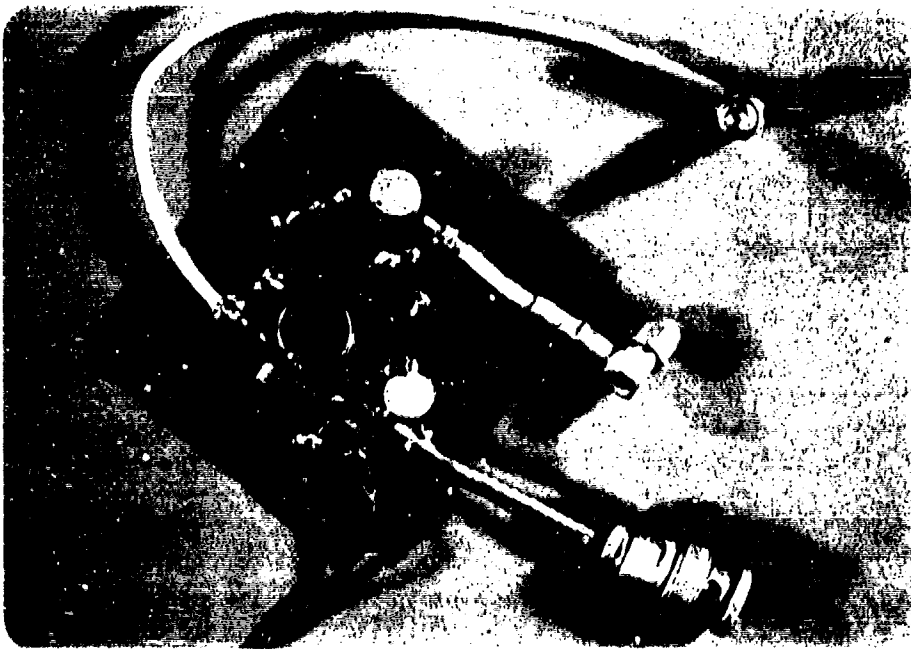
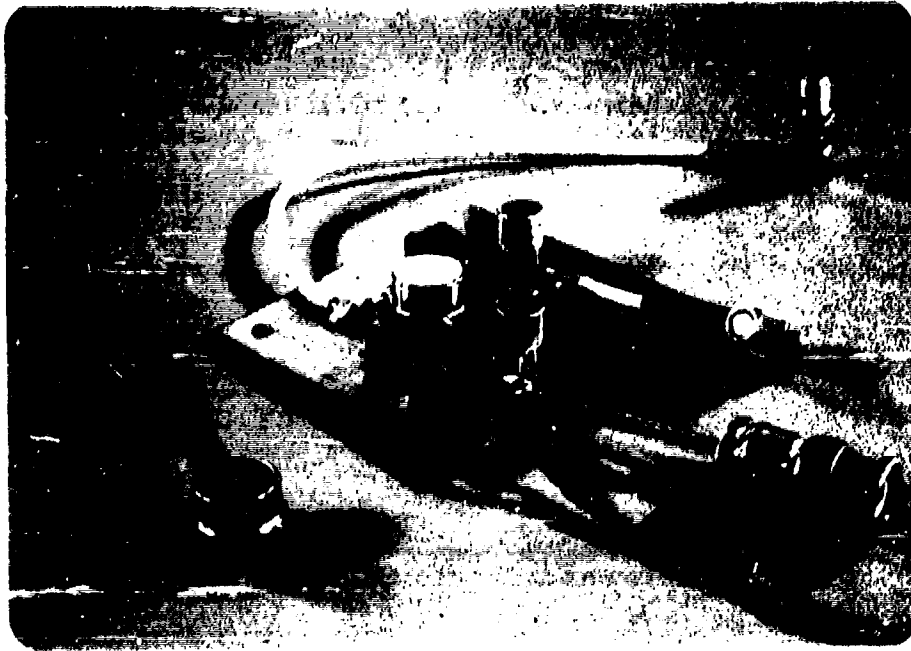


Figure 7 -- Test circuit.

in one lot and 50% yield was achieved in the other. Although some of the devices failed at high frequencies, there was no indication of failure under static conditions. This indicates that presorting of future devices using high frequency tests may be required on future and larger hybrid circuits to improve yields. Most of the defective devices were reworked without much difficulty, however, the reworked devices followed the same yields as when originally fabricated. This, again, leads to the conclusion that the yields were governed by the quality of the CA 3049L chips.

V. Conclusion

Although the end result of this project was a success, many improvements could be made to reduce the cost and improve circuit performance. Thick film hybrid technology could be introduced, decreasing the cost substantially, while shortening the fabrication time. Passive components could also be added, thus reducing external circuitry and improving the frequency response. Eventually, the printed circuit board would be replaced with a hybrid circuit optimizing the geometry for improved frequency and power characteristics. Such capability will be a must for future microwave circuit laboratories.

A more advanced approach would be to stay with thin film technology, but instead of fabricating the circuit on a ceramic substrate, the devices would be fabricated on an active wafer such as

silicon or gallium arsenide. This would allow the fabrication of balanced active components in the substrate, thereby improving system versatility. Although the initial investment would be far greater than that required for thick film, pace with state of the art advances could be maintained.

Evaporation Procedures*

1. Turn on Diffusion pump (30 minutes prior to Evaporation).
2. Open Foreline valve.
3. Open Nitrogen tank.
4. Open vent valve (wait 2 or 3 minutes).
5. Lift bell jar.
6. Close vent valve and Nitrogen tank.
7. Clean 2 tungsten "boat" filaments, the ceramic boards to be used and 2 sections of aluminum wire.
8. Attach "boat" filaments in parallel to the evaporator electrodes.
9. Coil tightly the 2 sections of aluminum wire and set them inside the filaments.
10. Lower bell jar.
11. Fill cold trap with liquid Nitrogen.
12. Open Roughing valve (wait 2 or 3 minutes until TC2 reaches 80 microns)
13. Close Roughing valve and then open Foreline valve.
14. Open High Vacuum valve.
15. Turn on Cold Cathode gauge.
16. Keep High Vacuum valve on until Cold Cathode gauge reaches 4×10^{-6} Torr.
17. Turn off Cold Cathode gauge.

* All switches are delayed, light indicates that switch is ON.

Evaporation procedure, cont'd...

18. Turn on filament power.
19. Increase filament current to 20% .
20. Let aluminum out gas (melt completely).
21. Remove shutter.
22. Increase filament current to 40% (wait 3 minutes) .
23. Decrease current and turn filament power off.
24. Close High Vacuum valve (wait 5 to 10 minutes) .
25. Follow steps 2 through 6.
26. Clean Belljar and base plate.
27. Follow steps 20 through 13, except step 11.
28. Turn Diffusion pump off if no other evaporation will be done.
29. Leave mechanical pump on.

Photo-Lithography Procedures

1. Turn on timers for ovens (to allow warm-up period).
Set prebake oven (on left) to $90^{\circ} \pm 5^{\circ}\text{C}$. Postbake oven (on right) to $120^{\circ} \pm 5^{\circ}\text{C}$.
2. Turn on hotplate (dial at ≈ 225) and heat 25 ml of aluminum etch to $75^{\circ} \pm 5^{\circ}\text{C}$.
3. Spin positive photo-resist onto metallized ceramic boards (3500 RPM for 30 seconds).
4. Prebake for 20 minutes ($90^{\circ} \pm 5^{\circ}\text{C}$).
5. Turn on Cobilt 400A Aligner. Follow procedures posted near aligner and expose for 4.5 minutes.
6. Immerse in positive photo resist developer for 30-50 seconds (until pattern is clear and build-up around edges is gone).
7. Rinse in 2 Mega-ohm H_2O and dry with N_2 .
8. Postbake for 20 minutes ($120^{\circ} \pm 5^{\circ}\text{C}$).
9. Etch in hot Aluminum Etch for 30-40 seconds.
10. Clean with acetone (scrub gently with Q-tip to remove all photo-resist).

Sawing Procedures

1. Select blade or blades of desired thickness and mount onto the shaft using spacers and tightening the nut at the end of the shaft.
2. Secure object onto cutting pad with "sticky" wax.
3. Mount and secure pad onto holder.
4. Turn power switch to "On" position.
5. Mount cutting pad and holder onto the sawing platform and operate clamp switch to secure holder.
6. Start water flow and coolant pump.
7. Set in/out controls for cutting speeds.
8. Lower head using switch and set desired cutting depth.
Be sure to cut thru the object and partially into the sawing pad.
9. Prime butting blade with primer block.
10. Determine width and angle of cut.
11. Operate in/out switch to move cutting platform and cut object.
12. When finished, return equipment to original state and turn power off.

Bonder Procedures

1. Turn power switch to "On".
2. Turn bonder power switch to "On".
3. Set power stat to 56 (controls tip temperature).
4. Set degrees centigrade at 300° to control platform temperature.
5. Open valves on Hydrogen and Formine gas tanks and adjust them to 5 psi each. Open flow valve mounted on back of bonder table. Adjust platform gas supply to 1½. Light Cutting torch.
6. Allow platform to heat to 300°C before proceeding with bonding operation.
7. Focus microscope on tip, find ball at end of gold wire.
8. Operate "Spool" switch to suck gold ball up into end of tip.
9. Refocus microscope on header and bring tip down into position.
10. Press button on the tip control handle which stops air flow to the platform.
11. Release tip control handle and check for good bond to header. *
12. Reposition tip at next bonding target and repeat steps 9, 10, and 11. (This procedure is called a "Stitch" bond.)
13. Push "cutting flame" button to sever gold wire.
14. Repeat steps (7) through (13) for additional bonds.

* If bond is not made, lower tip into position and press button again, holding tip control lever in position for several seconds.

APPENDIX C

APPROPRIATE RELATIONSHIPS FOR THE KALMAN TRACKING LOOP EXPERIMENT

In this appendix, equations are given which relate bit error rate to the tracking errors in the PN code. These equations were used to obtain the theoretical values given in Figure V-3. Also given are the curves from which the model parameters for the various Kalman predictors were chosen.

A. BIT ERROR RATE vs CODE TRACKING ERRORS

The bit error rate is related to the code tracking errors (for large spectral spreading ratios) by

$$P_E = 1/2 \int_0^1 \exp(-r \cdot \ell_1^2) p(\ell_1 | k/2) d\ell_1 \quad (A1)$$

where

$$p(\ell_1 | k/2) = \frac{1}{\sqrt{2\pi} \sigma_{\epsilon\Delta}} \exp \left\{ \frac{-(\ell_1 - 1 + \bar{\epsilon}_\Delta)^2}{2\sigma_{\epsilon\Delta}^2} \right. \\ \left. + \exp \frac{-(\ell_1 - 1 - \bar{\epsilon}_\Delta)^2}{2\sigma_{\epsilon\Delta}^2} \right\} U(1 - \ell_1) . \quad (A2)$$

In these equations

P_E = probability of a bit error

r = E_b/N_0 (energy per bit/single sided noise spectral density)

k = spectral spreading factor

k_1 = normalized magnitude of the signal vector

$\bar{\epsilon}_\Delta$ = average tracking offset (bias)

$\sigma_{\epsilon\Delta}$ = standard deviation of the tracking error.

A complete description and derivation of these equations is given in reference [10] (see Section V for this reference).

B. NOISE PERFORMANCE OF A KALMAN SDDL

The parameters of the four Kalman predictors were chosen so that the four predictors would have different noise performances. The relationship between the noise performance and the parameters is shown in Figure C1 (extracted from reference [4] in Section V). Here \tilde{P}_{in} is the tracking jitter (rms), σ_ξ is the open loop measurement jitter given by [11, Equation (69)]

$$\sigma_\xi = \frac{\Delta}{2} \left[\frac{1.215}{E_c/N_0} \right]^{1/2} \quad \text{for } E_c/N_0 > 10, \quad (A3)$$

E_c is the energy in the clock pulse,

N_0 is the single sided noise spectral density, and

ρ , σ_v , λ^2 , and σ_T are the parameters which were selected.

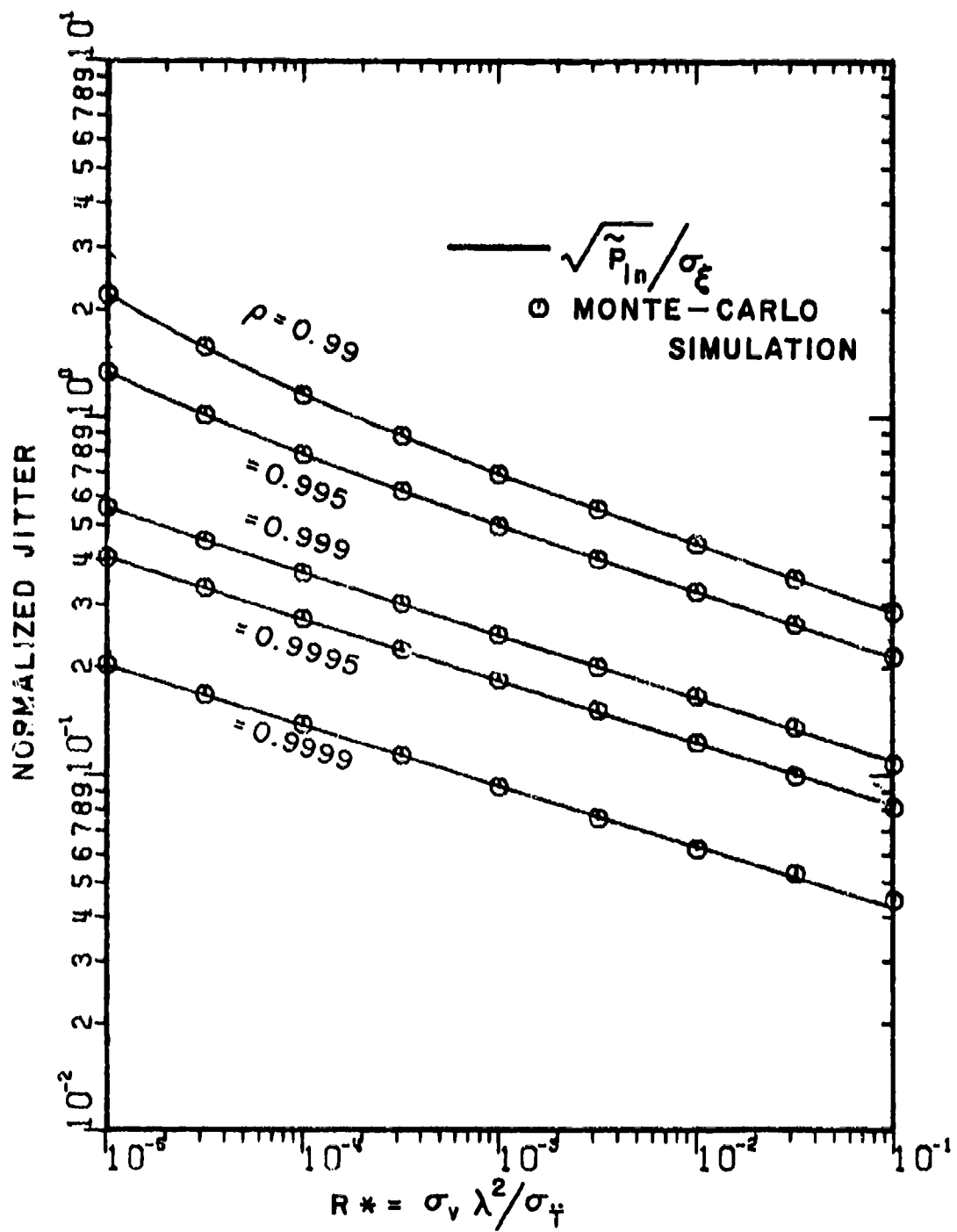


Figure C1. The noise performance of the Kalman predictors as a function of model parameters.

C. NOISE PERFORMANCE OF FOUR SAMPLE AVERAGES

The jitter performance of the four sample averager is given by [11, Equation (68)]

$$\sigma_e = \left[\frac{1}{N_C} \left(\frac{A_C}{2-A_C} \right) \right]^{1/2} \sigma_\xi \quad (A4)$$

where σ_e is the rms clock jitter

N_C is the number of samples averaged (4)

A_C is the loop gain (unity), and

σ_ξ is given in Equation (A3).